NOTICE

The quality of this microform is heavily dependent upon the quality of the original thesis submitted for microfilming. Every effort has been made to ensure the highest quality of reproduction possible.

If pages are missing, contact the university which granted the degree.

Some pages may have indistinct print especially if the original pages were typed with a poor typewriter ribbon or if the university sent us an inferior photocopy.

Reproduction in full or in part of this microform is governed by the Canadian Copyright Act, R.S.C. 1970, c. C-30, and subsequent amendments.

AVIS

La qualité de cette microforme dépend grandement de la qualité de la thèse soumise au microfilmage. Nous avons tout fait pour assurer une qualité supérieure de reproduction.

S'il manque des pages, veuillez communiquer avec l'université qui a conféré le grade.

La qualité d'impression de certaines pages peut laisser à désirer, surtout si les pages originales ont été dactylographiées à l'aide d'un ruban usé ou si l'université nous a fait parvenir une photocopie de qualité inférieure.

La reproduction, même partielle, de cette microforme est soumise à la Loi canadienne sur le droit d'auteur, SRC 1970, c. C-30, et ses amendements subséquents.

ISBN 0-315-56068-1

Canada

An Investigation of Vibration Isolation Systems Using Active, Semi-active and Tunable Passive Mechanisms with Applications to Vehicle Suspensions

Hong Su

A Thesis

in

The Department

of

Mechanical Engineering

Presented in Partial Fulfillment of the Requirements
for the Degree of Doctor of Philosophy at
Concordia University
Montreal, Quebec, Canada

April 1990

CONCORDIA UNIVERSITY
Division of Graduate Studies

This is to certify that the thesis prepared

By: Hong Su

Entitled: An Investigation of Vibration Isolation Systems Using Active, Semi-active and Tunable Passive Mechanisms with Applications to Vehicle Suspensions

and submitted in partial fulfillment of the requirements for the degree of

Doctor of Philosophy

complies with the regulations of the University and meets the accepted standards with respect to originality and quality.

Signed by the final examining committee:

Dr. M.E. Szabo — Chair, Dean of Graduate Studies

Dr. R.J. Rogers — External Examiner

Dr. H.B. Poorooshasb — External to Program

Dr. S. Sankar — Examiner

Dr. A. Hemami — Examiner

Dr. T.S. Sankar — Thesis Co-Supervisor

Dr. S. Rakheja — Thesis Co-Supervisor

Approved by _____
Chair of Department or Graduate Program Director

April 19 1990

_____
Dean of Faculty

ABSTRACT

An Investigation of Vibration Isolation Systems
Using Active, Semi-active and Tunable Passive Mechanisms
with Applications to Vehicle Suspensions

Hong Su, Ph.D.
Concordia University, 1990

In this dissertation, an analytical investigation on active, semi-active and passive vibration control mechanisms is presented in order to achieve improved shock and vibration isolation of mechanical systems, especially ground vehicle applications.

A hybrid active vibration isolation system, incorporating an electro-magnetic force generator along with passive damping and spring elements, is mathematically modeled based on fundamental physical laws and taking into account the generator dynamics. Complete vibration isolation characteristics of the hybrid active control system are evaluated for various feedback variables and control schemes, using numerical simulations. Influence of the force generator dynamics on vibration isolation performance is illustrated through the simulation results.

A concept of tunable pressure limiting modulation is proposed in hydraulic damper systems. A hydraulic orifice damper is modified by using the proposed tunable pressure limiting modulation to achieve variable damping in vibration isolation systems, without requiring any external energy source, sophisticated control devices and feedback instrumentation that are essential for active and semi-active isolators. The fluid flow equations are employed to develop the nonlinear

mathematical model of the hydraulic damper, incorporating the fluid and mechanical compliance, and the dynamics of the pressure limiting mechanism. The computer simulation reveals that the shock and vibration isolation performance of the tunable pressure limited hydraulic damper systems is comparable to that of the semi-active 'on-off' vibration control systems.

A generalized harmonic linearization technique, based on a principle of energy similarity of dynamic elements, is proposed to derive equivalent linear representations of both nonlinear damping and spring elements, in the frequency domain. An analysis of the nonlinear in-plane vehicle model, with air-springs, orifice damping and pressure limiting modulation due to tunable hydraulic shock absorbers, is carried out to establish the stochastic response to random road inputs in terms of power spectral density, and to illustrate the improved vehicle ride performance due to tunable shock absorbers.

An interconnected hydro-pneumatic suspension with tunable pressure limiting mechanism is presented to achieve improved vehicle ride and handling performance. Analysis of a roll plane model of a vehicle employing the tunable interconnected suspension shows that the connections of fluid flow within the interconnected suspension provide an enhanced static roll stability; while the tunable pressure limiting modulation between the strut and the accumulator of each suspension unit offers an improved vehicle ride performance.

ACKNOWLEDGEMENTS

The author wishes to express his sincere appreciation to his thesis supervisors, Dr. T. S. Sankar and Dr. S. Rakheja, for initiating the study topic and providing continued guidance throughout the course of this investigation.

Thanks are due to the colleagues, faculty and staff at the Mechanical Engineering Department, Computer Centre, and CONCAVE Research Centre of the Concordia University, for their contributions to this effort.

The financial support provided by the assistantships and fellowships funded by the CONCAVE Research Centre of the Department of Mechanical Engineering, Concordia University and the NSERC research grant OGP 0007104 awarded to Dr. T. S. Sankar, and the international student tuition fee remission fellowships funded by the Quebec Government, Canada, are gratefully acknowledged.

Finally, the author would like to express his special thanks to his wife and members of his family, for their encouragement.

TABLE OF CONTENTS

		Page
LIST OF FIGURES		xii
LIST OF TABLES		xxii
NOMENCLATURE		xxiii
CHAPTER 1	INTRODUCTION AND LITERATURE REVIEW	1
1.1	General	1
1.2	Review of Previous Investigations	3
1.2.1	Passive Vibration Isolation Systems and Hydraulic Dampers	3
1.2.2	Active Vibration Isolation Systems	7
1.2.3	Vibration Isolation Systems With Semi-Active or Sequential Damping	11
1.2.4	Interconnected Hydro-pneumatic Suspensions	14
1.2.5	Analytical Techniques for Nonlinear Stochastic Systems	17
1.2.5.1	Markov Methods	18
1.2.5.2	Perturbation Methods	21
1.2.5.3	Simulation Methods	22
1.2.5.4	Equivalent Linearization Methods	24
1.3	Scope of the Investigation	27
1.3.1	Objective of the Investigation	28
CHAPTER 2	AN ACTIVE VIBRATION ISOLATION SYSTEM USING ELECTROMAGNETIC FORCE GENERATOR	32
2.1	Introduction	32
2.2	Development of Active Vibration Control System Model	34
2.3	Generalized Control Scheme	39

TABLE OF CONTENTS (Continued) Page

2.4 Stability Analysis of Active Vibration Control System . 43

2.5 Vibration Isolation Characteristics Using Control Laws with Individual Variables 44

2.5.1 Absolute Position Control 45

2.5.2 Absolute Velocity Control 45

2.5.3 Absolute Acceleration Control 47

2.5.4 Relative Position Control 49

2.5.5 Relative Velocity Control 49

2.5.6 Relative Acceleration Control 51

2.6 Vibration Isolation Characteristics Using Control Laws with Combined Variables 51

2.6.1 Combined Absolute Velocity and Relative Position Control . . 52

2.6.2 Combined Absolute Velocity and Acceleration Control 54

2.6.3 Combined Absolute Velocity, Acceleration and Relative Position Control . 56

2.6.4 Combined Absolute Position, Velocity and Acceleration Control . 57

2.6.5 Combined Absolute Position, Velocity and Relative Position Control . 60

2.7 Summary 62

CHAPTER 3 **ANALYSIS OF AN IDEAL TUNABLE PRESSURE LIMITED HYDRAULIC DAMPER** 64

3.1 Introduction 64

3.2 Mathematical Modeling of Vibration Isolation System with Hydraulic Damper . . . 66

3.2.1 Equation of Motion 66

TABLE OF CONTENTS (Continued) Page

3.2.2 Static Equilibrium Equations 68

3.2.3 Dynamic Forces due to Hydraulic Damper . . 69

3.3 Semi-active 'On-off' Dampers 73

3.4 Concept of Tunable Pressure Limited Hydraulic Damper . . 75

3.5 Damping Characteristics of Tunable Pressure Limited Damper . . . 79

3.6 Tuning Methodology 80

3.7 Vibration Isolation Characteristics of Tunable Pressure Limited Hydraulic Damper . 86

3.8 Shock Isolation Characteristics of Tunable Pressure Limited Hydraulic Damper . . . 103

3.9 Summary 116

CHAPTER 4 ANALYSIS OF TUNABLE PRESSURE LIMITED DAMPER WITH FLUID AND MECHANICAL COMPLIANCE AND VALVE DYNAMICS . . . 118

4.1 Introduction 118

4.2 Development of Mathematical Model 119

4.2.1 Equations of Motion 121

4.2.2 Flow Equations 123

4.2.3 Pressure Equations 130

4.3 Dynamic Characteristics of Tunable Damper 131

4.4 Vibration Isolation Performance 146

4.5 Shock Isolation Performance 157

4.6 Summary 164

TABLE OF CONTENTS (Continued)

		Page
CHAPTER 5	RIDE DYNAMIC ANALYSIS OF ROAD VEHICLES EMPLOYING TUNABLE PASSIVE SUSPENSION	166
5.1	Introduction	166
5.2	Development of Vehicle Models	167
5.2.1	A Quarter Vehicle Model	168
5.2.2	An In-plane Vehicle Model	170
5.3	Deterministic Analysis of Quarter Vehicle Model	172
5.3.1	Vibration Transmissibility Characteristics	174
5.3.2	Transient Response Characteristics	180
5.4	Development of A Generalized Discrete Harmonic Linearization Technique for Stochastic Analysis of Nonlinear Vehicle Models	187
5.4.1	Principle of Energy Similarity of Dynamic Elements	189
5.4.2	Computation of Equivalent Linear Coefficients	191
5.4.3	Random Response Analysis	199
5.5	Stochastic Analysis of In-plane Vehicle Model	203
5.5.1	Random Road Excitation	203
5.5.2	Dynamic Analysis of In-plane Vehicle Model	208
5.6	Summary	220
CHAPTER 6	ANALYSIS OF AN INTERCONNECTED SUSPENSION WITH TUNABLE DAMPING CONTROL	222
6.1	Introduction	222
6.2	Development of Roll Plane Vehicle Model	224
6.3	Modeling of Independent Hydro-pneumatic Suspension	230

TABLE OF CONTENTS (Continued) Page

6.3.1 Static Equilibrium Equations 230

6.3.2 Fluid Flow Equations 233

6.3.3 Pressure Equations 234

6.3.4 Dynamic Forces of Independent Suspension . . 235

6.4 Modeling of Interconnected Hydro-pneumatic Suspension . . . 236

6.4.1 Static Equilibrium Equations 238

6.4.2 Fluid Flow Equations 241

6.4.3 Pressure Equations 244

6.4.4 Dynamic Forces of Interconnected Suspension 247

6.5 Modeling of Tunable Interconnected Hydro-pneumatic Suspension 249

6.5.1 Fluid Flow Equations 251

6.5.2 Pressure Equations 257

6.5.3 Dynamic Forces of Tunable Interconnected Suspension . 259

6.5.4 Equations of Motion of Valve Spools 259

6.6 Analysis of Vehicle Roll During Steady Turning . 261

6.6.1 External Roll Moments 261

6.6.2 Roll Response of Vehicle Model 263

6.7 Dynamic Ride Performance Evaluation 273

6.7.1 Transient Response Characteristics 273

6.7.2 Frequency Response Characteristics 287

6.8 Summary 305

TABLE OF CONTENTS (Continued) Page

CHAPTER 7 CONCLUSIONS AND RECOMMENDATIONS 307

7.1 General 307

7.2 Highlights of the Investigation 308

7.2.1 Vibration Isolation Performance of Electro-magnetic Active Control Systems Including the Influence of Force Generator Dynamics 309

7.2.2 Concept of Tunable Pressure Limiting Modulation . . . 309

7.2.3 Significance of Fluid Compliance and Valve Dynamics . . . 311

7.2.4 Development of Generalized Discrete Harmonic Linearization Technique 312

7.2.5 Development of Tunable Interconnected Hydro-pneumatic Vehicle Suspension . . . 313

7.3 Conclusions 314

7.4 Recommendations for Future Work 316

REFERENCES 319

LIST OF FIGURES

FIGURE		Page
2.1	A schematic of SDOF hybrid active vibration isolation system	35
2.2	An electro-magnetic active force generator model	35
2.3	Block diagram representation of hybrid active vibration control system	41
2.4	Vibration transmissibility of hybrid active system employing absolute position feedback (ζ=0.3)	46
2.5	Vibration transmissibility of hybrid active system employing absolute velocity feedback (ζ=0.3)	46
2.6	Vibration transmissibility of hybrid active system employing absolute acceleration feedback (ζ=0.3)	48
2.7	Vibration transmissibility of hybrid active system employing relative position control (ζ=0.3)	48
2.8	Vibration transmissibility of hybrid active system employing relative velocity control (ζ=0.3)	50
2.9	Vibration transmissibility of hybrid active system employing relative acceleration control (ζ=0.3)	50
2.10	Vibration transmissibility of hybrid active system employing absolute velocity and relative position control (ζ=0.1, G_4/k=1.)	53
2.11	Vibration transmissibility of hybrid active system employing absolute velocity and relative position control (ζ=0.1, ζ_x=0.7)	53
2.12	Vibration transmissibility of hybrid active system employing absolute velocity and acceleration control (ζ=0.1, ζ_x=0.7)	55
2.13	Vibration transmissibility of hybrid active system employing absolute velocity, acceleration and relative position control (ζ=0.1, ζ_x=0.7, G_3/m=1.0)	55
2.14	Vibration transmissibility of hybrid active system employing absolute position, velocity and acceleration control (ζ=0.1, ζ_x=0.7, G_1/k=1.0)	58

LIST OF FIGURES (Continued)

FIGURE		Page
2.15	Vibration transmissibility of hybrid active system employing absolute position, velocity and acceleration control (ζ=0.1, ζ_x=0.7, G_3/m=1.0)	58
2.16	Vibration transmissibility of hybrid active system employing absolute position, velocity and relative position control (ζ=0.1, ζ_x=1.0, G_1/k=0.5)	61
2.17	Vibration transmissibility of hybrid active system employing absolute position, velocity and relative position control (ζ=0.1, ζ_x=1.0, G_4/k=-0.5)	61
3.1	Model representation of a SDOF vibration isolation system with (a) fixed damping, and (b) variable damping	67
3.2	Schematic of a passive hydraulic damper	67
3.3	Schematic of a tunable pressure limited hydraulic damper with two relief valves	78
3.4	Pressure differential characteristics of a tunable pressure limited damper with respect to relative velocity	82
3.5	Damping characteristics of a tunable pressure limited damper with respect to relative velocity	83
3.6	Pressure differential characteristics of a tunable pressure limited damper system with respect to excitation frequency	85
3.7	Damping characteristics of a tunable pressure limited damper system with respect to excitation frequency	85
3.8	Comparison of steady state acceleration response of mass with tunable damper, and 'on-off' dampers I and II, at ω/ω_n=1	89
3.9	Steady state acceleration response of mass with semi-active 'on-off' damper I, at ω/ω_n=3	91
3.10	Steady state acceleration response of mass with semi-active 'on-off' damper II, at ω/ω_n=3	92
3.11	Steady state acceleration response of mass with tunable pressure limited damper, at ω/ω_n=3	93
3.12	Displacement transmissibility of vibration isolation system employing tunable damper and semi-active 'on-off' dampers	96

LIST OF FIGURES (Continued)

FIGURE		Page
3.13	Velocity transmissibility of vibration isolation system employing tunable and semi-active 'on-off' dampers	97
3.14	Displacement transmissibility of vibration isolation system employing tunable damper with various values of tuning factor	99
3.15	Velocity transmissibility of vibration isolation system employing tunable damper with various values of tuning factor	100
3.16	Acceleration transmissibility of vibration isolation system employing tunable damper with various values of tuning factor	101
3.17	Displacement transmissibility of vibration isolation system employing tunable damper with various values of tuning factor	102
3.18	Displacement response of mass with tunable, semi-active 'on-off' and fixed orifice dampers to rounded step input (η=10)	105
3.19	Velocity response of mass with tunable, semi-active 'on-off' and fixed orifice dampers to rounded step input (η=10)	106
3.20	Acceleration response of mass with tunable, semi-active 'on-off' and fixed orifice dampers to rounded step input (η=10)	107
3.21	Relative displacement response of system employing tunable, semi-active 'on-off' and fixed orifice dampers to rounded step input (η=10)	108
3.22	Displacement response of mass employing tunable damper for various values of tuning factor to rounded step input (η=10)	110
3.23	Velocity response of mass employing tunable damper for various values of tuning factor to rounded step input (η=10)	111
3.24	SDR response of mass employing tunable, semi-active 'on-off' and fixed orifice dampers to rounded step input	113
3.25	SVR response of mass employing tunable, semi-active 'on-off' and fixed orifice dampers to rounded step input	113

LIST OF FIGURES (Continued)

FIGURE		Page
3.26	SAR response of mass employing tunable, semi-active 'on-off' and fixed orifice dampers to rounded step input	114
3.27	RDR response of system employing tunable, semi-active 'on-off' and fixed orifice dampers to rounded step input	115
4.1	Schematic of vibration isolation system with tunable pressure limited hydraulic damper (a) tunable variable damping system (b) tunable pressure limited damper	120
4.2	Schematic of a port configuration of pressure limiting valve	129
4.3	Force-displacement characteristics of vibration isolation system with fixed orifice and tunable dampers ($\beta_e = 6.9\times10^8$ (Pa), $\omega/\omega_n=2.0$)	135
4.4	Force-displacement characteristics of tunable damper with ideal and higher order models ($\beta =6.9\times10^8$ (Pa)), ($\omega/\omega_n=2.0$)	136
4.5	Pressure differential characteristics of tunable pressure limited damper system with respect to excitation frequency	138
4.6	Damping force-displacement characteristics of tunable damper with various bulk moduli ($\beta_e=6.9\times10^8$ (Pa), $\omega/\omega_n=0.5$)	140
4.7	Damping force-displacement characteristics of tunable damper with various bulk moduli ($\beta_e=6.9\times10^8$ (Pa), $\omega/\omega_n=2.0$)	141
4.8	Damping force-displacement characteristics of tunable damper with various bulk moduli ($\beta_e=6.9\times10^8$ (Pa), $\omega/\omega_n=5.0$)	141
4.9	Force-displacement characteristics of gas-spring component with ideal and higher order models ($\beta =6.9\times10^8$ (Pa)), ($\omega/\omega_n=0.5$)	143
4.10	Force-displacement characteristics of gas-spring component with ideal and higher order models ($\beta =6.9\times10^8$ (Pa)), ($\omega/\omega_n=1.0$)	143
4.11	Force-displacement characteristics of gas-spring component with ideal and higher order models ($\beta =6.9\times10^8$ (Pa)), ($\omega/\omega_n=5.0$)	144
4.12	Total force-displacement characteristics of tunable damper with various bulk moduli ($\beta_e=6.9\times10^8$ (Pa), $\omega/\omega_n=5.0$)	145

LIST OF FIGURES (Continued)

FIGURE		Page
4.13	Transient force of tunable damper with ideal and higher order models (β =6.9x10^8 (Pa)) due to rounded step input (η=10)	147
4.14	Transient force of tunable damper with various bulk moduli (β_e=6.9x10^8 (Pa)) due to rounded step input (η=10)	148
4.15	Displacement transmissibility of vibration isolation system employing fixed orifice and tunable dampers β_e=6.9x10^8 (Pa)	150
4.16	Velocity transmissibility of vibration isolation system employing fixed orifice and tunable dampers β_e=6.9x10^8 (Pa)	150
4.17	Displacement transmissibility of vibration isolation system employing tunable damper with ideal and higher order models (β_e=6.9x10^8 (Pa)), (ν=1)	152
4.18	Acceleration transmissibility of vibration isolation system employing tunable damper with ideal and higher order models (β_e=6.9x10^8 (Pa)), (ν=1)	152
4.19	Relative displacement transmissibility of vibration isolation system employing tunable damper with ideal and higher order models (β_e=6.9x10^8 (Pa)), (ν=1)	153
4.20	Displacement transmissibility of vibration isolation system employing tunable damper with various bulk moduli (β_e=6.9x10^8 (Pa)), (ν=1)	155
4.21	Velocity transmissibility of vibration isolation system employing tunable damper with various bulk moduli (β_e=6.9x10^8 (Pa)), (ν=1)	155
4.22	Velocity transmissibility of vibration isolation system employing tunable damper with various values of tuning factor (β_e=6.9x10^8 (Pa))	156
4.23	Transient displacement response of shock isolation system employing fixed orifice and tunable dampers(β_e=6.9x10^8(Pa))	159
4.24	Transient velocity response of shock isolation system employing fixed orifice and tunable dampers(β_e=6.9x10^8(Pa))	160
4.25	Transient displacement response of shock isolation system employing tunable damper with ideal and higher order models (β_e=6.9x10^8 (Pa)), (ν=1)	161

LIST OF FIGURES (Continued)

FIGURE		Page
4.26	Transient velocity response of shock isolation system employing tunable damper with ideal and higher order models (β_e=6.9x10^8 (Pa)), (ν=1)	161
4.27	Transient displacement response of shock isolation system employing tunable damper with various bulk moduli (β_e=6.9x10^8 (Pa), (ν=1)	162
4.28	Transient displacement response of shock isolation system employing tunable damper with various bulk moduli (larger variation) (β_e=6.9x10^8 (Pa), (ν=1)	162
4.29	Transient velocity response of shock isolation system employing tunable damper with various bulk moduli (β_e=6.9x10^8 (Pa), (ν=1)	163
5.1	Schematic of a quarter vehicle model	169
5.2	Schematic of an in-plane bounce and pitch vehicle model	169
5.3	Velocity transmissibility of sprung mass of quarter vehicle model employing tunable and fixed orifice shock absorbers	175
5.4	Displacement transmissibility of sprung mass of quarter vehicle model employing tunable and fixed orifice shock absorber	178
5.5	Velocity transmissibility of sprung mass of quarter vehicle model employing tunable shock absorber with various values of tuning factor	179
5.6	Representation of a bump road input	181
5.7	Transient displacement response of sprung mass of quarter vehicle model employing tunable and fixed orifice shock absorbers	183
5.8	Transient velocity response of sprung mass of quarter vehicle model employing tunable and fixed orifice shock absorbers	184
5.9	Transient displacement response of unsprung mass of quarter vehicle model employing tunable and fixed orifice shock absorbers	185
5.10	Transient velocity response of sprung mass of quarter vehicle model employing tunable and fixed orifice shock absorbers (v=5 m/s)	186

LIST OF FIGURES (Continued)

FIGURE		Page
5.11	Damping force of a tunable shock absorber	194
5.12	Gas-spring force of a shock absorber	197
5.13	A flow diagram of simulation procedure for random response of nonlinear vehicle models	202
5.14	Displacement PSD of a random road input (v=20 m/s)	207
5.15	Bounce acceleration PSD of vehicle sprung mass with tunable and fixed orifice shock absorbers	210
5.16	Pitch acceleration PSD of vehicle sprung mass with tunable and fixed orifice shock absorbers	211
5.17	Vertical acceleration PSD of front unsprung mass with tunable and fixed orifice shock absorbers	213
5.18	Vertical acceleration PSD of rear unsprung mass with tunable and fixed orifice shock absorbers	214
5.19	Bounce acceleration PSD of vehicle sprung mass with tunable shock absorber for various values of tuning factor	216
5.20	Pitch acceleration PSD of vehicle sprung mass with tunable shock absorber for various values of tuning factor	217
5.21	Bounce acceleration PSD of vehicle sprung mass with fixed fixed orifice and tunable shock absorbers(various ν_f and ν_r)	218
5.22	Pitch acceleration PSD of vehicle sprung mass with fixed fixed orifice and tunable shock absorbers(various ν_f and ν_r)	219
6.1	Representation of roll plane model of a road vehicle	226
6.2	Schematic of hydro-pneumatic shock absorber	231
6.3	Schematic of roll plane model of vehicle employing independent hydro-pneumatic suspension	231
6.4	Schematic of roll plane model of interconnected hydro-pneumatic suspension	237
6.5	Schematic of roll plane model of tunable interconnected hydro-pneumatic suspension (a) Tunable interconnected Suspension (b) Pressure relief valve	250
6.6	External roll moments acting upon sprung mass	262

LIST OF FIGURES (Continued)

FIGURE		Page
6.7	A rounded step overturning moment acting on vehicles during steady turning	262
6.8	Transient roll angle response of sprung mass of vehicle employing independent and interconnected suspensions for a_t=0.5 m/s^2	264
6.9	Transient roll angle velocity response of sprung mass of vehicle employing independent and interconnected suspensions for a_t=0.5 m/s^2	264
6.10	Transient roll angle response of sprung mass of vehicle employing interconnected and tunable interconnected (ν=0.3) suspensions for a_t=1.0 m/s^2	266
6.11	Transient roll angle velocity response of sprung mass of vehicle employing interconnected and tunable interconnected (ν=0.3) suspensions for a_t=1.0 m/s^2	267
6.12	Transient roll angle response of sprung mass of vehicle employing independent, interconnected and tunable interconnected (ν=0.3) suspensions for a_t=1.0 m/s^2	269
6.13	Transient roll angle response of unsprung mass of vehicle employing independent and interconnected suspensions for a_t=0.5 m/s^2	270
6.14	Transient displacement response of sprung mass of of vehicle employing independent and interconnected suspensions for a_t=0.5 m/s^2	272
6.15	Transient displacement response of sprung mass of vehicle employing interconnected and tunable interconnected (ν=0.3) suspensions for a_t=1.0 m/s^2 (a) Displacement road input to right tire, (b) A rounded step displacement input	272
6.16	Schematic of road input to roll plane model of a road vehicle	274
6.17	Transient displacement response of sprung mass of vehicle employing independent, interconnected and tunable interconnected (ν=1) suspensions	277
6.18	Transient velocity response of sprung mass of vehicle employing independent, interconnected and tunable interconnected (ν=1) suspensions	278
6.19	Transient roll angle response of sprung mass of vehicle employing independent, interconnected and tunable interconnected (ν=1) suspensions	279

LIST OF FIGURES (Continued)

FIGURE		Page
6.20	Transient displacement response of sprung mass of vehicle employing interconnected and tunable interconnected (ν=1) suspensions (β_e=6.9x10^8 (Pa))	282
6.21	Transient velocity response of sprung mass of vehicle employing interconnected and tunable interconnected (ν=1) suspensions (β_e=6.9x10^8 (Pa))	283
6.22	Transient roll angle response of sprung mass of vehicle employing interconnected and tunable interconnected (ν=1) suspensions (β_e=6.9x10^8 (Pa))	283
6.23	Transient angle velocity response of sprung mass of vehicle employing interconnected and tunable interconnected (ν=1) suspensions (β_e=6.9x10^8 (Pa))	284
6.24	Transient displacement response of unsprung mass of vehicle employing interconnected and tunable interconnected (ν=1) suspensions (β_e=6.9x10^8 (Pa))	285
6.25	Transient roll angle response of unsprung mass of vehicle employing interconnected and tunable interconnected (ν=1) suspensions (β_e=6.9x10^8 (Pa))	286
6.26	Transient displacement response of sprung mass of vehicle employing interconnected, and high order and ideal tunable interconnected suspensions	288
6.27	Transient velocity response of sprung mass of vehicle employing higher order and ideal tunable interconnected suspensions	289
6.28	Transient roll angle response of sprung mass of vehicle employing higher order and ideal tunable interconnected suspensions	290
6.29	Transient angle velocity response of sprung mass of vehicle employing higher order and ideal tunable interconnected suspensions	290
6.30	Displacement transmissibility of sprung mass of vehicle employing interconnected and tunable interconnected (ν=1) suspensions (β_e=6.9x10^8 (Pa))	292
6.31	Roll angle transmissibility of sprung mass of vehicle employing interconnected and tunable interconnected (ν=1) suspensions (β_e=6.9x10^8 (Pa))	294

LIST OF FIGURES (Continued)

FIGURE		Page
6.32	Displacement transmissibility of unsprung mass of vehicle employing interconnected and tunable interconnected (ν=1) suspensions (β_e=6.9x10^8 (Pa))	296
6.33	Roll angle transmissibility of unsprung mass of vehicle employing interconnected and tunable interconnected (ν=1) suspensions (β_e=6.9x10^8 (Pa))	296
6.34	Displacement transmissibility of sprung mass of vehicle employing interconnected, higher order and ideal tunable interconnected (ν=1.0) suspensions	298
6.35	Roll angle transmissibility of sprung mass of vehicle employing interconnected, higher order and ideal tunable interconnected (ν=1.0) suspensions	298
6.36	Relative displacement transmissibility of right suspension unit with interconnected, higher order and ideal tunable interconnected (ν=1.0) suspensions	299
6.37	Displacement transmissibility of sprung mass of vehicle employing tunable interconnected suspensions (ν=0.7, 1.0 and 1.3)	303
6.38	Roll angle transmissibility of sprung mass of vehicle employing tunable interconnected suspensions (ν=0.7, 1.0 and 1.3)	303
6.39	Relative displacement transmissibility of right suspension unit with tunable interconnected suspensions (ν=0.7, 1.0 and 1.3)	304

LIST OF TABLES

TABLE		Page
3.1	Simulation Parameters of Tunable Pressure Limited Hydraulic Damper System	88
4.1	Simulation Parameters of Tunable Pressure Limited Hydraulic Damper System	132
4.2	Simulation Parameters of Tunable Pressure Limiting Valves	133
5.1	Simulation Parameters of Quarter Vehicle Model	173
5.2	Simulation Parameters of Tunable In-plane Two Axle Vehicle Suspension	204
5.3	Data of Random Road Input	206
6.1	Simulation Parameters of the Roll Plane Vehicle Model	228
6.2	Simulation Parameters of Hydro-pneumatic Suspension	232
6.3	Simulation Parameters of Interconnected Hydro-pneumatic Suspension	239
6.4	Simulation Parameters of Tunable Interconnected Hydro-pneumatic Suspension	252

NOMENCLATURE

a_e	area of relief valve opening (m^2)
a_t	lateral acceleration (m/s^2)
a_r	area of spool end of relief valve (m^2)
a_1, a_2	areas of orifice (m^2)
A	constant time-invariable state matrix
A_{cj}	area of piston face of jth shock absorber (m^2)
A_p	area of the piston on the rad side (m^2)
A_r	rod cross section area of the damper (m^2)
A_1	constant coefficient of generator (m^{-1})
A_2	constant coefficient of magnetic field ($N \cdot m/A^2$)
B_1	constant control matrix
B_2	constant disturbance matrix
c	viscous damping coefficient of passive damper ($N \cdot s/m$)
c_{eq}	local equivalent damping coefficient ($N \cdot s/m$)
c_{rc}, c_{re}	viscous damping coefficients of valves ($N \cdot s/m$)
C	orifice damping coefficient (kg/m)
C_d	orifice discharge coefficient
c_t	damping coefficients of tire ($N \cdot s/m$)
D	inside pipe diameter (m)
DOF	degree of freedom
e	constant e = 2.71828
E	processed energy function ($N \cdot m$)
f	temporal frequency (Hz)
f_a	gas-spring force (N)
f_c	centrifugal force (N)

NOMENCLATURE (Continued)

f_{cp}	control force due to passive elements (N)
f_{ca}	control force due to active element (N)
f_d	damping force due to damper (N)
f_{dc}	total dynamic force due to damper (N)
f_k	restoring force generated by linear spring (N)
f_r	force acting on valve spool (N)
F_0	damper force corresponding to static equilibrium position of the system (N)
g	gravity acceleration (m/s^2)
$G_1, G_2 \ldots G_6$	control gain coefficients
h_1	height of sprung mass center above the ground (m)
h_2	height of sprung mass center with respect to the roll center (m)
[H]	complex frequency response function matrix
i	unit imaginary number = $\sqrt{-1}$
I_a	armature current (A)
I_f	constant field current (A)
I_s	pitch mass moment of inertia of suspension ($kg \cdot m^2$)
I_1	roll mass moment of inertia of suspension ($kg \cdot m^2$)
I_2	roll mass moment of inertia of beam axle assembly ($kg \cdot m^2$)
J	subscript for jth shock absorber
k	stiffness coefficient of linear spring (N/m)
k_r	stiffness coefficient of relief valve (N/m)
k_s	stiffness coefficient of suspension spring (N/m)
k_t	stiffness coefficient of tire (N/m)
k_{eq}	local equivalent stiffness coefficient (N/m)

NOMENCLATURE (Continued)

$k_1, k_2 \ldots k_6$	control gains due to active feedback
K_a	constant coefficient of force = $A_1 A_2 I_f$ (N/A)
ℓ	stroke of hydraulic damper (m), and subscript for jth shock absorber
ℓ_f, ℓ_r, ℓ_t	distances from shock absorbers to sprung mass center, respectively (m)
ℓ_{fr}	vehicle wheelbase (m)
ℓ_{wl}, ℓ_{wr}	distances between tires and center of gravity of the unsprung mass, respectively (m)
ℓ_1	stroke of chamber I of shock absorber (m)
ℓ_2	stroke of chamber II of shock absorber (m)
L	length of pipe (m), and constant armature inductance (H)
L_r	distance between two centers of the port arcs (m)
m	mass of the main body (kg), and number of input variables
m_r	spool mass of relief valve (kg)
m_s	sprung mass of the vehicle (kg)
m_u	unsprung mass of the vehicle (kg)
m_1	sprung mass of the suspension (kg)
m_2	unsprung mass of the beam axle assembly (kg)
n	number of degrees of freedom of the system, and number of orifice on the piston
N	number of discrete excitation frequencies
p_a	initial charge pressure (Pa)
p_{ab}	pressure differential = $(p_a - p_b)$
PSD	power spectral density
p_0	static internal pressure of hydraulic damper (Pa)
p_1	instantaneous pressure in chamber I (Pa)

NOMENCLATURE (Continued)

p_2	instantaneous pressure in chamber II (Pa)
p_3	instantaneous pressure in gas chamber III (Pa)
$(p_{12})_o$	preset pressure limiting value (Pa)
Q_{cy}	volume flow rate through cylinder orifice (m^3/s)
Q_{e1}	volume flow rate due to compliance in chamber I (m^3/s)
Q_{e2}	volume flow rate due to compliance in chamber II (m^3/s)
Q_{m1}	rate of change of fluid volume in chamber I (m^3/s)
Q_{m2}	rate of change of fluid volume in chamber II (m^3/s)
Q_{m3}	rate of change of gas volume in chamber III (m^3/s)
Q_{or}	volume flow rate through orifices (m^3/s)
Q_{re}	volume flow rate through relief valves (m^3/s)
Q_{12}	volume flow rate from chamber I to II (m^3/s)
$Q_{2\ell 1r}$	volume flow rate from chamber II_ℓ to chamber I_r (m^3/s)
$Q_{2r1\ell}$	volume flow rate from chamber II_r to chamber I_ℓ (m^3/s)
Q_{32}	volume flow rate from chamber III to II (m^3/s)
r	radius of the half round bump (m), and subscript for right shock absorber
R	Reynold's number of fluid flow, radius of road curve (m), and constant armature resistance (Ω)
R_r	radius of the port arc (m)
RDR	shock relative displacement ratio
s	Laplace variable
s(f)	temporal spectral density (m^2/hz)
$s_{fr}(f)$	cross-spectral density of road input (m^2/hz)
sgn(·)	sign function = $\begin{cases} +1, & (\cdot) > 0 \\ -1, & (\cdot) < 0 \end{cases}$

NOMENCLATURE (Continued)

$[s_i]$	input power spectral density matrix
$[s_x]$	response power spectral density matrix
$[s_{xi}(f)]$	temporal displacement spectral density matrix of road excitation
$s(\mu)$	spatial spectral density of road roughness (m^3/cycle)
$s,\mu_0)$	roughness coefficient and amplitude of the spectral density at reference spatial frequency μ_0 (m^3/cycle)
SAR	shock acceleration ratio
SDR	shock displacement ratio
SVR	shock velocity ratio
t	time (s)
$T_{\iota\phi}$	moment due to lateral displacement of the sprung mass center by means of roll motion (N·m)
$T_{p\phi}$	primary overturning moment due to lateral acceleration during curve maneuver (N·m)
$T_{s\phi}$	total external moment acting on sprung mass (N·m)
T_r	vibration transmissibility
u	instantaneous coordinate of the vehicle (m), and control law of the system
u_0	initial position of vehicle away from the center (m)
v	forward speed of vehicle (m/s)
V_a	initial volume of gas chamber III (m^3)
V_{ro}	equivalent volume due to connecting pipe (m^3)
V_0	static volume of gas chamber III (m^3)
V_1	instantaneous volume of chamber I (m^3)
V_2	instantaneous volume of chamber II (m^3)

NOMENCLATURE (Continued)

V_3	instantaneous volume of gas chamber III (m^3)
$v(t)$	input control voltage of active system (V)
w	excitation input to the active system
w_1, w_2	constants characterizing road waviness
W_j	static load transferred on jth shock absorber (N)
W_ℓ, W_r	static loads on left and right shock absorbers (N)
x	vertical displacement of sprung mass (m)
x_1	base input displacement (m)
x_s	bounce displacement of sprung mass (m)
x_u	vertical displacement of unsprung mass (m)
x_1, x_2	bounce displacements of front and rear unsprung masses, respectively (m)
X_1	amplitude of base excitation (m)
X_{max}	maximum value of the step displacement (m)
X_{st}	static deflection of damper (m)
X	state variable vector
y_c, y_e	coordinates characterizing displacements of compression and extension spools, respectively (m)
y_ℓ, y_r	coordinates characterizing displacements of left and right spools, respectively (m)
Y_0	preset displacement of relief valve (m)
z	relative displacement of the system = $x - x_1$ (m)
$z_{1\ell}$, z_{1r}	relative displacements of the left and right tires, respectively (m)
z_ℓ, z_r	relative displacements of the left and right suspension units, respectively (m)

NOMENCLATURE (Continued)

z_1, z_2	front and rear relative displacements of suspension, respectively (m)
Z	amplitude of displacement across the element (m)
α	damping force coefficient (m^2)
β	damping parameter
β_c	bulk modulus of container (Pa)
β_e	effective bulk modulus (Pa)
$\beta_{eq}\|_{\omega=\omega n}$	equivalent damping parameter at resonance
β_ι	bulk modulus of liquid fluid (Pa)
β_o	damping parameter of orifice damper
γ	polytropic exponent, $1 \leq \gamma \leq 1.4$
ε	counter electromotive force (emf) (V), and force reduction coefficient when the orifice is modulated to its maximum opening
ζ	viscous damping ratio
ζ_x, ζ_z	damping ratios due to active vibration control
η	shock severity parameter
θ_s	coordinate of pitch angle of sprung mass (rad)
μ	absolute viscosity of fluid ($N \cdot s/m^2$), and spatial frequency (cycles/m)
μ_x, μ_z	mass ratios due to active vibration control
μ_0	reference spatial frequency = $1/2\pi$ (cycles/m)
ν	tuning factor of pressure limited damper
ν_x, ν_z	stiffness ratio due to active vibration control
ρ	mass density of fluid (kg/m^3)

NOMENCLATURE (Continued)

τ	time delay between the front and rear wheels (s), and time constant of force generator system = L / R (s)
ϕ	magnetic flux (Wb)
ϕ_s, ϕ_u	general coordinates characterizing roll angles of the sprung and unsprung masses, respectively (rad)
τ'	time constant ratio = $\tau\ \omega_n$
ω	angular frequency (rad/s)
ω_n	angular natural frequency of system (rad/s)
ω_j	discrete excitation frequency (rad/s)
$(\dot{\ }), (\ddot{\ })$	first and second derivatives with respect to time
$[\cdot]^{-1}$	inverse matrix of $[\cdot]$
$(^*)$	complex conjugate operator
$\lvert(\cdot)\rvert$	magnitude of $(\cdot)$

CHAPTER 1

INTRODUCTION AND LITERATURE REVIEW

1.1 General

Design of an effective shock and vibration isolation system to protect mechanical systems or the human body from shock and vibration environments involves the selection of appropriate spring and damping mechanisms. Specifically, the damping characteristics play a major role in shaping the shock and vibration response performance of the isolation system. Shock and vibration isolation can, in general, be realized by passive, active or semi-active vibration control elements.

The restoring and dissipative forces, in a passive vibration control system, are generated purely due to the relative deflection and relative velocity, across the passive elements, such as springs and dampers of various types. Passive vibration isolation systems thus do not require any external power source and offer simple, inexpensive and reliable means to achieve shock and vibration control. However, passive vibration isolation systems possess inherent performance limitations due to their fixed parameters, such as damping. It has been established that vibration isolation systems with variable parameters can considerably improve vibration attenuation performance.

The control forces, in an active vibration control system, are generated via active force generators, and change with variations in excitation and response characteristics. Active vibration control systems can supply energy, when required, as well as dissipate energy, whereas passive systems can only dissipate or temporarily store energy. Investigations carried out during the past decade have shown that desired damping and restoring forces can be achieved via appropriate

feedback control schemes leading to improved vibration isolation performance. The major disadvantages of active vibration control systems include the requirement of an external energy source and a sophisticated control system with a number of sensors. The implementation of such active vibration isolation systems is thus severely limited due to the increased cost, complexity and weight. However, active vibration isolation systems are used where the performance benefits outweigh these limitations.

Semi-active vibration isolation systems generate damping forces passively, while the damping parameters are modulated using an active control system. Semi-active vibration control systems offer an excellent compromise between the performance benefits of active systems and the simplicity of passive vibration isolation systems. Semi-active vibration control systems require only low electrical power for necessary signal processing and can provide improved shock and vibration isolation performance as compared with that of passive ones. Although the hardware requirements of a semi-active vibration isolation system are considerably simpler than those of an active one, the general use of semi-active vibration isolation systems still remains limited due to the requirement of comprehensive instrumentation and control devices.

Vehicle suspensions invariably employ either linear or nonlinear passive vibration isolators to protect the structure, cargo and human occupants from shock and vibration inputs arising from tire-terrain interactive dynamics. High power and mobility requirements of modern vehicles necessitate the suspension design to achieve improved ride comfort and driver safety. In view of the performance limitations of passive vehicle suspensions, numerous semi-active and active vibration

isolation systems have been proposed to achieve satisfactory vehicle ride.

The objective of this dissertation is to investigate passive, active and semi-active vibration control systems in order to achieve an improved shock and vibration isolation performance for mechanical systems specifically for vehicle systems. In view of the complex hardware requirements of semi-active and active vibration control systems, the primary focus of the study is directed towards tunable passive vibration control systems to achieve improved performance. Methodologies for modeling and techniques for effective analysis of the system are presented and employed.

1.2 Review of Previous Investigations

Literature in shock and vibration control and vehicle suspension design constitutes a variety of investigations concerning the development of improved passive elements, advanced active and semi-active control systems, and modified suspensions. A review of the relevant literature is presented in the following subsections in order to develop the objective of this dissertation.

1.2.1 Passive Vibration Isolation Systems and Hydraulic Dampers

Mechanical vibration energy is dissipated due to the damping within a dynamic system. Dampers are, therefore, critical components in all passive mechanical vibration control systems [1]. Passive hydraulic dampers of various types are widely employed in shock and vibration isolation systems [2, 3, 4], specifically in vehicle suspensions such as in automobiles, motorcycles and aircraft landing gear [5, 6, 7].

Shock and vibration isolation performance characteristics of

passive isolators employing linear or nonlinear springs and dampers have been studied extensively [8]. Various forms of nonlinear damping were investigated in view of their vibration isolation characteristics by Ruzicka and Derby [9]. A single-degree-of-freedom model of a vibration isolation system employing nonlinear dampers with the relative velocity exponent varying between 0.5 and 5 was analyzed to determine vibration transmissibility. The study concluded that the preferred damping nonlinearity and damping value in a vibration isolation system depend on the vibration excitation characteristics and are based on a compromise between resonant vibration control and high-frequency vibration isolation. The shock isolation performance of a passive isolator with linear spring and quadratic law damper was investigated by Hundal [10]. The study proposed a closed form solution of the equation for the isolator and the design of an optimal quadratic law damper.

Shock absorbers used in passive vehicle suspensions have been extensively investigated via analytical and experimental studies. Karadayi and Masada [11] developed a nonlinear analytical model of a shock absorber based on experimental results. The shock absorber model incorporated various damping nonlinearities including asymmetric damping, dry friction, hysteresis due to fluid compressibility and backlash. A shock absorber model including coulomb friction was investigated by Mercer and Rees [12]. The study minimized both the transmitted shock and relative displacement by adapting a variable friction force to achieve an optimum shock isolator. The impact characteristics of a shock absorber used in freight cars was studied by Freudenstein [13]. The analysis discussed the influence of masses, impact speed, closure time, Coulomb damping, and compliance distribution

within the lading, on the shock isolation performance. Various optimization techniques have been implemented to determine optimal parameters of shock and vibration isolation systems with respect to specified input excitation and performance criteria [14, 15].

Analytical and experimental studies have established that the damping characteristics of shock absorbers are strongly influenced by the operating temperature, fluid compressibility and entrained air [4, 7]. Air spring suspensions with separated gas chambers have been proposed in recent years [16]. Moulton and Best [17] proposed the design of a hydro-gas suspension to achieve improved ride and handling performance of vehicles. Chu and Li [18] developed an analytical model of the hydro-gas suspension system to evaluate the vibration isolation performance. The analysis of the basic characteristics of the hydro-gas suspension indicates that the stiffness of the suspension varies with respect to the system mass and the restoring force is nonlinear and asymmetric. The nonlinearities due to orifice damping and gas spring of a hydro-pneumatic suspension were discussed by Lin and Xi [19]. Their study further analyzed the performance characteristics of the hydro-pneumatic suspension for stochastic input excitations. Liquid springs have also been proposed and analyzed to achieve improved shock isolation performance [20].

The magnitude of the damping force developed due to orifice flows within a shock absorber is primarily related to the square of the relative velocity across the shock absorber [10]. Here the damping force increases rapidly with the relative velocity response and yields poor vibration isolation performance. Certain valving mechanisms are therefore employed within shock absorbers to limit the magnitude of the

orifice damping force [4, 6]. Pressure relief valves are often used to limit the magnitude of the hydraulic damping force corresponding to high relative velocity response. The pressure relief valves are preset by the manufacturers to achieve desired damping characteristics. The spring rate of the relief valves is selected primarily to achieve high damping force around the resonant frequencies. Such fixed shock absorbers do not provide effective limiting of the damping force corresponding to high relative velocity response [4]. The shock absorbers with relief valves are often designed to yield asymmetric damping characteristics during compression and extension strokes. Burns and Sachs [21] developed a simple model of an asymmetric shock absorber and presented the influence of asymmetric damping on the ride comfort in terms of vibration isolation performance.

Van Vliet [22] developed an analytical model of a hydraulic shock absorber with a fixed relief valve. The relief valve is designed to open only during compression to limit the magnitude of maximum damping force. An unsymmetrical damping force and displacement relationship was established by computer simulation and test results.

In order to overcome the inherent performance limitations of a passive hydraulic damper with fixed damping characteristics due to constant orifice area, a number of damping mechanisms with variable orifice areas have been proposed. Asami et al [23] studied the damping characteristics of a hydraulic damper by varying the orifice area in the piston. A two stage variable area orifice hydraulic damper used in an impact absorber has been proposed and analyzed by Hundal [24].

The effects of fluid compressibility on the damping characteristics of the hydraulic damper and thus the shock and vibration isolation

performance of the isolator have been investigated by many researchers [24, 25, 26]. The significant influence of the fluid compressibility on the performance characteristics of landing gears was presented by Wahi [25] through test results. Shock absorber models considering compressible fluid were developed and analyzed by Wahi [25] and Mayne [26]. The shock isolation performance with the influence of compressibility of the fluid was presented via numerical analysis of a single fluid chamber impact absorber model. Hundal [24] also presented a parametric study to illustrate the influence of bulk modulus of the fluid on the performance characteristics of the two stage variable orifice impact absorbers. The simulation results indicated that the performance of a finely tuned variable area shock absorber is degraded if the fluid compressibility is considered.

1.2.2 Active Vibration Isolation Systems

Developments in control engineering provided a new approach to predict dynamic behavior of physical systems [27, 28]. Dynamic systems with adjustable dynamic characteristics can be realized using feedback control techniques [29]. It has been demonstrated that vibration isolation systems with parameters that change with excitation and response characteristics provide improved shock and vibration isolation performance [30, 31, 32].

Numerous active vibration isolation systems employing various force generators and control schemes have been proposed and investigated in recent years. Cavanaugh [33] first proposed a servo controlled pneumatic vibration isolation system. The active control force generated was proportional to the integral of the relative displacement response. The analysis of the single degree of freedom linear active vibration

isolation system demonstrated an improved vibration transmissibility. Hullender et al. [34] investigated the vibration control of vehicle systems using an active pneumatic suspension. The classical PID control scheme was employed in the proposed active suspension. The study concluded that the heave acceleration of the vehicle with active suspension could be reduced to only 38 percent of the heave acceleration response of optimally damped passive fluid suspension. A secondary lateral suspension employing active controlled pneumatic actuators has been investigated by Cho and Hedrick [35]. The active pneumatic suspension employed the acceleration and velocity response in a feedback control scheme. The comparison of experimental and analytical results revealed the significant influence of dynamics of the active actuator system. This study concluded that the car body lateral acceleration can be reduced by 46 percent with a power requirement of 5.7 kW. Iwata and Nakano [36] discussed optimal vibration control of active pneumatic suspensions by using a linear optimal control technique based on full state variable feedback.

Various active vibration isolation systems using servo-controlled hydraulic actuators have been proposed and investigated by Sutton [37], and Dominy and Bulman [38], respectively. The hydraulic actuator, energized through a fluid pump, provides the active force controlled via a hydraulic servo-valve, modulated through a linkage feedback mechanism. The analysis of a suspension using such active hydraulic actuators demonstrated [38] that the active system is able to minimize the sprung mass response to bump input excitations while maintaining a constant ride attitude.

Active electro-hydraulic vibration isolation systems employing

various control schemes have been proposed and analyzed by many researchers [39, 40, 41]. Electrically controlled servo-valves are employed to modulate the active control forces generated by the hydraulic actuator. Calcaterra et al. [39] investigated an active electro-hydraulic suspension employing a PID control scheme. Schubert and Ruzicka [40] proposed and analyzed an electro-hydraulic vibration isolation system using a feedback control scheme based on the absolute acceleration and relative displacement response variables, while the electro-hydraulic servo-valve is modeled as a second order subsystem. The theoretical and experimental results indicated that static deflection as well as vibration isolation performance of such an active control system can be improved over a broad-band excitation frequency range. Tanaka and Kikushima [41] proposed an electro-hydraulic vibration isolation system employing a force feedforward control to isolate the forces transmitted to the ground for a forging hammer machine. Dynamic compensators were designed to obtain adequate suppression of the transmitted force.

Seto [42] proposed and investigated an eddy-current force generator for active vibration control. The active force generated due to the controlled magnetic field is a function of the relative velocity sensed by the vibration control system. The analytical and experimental studies of a long overhung ram in a machine tool revealed that vibration transmitted during metal cutting processes can be suppressed considerably by employing the active eddy-current force generator. An active vibration control system employing an electromagnetic force generator was proposed and investigated by Ellis and Mote [43], for control of transverse vibrations of a circular saw, where the control

force generated was proportional to the relative velocity response. Nikolajsen et al [44] investigated an electromagnetic vibration control system for transmission systems, based on relative velocity feedback and showed that the shaft vibrations are damped significantly.

A concept of reliable fail-safe vibration control, comprising of active and passive force generator elements, was introduced by Guntur and Sankar [45]. Implementation of both active and passive elements in active vibration control systems has been proposed by other researchers [33, 35, 41]. Various active control schemes, including feedback and feedforward controls, were presented to demonstrate the potentials of such active vibration control systems.

The vibration isolation performance of active vibration control systems is often evaluated for ideal elements [32-45], while the dynamic characteristics of the active force generators are neglected. Buzan and Hedrick [46] modeled a pneumatic actuator in an active vibration control system as a dynamic sub-system and investigated the influence of dynamics of the pneumatic actuator on the vibration isolation performance. The study revealed that the actuator dynamics influences the suspension performance considerably.

Some control laws based on feedback of response variables have been proposed not only to obtain the desired performance characteristics, but also to realize a practical control scheme, and to compensate for the influence of dynamics of force generators. Thompson [47] investigated a suboptimal linear active suspension which considered only some variables in a partial state feedback control, instead of the state feedback. Klinger and Calzado [48] proposed a control scheme which took into account the compensation for dynamics of the force actuator, in an

active pneumatic suspension. It seems necessary, therefore, to investigate systematically the basic vibration isolation characteristics of various feedback variables, and the influence of the dynamics of the entire control system, including force generator, signal processing system and power amplifier, on the performance of active vibration isolation systems.

1.2.3 Vibration Isolation Systems With Semi-active Or Sequential Damping

In a vibration isolation system, the damping force tends to reduce the magnitude of mass acceleration only during a part of the vibration cycle and to increase it during the remaining part of the cycle. A number of sequential damping mechanisms have been proposed so that a high damping force is provided during that part of the cycle when it acts to reduce the magnitude of mass acceleration and a minimum damping force is generated during the remaining vibration cycle [49, 57]. Such a sequential damping is realized by modulating the orifice areas in a hydraulic damper using semi-active control.

Karnopp et al. [49] first proposed the concept of a semi-active vibration isolation system using a force generator based on 'skyhook' control. The damping force, proportional to absolute velocity response of the mass, is generated whenever the absolute and the relative velocities carry the same sign. Although hardware implementation of such a system is considerably simpler and less costly than that of an active vibration isolation system, the realization of skyhook control is still significantly complex.

A number of semi-active vibration isolators employing 'on-off' or sequential damping have been proposed and investigated in an attempt to further simplify the hardware implementations. Roley [50] and Margolis

et al [51] investigated some semi-active vibration isolation systems employing a force generator which generates a damping force as a function of the relative velocity. The passively generated damping force is modulated by using the control scheme proposed by Karnopp et al. [49]. The damping force is assumed to be proportional to relative velocity when the absolute and the relative velocities carry the same sign. The damping force is assumed to be zero when the sign of the absolute velocity response of the mass differs from that of the relative velocity response. Krasnicki [52] conducted experimental studies on a prototype semi-active 'on-off' damper and presented a comparison of analytical and experimental performance characteristics for harmonic excitations. The experimental study illustrated that the vibration transmissibility of the 'on-off' damper is comparable with that of the 'skyhook' semi-active damper proposed by Karnopp et al [49] in the low and resonant frequency regions. In the higher frequency region, however, the semi-active 'on-off' damper yields a poor vibration isolation performance.

The semi-active 'on-off' control scheme has been used in various applications by many investigators, such as multi-mode structures [53], tractor cabs [50], and military ground vehicles [54]. All the above studies clearly demonstrate that vibration control schemes with semi-active 'on-off' damping provide considerably superior vibration isolation performance to that provided by passive vibration control systems. However, measurement of absolute velocity of the mass poses considerable complexities, specifically at low excitation frequencies. Margolis [55], and Sharp and Hassan [56], proposed an absolute velocity and acceleration feedback control scheme to compensate for the error

caused by measurement of absolute velocity.

In view of the problems associated with the acquisition of absolute velocity at low excitation frequencies, Rakheja et al. [57] and Sireteanu [58] proposed a semi-active 'on-off' damping mechanism based upon directly measurable variables. The proposed damper generates a high damping force proportional to the square of the relative velocity response, when the sign of the relative velocity opposes that of the relative displacement. The damping force is reduced to a low value by modulating the orifice to its maximum opening, when the relative velocity and displacement carry the same sign. Sireteanu [58] analyzed the random response characteristics of vehicle suspensions employing the above sequential damping. The studies revealed that the vibration isolation performance of the sequential dampers is almost identical to that of the 'on-off' dampers proposed by Karnopp et al. [49] and Margolis et al. [51].

Semi-active 'on-off' controls yield large magnitude of jerk (rate of change of acceleration) around the discontinuity between the 'on' and 'off' states, similar to the bang-bang control [59]. Moreover, semi-active vibration isolation systems require a comprehensive instrumentation package and control devices. Thus the cost, complexities, and instabilities associated with chatter and drifting phenomena of semi-active 'on-off' control may still be the major obstacles for its general application.

Snowdon [60] proposed various concepts of dual-phase damping in vibration isolation systems and investigated their shock isolation performance. The damping ratio takes one of two constant values if the relative velocity of the dual-phase damper is either small or large. For

intermediate velocities, there is a linear transition from one level of the damping ratio to the other. Venkatesan and Kirshnan [61] analyzed the harmonic response of a vibration isolation system with a dual-phase damper. The analysis demonstrated that the absolute vibration transmissibility of the dual-phase damper system can be minimized by selecting appropriate dual-phase damping parameters. Guntur and Sankar [62] investigated the shock isolation characteristics of several dual-phase mechanisms. Venkatesan and Krishnan [63] proposed and investigated an application of the dual-phase damper in a landing gear during the touch-down of airplanes.

1.2.4 Interconnected Hydro-pneumatic Suspensions

Ride, handling and control of ground vehicles pose conflicting requirements on vehicle suspensions. A softer suspension provide better ride but poor stability and directional control. Improved handling performance requires a suspension that is neither stiff nor too soft. Vehicle suspensions are thus designed to achieve a compromise among the ride, handling and control performance requirements of the vehicles. However, a larger weighting is given to the control performance to ensure ground vehicle stability.

Concepts in interconnected vehicle suspensions have been proposed to achieve improved ride as well as handling and stability of road vehicles [31, 37]. Hydro-pneumatic vehicle suspensions with rising rate stiffness characteristics and almost constant natural frequency offer considerable potential for ride amplitude control, self-leveling, anti-roll and anti-pitch control via the interconnections [16, 18, 64].

A number of interconnected hydro-pneumatic suspensions have been proposed and investigated in an attempt to overcome the limitations of

the conventional passive suspensions and to improve the roll stability as well as ride performance of road vehicles. Felez and Vera [65] investigated interconnected passive hydro-pneumatic suspension systems for ride and roll response characteristics. The study demonstrated an improved anti-roll performance of the interconnected suspensions. Moulton and Best [66] proposed and analyzed an interconnected suspension system with rubber springs. Their investigation demonstrated an improved load distribution control of the vehicle. Meller [67] proposed and investigated an interconnected hydro-pneumatic suspension with a self-energizing pump system. The load dependent internal pump is energized by the relative movement between the axle and the vehicle body. The hydro-pneumatic leveling characteristics are hence realized via this suspension. Tanahashi et al. [68] proposed and investigated an interconnected and feedback modulated hydro-pneumatic suspension. The interconnected suspension provides a variable damping force with three levels by an electronic modulation system according to the vehicle running and road conditions. The theoretical and experimental studies demonstrated both improved ride comfort and handling characteristics of the vehicle.

Various interconnected suspensions with active and semi-active controls have been proposed and investigated by many researchers [69, 71]. Horton and Crolla [69] investigated interconnected suspensions incorporating semi-active feedback mechanisms. A mechanical linkage mechanism is used to control the hydraulic servo valve and thus the stiffness and damping characteristics of the suspension. An active suspension with interconnection between hydro-pneumatic shock absorbers was investigated by Crolla et al. [70]. The simulation study indicated

an improved ride comfort and body attitude control of the vehicle. Sutton [37] configured an active interconnected suspension using active hydraulic actuators. The results of the experimental simulation in the time domain indicated the potential advantages of the active interconnected suspension. Howard [71] investigated an active interconnected suspension for a three dimensional model of vehicle. The improved self-leveling, anti-roll and anti-pitch behaviors of the suspension were presented through computer simulation studies. Felez and Vera [65] also investigated a hydro-pneumatic suspension with active connection control. A three position servo valve was employed to control the fluid connection passages of the suspension. The study observed the hunting type of instability problem associated with the interconnected active suspension.

Studies conducted on interconnected vehicle suspensions have established that the vehicle roll stability in general can be improved considerably. Although active and semi-active interconnected suspensions provide superior shock and vibration isolation as well as improved road holding ability, the implementation of such systems has been limited due to the associated high costs, complexities and poor stability [37, 65].

1.2.5 Analytical Techniques for Nonlinear Stochastic Systems

Since linear systems are much easier and economical to analyze than nonlinear systems, nonlinear mechanical systems are often analyzed by assuming linear characteristics. Vehicle suspension systems often exhibit nonlinearities associated with coulomb friction, orifice flows, air springs, leaf springs, etc. Often critical effects of nonlinear suspension thus can not be simulated via linear theory, specifically when the system nonlinearities are strong and the system does not

operate in a small range, as in the cases of coulomb friction and logical state changes. For the analytical models presented in this study, such as hydraulic dampers and tunable pressure limiting mechanisms, the nonlinearities are relatively strong and play dominant roles in their dynamic characteristics [12, 72]. Road surfaces traversed by vehicles are random in nature and the input excitations to vehicles should be described stochastically. Hence, the ride performance of the nonlinear vehicle models should be evaluated by a stochastic approach.

In this section, the available techniques that can be adopted to solve nonlinear dynamic systems subjected to stochastic excitations are reviewed. The major advantages and limitations of these techniques are examined with emphasis on applications to multi-degree-of-freedom vehicle suspensions with nonlinearities associated with orifice damping, air springs and tunable pressure limiting mechanisms, so that a suitable method may be selected for stochastic analysis of the proposed vehicle suspension with tunable dampers.

Various analytical techniques have been developed to predict the response characteristics of nonlinear dynamic systems to random excitations [73-77]. These nonlinear analytical techniques employ various approaches, such as

i) Markov methods,

ii) perturbation methods,

iii) simulation methods, and

iv) equivalent linearization methods.

1.2.5.1 Markov Methods

When the future state of a system response process depends only on

the most recently known state, then it is defined as a Markov process [78]. A Markov random process is completely described in terms of its first and transition probability densities or the statistical moments. Roberts [74] discussed a number of analytical techniques dealing with Markov processes. The response process of a system with Markov process properties can be derived using two approaches:

(i) Fokker-Planck equation and

(ii) moment equation.

Fokker-Planck Equation

The transition probability density function of the response process of nonlinear systems, subject to a white noise (or filtered white noise) excitation, is governed by the Fokker-Planck equation. The required statistics of the response process are then completely defined by its transition density function. Ariaratnam [79] and Caughey [80] derived the Fokker-Planck equation of discrete nonlinear dynamic systems subjected to white random excitation. Ariaratnam [79] analyzed a two-degree-of-freedom suspension with nonlinear springs, and derived closed form solutions for some simple cases with stationary processes. It has been established that the Fokker-Planck equation approach offers the advantage of providing an exact solution for response statistics [73, 81, 82]. However, the complete solution of the equation is available only for a limited class of problems. The dynamic systems with nonlinearities involving velocities and their couplings and non-stationary random processes still remain to be solved.

In view of the difficulty of deriving exact closed form solutions of the Fokker-Planck equation, various approximate methods to solve this kind of parabolic differential equation have been developed, which can

be classified as:

(1) approximate analytical methods, and

(2) approximate numerical methods.

The stochastic averaging methods are a class of approximate analytical methods, in which rapid fluctuations in variable amplitudes and phases are averaged with respect to time to provide simpler equations for slowly varying quantities [83]. Crandall and Zhu [75] discussed various different stochastic averaging methods in order to generate the slowly varying quantities. Although stochastic averaging methods have been extensively applied to some nonlinear random systems, the major limitation of the stochastic averaging method is that it can not account for the effect of strong nonlinearity in restoring force terms [75, 84].

Numerical methods offer an alternative way to solve the Fokker-Planck equation. Since the Fokker-planck equation is essentially a parabolic partial differential equation, it can, in principle, be solved numerically. A finite difference method was proposed by Roberts [85] for solving the Fokker-Planck equation. Langley [86] discussed a finite element method to compute stationary solutions of Fokker-Planck equations and obtained very satisfactory results for a single-degree-of-freedom Duffing oscillator. Effective numerical methods for solving higher dimensional Fokker-Planck equations of multi-degree-of-freedom systems still remain to be developed [76].

The Fokker-Planck equations of dynamic systems with nonlinearities involving velocities, or inertial or damping coupling between the general coordinates, also remain to be solved [87, 88]. Therefore, the Fokker-Planck equation approach is not suitable for nonlinear suspension

systems considered in this dissertation.

Moment Equation

The moment equation approach can yield statistical moments of the response of a nonlinear system subject to random excitations, assuming the response as a Markov process [89]. A set of differential equations for the statistical moments of the response can be derived either from the equations of motion or from the associated Fokker-Planck equations. A set of coupled ordinary differential equations can thus be derived and solved to yield nonlinear response characteristics. The inherent limitation of the moment equation approach is that there are always more unknown moments than the number of equations for nonlinear systems and exact solutions can never be obtained [90].

Approximate solutions to moment equations have been proposed based on the following assumptions [75]:

(a) certain higher order moments can be neglected,

(b) the neglected higher order moments can be related to lower order moments in a certain manner.

Therefore, it is necessary to introduce a closure approximation technique to generate the results. Iyenger and Dash [91] presented a study on random vibration response of nonlinear systems by using the Gaussian closure approximation technique. The Gaussian closure technique relates the higher order moments to lower order moments in the same way that moments of Gaussian processes are related. It has, however, been pointed out by Roberts and Dunne [92] that the Gaussian closure approximations sometimes produce poor, and even completely erroneous, results.

Crandall [89] systematically discussed the Non-Gaussian closure

approximation techniques and pointed out that such methods offer the potentials to improve considerably the accuracy of the results. Various non-Gaussian closure methods have been proposed and tested for special cases [90, 93]. Although good results for some cases, even for some multi-degree-of-freedom nonlinear systems, have been obtained by using these methods, the reliability of the non-Gaussian closure techniques has not yet been proven [75].

It can be seen that both Fokker-Planck equation and moment equation approaches for Markov processes have limitations in applications to the multi-degree-of freedom nonlinear suspension models with nonlinearities associated with orifice damping, air-spring and tunable pressure limiting mechanisms. The Markov methods are, therefore, not suitable for the nonlinear vehicle models proposed in this thesis.

1.2.5.2 Perturbation Methods

In this technique, the magnitude of the nonlinearity in a system is assumed to be controlled by a small perturbation parameter ε. The response of the system is established in terms of a power series in ε. Substituting the power series solution into the original nonlinear equations of motion and equating the coefficients of like powers of the nonlinear parameter, a set of successive linear differential equations are evaluated in terms of the power series of the solution [94].

This classical approach for deterministic nonlinear problems was first applied to stochastic nonlinear vibration problems by Crandall [95]. The statistics of the response solution are evaluated in the same manner as the deterministic response. Various applications of this method have been proposed to analyze stochastic dynamic systems possessing limited amounts of nonlinearities [74]. Chu and Li [18]

analyzed the dynamic characteristics of a nonlinear suspension system employing hydro-pneumatic shock absorbers by using the perturbation method. The influence of the air-spring parameters of the shock absorbers on ride performance was presented. The analytical investigations of various nonlinear stochastic systems have been proposed by Manning [96] and Tung [97].

The perturbation series is usually an asymptotic power series. For small ε higher order perturbation can improve the accuracy of the solution. For large ε, however, the perturbation may worsen the accuracy of the results. The advantages of the perturbation methods include that it is a simple and effective technique for the analysis of systems with weak nonlinearities. Furthermore, the method is not restricted to cases of uncorrelated excitations. The major limitation of this approach is, however, that the stochastic system, in addition to possessing only weak nonlinearities, must contain some finite amount of linear viscous damping so that the solution of the successive linearized equations would be in a bounded form. Since the nonlinear suspension systems, to be investigated in this dissertation, are characterized by strong nonlinearities such as orifice damping, air springs and tunable pressure limiting mechanisms, the perturbation methods are considered inappropriate.

1.2.5.3 Simulation Methods

This approach, also referred to as the Monte Carlo method, can be described by following three steps [75]:

1) generation of a large number of sample functions of the excitation process, with desired statistical properties;
2) computation of the corresponding sample functions of the response

process, based on the dynamic model of the system and a finite number of 'typical' initial conditions;

3) statistically processing the response characteristics to obtain the desired response statistics.

In principle, the approach is very general and applicable to the stationary or nonstationary response of systems of any degree of complexity. However, it requires a large number of representative simulations of the system response yielding an ensemble of state trajectories. The statistics of the response, such as mean, covariance, etc., are then estimated with certain confidence limits. For stationary, ergodic processes the method is simplified due to the fact that temporal averaging needs only one input/output realization of sufficient duration [98].

The simulations can be performed either on a digital computer or an analog computer depending on the way the system is modeled. The excitation process for an analog simulation is obtained from a random signal generator and filters. The white noise excitation for a digital computer simulation, on the other hand, can be generated directly from a sequence of independent random numbers with a normal distribution [99]. For non-white noise excitation a digital filter can be constructed to operate on a white noise and thus to obtain the desired spectrum. If the frequencies are equally spaced, implementation of simulation on a digital computer can be made considerably more efficient by using the FFT algorithm [100]. Various other simulation methods have been discussed by Roberts [75].

The advantages of simulation methods over other methods include the flexibility that it can be readily extended to the case of

multidimensional and multivariate processes [101], and possesses better error diagnostic capability. The major drawback of simulation methods is the computation time and cost. The statistical uncertainty in the response statistics decreases in proportion to $n^{-1/2}$ (n = number of sample excitations), while the cost increases is essentially proportional to n. To gain one additional significant figure in the results requires a hundredfold increase in cost [75]. For this reason, the simulation methods are usually used to provide a basis for assessing the validity and accuracy of other approximate methods when the exact solution is not available. This method is, therefore, not considered appropriate for the analysis of the proposed nonlinear vehicle system.

1.2.5.4 Equivalent Linearization Methods

Well established linear analytical tools provide a powerful and convenient approach to analyze the characteristics of linear stochastic systems. Equivalent linearization methods make use of merit of the linear analytical tools for certain classes of nonlinear systems. The equivalent linearization methods are based on the concept of replacing the nonlinear system by a related linear system according to a specified criterion such that the difference between response characteristics of the two systems is a minimum [102]. Though there are various linearization methods based on different criteria, they can be classified into two approaches according to the domain in which the mathematical model of the system is established:

1) time domain linearization approaches;

2) frequency domain linearization approaches.

In time domain linearization approaches, the following two techniques are available in the analysis of nonlinear stochastic

systems:

(a) Statistical linearization techniques

(b) Piece-wise linearization technique

Statistical Linearization Techniques

Statistical linearization techniques are an extension of the describing function method of Krylov and Bogoliubov in control theory for deterministic excitations [103]. The first development of a suitable equivalent linearization procedure for stochastically excited nonlinear systems was introduced by Caughey [88] and Booton [102]. Here, nonlinear stiffness and damping elements are replaced by optimal linear elements by minimizing the mean square errors between the nonlinear and linear equations. Iwan and Patula [104] presented various minimization criteria for the statistical linearization technique and discussed their relative merits and demerits.

The statistical linearization technique is not limited by the restrictions on excitation and dissipation often encountered in other approximation approaches. Therefore, it can been applied to a broad class of vibration problems with many degrees-of-freedom. If the excitation is Gaussian distributed, the procedure is simple to implement. Roberts [75] discussed the statistical linearization method and its applications, and pointed out that the errors in mean square response remain quite modest even for large nonlinearities. However, difficulties are encountered when the nonlinear characteristics are discontinuous [105], as in Coulomb friction and logical state control. Since the proposed nonlinear models of vehicle systems have logical state control due to a tunable pressure limiting mechanism, the statistical linearization method is not applicable to the vehicle models

discussed in this dissertation.

Piece-wise Linearization Technique

This technique is used when the nonlinearities of a system vary with time. Here, the nonlinear system is replaced by a set of equivalent linear representations in discrete time. The piece-wise linear representation of the system model within each time interval is predetermined by using deterministic approaches. The stochastic response is established by evaluating response of the piece-wise linear model to random excitations, within each time interval. Kumar et al. [106] investigated the stochastic response of gears by using the piece-wise linearization technique. The nonlinear time variant model of the gear at different contact positions is expressed by an equivalent piece-wise time discrete model in terms of state transition matrix. This technique is limited to the cases where the nonlinearities of systems are only functions of time and the piece-wise linear models can be predetermined. Since the nonlinearities of the proposed vehicle systems are functions of response variables and can not predetermined without knowing excitations, this method is not adoptable for the analysis of the nonlinear vehicle models in this investigation.

Frequency Domain Linearization Approaches

When excitations to a nonlinear system can be represented in the frequency domain, this linearization technique can replace the nonlinear system by a frequency dependent linear model based on the minimization of the difference between the two systems with respect to a specified criterion. The deterministic linearization in the frequency domain was first developed by Thomson [107]. Various nonlinear damping elements in steady state harmonic vibratory systems are replaced by the equivalent

1.3 Scope of the Investigation

In the previous pages it has been established that passive vibration isolators exhibit inherent performance limitations. While semi-active and active vibration isolators with variable parameters offer superior isolation performance, the increased cost and complexities prohibit their general implementation. It is further established that low cost, simple and reliable passive vibration isolators with variable parameters are extremely desirable to achieve improved shock and vibration isolation performance. Modified passive vibration isolators with tunable characteristics are proposed and analyzed in this thesis with the objective of achieving improved shock and vibration isolation performance of mechanical systems, in particular for vehicle systems. Semi-active sequential dampers are also investigated to demonstrate the relative performance characteristics of tunable hydraulic dampers. The vibration isolation performance of active vibration isolators is also investigated incorporating the generator dynamics.

1.3.1 Objective of the Investigation

The overall objective of this research investigation is to contribute towards attainment of effective vibration isolators, specifically for vehicle suspensions, in order to achieve improved shock and vibration isolation performance. The specific objectives of the study may be summarized as follows:

(i) Investigate active vibration control systems employing various feedback control schemes in view of their vibration isolation performance and discuss the influence of dynamics associated with the force generators.

viscous damping elements, which are calculated by equating the energy dissipated per cycle of the nonlinear damping elements to that of an equivalent viscous damper. This simple and practical technique has been widely used in many deterministic nonlinear dynamic systems [108].

A discrete harmonic linearization method, which is an extension of the frequency domain linearization to stochastic nonlinear systems subject to random excitations, was introduced by Rakheja [105]. It replaces different nonlinear damping mechanisms by an array of equivalent viscous damping coefficients within specified frequency intervals over the entire frequency range of interest. The set of localized linear systems thus developed is a function of corresponding discrete frequency and amplitude of excitation. Various linearization methods in the frequency domain based on different equivalent criteria and accuracy of the methods have been presented by Rakheja et al. [109].

The discrete harmonic linearization method presents a very simple approach to analyze stochastic response of nonlinear systems with many degrees-of-freedom The response of the nonlinear system is directly obtained in terms of the power spectral density (PSD) function by matrix multiplication of the linearized frequency response function and the input power spectral density function. The major limitation of this technique is that it is restricted to stationary excitations. Another limitation is that the techniques proposed have dealt with only nonlinear damping elements and can not provide an equivalent linear stiffness for a nonlinear restoring element. This restriction to nonlinear restoring elements may be removed by a generalized discrete harmonic linearization technique that is proposed in this investigation.

(ii) Investigate the performance potentials of passive hydraulic dampers with tunable parameters.

(iii) Investigate the performance characteristics of passive vibration systems employing tunable hydraulic damper in relation to the semi-active sequential dampers.

(iv) Develop appropriate techniques for the evaluation of the stochastic ride response of vehicle suspension employing nonlinear tunable shock absorbers.

(v) Configure and analyze the interconnected vehicle suspension with tunable parameters in order to achieve improved ride and roll stability performance.

The proposed study is carried out in the following four phases in order to realize the above objectives:

(i) Investigate vibration isolation performance of an active vibration control system employing an electro-magnetic force generator and evaluate the influence of the dynamics of the force generator.

(ii) Configure a tunable passive hydraulic damper and investigate its shock and vibration isolation performance.

(iii) Evaluate the random ride response of vehicle suspension employing tunable hydraulic damper.

(iv) Configure a tunable interconnected vehicle suspension, and investigate the vibration attenuation and roll performance characteristics.

In Chapter 2, an active vibration isolation control system using an electro-magnetic force generator in conjunction with passive spring and damping elements is investigated. A mathematical model of the active

vibration isolator incorporating the dynamics of the force generator is developed. A generalized control scheme is proposed in order to evaluate the vibration isolation characteristics of the active system incorporating the effects of generator dynamics. Simulation results of the active system with various independent as well as combined controls are presented and discussed. The effects of generator dynamics and the stability of the active control system are emphasized.

In Chapter 3, a passive hydraulic damper with constant orifice area is analyzed in view of the damping and vibration isolation characteristics. The concept of a pressure limited hydraulic damper is derived and the associated tuning methodology is presented. The shock and vibration isolation performance characteristics of the isolator employing a tunable pressure limited hydraulic damper are compared with those employing semi-active sequential dampers.

In Chapter 4, a higher order mathematical model of the tunable hydraulic damper is developed, incorporating the fluid and mechanical compliance, and the dynamics of the tunable pressure relief mechanism. Nonlinear differential equations characterizing the dynamics of an isolator using a tunable damper are solved via numerical integration. The results are discussed to demonstrate the influence of the dynamics of the pressure relief mechanism and fluid compliance on the shock and vibration isolation performance of the tunable hydraulic damper.

In Chapter 5, ride performance potentials of vehicle suspensions employing the modified tunable shock absorbers are evaluated for both deterministic and stochastic excitations. Two ride dynamic models are developed, namely a quarter car model and an in-plane vehicle model, to investigate the ride performance potentials of tunable shock absorbers.

The quarter car model is first evaluated in the time and frequency domains for deterministic inputs. The dynamic ride performance is presented in terms of shock and vibration isolation characteristics. A generalized discrete harmonic linearization technique, based upon local linearization techniques, is developed to obtain the vehicle ride response to stochastic terrain excitations. The stochastic ride response of the in-plane vehicle model with tunable shock absorbers is presented in terms of the response power spectral density.

In Chapter 6, roll plane models of vehicles with independent and interconnected suspensions are developed to investigate the ride and roll performance potentials of interconnected vehicle suspensions. Interconnected vehicle suspensions employing constant orifice and tunable pressure limited mechanisms are analytically modeled and investigated. The roll plane vehicle system employing tunable interconnected suspension is modeled incorporating the effective bulk modulus of the fluid and the dynamics of relief mechanisms. The roll response characteristics of the interconnected suspensions is evaluated for a typical cornering maneuver. The ride performance potentials of tunable interconnected suspension are demonstrated in both time and frequency domains in terms of shock and vibration isolation characteristics.

In chapter 7, highlights of the results obtained and the general conclusions drawn are presented along with an outline for the future work.

CHAPTER 2

AN ACTIVE VIBRATION ISOLATION SYSTEM USING ELECTRO-MAGNETIC FORCE GENERATOR

2.1 Introduction

In general, vibration isolation of mechanical systems can be achieved through either passive or active vibration control systems. Although passive vibration isolation systems offer simple and reliable means to protect mechanical systems from vibration environment, the inherent performance limitations of passive vibration isolators are well known. An active shock and vibration isolation system with parameters that change with respect to the excitation and response characteristics of the system can provide significantly superior vibration isolation performance. Active vibration control systems can supply energy when required as well as dissipate energy, whereas a passive vibration control system can only dissipate or temporarily store energy. The major disadvantages of active systems include the requirements of an external energy source and a sophisticated control system with a number of sensors. Increased cost, complexity and weight of the active vibration isolation systems impose a limitation on the general application of such systems, however active vibration isolators are used where the performance benefits outweigh these limitations.

In the past twenty years various active vibration isolation systems have been proposed and investigated extensively [31, 37, 122]. Many efforts have been made to predict the dynamic performance of active vibration control systems in various applications [123, 124]. An active vibration control system employing an electro-magnetic force generator

was analyzed by Ellis and Mote [43] for the attenuation of transverse vibrations of a circular saw. Nikolajsen et al. [44] investigated an electro-magnetic force generator to achieve the active control of transmission shaft vibrations. Active electromagnetic suspensions were investigated by Hogan and Hubbard [125], and Weinberg [128], respectively. The vibration isolation performance of active vibration control systems is often evaluated for ideal elements [32-45], while the dynamic characteristics of the active force generator are neglected. Buzan and Hedrick [46] investigated the influence of the dynamics of a pneumatic actuator on the vibration isolation performance of the active vibration control system. The study revealed that the actuator dynamics influences the suspension performance considerably.

In this chapter, an analytical investigation of vibration isolation performance of a hybrid active vibration control system, incorporating an electro-magnetic force generator along with passive spring and damping elements, is presented. The electro-magnetic force generator is modeled as a first order dynamic subsystem, and a general control scheme is formulated by including absolute and relative response variables of the system. The basic vibration isolation characteristics of the feedback vibration control employing individual variables are first presented and discussed in view of the dynamics of the force generator. The vibration isolation performance of the electro-magnetic active system with combined variable control schemes is, secondly, evaluated and compared with that of the ideal model to demonstrate the significance of force generator dynamics. Active control schemes are proposed and investigated based on the basic vibration isolation

characteristics of individual variables, with the effects of generator dynamics. The limiting values of various control gains are established through stability analysis of the active vibration control system.

2.2 Development of Active Vibration Control System Model

A single-degree-of-freedom hybrid fail-safe vibration control system is configured by integrating an active force generator to a conventional passive vibration isolation system, as shown in Figure 2.1. The hybrid active vibration isolation system is configured in view of following advantages:

1) improved reliability of the vibration control system [45];

2) reduced power level requirement of the active generator.

The equation of motion of the hybrid active vibration control system is developed and expressed in terms of control forces generated by both active and passive components:

$$m\,\ddot{x}(t) + f_{cp}(t) + f_{ca}(t) = 0. \tag{2.1}$$

where,

m = mass of the system (kg)

x = vertical displacement coordinate of the mass (m)

f_{cp} = control force due to passive elements (N)

f_{ca} = control force due to active element (N)

The passive control force offered by the passive spring and damper is dependent upon the element coefficients and relative movement of the system. Assuming linear coefficients, the passive control force can be expressed as:

$$f_{cp}(t) = k\,z(t) + c\,\dot{z}(t) \tag{2.2}$$

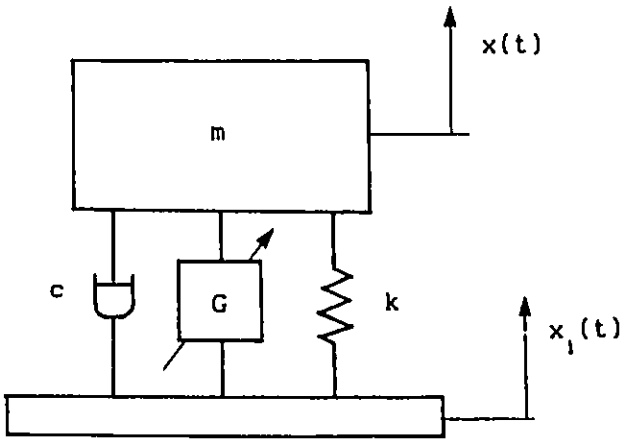

FIGURE 2.1 A schematic of SDOF hybrid active vibration isolation system

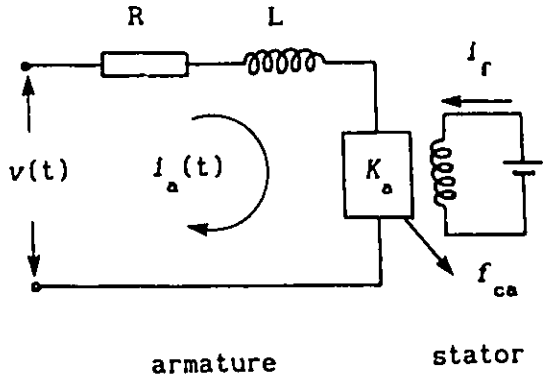

FIGURE 2.2 An electro-magnetic active force generator model

where,

k = stiffness coefficient of spring (N/m)

c = viscous damping coefficient of damper (N·s/m)

z = relative displacement of the system (m), defined by

$$z(t) = x(t) - x_i(t) \tag{2.3}$$

x_i = base input displacement (m)

The active control force generated by active force generator G, is dependent upon the dynamics of the force generator, control laws and control gains. The active control force can be generated via hydraulic or pneumatic actuators coupled with wide band servo-valve and external hydraulic or pneumatic power source [40, 46]. Ellis and Mote [44] and Nikolajsen et al. [45] proposed that the active control force can also be realized via electro-magnets with a lesser degree of complexity.

An electro-magnetic active force generator model, as shown in Figure 2.2, is selected for this investigation. The electro-magnetic force generator consists of a stator and an armature. The stator provides a magnetic field through a constant electric current, while the armature generates an active force by means of interactions of armature current and stator magnetic field. The armature circuit is represented by a resistor and inductor circuit subject to the control voltage. The stator mass of the force generator is lumped to the base, while the mass of the armature is lumped with system mass. The control force, generated by the electro-magnet, is proportional to the product of armature current and magnetic flux strength of the field [126, 128]:

$$f_{ca}(t) = A_1 \phi i_a(t) \tag{2.4}$$

where,

A_1 = constant coefficient of generator (m^{-1})

i_a = armature current (A)

ϕ = magnetic flux (Wb)

Assuming an unsaturated magnetic field, the flux ϕ is then proportional to the constant field current and expressed as:

$$\phi = A_2 \, i_f \tag{2.5}$$

A_2 = constant coefficient of magnetic field ($N \cdot m/A^2$)

i_f = constant field current (A)

Substituting equation (2.5) into (2.4) yields the following:

$$f_{ca}(t) = K_a \, i_a(t) \tag{2.6}$$

where,

$K_a = A_1 \, A_2 \, i_f$, constant coefficient of force (N/A)

Equation (2.6) reveals that the active control force can be expressed as a linear function of the armature current. The armature current can be, further, related to control voltage, armature resistance, armature inductance and the counter emf induced by the relative motion of the armature with respect to the stator, and expressed as:

$$L \frac{d \, i_a(t)}{d \, t} + R \, i_a(t) + \varepsilon(i_a, \dot{z}) = v(t) \tag{2.7}$$

where,

$v(t)$ = input control voltage of active system (V)

R = constant armature resistance (Ω)

L = constant armature inductance (H)

ε = counter electromotive force , emf, (V)

State Equation of the Active System

Assume that the influence of eddy currents due to counter electromotive force (emf) is negligible as compared with that of the input control voltage [128]. A set of state variables is selected and defined as the following:

$$x_1(t) = z(t) \tag{2.8}$$

$$x_2(t) = \dot{x}(t) \tag{2.9}$$

$$x_3(t) = i_a(t) \tag{2.10}$$

The corresponding state differential equations car be then obtained from equations (2.1) to (2.10), and expressed as:

$$\dot{X}(t) = A\,X(t) + B_1\,u(t) + B_2\,w(t) \tag{2.11}$$

where,

X = state variable vector

u = control input to the system

w = excitation input to the system

A = constant time-invariable state matrix

B_1 = constant control vector

B_2 = constant disturbance vector

and

$$X = \begin{Bmatrix} x_1 \\ x_2 \\ x_3 \end{Bmatrix}, \; u = v(t) \text{ and } w = \dot{x}_1(t) \tag{2.12}$$

$$A = \begin{bmatrix} 0. & 1. & 0. \\ -\frac{k}{m} & -\frac{c}{m} & -\frac{K_a}{m} \\ 0 & 0 & -\frac{R}{L} \end{bmatrix} \tag{2.13}$$

$$B_1 = \begin{Bmatrix} 0. \\ 0. \\ \frac{1}{L} \end{Bmatrix} \quad \text{and} \quad B_2 = \begin{Bmatrix} -1. \\ \frac{c}{m} \\ 0. \end{Bmatrix} \tag{2.14}$$

2.3 Generalized Control Scheme

For a complete controllable nth order system, a control law based on n linearly independent state variables is sufficient for a full state feedback control of the system [103]. A number of active control schemes employing various feedback variables, that may include absolute response variables, such as position, velocity and acceleration of the mass, and relative response variables, such as relative displacement, relative velocity and relative acceleration of the mass with respect to the isolator base, have been proposed in the literature [35, 43, 47]. The choice of feedback variables is often made to obtain a practical control scheme [47], desired performance characteristics and/or to compensate for the influence of the dynamics of force generating actuators [48].

A General Control Law for the Active Vibration Control System

In order to examine systematically the vibration isolation performance based on various feedback variables, a general control law is formulated as a combination of absolute, as well as relative response variables:

$$u(t) = k_1 x(t) + k_2 \dot{x}(t) + k_3 \ddot{x}(t) + k_4 z(t) + k_5 \dot{z}(t) + k_6 \ddot{z}(t) \tag{2.15}$$

Where,

k_1 = control gain due to absolute position (V/m)

k_2 = control gain due to absolute velocity (V·s/m)

k_3 = control gain due to absolute acceleration ($V \cdot s^2/m$)

k_4 = control gain due to relative position (V/m)

k_5 = control gain due to relative velocity (V·s/m)

k_6 = control gain due to relative acceleration (V·s^2/m)

Transfer Function of the Active System

The performance characteristics of active vibration isolation system are evaluated in terms of transmissibility characteristics. Taking Laplace transform of equations (2.11) to (2.15), a block diagram of the active vibration isolation system, incorporating an electro-magnetic force generator, a passive spring and a viscous damper, is formulated as shown in Figure 2.3. The transfer function of the hybrid active vibration isolation system can thus be expressed as:

$$\frac{X(s)}{X_1(s)} = \left(\frac{(G_6 + \tau c)s^2 + (G_5 + c + \tau k)s + (G_4 + k)}{\tau m s^3 + (G_3 + G_6 + \tau c + m)s^2 + (G_2 + G_5 + \tau k + c)s + (k + G_1 + G_4)} \right) \quad (2.16)$$

where, s is the Laplace variable, and

$$G_i = \frac{K_a}{R} k_i \ , \ i = 1, \ldots, 6 \quad (2.17)$$

$$\tau = L / R \quad (2.18)$$

For an ideal active vibration isolation system, where the dynamics of the electro-magnetic force generator are neglected ($\tau = 0.$), the transfer function of equation (2.16) reduces to that of a second order system as given by:

$$\frac{X(s)}{X_1(s)} = \left(\frac{G_6 s^2 + (G_5 + c)s + (G_4 + k)}{(G_3 + G_6 + m)s^2 + (G_2 + G_5 + c)s + (k + G_1 + G_4)} \right) \quad (2.19)$$

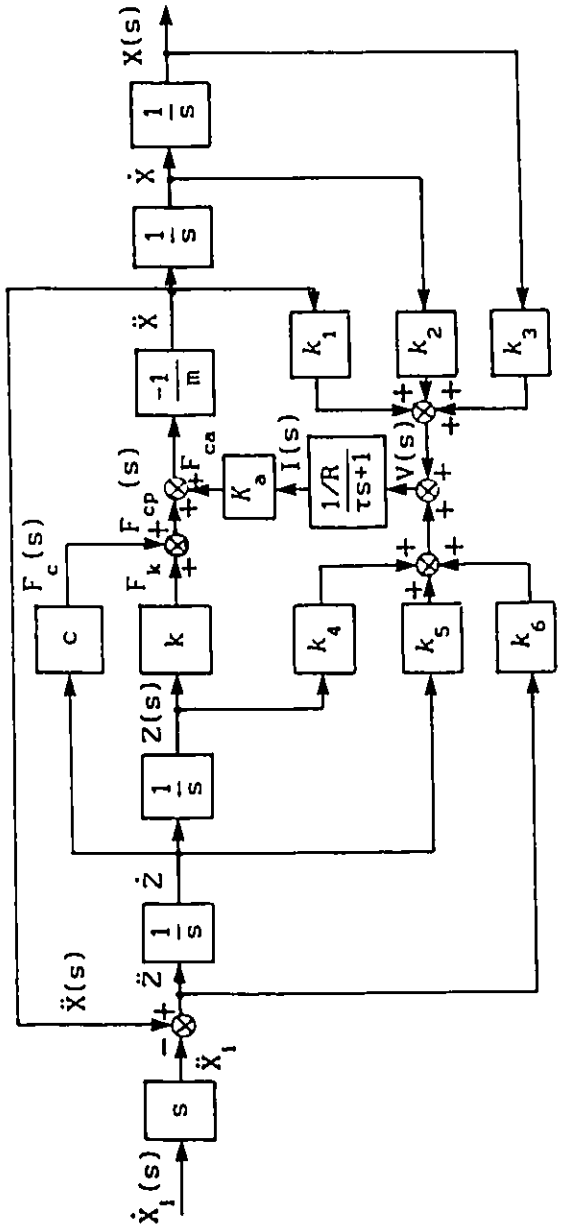

FIGURE 2.3 Block diagram representation of hybrid active vibration control system

An examination of the ideal active vibration control system based on equation (2.19) reveals that:

1) the stiffness characteristics of the active vibration isolation system are influenced by the gains of the absolute and relative position feedback (G_1 and G_4);
2) absolute velocity and relative velocity feedback gains (G_2 and G_5) affect the damping characteristics of the system; and
3) absolute and relative acceleration gains (G_3 and G_6) influence the inertial properties of the active system.

The active control force can thus be generated and varied with respect to response and excitation variables to achieve the desired performance characteristics of the active vibration control system.

A comparison of equations (2.16) and (2.19) reveals that dynamic characteristics of the active force generator also affect the properties of the active vibration control system and thus may cause certain distortions in both amplitude and phase of the control force with respect to excitation frequency. Specifically, the distortions in phase can alter the nature of the control force significantly.

Transmissibility Function of the Active Vibration Control System

The vibration transmissibility of the active vibration control system, employing the feedback from absolute as well as relative response variables, is obtained from equation (2.16) and expressed as a function of non-dimensionalized variables as follows:

$$T_r = \left|\frac{X(\omega)}{X_i(\omega)}\right| =$$

$$\left[\frac{\left[(1+\nu_z) - (2\zeta\tau' + \mu_z)\left(\frac{\omega}{\omega_n}\right)^2\right]^2 + \left[\left(\tau' + 2\zeta(1 + \frac{\zeta_z}{\zeta})\right)\left(\frac{\omega}{\omega_n}\right)\right]^2}{\left[(1+\nu_z+\nu_x) - \left(2\zeta\tau' + (1+\mu_z+\mu_x)\right)\left(\frac{\omega}{\omega_n}\right)^2\right]^2 + \left[\left(\tau' + 2\zeta(1+\frac{\zeta_x}{\zeta}+\frac{\zeta_z}{\zeta})\right)\left(\frac{\omega}{\omega_n}\right) - \tau'\left(\frac{\omega}{\omega_n}\right)^3\right]^2}\right]^{\frac{1}{2}}$$

...(2.20)

where,

ω = angular excitation frequency (rad/s)

ω_n = angular undamped natural frequency of system (rad/s)

and

$$\omega_n^2 = \frac{k}{m} \; ; \quad \zeta = \frac{c}{2\sqrt{mk}} \; ; \quad \tau' = \tau\,\omega_n$$

$$\nu_x = \frac{G_1}{k} \; ; \quad \zeta_x = \frac{G_2}{2\sqrt{mk}} \; ; \quad \mu_x = \frac{G_3}{m}$$

$$\nu_z = \frac{G_4}{k} \; ; \quad \zeta_z = \frac{G_5}{2\sqrt{mk}} \; ; \quad \mu_z = \frac{G_6}{m} \qquad (2.21)$$

2.4 Stability Analysis of Active Vibration Control System

Active control systems are often conditionally stable systems. It is apparent from (2.16) that the characteristic equation for the active vibration control system incorporating an electro-magnetic force generator is of third order. For a stable active vibration isolation system, the following conditions on limiting gain values are obtained, based on the Routh-Hurwitz stability criterion [103]:

$$\nu_x + \nu_z > -1$$

$$2\zeta_x + 2\zeta_z > -(\tau' + 2\zeta)$$

$$\mu_x + \mu_z > -(1 + 2\zeta\tau')$$

and

$$\left(1 + \mu_x + \mu_z + 2\zeta\tau'\right)\left[\tau' + 2\zeta\left(1 + \frac{\zeta_x}{\zeta} + \frac{\zeta_z}{\zeta}\right)\right] > \tau'\left(1 + \nu_x + \nu_z\right) \qquad (2.22)$$

In the evaluation of vibration isolation performance of various control schemes, the limiting values of feedback gains of various variables are determined from equation (2.22) in order to ensure stability of the active control system.

2.5 Vibration Isolation Characteristics Using Control Law with Individual Variables

Vibration isolation characteristics of active vibration control system with an electro-magnetic force generator are investigated for feedback from various response and excitation variables. The non-dimensional time constant of the first order subsystem model, the electro-magnetic force generator, is selected as $\tau'=0.3$. Damping ratio due to passive element is assumed to be, $\zeta=0.3$. The influence of the dynamics of force generator on the performance characteristics is emphasized for the feedback control schemes employed. Transmissibility characteristics of the active vibration control system using electro-magnetic force generator ($\tau'=0.3$) are thus compared with those of the ideal vibration control system ($\tau'=0.$), for various values of control variable gains to demonstrate the significance of the generator dynamics.

In this section, the vibration isolation characteristics of the hybrid active system, employing the six individual response variables, respectively, are presented and evaluated in terms of vibration transmissibility of the system. The basic vibration isolation

performance of the active control system based on individual variables is established and discussed, in view of dynamics of the force generator.

2.5.1 Absolute Position Control

Equation (2.20) is computed to establish the transmissibility response of the active vibration control system using an ideal ($\tau'=0$) as well as the electro-magnetic force generator with first order dynamics ($\tau'=0.3$). Vibration transmissibility of the active vibration control system employing absolute position feedback, often referred to as a *skyhook spring*, is compared with that of an ideal vibration control system, as shown in Figure 2.4. It is observed that static as well as resonant response values of the ideal vibration control system decrease as the gain G_1 is increased (for $G_1>0$). However, due to dynamics of the force generator, peak response of the actual force generator model increases considerably as the absolute position gain value is increased. The generator dynamics, therefore, deteriorate the vibration isolation performance employing the absolute position feedback, except for $G_1<0$. The electro-magnetic force generator reveals better performance than that of an ideal system, when negative absolute position gain value within the stable range is employed.

It can be also seen that as the feedback gain value of the absolute position control is increased, the natural frequency of the system increases due to the stiffness characteristics of the position feedback control.

2.5.2 Absolute Velocity Control

A vibration isolation control system employing an absolute velocity

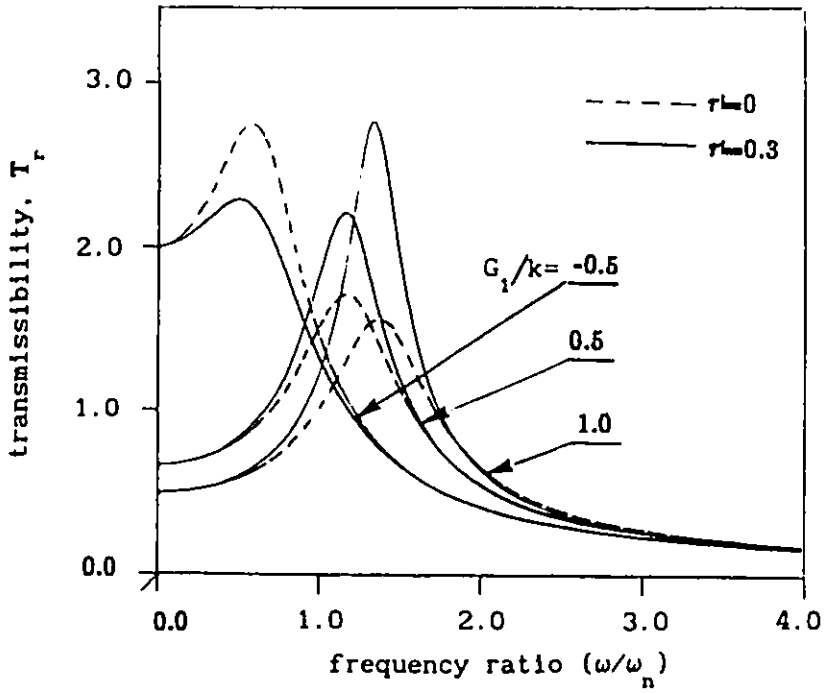

FIGURE 2.4 Vibration transmissibility of hybrid active system employing absolute position feedback (ζ=0.3)

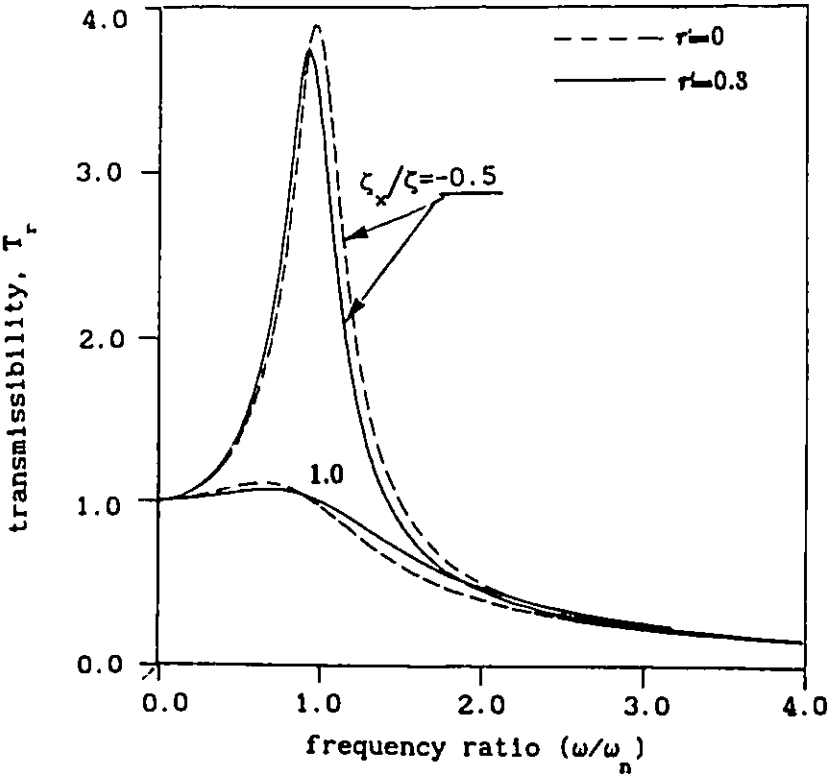

FIGURE 2.5 Vibration transmissibility of hybrid active system employing absolute velocity feedback (ζ=0.3)

feedback is also referred to as a *skyhook damper* [49]. Transmissibility characteristics of the hybrid active vibration control system using either an electro-magnetic or an ideal force generator, when absolute velocity feedback is employed, are shown in Figure 2.5. It can be seen that transmissibility response decreases considerably irrespective of the excitation frequency, as the feedback gain G_2 is increased. The absolute velocity feedback, therefore, yields a significantly improved vibration isolation performance. A comparison of the response characteristics of the electro-magnetic force generator ($\tau'=0.3$) with that of an ideal system reveals that the generator dynamics have only minimal effect on the performance.

2.5.3 Absolute Acceleration Control

The transmissibility response of hybrid active vibration isolation system employing mass acceleration feedback control, with various feedback gain values, is presented in Figure 2.6. The peak response of an ideal system increases as the acceleration feedback gain G_3 is increased. However, the peak response value decreases when the dynamics of the force generator are taken into consideration, as shown in Figure 2.6. The dynamics due to the generator, thus, yield an improved vibration isolation performance with absolute acceleration feedback control.

Since absolute acceleration feedback influences the mass characteristics of the vibration isolation system, the resonant frequency of the actively controlled vibration isolation system decreases with an increase in the gain value G_3.

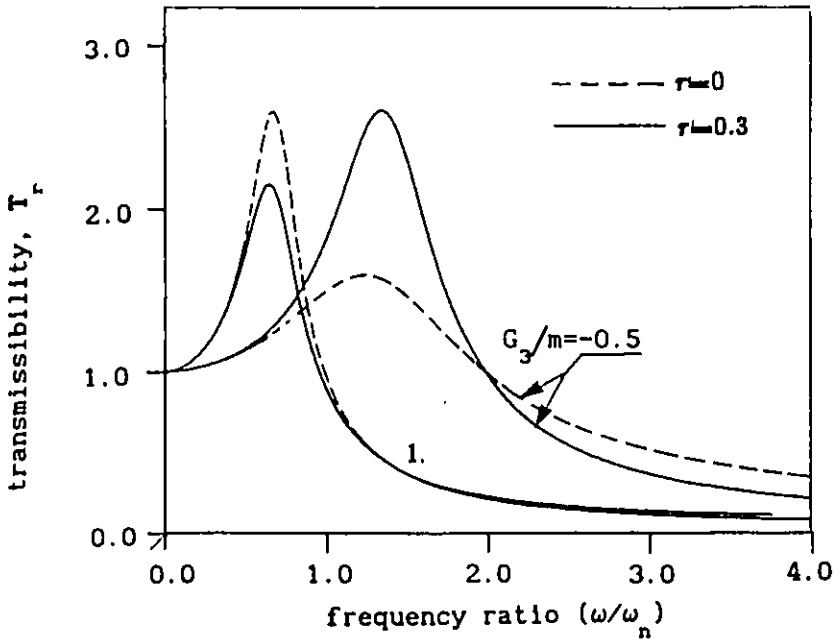

FIGURE 2.6 Vibration transmissibility of hybrid active system employing absolute acceleration feedback (ζ=0.3)

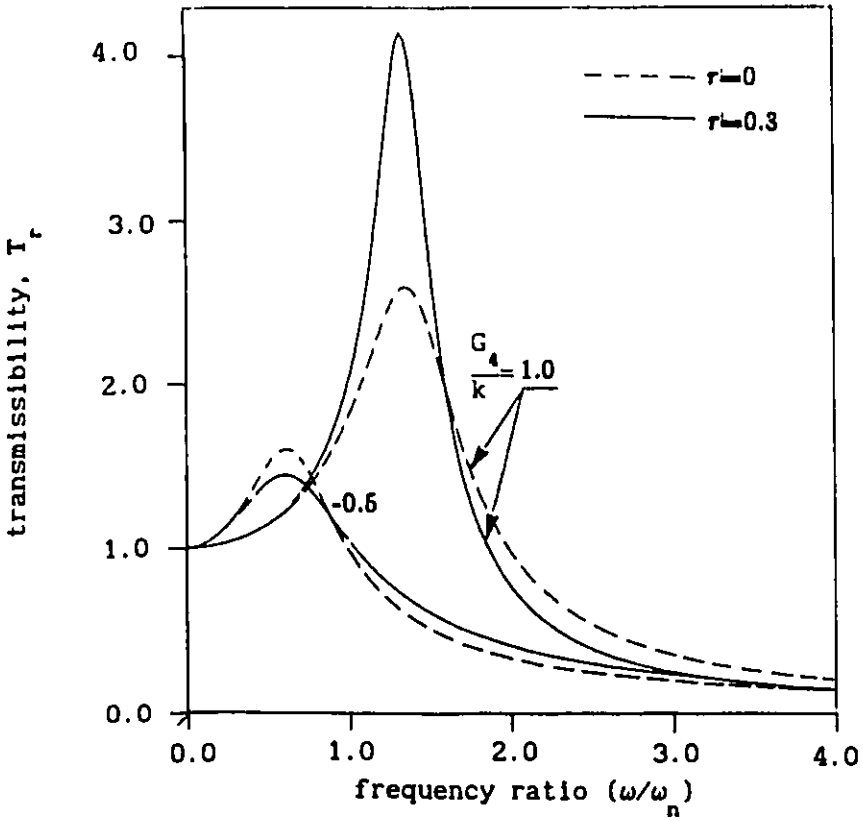

FIGURE 2.7 Vibration transmissibility of hybrid active system employing relative position control (ζ=0.3)

2.5.4 Relative Position Control

Transmissibility characteristics of the hybrid active vibration control system based on relative position control are illustrated in Figure 2.7. It is observed that the peak response of active system due to individual relative position control increases as the gain value G_4 is increased. A comparison of transmissibility characteristics of ideal and electro-magnetic actuator ($\tau'=0.3$) reveals that vibration isolation performance is severely deteriorated due to the dynamics of the actuator, for relative position control with $G_4>0$. However, the transmissibility response due to actuator dynamics coupled with negative gain value ($G_4<0.$) is observed to be superior to that of an ideal controller. The natural frequency of active system based on relative position control also increases due to its stiffness characteristics.

2.5.5 Relative Velocity Control

Transmissibility characteristics of relative velocity controlled active vibration control system are shown in Figure 2.8. It can be seen that response of vibration control system with both ideal and electro-magnetic force generators is basically similar to that of a passive system. However, the peak response amplitude as well as the natural frequency of the electro-magnetic force generator is slightly higher than that of the ideal system for positive gain values ($\zeta_z>0$), due to the influence of generator dynamics. For a negative gain value, a significant resonant peak is obtained due to reduced damping value of the active control system. The amplitude of resonant peak decreases slightly when the dynamics of the force generator are taken into

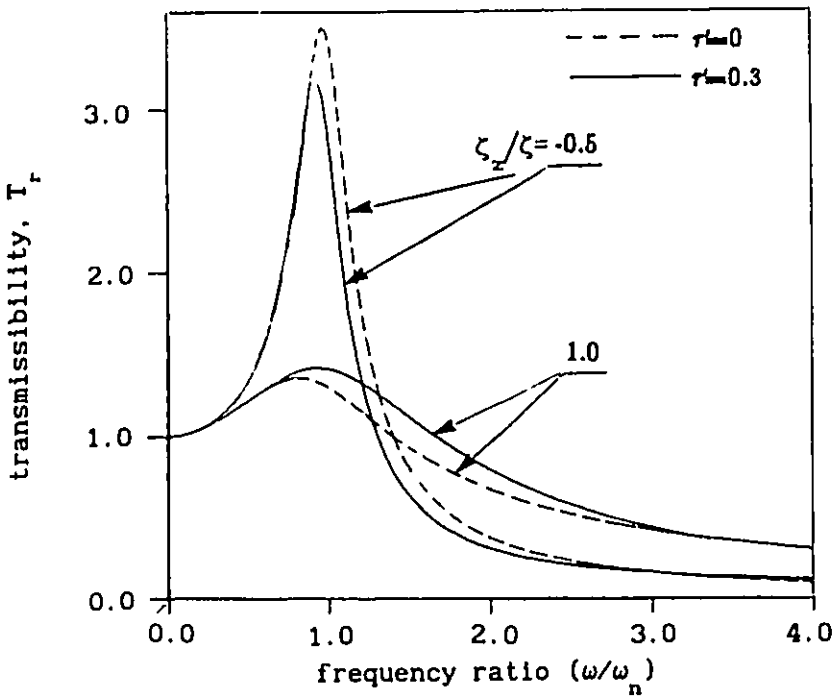

FIGURE 2.8 Vibration transmissibility of hybrid active system employing relative velocity control (ζ=0.3)

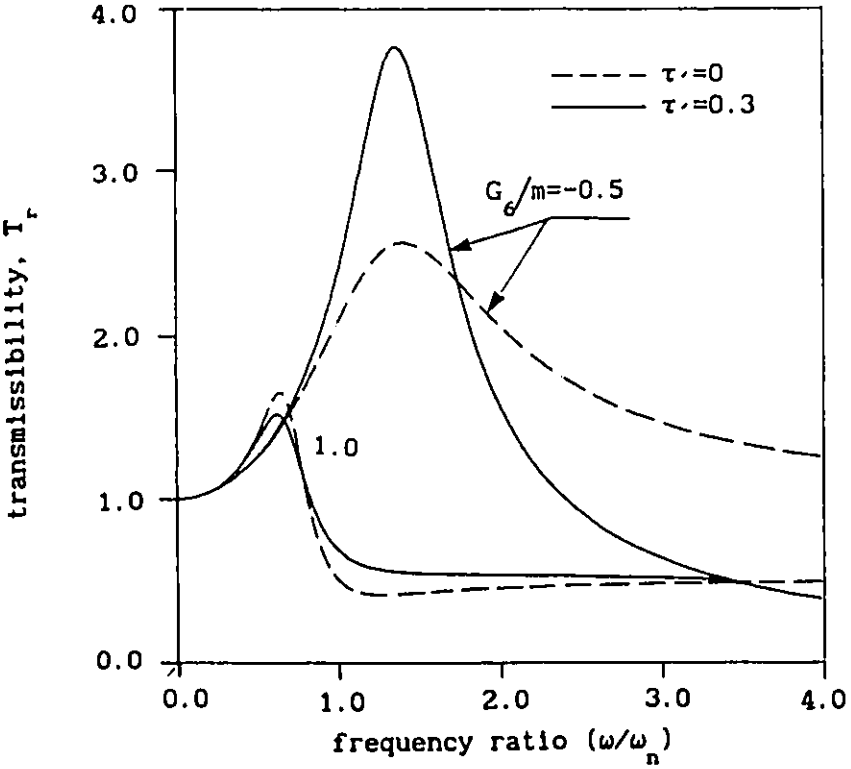

FIGURE 2.9 Vibration transmissibility of hybrid active system employing relative acceleration control (ζ=0.3)

consideration.

2.5.6 Relative Acceleration Control

Transmissibility characteristics of hybrid active vibration control system based on only relative acceleration control, for both ideal and electro-magnetic force generator, are shown in Figure 2.9. The peak transmissibility response and natural frequency of the relative acceleration controlled system decreases considerably with increased gain values. The resonant peak response of the active system with the electro-magnetic force generator is smaller than that of the ideal one, for $G_6>0$. However, the transmissibility response of the ideal active system is significantly deteriorated with negative gain ($G_6<0$). Dynamics due to the generator further deteriorate the transmissibility response, as shown in Figure 2.9.

2.6 Vibration Isolation Characteristics Using Control Laws with Combined Variable Controls

Vibration isolation characteristics of the active vibration control system with, ideal as well as electro-magnetic actuators, are further investigated by employing the feedback from a combination of response and excitation variables, such that an effective vibration isolation can be achieved. The influence of the dynamics of the force generator on the transmissibility characteristics is investigated and discussed for various control laws. Control laws comprising of various response and excitation variables, for generation of active force, are selected based upon the performance characteristics presented in section 2.5.

2.6.1 Combined Absolute Velocity and Relative Position Control

Karnopp et al. [49], and Guntur and Sankar [45] have discussed the potential performance benefits of absolute velocity and relative position control, while neglecting the dynamics of the force generator. The control voltage applied at the electro-magnetic force generator by employing absolute velocity and relative position control can be expressed, from equation (2.15), as:

$$u = v(t) = k_2\dot{x}(t) + k_4 z(t) \qquad (2.23)$$

The transmissibility function of this active vibration isolation system is obtained from equations (2.11) and (2.23), and expressed as:

$$T_r = \left[\frac{\left[1+ \nu_z - 2\zeta\tau' \left(\frac{\omega}{\omega_n}\right)^2 \right]^2 + \left[\left(\tau' + 2\zeta\right)\left(\frac{\omega}{\omega_n}\right) \right]^2}{\left[(1+\nu_z) - (1.+2\zeta\tau')\left(\frac{\omega}{\omega_n}\right)^2 \right]^2 + \left[\left[2\zeta\left(1+\frac{\zeta_x}{\zeta}\right)+\tau'\right]\left(\frac{\omega}{\omega_n}\right) - \tau'\left(\frac{\omega}{\omega_n}\right)^3 \right]^2} \right]^{\frac{1}{2}} \qquad \ldots(2.24)$$

Figures 2.10 and 2.11 show the transmissibility characteristics of active vibration control system, when the active force is generated using absolute velocity and relative position control. The influence of absolute velocity gain (ζ_x) on the transmissibility characteristics for fixed relative position gain ν_z=1, and ζ=0.1 is presented in Figure 2.10. Response characteristics clearly reveal that peak transmissibility response of the active system with low absolute velocity gain (ζ_x=0.2) is deteriorated considerably due to the dynamics of the electro-magnetic force generator. However, the resonant transmissibility peak is suppressed as the velocity gain $G_2(\zeta_x)$ is increased. The absolute

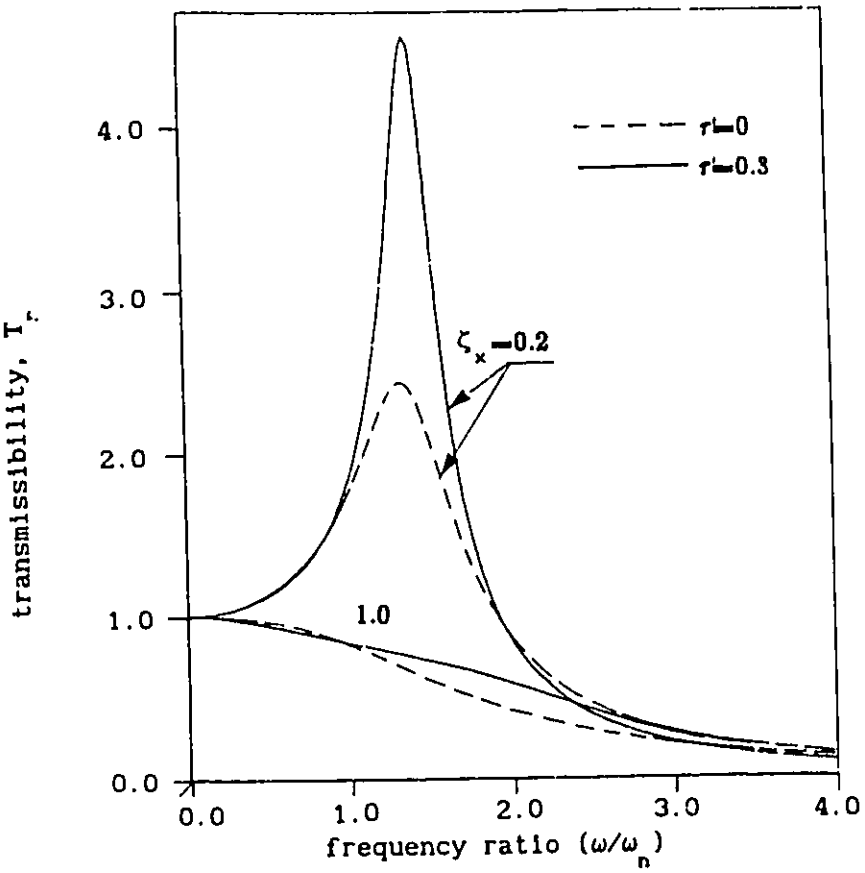

FIGURE 2.10 Vibration transmissibility of hybrid active system employing absolute velocity and relative position control (ζ=0.1, G_4/k=1.)

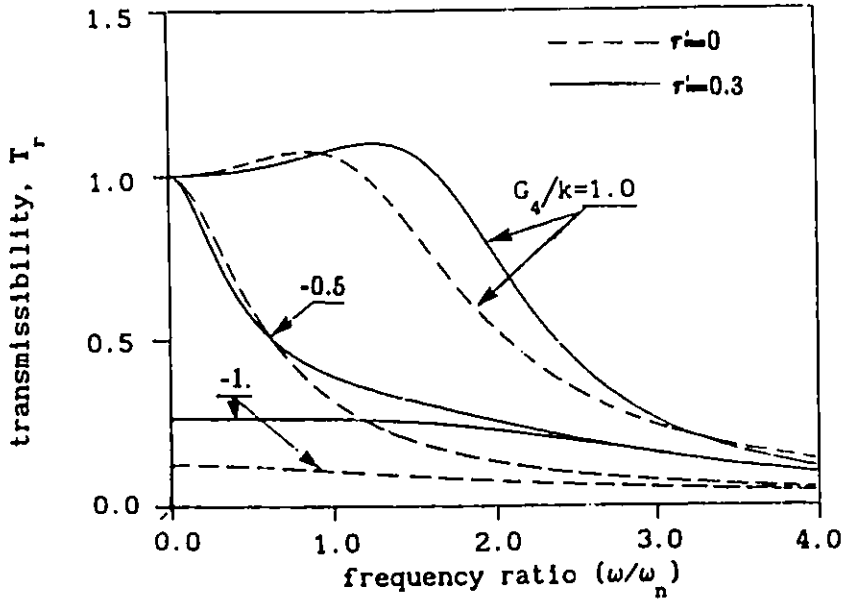

FIGURE 2.11 Vibration transmissibility of hybrid active system employing absolute velocity and relative position control (ζ=0.1, ζ_x=0.7)

velocity feedback is, therefore, desirable in an active vibration isolation control system. Transmissibility characteristics of the active control system with ζ_x=0.7 and various values of relative position gain (G_4 or ν_z) are shown in Figure 2.11. Response characteristics reveals that the vibration isolation performance can be improved considerably, for all excitation frequencies (including ω = 0.), when the gain $G_4(\nu_z)$ is decreased, as shown in Figure 2.11. However, for stability considerations, the gain value must be limited to $\nu_z \geq -1$.

2.6.2 Combined Absolute Velocity and Acceleration Control

Cho and Hedrick [35], and Guntur and Sankar [45] have investigated the performance of an active vibration control system based upon absolute velocity and acceleration control while neglecting the dynamics of the actuator. The control law corresponding to absolute velocity and acceleration feedback is obtained as:

$$u = v(t) = k_2\dot{x}(t) + k_3\ddot{x}(t) \tag{2.25}$$

The vibration transmissibility function is then expressed as:

$$T_r = \left[\frac{\left[1 - 2\zeta\tau'\left(\frac{\omega}{\omega_n}\right)^2\right]^2 + \left[\left(\tau' + 2\zeta\right)\left(\frac{\omega}{\omega_n}\right)\right]^2}{\left[\left[1-(1+\mu_x+2\zeta\tau')\left(\frac{\omega}{\omega_n}\right)^2\right]^2 + \left[\left[2\zeta\left(1+\frac{\zeta_x}{\zeta}\right) + \tau'\right]\left(\frac{\omega}{\omega_n}\right) - \tau'\left(\frac{\omega}{\omega_n}\right)^3\right]^2\right]}\right]^{\frac{1}{2}} \tag{2.26}$$

Transmissibility characteristics of the active vibration control system employing absolute velocity and acceleration feedback control are presented in Figure 2.12, where the absolute velocity gain is held fixed (ζ_x=0.7) and the acceleration feedback gain G_3 is varied. A comparison of response characteristics of both ideal and electro-magnetic force generator reveal that the dynamics of the electro-magnetic force

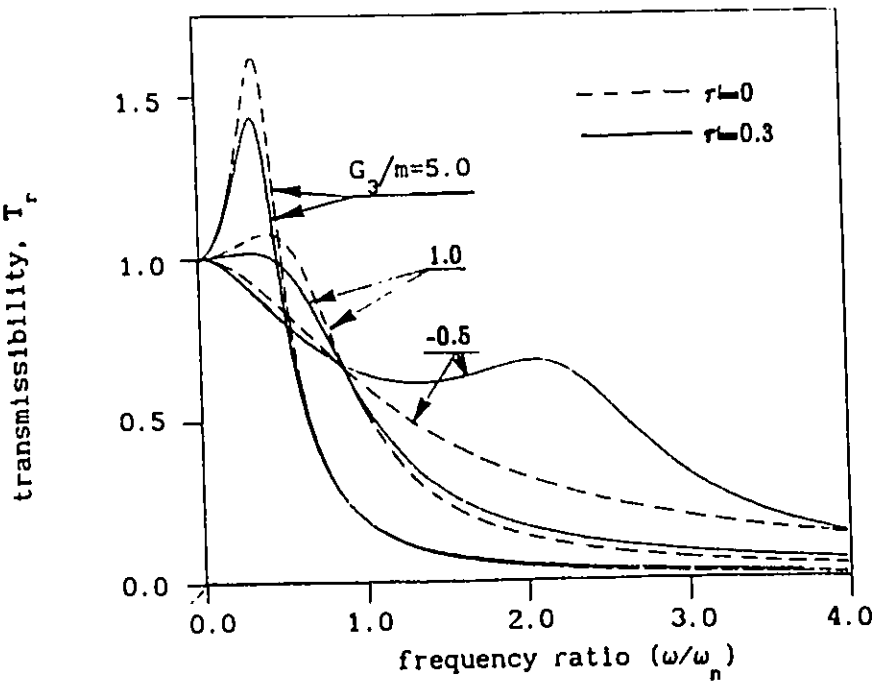

FIGURE 2.12 Vibration transmissibility of hybrid active system employing absolute velocity and acceleration control (ζ=0.1, ζ_x=0.7)

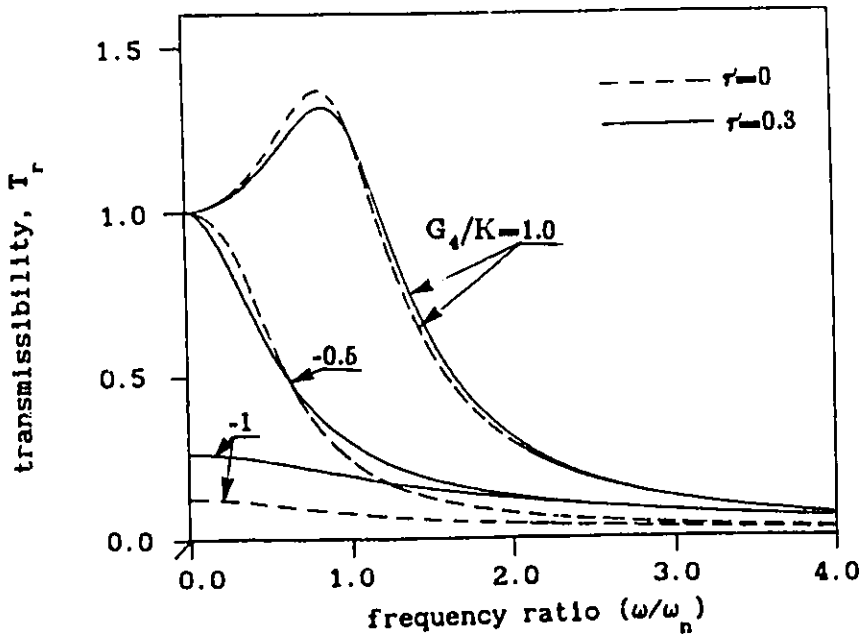

FIGURE 2.13 Vibration transmissibility of hybrid active system employing absolute velocity, acceleration and relative position control (ζ=0.1, ζ_x=0.7, G_3/m=0)

generator introduce a high peak at larger excitation frequency, when the gain G_3 is selected to be negative. It is obvious that the amplitude at high excitation frequency as well as the resonant frequency decreases as the acceleration feedback gain (G_3) is increased. However the peak transmissibility increases as the gain value is increased. For a positive acceleration feedback gain, moreover, the electro-magnetic force generator yields a lower peak response as compared with that of the ideal force generator.

2.6.3 Combined Absolute Velocity, Acceleration and Relative Position Control

Figure 2.7 revealed that a negative relative position control can reduce transmissibility response at low excitation frequencies. The vibration isolation performance of the active vibration control system is thus investigated for a combined relative position, absolute velocity and acceleration control. Thompson [47] proposed an active control scheme based upon this combined variable control with an ideal force generator and positive relative position feedback. The control law for such a vibration control system can be expressed as:

$$u(t) = v(t) = k_2\dot{x}(t) + k_3\ddot{x}(t) + k_4 z(t) \qquad (2.27)$$

The corresponding transmissibility function is then expressed as:

$$T_r = \left[\frac{\left[1 + \nu_z - 2\zeta\tau' \left(\frac{\omega}{\omega_n}\right)^2 \right]^2 + \left[\left(\tau' + 2\zeta \right) \left(\frac{\omega}{\omega_n}\right) \right]^2}{\left[(1+\nu_z) - (1.+\mu_x+2\zeta\tau') \left(\frac{\omega}{\omega_n}\right)^2 \right]^2 + \left[2\zeta\left(1+\frac{\zeta_x}{\zeta}\right)+\tau' \right] \left(\frac{\omega}{\omega_n}\right) - \tau' \left(\frac{\omega}{\omega_n}\right)^3 \right]^2} \right]^{\frac{1}{2}} \qquad \ldots(2.28)$$

Transmissibility characteristics of the active vibration control system with an ideal and an electro-magnetic actuator model are presented in Figure 2.13. The absolute velocity and acceleration feedback gains are held fixed (ζ_x= 0.7 and μ_x = 1.), while the relative position gain (ν_z) is varied. It can be observed that the active vibration isolation system provides superior transmissibility for negative values of relative position gain (ν_z<0). Specifically for ν_z=-1, at the threshold of the system stability, the static ratio is given by:

$$T_r\Big|_{\omega=0.} = \frac{2\zeta + \tau'}{2(\zeta + \zeta_x) + \tau'} \qquad (2.29)$$

The static ratio for the ideal force generator is obtained as 0.125, for ζ = 0.1 and ζ_x= 0.7, while the corresponding static ratio due to the dynamics of the actuator is observed to be 0.26.

2.6.4 Combined Absolute Position, Velocity and Acceleration Control

It has also been established that the positive position feedback (*skyhook spring*) can improve the static stiffness of a vibration control system. The vibration isolation performance of the active control system is thus investigated for the three absolute variable control. The corresponding control law is expressed as:

$$u = v(t) = k_1 x(t) + k_2 \dot{x}(t) + k_3 \ddot{x}(t) \qquad (2.30)$$

and the corresponding expression for vibration transmissibility is obtained as:

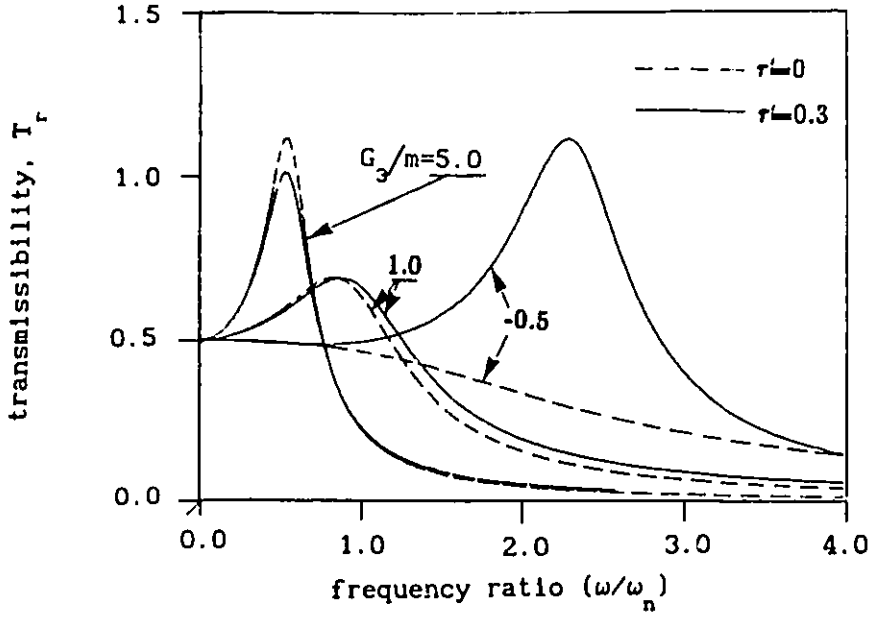

FIGURE 2.14 Vibration transmissibility of hybrid active system employing absolute position, velocity and acceleration control (ζ=0.1, ζ_x=0.7, G_1/k=1.0)

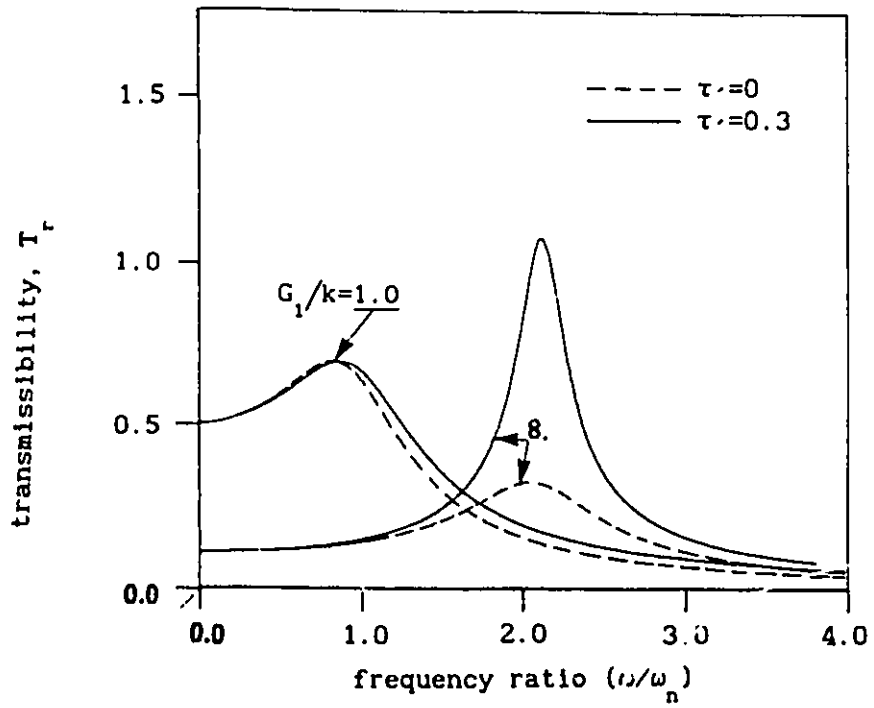

FIGURE 2.15 Vibration transmissibility of hybrid active system employing absolute position, velocity and acceleration control (ζ=0.1, ζ_x=0.7, G_3/m=1.0)

$$T_r = \left[\frac{\left[1. - 2\zeta\tau'\left(\frac{\omega}{\omega_n}\right)^2\right]^2 + \left[\left(\tau' + 2\zeta\right)\left(\frac{\omega}{\omega_n}\right)\right]^2}{\left[(1+\nu_x)-(1.+\mu_x+2\zeta\tau')\left(\frac{\omega}{\omega_n}\right)^2\right]^2 + \left[\left[2\zeta(1+\frac{\zeta_x}{\zeta})+\tau'\right]\left(\frac{\omega}{\omega_n}\right)-\tau'\left(\frac{\omega}{\omega_n}\right)^3\right]^2} \right]^{\frac{1}{2}}$$

...(2.31)

Vibration transmissibility characteristics of the active control system with ideal as well as electro-magnetic force generators are presented in Figures 2.14 and 2.15. The vibration isolation performance for fixed absolute velocity and position gains (ζ_y= 0.7 and ν_y= 1.), and various values of acceleration gain (G_3) is shown in Figure 2.14. It is observed that an increase in acceleration gain value results in lower resonant frequency and considerably larger resonant response. The influence of generator dynamics becomes significant for negative acceleration feedback gains. A comparison of results in Figures 2.12 and 2.14 reveals that the introduction of absolute position feedback (ν_x=1) reduces the static amplitude to 0.5. Figure 2.15 presents the transmissibility response due to variations in absolute position feedback gain. In the case of an ideal force generator, an increase in G_1 yields an increase in natural frequency, and decrease in static as well as peak transmissibility. However, the peak value is considerably higher when the dynamics of the force generator are taken into consideration, specifically for large absolute position gains (ν_x= 8.), as shown in Figure 2.15.

2.6.5 Combined Absolute Position, Velocity and Relative Position Control

It has been shown that the negative relative position feedback (ν_z) in an active control system can reduce vibration transmissibility at low excitation frequencies, however the stability of the system is affected unfavorably when ν_z approaches -1. The stability of the system can be improved by introducing absolute position feedback, as demonstrated in equation (2.15). The control law due to absolute position, velocity and relative position variable feedback is expressed as:

$$u = v(t) = k_1 x(t) + k_2 \dot{x}(t) + k_4 z(t) \qquad (2.32)$$

The corresponding transmissibility function is then expressed as:

$$T_r = \left[\frac{\left[1+ \nu_z - 2\zeta\tau' \left(\frac{\omega}{\omega_n}\right)^2 \right]^2 + \left[\left(\tau' + 2\zeta\right)\left(\frac{\omega}{\omega_n}\right) \right]^2}{\left[(1+\nu_x+\nu_z) - (1+2\zeta\tau')\left(\frac{\omega}{\omega_n}\right)^2 \right]^2 + \left[\left[2\zeta\left(1+\frac{\zeta_x}{\zeta}\right)+\tau'\right]\left(\frac{\omega}{\omega_n}\right) - \tau'\left(\frac{\omega}{\omega_n}\right)^3 \right]^2} \right]^{\frac{1}{2}} \qquad \ldots(2.33)$$

Equation (2.33) reveals that the static value of transmissibility approaches zero by letting $\nu_z = -1.$ and $\nu_x > 0$. The stiffness of such system becomes infinite, while the stability of the system will be assured due to positive value of absolute position control gain ν_x. Figure 2.16 shows the vibration transmissibility of the active control system, for fixed values of absolute position and velocity gains (ν_x = 0.5 and $\zeta_x = 1.$), and various values of relative position gain ν_z. It can be observed that transmissibility response at extremely low frequencies decreases considerably as the gain ν_z is decreased, and the response approaches zero for the relative position gain $\nu_z = -1$. The vibration

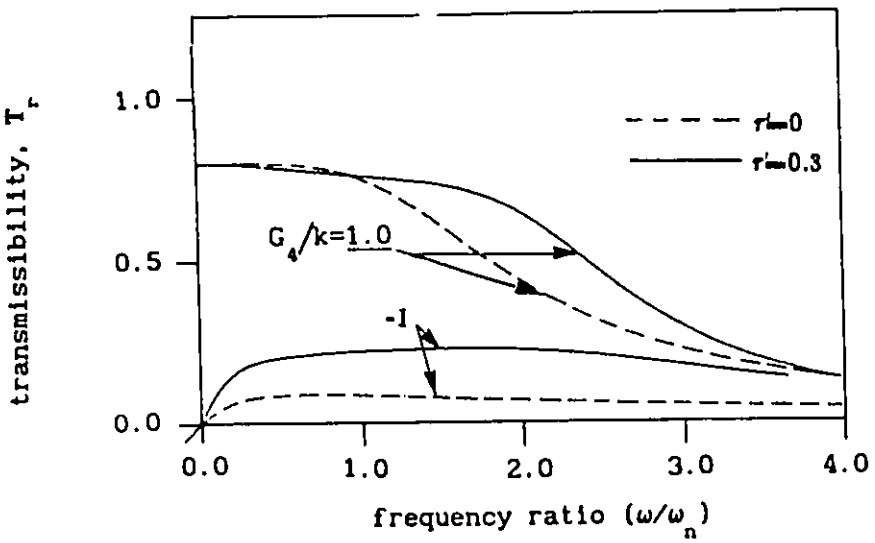

FIGURE 2.16 Vibration transmissibility of hybrid active system employing absolute position, velocity and relative position control (ζ=0.1, ζ_x=1.0, G_1/k=0.5)

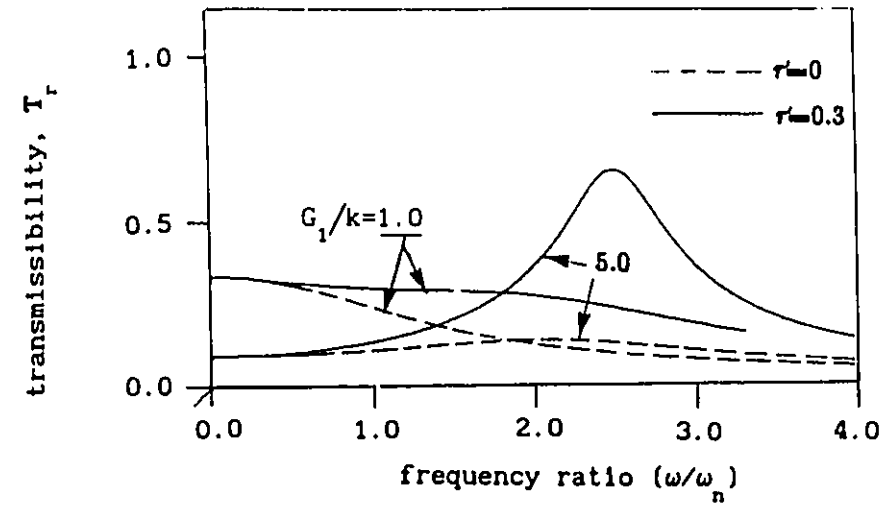

FIGURE 2.17 Vibration transmissibility of hybrid active system employing absolute position, velocity and relative position control (ζ=0.1, ζ_x=1.0, G_4/k=-0.5)

isolation performance of the active control system is deteriorated considerably when the dynamics of the force generator are incorporated, as shown in Figure 2.16. Vibration transmissibility of the hybrid active control system, for various values of absolute position feedback gain (ν_x), while the absolute velocity and relative position gains are held fixed ($\zeta_x = 1.$ and $\nu_z = -0.5$) is shown in Figure 2.17. It can be seen that response amplitude can be reduced considerably at low excitation frequencies by introducing large values of absolute position gain ν_x. However, too large a value of the gain ν_x yields a high peak at higher excitation frequencies due to the dynamics of the electro-magnetic force generator.

2.7 Summary

In this chapter, vibration isolation characteristics of a hybrid active vibration control system, incorporating an electro-magnetic force generator, and passive spring and damping elements, are presented, based on various control schemes. The electro-magnetic force generator is modeled as a first order dynamic subsystem. The simulation results are obtained for various controls based on feedback from individual and combined absolute and relative response variables. Vibration isolation performance of the active system due to individual variable controls indicates that each response variable can only effect some aspects of the transmissibility characteristics. The vibration isolation characteristics of the active system with an ideal as well as an electro-magnetic force generator are presented and discussed to demonstrate the significance of dynamics of the force generator. The

vibration isolation performance of the active system, in general, is adversely affected by the generator dynamics. However, in certain cases, the generator dynamics can yield an improved vibration isolation performance, depending upon the feedback variables and control gains. An active control scheme, based upon absolute position, velocity and relative position control, yields considerably superior vibration isolation performance. Stability analysis of the active vibration control system is also carried out to determine the limiting values of various response variable feedback gains.

CHAPTER 3

ANALYSIS OF AN IDEAL TUNABLE PRESSURE LIMITED HYDRAULIC DAMPER

3.1 Introduction

Passive springs and dampers of various types are widely used in mechanical vibration isolation systems, such as vehicle suspensions. Although conventional passive vibration control elements offer a simple, inexpensive and reliable means to protect mechanical systems and human bodies from shock and vibration disturbances, the most obvious performance limitation associated with passive elements is exhibited due to the inherently fixed damping characteristics. Heavily damped vibration isolators are desirable to suppress the resonant vibration of a mechanical system, while attenuation of vibration at higher excitation frequencies require lightly damped isolators. In order to overcome the inherent performance limitation of conventional passive vibration isolation systems, it is desirable to develop vibration isolation systems with variable parameters which could be varied with respect to the changing excitations or response variables.

Active vibration isolation systems, with automatically controlled parameters that change with variations in excitation and response variables, can provide superior shock and vibration isolation performance, as illustrated in Chapter 2. However, the requirements of an external energy source, actuators, control devices and sensors limit the general implementation of active vibration control systems [31, 32]. The implementation of active means of vibration isolation has been limited to cases in which the performance benefits outweigh the

disadvantages associated with costs and complexities.

Alternatively, semi-active vibration isolation systems actively modulate the passively generated isolator forces, and thus offer a compromise between the performance benefits of an active and the simplicity of a passive vibration isolation system. A semi-active vibration isolator, with either continuous or sequential variations in damping parameter, requires only low level electrical power for necessary signal processing, and provides improved vibration isolation performance as compared with that of a passive vibration isolator [56, 57]. However, semi-active vibration isolators still require a comprehensive instrumentation package and control devices. Moreover, measurement of certain semi-active control variables may pose complexities, specifically for low excitation frequencies. Semi-active 'on-off' control yields a large magnitude of jerk around the discontinuity between the 'on' and 'off' states [59].

Hydraulic shock absorbers used in vehicle suspensions invariably employ valving mechanisms to limit the magnitude of damping force due to orifice flows [6, 22]. The valve may be opened during the compression or extension strokes in certain conditions to yield a reduced damping force. The pressure relief valves are preset by the manufacturers to achieve desired damping characteristics. The spring rate of the relief valves is primarily selected to achieve high damping force around the resonant frequencies. Such shock absorbers thus do not provide effective limiting of the damping force corresponding to high relative velocity response [6, 22].

In this chapter, a passive hydraulic damper with fixed orifice area

is analyzed in view of the damping and vibration isolation characteristics. Two semi-active 'on-off' control schemes, proposed by Rakheja [105] and Margolis et al. [51], respectively, are examined by applying them to a vibration isolation system with a hydraulic damper. An alternative passive control scheme based on a concept of tunable pressure limiting modulation is proposed to achieve variable sequential damping. The associated tuning methodology is presented to obtain effective vibration resonant control as well as improved vibration isolation. The shock and vibration isolation performance characteristics of a passive vibration isolator employing tunable hydraulic damper are investigated through computer simulation and compared with those of vibration isolators employing fixed orifice hydraulic and semi-active 'on-off' dampers.

3.2 Mathematical Modeling of Vibration Isolation System with Hydraulic Damper

Figures 3.1 (a) and (b) illustrate the model representation of a base excited single-degree-of-freedom (SDOF) vibration isolation system employing fixed and variable damping elements, respectively. A schematic of the fixed orifice hydraulic damper employed in the vibration isolation system is shown in Figure 3.2.

3.2.1 Equation of Motion

The equation of motion of the SDOF system employing a linear spring and a passive hydraulic damper shown in Figure 3.1 can be expressed as:

$$m\ddot{x}(t) + f_k(t) + f_{ds}(t) = 0 \qquad (3.1)$$

where,

m = mass of the main body (kg)

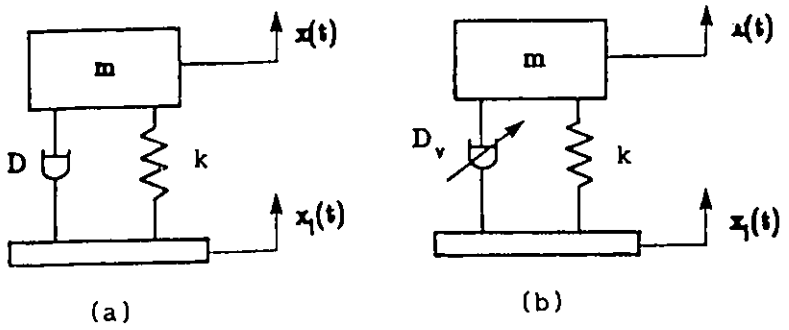

FIGURE 3.1 Model representation of a SDOF vibration isolation system with (a) fixed damping, and (b) variable damping

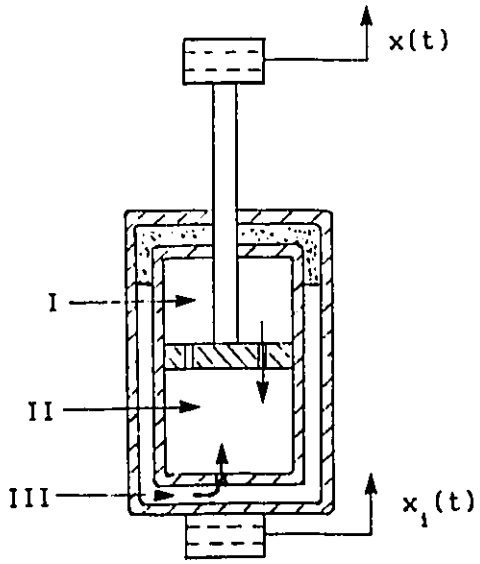

FIGURE 3.2 Schematic of a passive hydraulic damper

x = vertical displacement coordinate of the mass (m)

t = time (sec)

f_k = restoring force generated by linear spring k (N)

f_{ds} = total dynamic force due to hydraulic damper D (N)

The restoring force, $f_k(t)$, generated by linear spring, is expressed as:

$$f_k(t) = k\ z(t) \tag{3.2}$$

where,

$$z = x - x_i \tag{3.3}$$

k = stiffness coefficient of linear spring (N/m)

z = relative displacement of the system (m)

x_i = input displacement at the base (m)

The total dynamic force, $f_{ds}(t)$, generated by the fixed orifice hydraulic damper shown in Figure 3.2, consists of restoring and damping forces due to pressurized gas column and orifice flows, respectively:

$$f_{ds}(t) = f_d(t) + f_a(t) \tag{3.4}$$

f_a = restoring force due to gas-spring of the damper (N)

f_d = orifice damping force of the damper (N)

The restoring and damping forces generated by the hydraulic damper are derived in the following subsections.

3.2.2 Static Equilibrium Equations

The hydraulic pressure within the hydraulic damper corresponding to the static equilibrium is related to the static load, linear spring stiffness, and static deflection by:

$$mg = k\ X_{st} + p_0 A_r \tag{3.5}$$

where,

X_{st} = static deflection of the system (m)

p_0 = static internal pressure of hydraulic damper (Pa)

A_r = cross section area of the piston rod (m^2)

Assuming a polytropic process, the static pressure can be related to the initial charge pressure in the gas chamber III:

$$p_0 = p_a \left(V_a / V_0 \right)^{\gamma} \tag{3.6}$$

where,

p_a = initial charge pressure (Pa)

V_a = initial volume of gas chamber III (m^3)

V_0 = static volume of gas chamber III (m^3)

γ = polytropic exponent, $1 \leq \gamma \leq 1.4$, (γ=1 for isothermal process; γ=1.4 for adiabatic process)

Assuming incompressible fluid, the static deflection can be related to the change in the gas volume:

$$X_{st} = \frac{V_a - V_0}{A_r} \tag{3.7}$$

The nonlinear algebraic equations (3.5) to (3.7) are solved simultaneously using an iterative method to yield the values of the pressure, volume and deflection of the hydraulic damper corresponding to the static equilibrium position.

3.2.3 Dynamic Forces due to Hydraulic Damper

Assuming negligible seal friction, the total dynamic force generated by the hydraulic damper is determined by taking into account all the pressures acting upon the piston with respect to the static equilibrium position as:

$$f_{ds}(t) = (p_1 - p_0)\ A_p - (p_2 - p_0)(A_p + A_r) \tag{3.8}$$

where,

p_1 = instantaneous pressure in chamber I (Pa)

p_2 = instantaneous pressure in chamber II (Pa)

A_p = area of the piston on the rod side (m^2)

Define a pressure differential as:

$$p_{ij} = p_i - p_j \tag{3.9}$$

Equation (3.8) can be expressed in terms of the pressure differentials across the piston and cylinder orifices through a simple manipulation:

$$f_{ds}(t) = p_{12}\ A_p + p_{32}\ A_r - p_{30}\ A_r \tag{3.10}$$

where,

p_3 = instantaneous pressure in gas chamber III (Pa)

The pressure differentials, p_{12}, p_{32} and p_{30} in equation (3.10), can be derived from fluid flows equations and polytropic process of compressed gas, respectively, as presented in the followings.

Fluid Flow Equations

During compression and extension of the hydraulic damper, shown in Figure 3.2, the fluid flows through orifices in the piston and cylinder. Assuming incompressible fluid, the turbulent flow through the orifices can be related to the pressure differential across the orifices. For n identical orifices on the piston, the fluid flow across the piston orifices is expressed as:

$$Q_{12}(t) = n\ C_{d1}\ a_1 \sqrt{\frac{2\ |p_{12}|}{\rho}}\ \mathrm{sgn}(p_{12}) \tag{3.11}$$

where,

Q_{12} = flow rate through orifices from chamber I to II (m^3/s)

C_{d1} = discharge coefficient of piston orifice

a_1 = orifice area of piston (m^2)

ρ = mass density of fluid (kg/m^3)

$$\text{sgn}(\cdot) = \begin{cases} +1 , & (\cdot) > 0 \\ -1 , & (\cdot) < 0 \end{cases}$$

The fluid flow across the cylinder orifice is similarly expressed as:

$$Q_{32}(t) = C_{d2}\, a_2 \sqrt{\frac{2\,|p_{32}|}{\rho}}\, \text{sgn}(p_{32}) \tag{3.12}$$

where,

Q_{32} = flow rate through orifice from chamber III to II (m^3/s)

C_{d2} = discharge coefficient of cylinder orifice

a_2 = area of cylinder orifice (m^2)

The change rate of fluid volume in chamber I caused by the relative motion of the hydraulic damper is given by:

$$Q_{m1}(t) = A_p\, \dot{z}(t) \tag{3.13}$$

where,

Q_{m1} = rate of change of fluid volume in chamber I (m^3/s)

$\dot{z}$ = relative velocity of the damper (m/s)

Similarly, the change rate of fluid volume in chamber II is given by:

$$Q_{m2}(t) = (A_p + A_r)\, \dot{z}(t) \tag{3.14}$$

where,

Q_{m2} = rate of change of fluid volume in chamber II (m^3/s)

The fluid continuity condition gives the following relationships:

$$Q_{m1}(t) = Q_{12}(t) \tag{3.15}$$

$$Q_{m2}(t) = Q_{12}(t) + Q_{32}(t) \tag{3.16}$$

Pressure Equations

The pressure differentials due to the orifice flows can be obtained from the flow equations. Equations (3.11) through (3.16) yield the following expressions for pressure differentials p_{12} and p_{32}:

$$p_{12} = \frac{\rho}{2\, n^2 C_{d1}^2} \left(\frac{A_p}{a_1}\right)^2 |\dot{z}|\dot{z} \tag{3.17}$$

$$p_{32} = \frac{\rho}{2\, C_{d2}^2} \left(\frac{A_r}{a_2}\right)^2 |\dot{z}|\dot{z} \tag{3.18}$$

The instantaneous pressure of the gas chamber is determined assuming polytropic process and given by:

$$p_3 = p_0 \left(V_0 / V_3 \right)^{\gamma} \tag{3.19}$$

where,

V_3 = instantaneous volume of gas chamber III (m^3), and

$$V_3(t) = V_0 + A_r\, z(t) \tag{3.20}$$

The pressure differential p_{30} is then obtained from equations (3.19) and (3.20) as:

$$p_{30} = \left(\frac{V_0^{\gamma} - (V_0 + A_r\, z)^{\gamma}}{(V_0 + A_r\, z)^{\gamma}} \right) p_0 \tag{3.21}$$

Upon substituting equations (3.17), (3.18) and (3.21) into equation (3.10), the total dynamic force generated by the hydraulic damper is obtained as:

$$f_{ds}(z,\ \dot{z},\ t) = \frac{\rho}{2}\left[\frac{A_p}{n^2 C_{d1}^2}\left(\frac{A_p}{a_1}\right)^2 + \frac{A_r}{C_{d2}^2}\left(\frac{A_r}{a_2}\right)^2\right]|\dot{z}|\dot{z}$$

$$+ \left[\frac{(V_0 + A_r\ z)^{\gamma} - V_0^{\gamma}}{(V_0 + A_r\ z)^{\gamma}}\right] A_r\ p_0 \qquad (3.22)$$

A comparison of equations (3.4) and (3.22) reveals that the total dynamic force generated by the hydraulic damper comprises of a nonlinear orifice damping force and a nonlinear gas-spring restoring force expressed, respectively, by:

$$f_d(\dot{z},\ t) = \frac{\rho}{2}\left[\frac{A_p}{n^2 C_{d1}^2}\left(\frac{A_p}{a_1}\right)^2 + \frac{A_r}{C_{d2}^2}\left(\frac{A_r}{a_2}\right)^2\right]|\dot{z}|\dot{z} \qquad (3.23)$$

and

$$f_a(z,\ t) = \left[\frac{(V_0 + A_r\ z)^{\gamma} - V_0^{\gamma}}{(V_0 + A_r\ z)^{\gamma}}\right] A_r\ p_0 \qquad (3.24)$$

3.3 Semi-active 'On-off' Dampers

It has been established that the damping force tends to decrease the amplitude of mass acceleration only during a part of the vibration cycle, while the amplitude of mass acceleration increases in the remaining part of the cycle due to the passive damping [49, 57]. Equation (3.23) reveals that the magnitude of the damping force becomes predominant for large value of the relative velocity and thus yields poor vibration isolation performance. In order to overcome the inherent limitations of a vibration isolation system comprising of a passive damping mechanism, various semi-active 'on-off' damping mechanisms have been proposed and analyzed. Two semi-active 'on-off' control schemes

based upon directly measurable response variables, proposed by Rakheja [105] and Margolis et al. [51], have been considered practical and investigated with emphasis on applications by many other researchers [58, 52, 53].

Semi-active Control Scheme I

Rakheja [105] established that the damping force tends to attenuate the mass acceleration only when the damping force opposes the relative displacement of the vibration isolation system. Thus an 'on-off' control scheme is configured to modulate the damping force through the relative displacement of the system:

$$f_{d1} = \begin{cases} C\,|\dot{z}|\dot{z} , & \text{for } z\,\dot{z} < 0 \\ \varepsilon\,C\,|\dot{z}|\dot{z} , & \text{for } z\,\dot{z} > 0 \end{cases} \tag{3.25}$$

where,

f_{d1} = 'on-off' damping force due to control scheme I by Rakheja [105] (N)

ε = force reduction coefficient when the orifice is modulated to its maximum opening

C = orifice damping coefficient (kg/m), and given by:

$$C = \frac{\rho}{2}\left[\frac{A_p}{n^2 C_{d1}^2}\left(\frac{A_p}{a_1}\right)^2 + \frac{A_r}{C_{d2}^2}\left(\frac{A_r}{a_2}\right)^2\right] \tag{3.26}$$

Semi-active Control Scheme II

Karnopp et al. [49] established that the amplitude of mass acceleration can be reduced when the absolute velocity of the mass carries the same sign as the relative velocity across the damper. An 'on-off' damper control scheme, based upon the sign of absolute and relative velocities, has been proposed and analyzed by Margolis et al

[51]:

$$f_{d2} = \begin{cases} C\,|\dot{z}|\dot{z} , & \text{for } \dot{x}\,\dot{z} > 0 \\ \varepsilon\,C\,|\dot{z}|\dot{z} , & \text{for } \dot{x}\,\dot{z} < 0 \end{cases} \qquad (3.27)$$

where,

f_{d2} = 'on-off' damping force due to scheme II by Margolis et al. [51] (N)

The objective of these control schemes is to attain the maximum damping force from the damper when it acts to reduce the amplitude of mass acceleration, while the damping force is reduced to a minimum when it acts to increase the magnitude of mass acceleration. Such a sequential damping mechanism can be realized by implementing a two-position 'on-off' valve to a conventional hydraulic orifice damper. The 'on-off' valve utilizes feedback signals of the relative velocity and either absolute velocity or relative displacement response of the vibration isolation system. Thus, the realization of sequential damping via semi-active 'on-off' schemes requires measurement of response variables and manipulation of measured signals to generate a command signal. The time delays associated with the instrumentation package and control device often limit the performance of an 'on-off' mechanism. Moreover, an 'on-off' damping mechanism yields a significant magnitude of jerk of isolator mass around the discontinuity.

3.4 Concept of Tunable Pressure Limited Hydraulic Damper

Alternatively, variations in damping may be realized through tunable pressure relief valves, where the command signal is generated from the pressure differential p_{12}. From equations (3.17) and (3.18) it can be seen that the ratio of pressure differentials p_{32} and p_{12} is a

constant:

$$\frac{p_{32}(t)}{p_{12}(t)} = \left(\frac{C_{d1}}{C_{d2}} \frac{na_1}{a_2} \frac{A_r}{A_p}\right)^2 = \text{constant} \qquad (3.28)$$

From equations (3.17), (3.18), (3.23) and (3.28), the damping force of the hydraulic damper can be expressed as a proportional function of pressure differential p_{12} alone:

$$f_d(t) = \alpha\, p_{12}(t) \qquad (3.29)$$

where

α = damping force coefficient (m^2), given by:

$$\alpha = A_p + \left(\frac{C_{d1}}{C_{d2}}\right)^2 \left(\frac{na_1}{a_2}\right)^2 \left(\frac{A_r}{A_p}\right)^2 A_r \qquad (3.30)$$

From equations (3.17) and (3.29) it is evident that the pressure differential p_{12} and thus the damping force is dependent upon the square of relative velocity across the hydraulic damper. For a constant amplitude of excitation, the magnitude of the damping force becomes predominant at high excitation frequencies and thus yields poor vibration isolation performance. The vibration isolation performance of the system employing such hydraulic damper can be improved by limiting the magnitude of damping force at high excitation frequencies. Equation (3.29) reveals that the damping force can be conveniently limited by limiting the pressure differential p_{12}. Thus a sequential damper similar to a semi-active damper can be achieved by using a pressure limiting valve with a tunable preset limiting value $(p_{12})_0$. Assuming the effects of the relief valve dynamics to be negligible, an ideal control scheme of the tunable pressure limited hydraulic damper can be expressed as:

$$f_{d3} = \begin{cases} \alpha\, p_{12}\,, & |p_{12}| < (p_{12})_0 \\ \alpha\, (p_{12})_0 \mathrm{sgn}(p_{12}), & \text{otherwise} \end{cases} \tag{3.31}$$

where,

f_{d3} = damping force of tunable pressure limited damper (N)

$(p_{12})_0$ = tunable preset pressure limiting value (Pa)

The control scheme in equation (3.31) can be realized by configuring a hydraulic damper with tunable pressure relief valves, as shown in Figure 3.3. The compression and extension relief valves, used across the piston, limit the pressure differential across the piston to a preset limiting value $(p_{12})_0$. When the magnitude of the pressure differential p_{12} is less than the preset limiting value $(p_{12})_0$ of the relief valves, the relief valves remain closed and thus the shock absorber acts as a conventional one. However, when the magnitude of the pressure p_{12} exceeds the preset value $(p_{12})_0$, the relief valve opens. The damping force is then reduced by permitting the fluid flow through the open relief valves. It can be seen that variable damping characteristics can be realized entirely passively, using the above control scheme. The proposed scheme does not require any instrumentation package which semi-active systems require. As shown in Figure 3.3, the pressure relief valves can be appropriately tuned to yield desirable damping characteristics for different base excitations. The tunable limiting pressure is obtained by setting the overlap displacement of the mechanism (Y_0), and the suitable spring rate of the valve can be selected to make the pressure-velocity relationship close to that of the ideal control scheme.

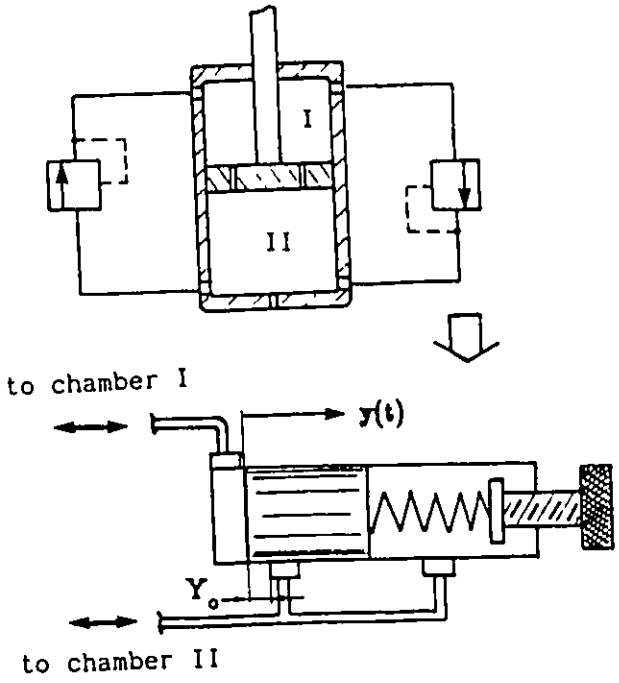

FIGURE 3.3 Schematic of a tunable pressure limited hydraulic damper with two relief valves

3.5 Damping Characteristics of Tunable Pressure Limited Damper

In order to evaluate the damping characteristics of the proposed hydraulic damper, a damping parameter β is defined as the ratio of the damping force f_d to the linear critical damping force of a single degree of freedom vibration isolation system as follows:

$$\beta = f_d \,/\, (2\sqrt{mk}\ |\dot{z}|) \tag{3.32}$$

β = damping parameter

For a linear passive vibration isolation system the damping parameter is simply the damping ratio of the system. However, for nonlinear dampers, the damping parameter is no longer a constant.

Fixed Orifice Hydraulic Damper

From equations (3.17), (3.29) and (3.32), the damping parameter of a fixed orifice passive hydraulic damper is obtained as:

$$\beta = \frac{\alpha}{2\sqrt{mk}} \left(\frac{\rho}{2\ n^2 C_{d1}^2}\right)\left(\frac{A_p}{a_1}\right)^2 |\dot{z}| \tag{3.33}$$

where β is the damping parameter of a fixed orifice damper. Equation (3.33) shows that the damping parameter of the conventional orifice damper is proportional to the magnitude of relative velocity.

Tunable Pressure Limited Hydraulic Damper

The damping parameter of an ideal tunable pressure limited hydraulic damper can be obtained from equations (3.31) and (3.32):

$$\beta = \begin{cases} \dfrac{\alpha}{2\sqrt{mk}} \left(\dfrac{\rho}{2\ n^2 C_{d1}^2}\right)\left(\dfrac{A_p}{a_1}\right)^2 |\dot{z}| \ , & |p_{12}| < (p_{12})_0 \\ \alpha\ (p_{12})_0 \,/\, (2\sqrt{mk}\ |\dot{z}|) \ , & \text{otherwise} \end{cases} \tag{3.34}$$

Equation (3.34) reveals that the damping parameter of the tunable pressure limited hydraulic damper is proportional to the magnitude of the relative velocity response, when $|p_{12}|<(p_{12})_0$, as in the case of a conventional hydraulic orifice damper. However, as the relative velocity response increases, the pressure differential p_{12} exceeds the limiting value of $(p_{12})_0$. The pressure relief valves open to limit the pressure differential p_{12} around the preset pressure $(p_{12})_0$, and the corresponding damping parameter is therefore obtained as inversely proportional to the magnitude of the relative velocity response.

3.6 Tuning Methodology

In view of vibration isolation performance, it is desirable to achieve a high value of damping parameter around the resonant frequency such that the resonant peak can be appropriately controlled. On the other hand, it is also desirable to produce a low value of damping parameter at high excitation frequencies to isolate the mass effectively. The modified hydraulic damper with tunable damping characteristics, expressed in equation (3.34), can meet the above requirements for effective isolation of the mass from base excitations.

An initial estimate of the preset limiting pressure $(p_{12})_0$ can be obtained from the linear system's response. For a base excited single degree-of-freedom vibration isolator, the maximum value of equivalent damping parameter β_{eq} (ratio of linear damping coefficient to the critical damping coefficient) is determined in view of the resonant response. The damping ratio can be related to the relative velocity response corresponding to the vibration isolator's resonance in the

following manner:

$$\beta_{eq}|_{\omega=\omega n} = |\dot{x}_1| / 2|\dot{z}| \qquad (3.35)$$

where,

$\beta_{eq}|_{\omega=\omega n}$ = equivalent damping parameter at resonance

ω = angular frequency (rad/s)

ω_n = angular undamped natural frequency of the isolator (rad/s)

In order to realize an appropriate control of the resonant peak, the minimum value of limiting pressure corresponding to the natural frequency is thus obtained from equations (3.34) and (3.35):

$$(p_{12})_0|_{\omega=\omega n} = k\ X_1 / \alpha \qquad (3.36)$$

$(p_{12})_0|_{\omega=\omega n}$ = limiting pressure value at resonance (Pa)

X_1 = amplitude of base excitation (m)

In order to achieve effective vibration isolation the limiting pressure is selected as:

$$(p_{12})_0 = \nu\ (k\ X_1 / \alpha) \qquad (3.37)$$

where,

ν = tuning factor of pressure limited hydraulic damper

The ratio of pressure differential p_{12} to the static pressure p_0 is established for various values of pressure limiting factors ν, assuming an ideal pressure limiting control scheme. The pressure ratio characteristics of the hydraulic damper are presented against the non-dimensional relative velocity response, as shown in Figure 3.4. It can be seen that the pressure differential of a fixed orifice passive hydraulic damper increase parabolically with respect to the relative velocity response. In case of a tunable pressure limited hydraulic

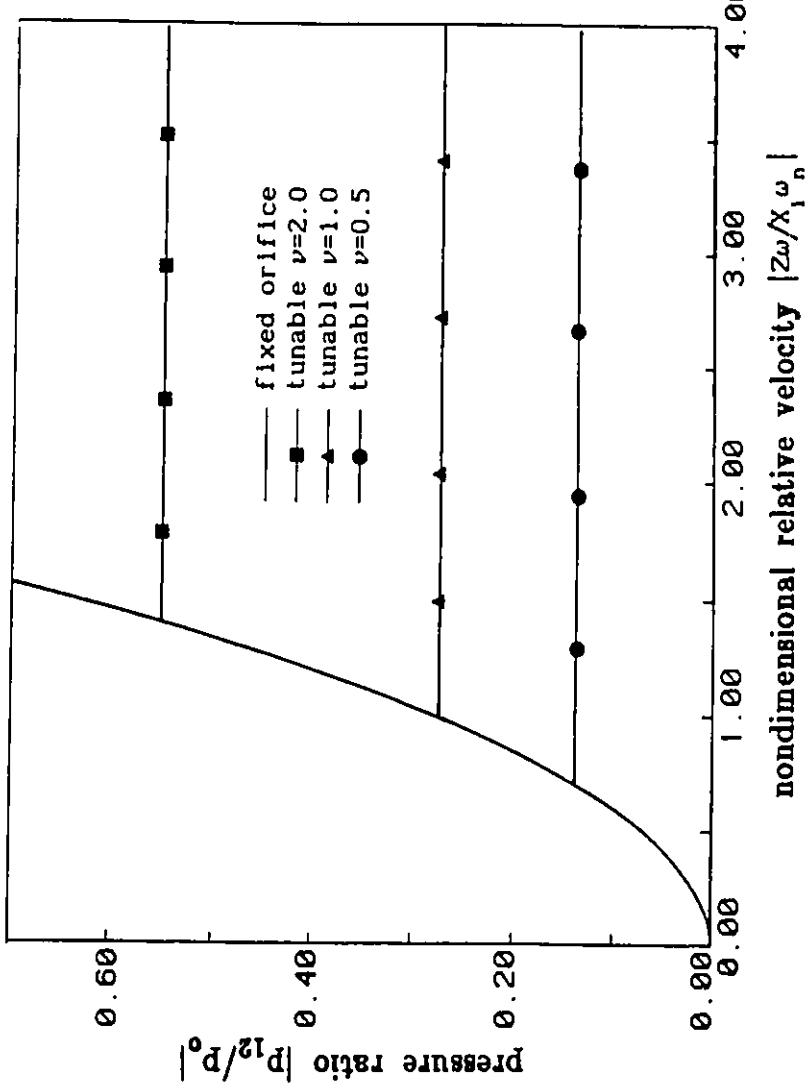

FIGURE 3.4 Pressure differential characteristics of a tunable pressure limited damper with respect to relative velocity

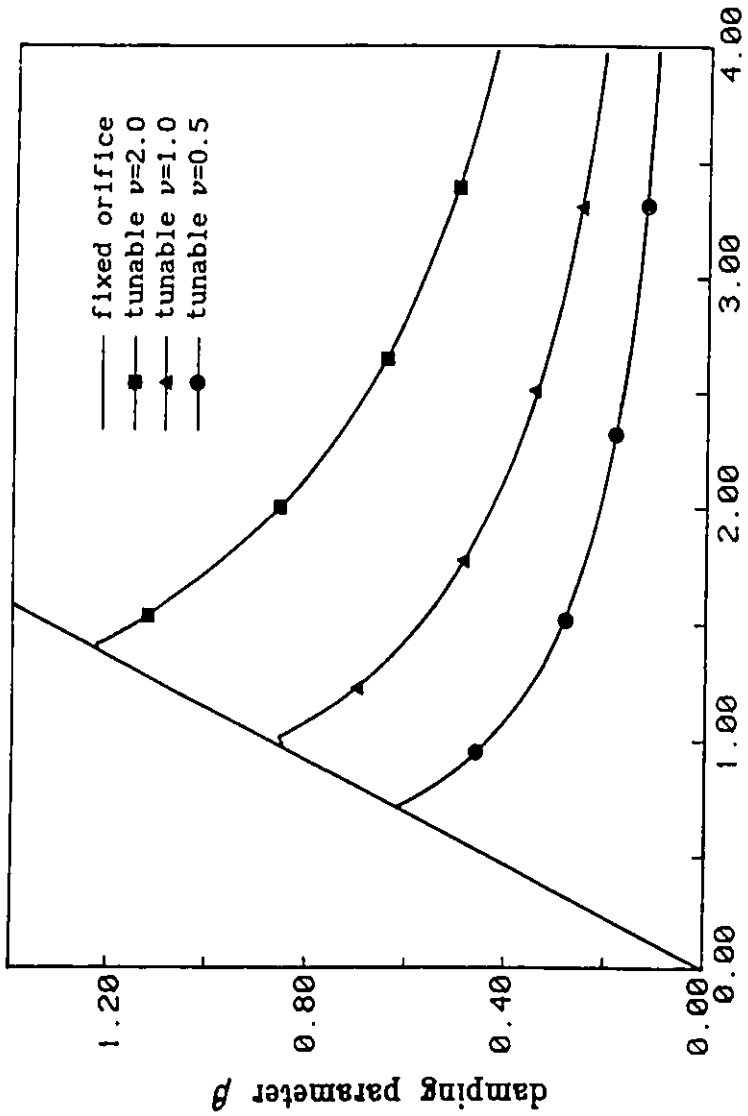

FIGURE 3.5 Damping characteristics of a tunable pressure limited damper with respect to relative velocity

damper the pressure differential increases parabolically corresponding to low relative velocity response until it approaches the limiting pressure value. The pressure differential p_{12} is, however, held around limiting value $(p_{12})_0$ as the relative velocity response increases. The pressure differential characteristics of the tunable pressure limited hydraulic damper are directly related to the tuning factor ν as shown in Figure 3.4. The corresponding damping parameters of both fixed orifice and tunable pressure limited dampers, computed from equations (3.33) and (3.34), are presented in Figure 3.5. It can be observed that the damping parameter of a fixed orifice passive hydraulic damper increases linearly with the relative velocity response. The damping parameter of a tunable pressure limited hydraulic damper is identical to that of a fixed orifice passive damper corresponding to low values of relative response. However, as the relative velocity response increases, the pressure differential across the piston is limited to $(p_{12})_0$, and the damping parameter is then obtained as inversely proportional to the relative velocity response, as shown in Figure 3.5. An ideal tunable pressure limited damper thus yields a peak damping parameter when p_{12} approaches $(p_{12})_0$ and the damping parameter decreases due to the open of relief valves.

The damping characteristics of an ideal tunable hydraulic damper are further investigated for a base excited SDOF vibration isolation system shown in Figure 3.1 (b). Figure 3.6 presents the pressure differential characteristics of a SDOF vibration isolation system with fixed orifice and tunable pressure limited damper, subjected to constant amplitude harmonic base excitations. The pressure differential p_{12} of

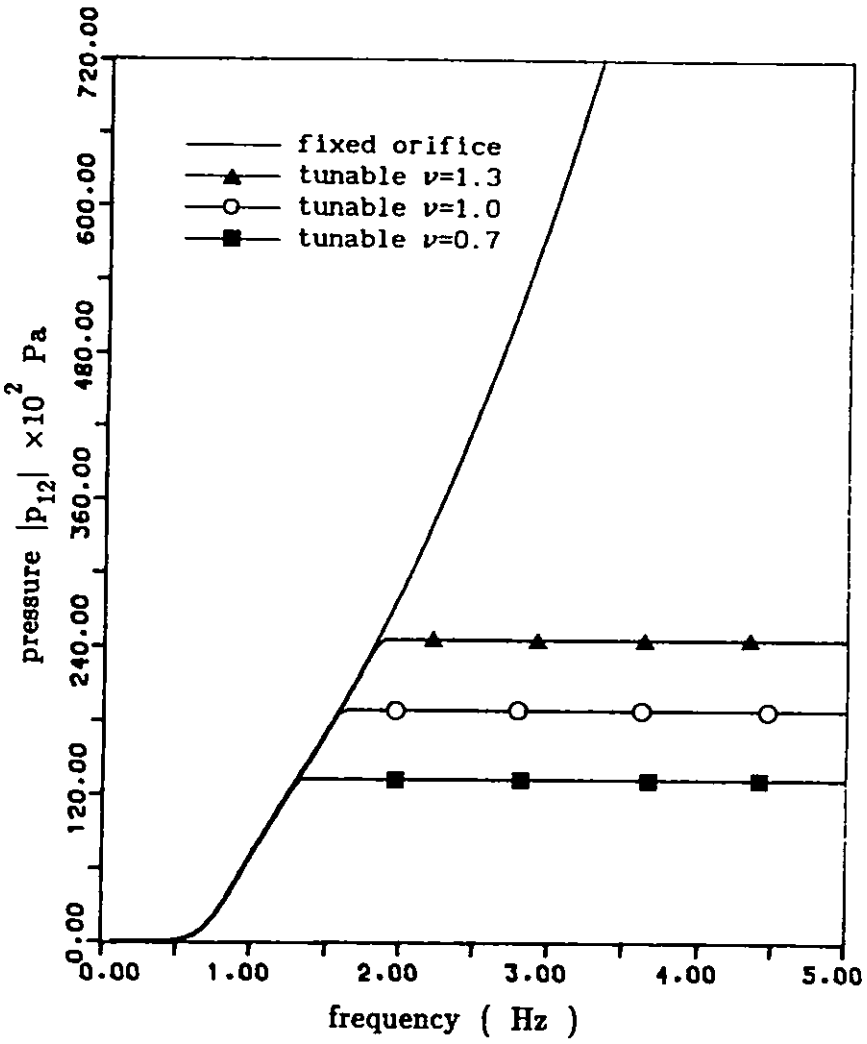

FIGURE 3.6 Pressure differential characteristics of a tunable pressure limited damper system with respect to excitation frequency

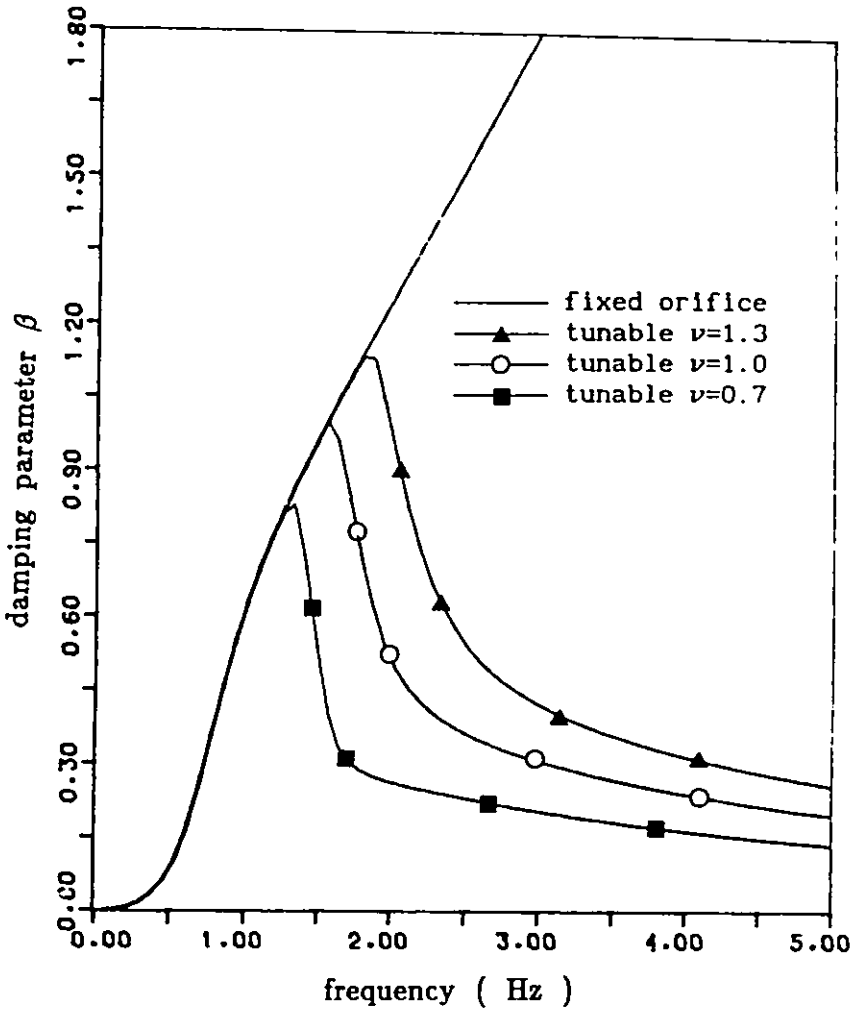

FIGURE 3.7 Damping characteristics of a tunable pressure limited damper system with respect to excitation frequency

the fixed orifice damper increases very rapidly with increase in excitation frequency. However, the pressure differential p_{12} of the tunable pressure limited damper is held around the $(p_{12})_0$ as the excitation frequency is increased. The value of pressure differential p_{12} at high excitation frequency is determined by the tuning factor ν of the pressure limited hydraulic damper as shown in Figure 3.6. The damping characteristics of the fixed orifice and the tunable pressure limited dampers are presented in Figure 3.7. It is observed that the damping parameter of the pressure limited damper is identical to that of the fixed orifice damper at low excitation frequencies. However, at higher excitation frequencies, the pressure differential p_{12} exceeds the preset pressure and the damping parameter decreases due to flows through the open relief valves. The damping characteristics of the modified damper can thus be tuned by selecting the tuning factor ν as shown in Figure 3.7. It is observed that a lower value of tuning factor ν causes the relief valves to start to open at a lower excitation frequency, and to result in more reduction in the damping value, and vice versa. In order to achieve high damping at resonance and low damping at higher excitation frequencies, the selection of the tuning factor of a tunable pressure limited hydraulic damper, therefore, is of importance for both effective resonant vibration control and vibration isolation.

3.7 Vibration Isolation Characteristics of Tunable Pressure Limited Hydraulic Damper

The nonlinear differential equation (3.1) is solved in conjunction with equations (3.3), (3.22), (3.25), (3.27), (3.31) and (3.37) for harmonic and rounded step displacement excitations to evaluate the

vibration and shock isolation performance of the vibration isolation system employing fixed orifice, tunable pressure limited and semi-active 'on-off' dampers. The equation of motion is solved using a numerical integration technique and the corresponding simulation parameters are listed in Table 3.1. The vibration and shock isolation characteristics of the ideal tunable pressure limited hydraulic damper are presented and discussed in relation with those of the fixed orifice passive and ideal semi-active 'on-off' dampers in this and the next sections.

The vibration isolation performance of the system employing tunable pressure limited hydraulic damper is evaluated in terms of the following two characteristics of the system and compared with those of the semi-active 'on-off' and fixed orifice passive dampers:

1) steady state harmonic response;

2) vibration transmissibility.

Steady State Harmonic Response

The steady state time history of mass acceleration response is obtained for the vibration isolation system employing the tunable pressure limiting hydraulic damper and two semi-active 'on-off' isolators, when subject to harmonic base excitation.

The non-dimensional steady state acceleration response ($\ddot{x}/X_1\omega^2$) of the mass corresponding to excitation frequency $\omega = \omega_n$ is presented in Figure 3.8. It is observed that the amplitudes of mass acceleration response of vibration isolation system employing all the three dampers are almost identical. However, the acceleration response characteristics of vibration isolation system with both semi-active 'on-off' dampers exhibit discontinuities at the time of switching, and the acceleration

TABLE 3.1

Simulation Parameters of Tunable Pressure Limited Hydraulic Damper System

SYMBOL	DESCRIPTION	PARAMETER VALUE
m	Mass of the system	65 kg
k	Stiffness coefficient	4000 N/m
ρ	Mass density of fluid	797 kg/m^3
A_p	Area of piston on rod side	2.03×10^{-3} m^2
A_r	Area of rod cross section	1.27×10^{-4} m^2
C_{d1}, C_{d2}	Discharge coefficient	0.7
a_1	Orifice area of piston	1.35×10^{-5} m^2
a_2	Orifice area of cylinder	1.35×10^{-5} m^2
γ	Polytropic exponent	1.4
p_{at}	Atmospheric pressure	101300 Pa
p_a	Initial charge pressure	15×10^5 Pa
V_a	Initial gas volume	2.8×10^{-4} m^3
n	Number of orifices on piston	4
X_1	Input amplitude	0.05 m

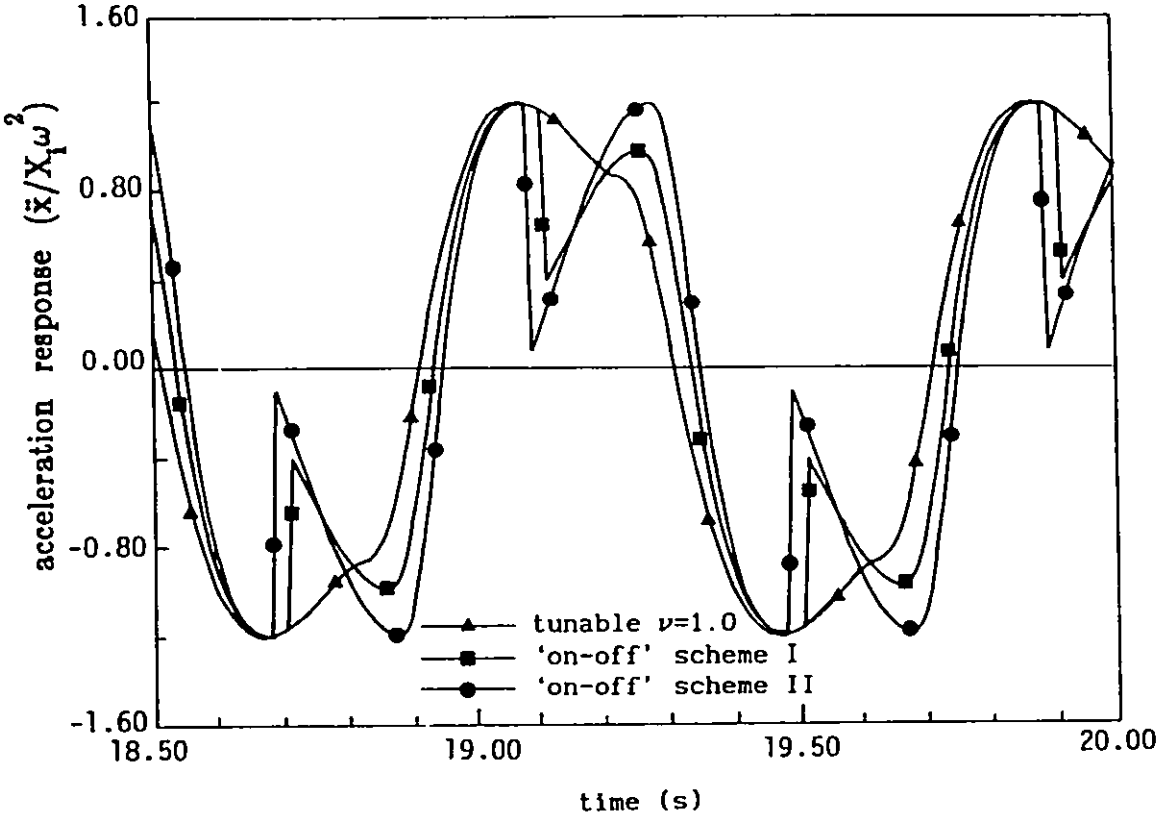

FIGURE 3.8 Comparison of steady state acceleration response of mass with tunable damper, 'on-off' scheme I and 'on-off' scheme II, at $\omega/\omega_n=1$

response discontinuity associated with semi-active 'on-off' scheme II is more severe than that of scheme I. Such discontinuities in acceleration give rise to jerk of the system mass. The tunable pressure limited hydraulic damper, on the other hand, provides sequential damping by limiting the maximum value of damping and the acceleration response does not exhibit any discontinuities.

As the excitation frequency is increased, the amplitude of the orifice damping force increases considerably (as shown in Figure 3.6). At excitation frequency $\omega/\omega_n = 3.0$, steady state acceleration response of the vibration isolation system employing semi-active 'on-off' damper I, semi-active 'on-off' damper II and the tunable pressure limited hydraulic damper, are presented in Figures 3.9, 3.10 and 3.11, respectively. It can be seen from Figure 3.9 that the semi-active 'on-off' damper using control scheme I does not yield a discontinuity of the acceleration response at $\omega/\omega_n = 3.0$. However, the control scheme I results in an unsymmetrical acceleration response about the static equilibrium position leading to a drift in the displacement response. The non-dimensional maximum acceleration response value of the semi-active 'on-off' vibration isolator using the control scheme I, which is the acceleration transmissibility at excitation frequency $\omega/\omega_n = 3.0$, is found to be 0.711.

The time history of harmonic steady state acceleration response of the SDOF vibration isolation system using semi-active 'on-off' damper II at excitation frequency $\omega/\omega_n = 3.0$, is presented in Figure 3.10. The non-dimensional maximum acceleration response value of the vibration isolator, at excitation frequency $\omega/\omega_n = 3.0$, with semi-active 'on-off'

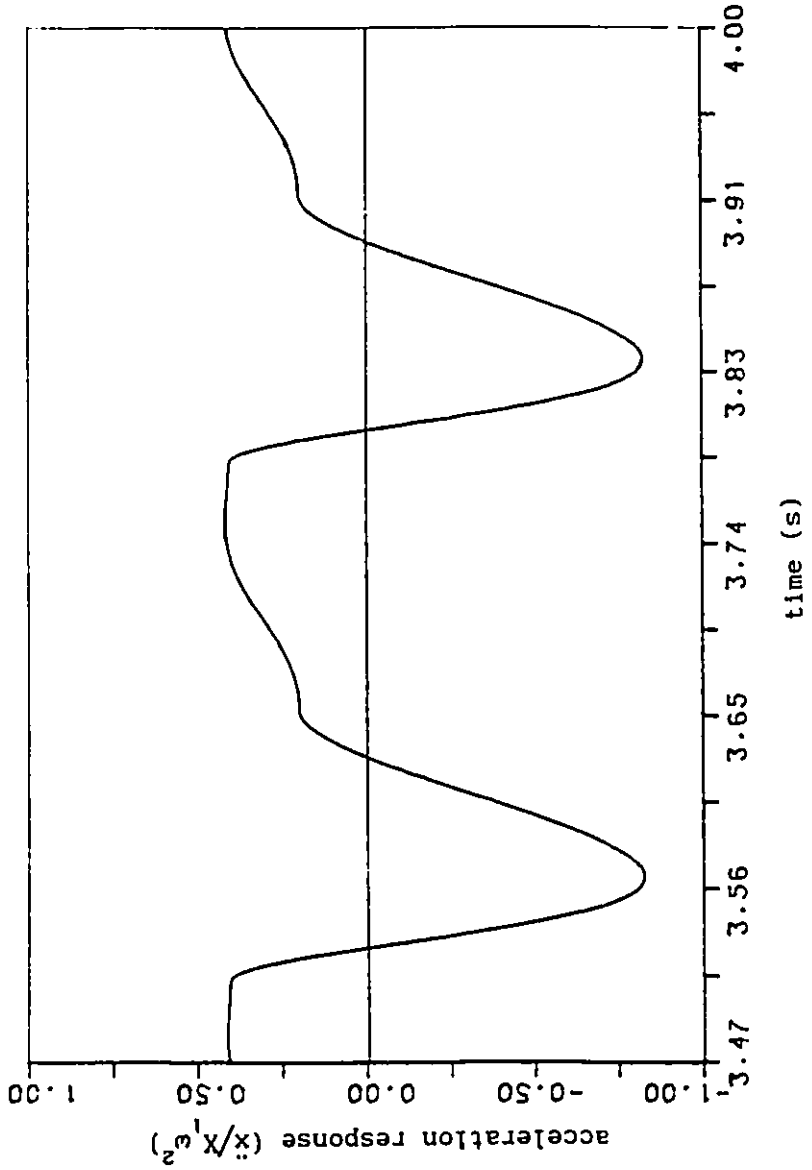

FIGURE 3.9 Steady state acceleration response of mass with semi-active 'on-off' damper I, at $\omega/\omega_n=3$

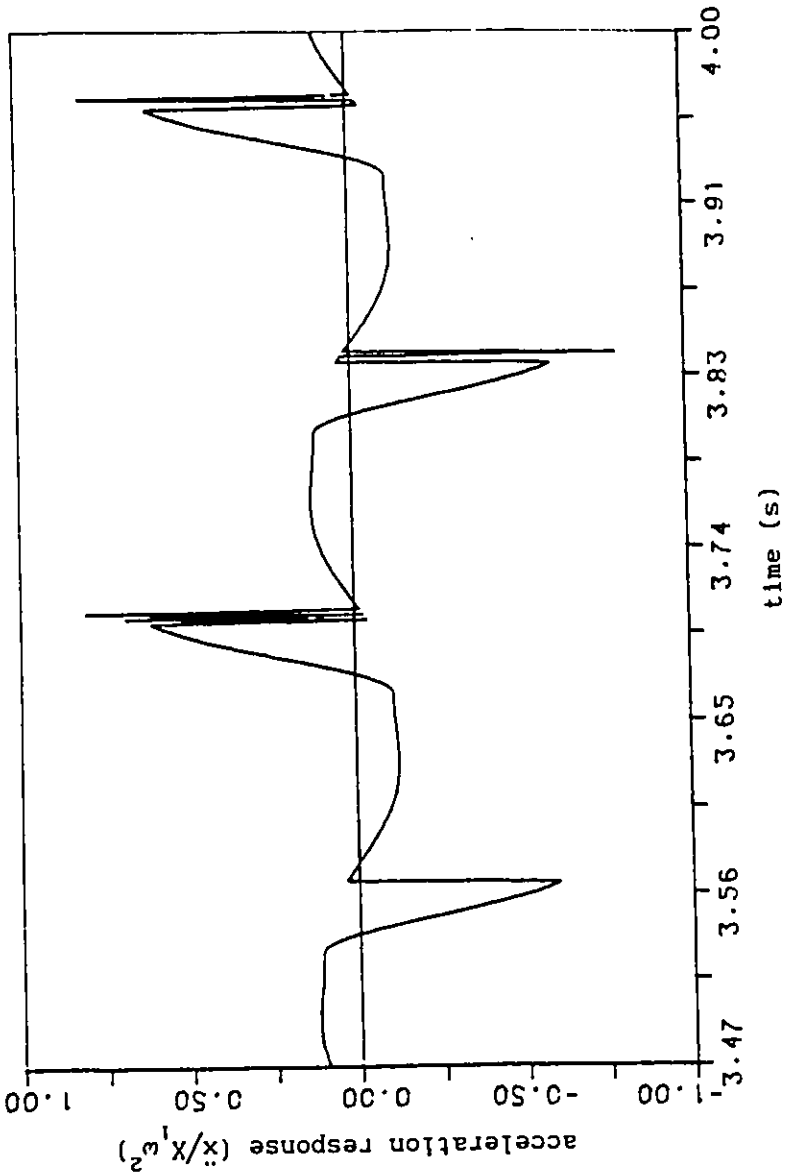

FIGURE 3.10 Steady state acceleration response of mass with semi-active 'on-off' damper II, at $\omega/\omega_n=3$

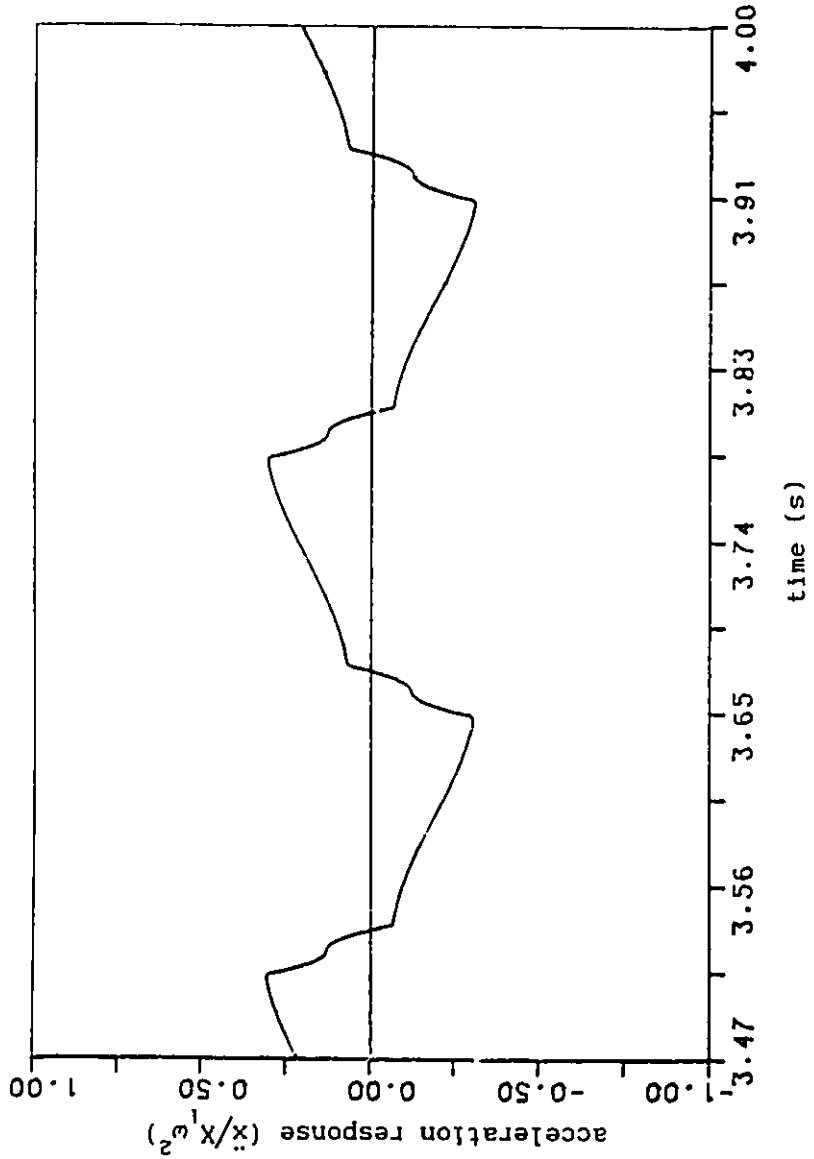

FIGURE 3.11 Steady state acceleration response of mass with tunable pressure limited damper, at $\omega/\omega_n = 3$

scheme II is found to be 0.79 and larger than that of the 'on-off' scheme I, while the area covered by the acceleration response, which is related to velocity transmissibility, due to semi-active 'on-off' scheme II is smaller than that of 'on-off' scheme I. It is obvious that the jerk introduced by the inherent discontinuous behavior of the semi-active 'on-off' damper II becomes even more severe, as the excitation frequency is increased. The chatter and extremely large jerk caused by semi-active 'on-off' scheme II deteriorates the performance of the semi-active 'on-off' damper [59].

Figure 3.11 presents the steady state acceleration response of the vibration isolation system employing a tunable pressure limited hydraulic damper at frequency $\omega/\omega_n = 3.0$. The non-dimensional maximum acceleration response value of the vibration isolator using a tunable damper at excitation frequency $\omega/\omega_n = 3.0$ is found to be 0.31 and the smallest one among the three dampers. Although the acceleration response does not appear to be very smooth due to the pressure limiting, the acceleration response of the tunable damper system is observed to be continuous. The jerk and the chatter caused by the 'on-off' type of sequential dampers can thus be eliminated by the proposed pressure limited hydraulic damper.

Vibration Transmissibility

The vibration transmissibility is obtained by computing the ratio of the amplitude of steady state response to that of harmonic base excitation, over the frequency range of interest. The transmissibility characteristics of the SDOF vibration isolation system using fixed orifice, tunable pressure limited and semi-active 'on-off' (based on

scheme II) dampers are evaluated via computer simulation. The response characteristics of the tunable damper are also presented for various values of tuning factors to illustrate the influence of the tuning parameter on the vibration isolation performance.

The displacement and velocity transmissibility characteristics of the vibration isolation system employing an ideal tunable pressure limited hydraulic damper (ν=1), a fixed orifice damper and an ideal semi-active 'on-off' damper are presented in Figures 3.12 and 3.13, respectively. It is obvious that the displacement, velocity and acceleration response transmissibilities of a nonlinear system are no longer identical as in the case of a linear system. A comparison of the response characteristics shows that the vibration isolation performance of the tunable pressure limited and 'on-off' dampers is superior to that of the fixed orifice damper. However, the peak velocity transmissibility of the 'on-off' damper is slightly deteriorated, while the peak transmissibility of the modified tunable damper is identical to that of the fixed orifice damper. The vibration isolation characteristics of the 'on-off' damper is superior to that of both fixed orifice and tunable dampers beyond the natural frequency. However, as the excitation frequency is further increased, the tunable pressure limited damper yields better vibration isolation performance than that of the 'on-off' damper.

The displacement, velocity and acceleration transmissibility characteristics of the isolator employing ideal tunable pressure limited hydraulic damper, corresponding to different values of the tuning factor ν, are compared with those of the isolator using fixed orifice damper,

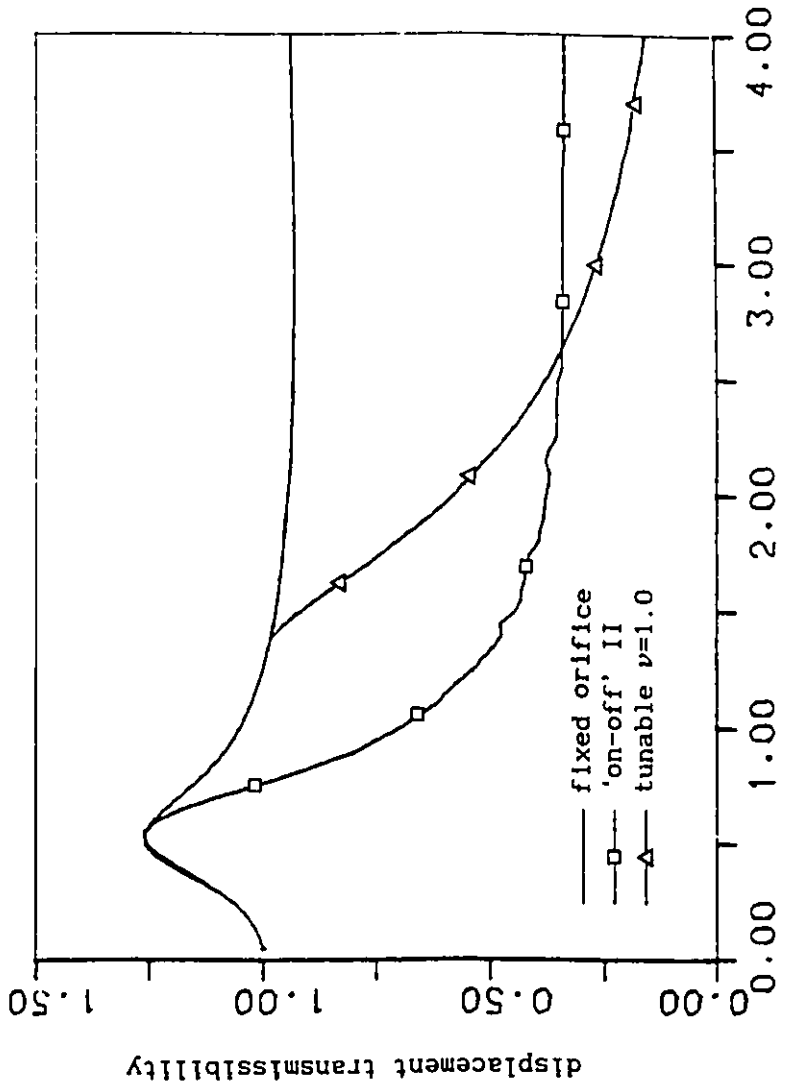

FIGURE 3.12 Displacement transmissibility of vibration isolation system employing tunable damper, 'on-off' dampers I and II

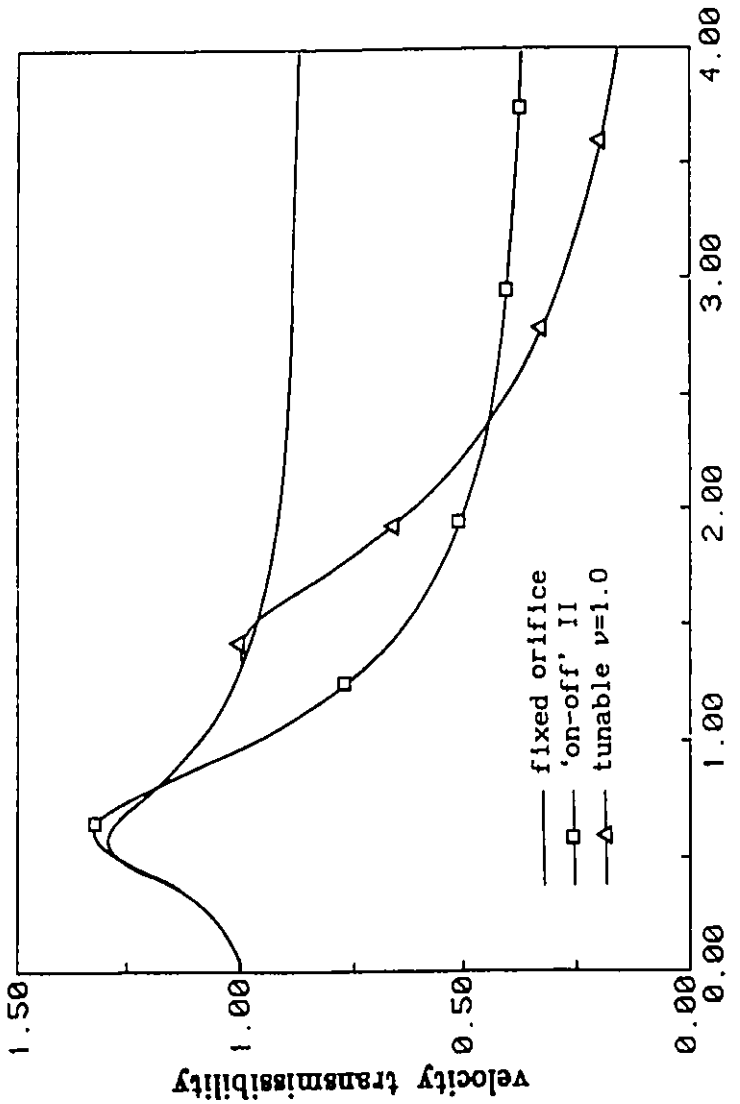

FIGURE 3.13 Velocity transmissibility of vibration isolation system employing tunable and semi-active 'on-off' dampers

as shown in Figures 3.14, 3.15 and 3.16, respectively. The transmissibility characteristics of the tunable damper are identical to that of the fixed orifice damper at low excitation frequencies. The ideal tunable damper continues to dissipate energy identical to that of fixed orifice damper around the natural frequency, and thus the resonant transmissibility ratios of both fixed and tunable dampers are identical. As the excitation frequency is increased, the pressure differential p_{12} increases due to the increase in relative velocity response. The pressure relief valve is thus opened to limit the pressure differential and thus the damping force around a constant value. At high excitation frequencies the vibration isolation performance of the tunable pressure limited damper is improved considerably for all values of pressure limiting factor within $0.8<\nu<1.5$, as shown in Figures 3.14 to 3.16.

From the simulation results, it is apparent that the vibration isolation performance beyond the natural frequency is strongly dependent upon the frequency at which pressure limitation occurs. A lower value of pressure tuning factor yields an improved vibration isolation performance corresponding to high frequency excitations. However, an extremely low value of tuning factor ν may result in a large transmissibility response when pressure differential approaches the limiting value, as shown in Figure 3.17. A low value of pressure tuning factor (ν=0.5) yields low damping near resonance and thus exhibits an excessively large transmissibility response, as shown in Figure 3.17. This peak can be suppressed by properly tuning the pressure limiting value according to the method presented in section 3.6. In order to make pressure limiting value greater than the minimum value given in equation

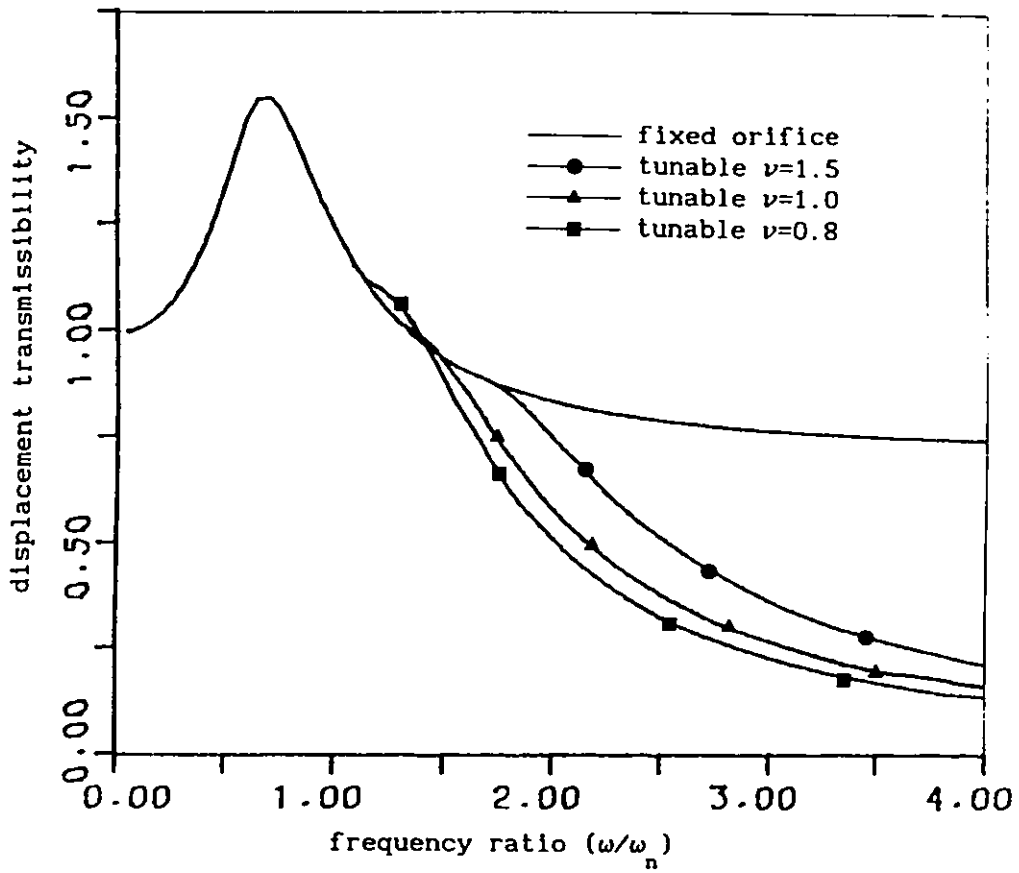

FIGURE 3.14 Displacement transmissibility of vibration isolation system employing tunable damper with various values of tuning factor

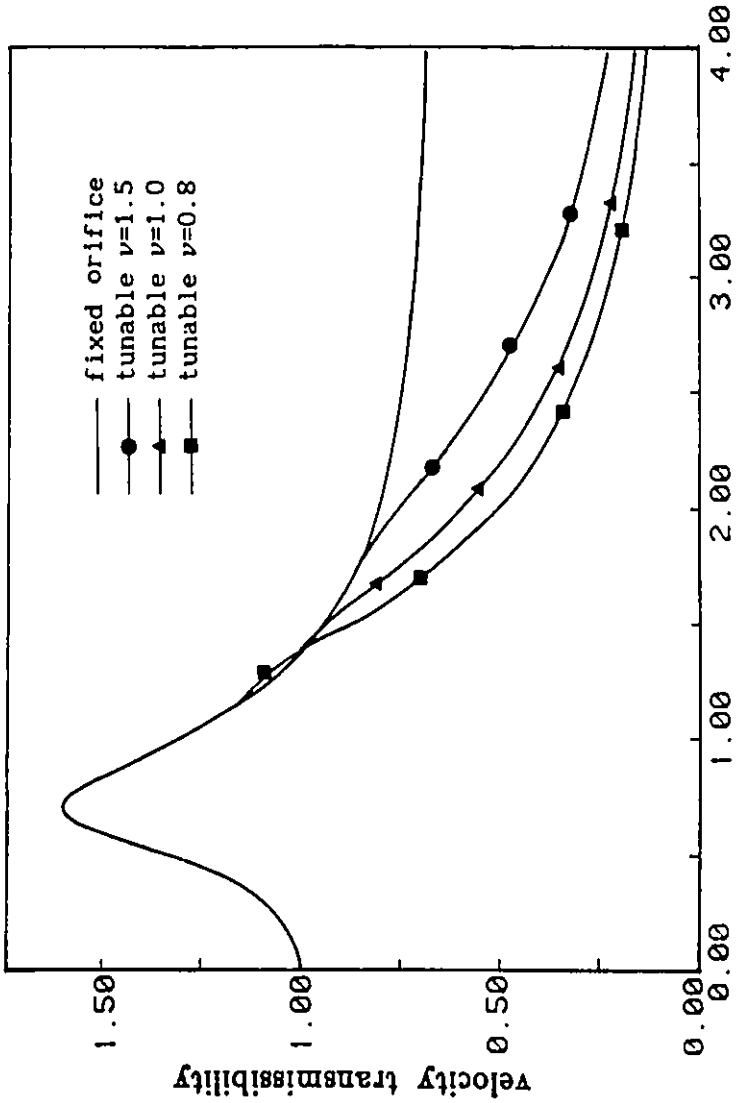

FIGURE 3.15 Velocity transmissibility of vibration isolation system employing tunable damper with various values of tuning factor

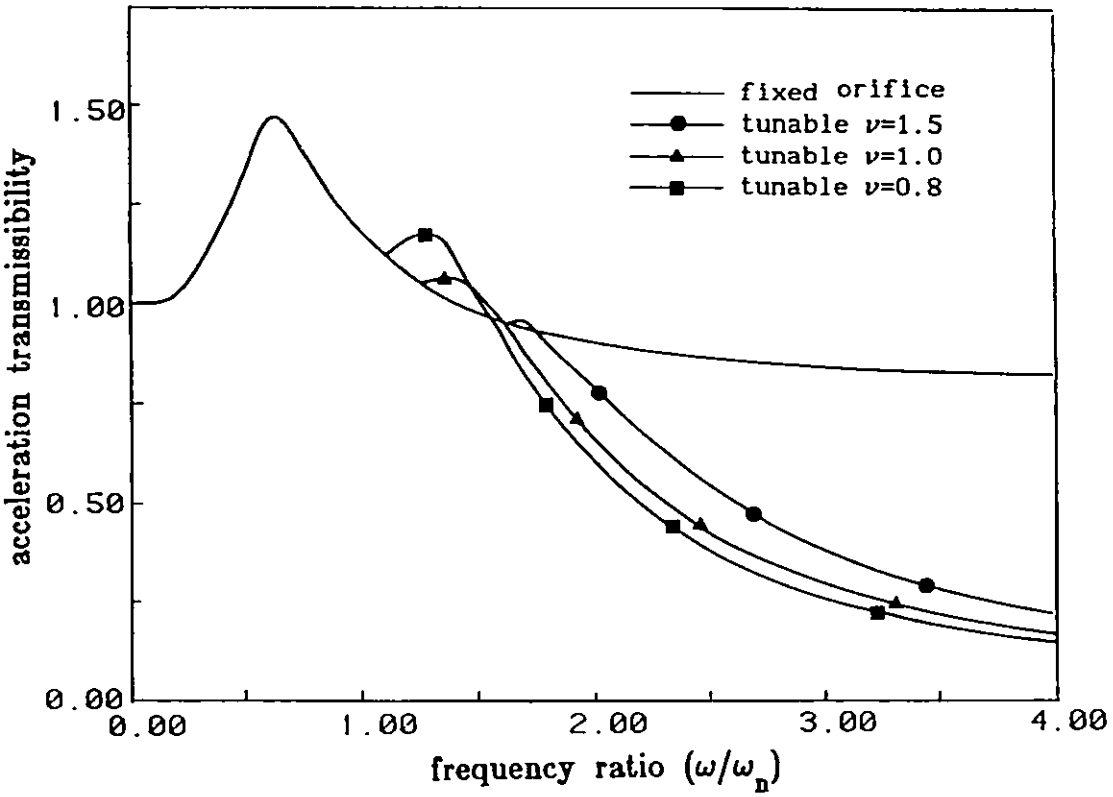

FIGURE 3.16 Acceleration transmissibility of vibration isolation system employing tunable damper with various values of tuning factor

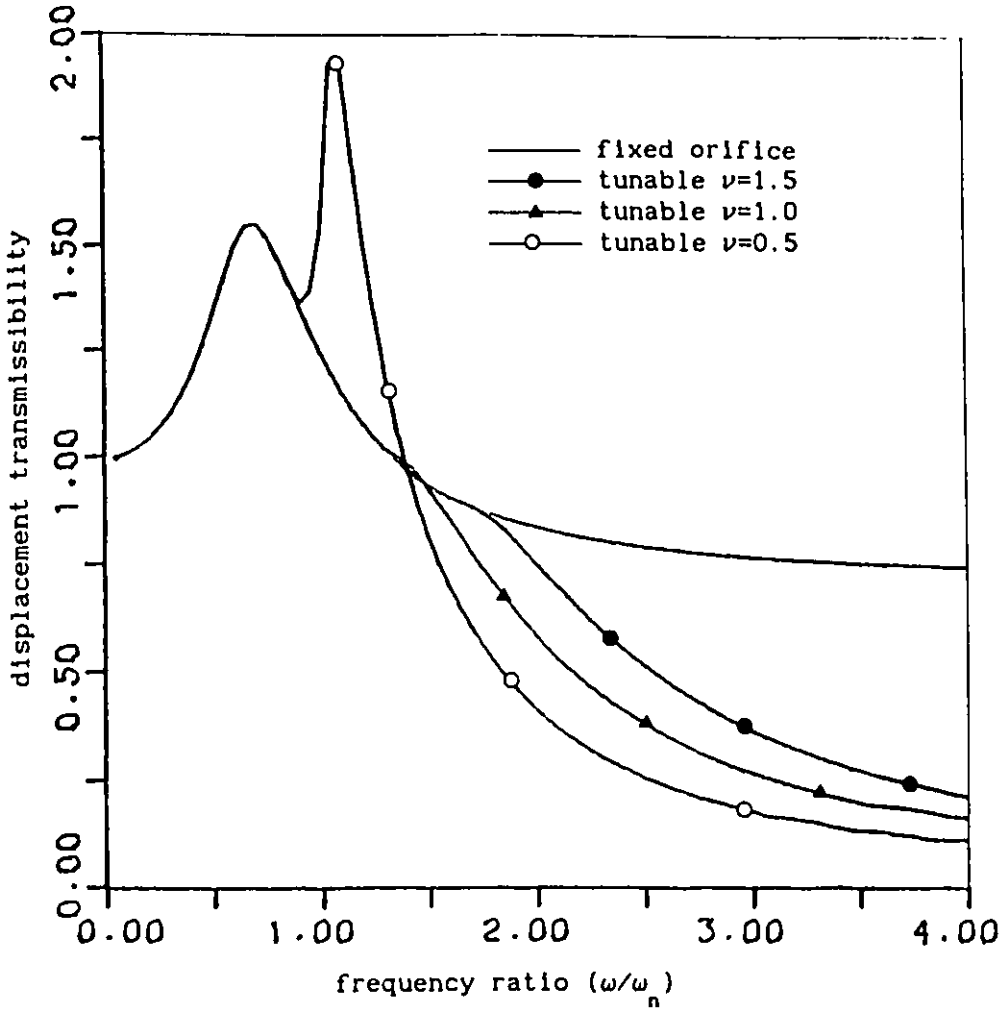

FIGURE 3.17 Displacement transmissibility of vibration isolation system employing tunable damper with various values of tuning factor

(3.36), the pressure tuning factor should be selected such that the pressure differential approaches the limiting value at excitation frequencies near $\sqrt{2}\ \omega_n$.

3.8 Shock Isolation Characteristics of Tunable Pressure Limited Hydraulic Damper

The shock isolation performance of the tunable pressure limited hydraulic damper is investigated for a rounded step displacement excitation at the base expressed as [60]:

$$x_1(t) = X_{max} \left(1 - e^{-\eta\ \omega_n t} (1 + \eta\ \omega_n t) \right) \tag{3.38}$$

where,

X_{max} = maximum value of the step displacement (m)

e = 2.71828

η = shock severity parameter

The corresponding velocity and acceleration excitation are given as the following, respectively:

$$\dot{x}_1(t) = (X_{max}\ \omega_n) \left(\eta\ e^{-\eta\ \omega_n t} (\eta\ \omega_n t) \right) \tag{3.39}$$

$$\ddot{x}_1(t) = (X_{max}\ \omega_n^2) \left(\eta^2\ e^{-\eta\ \omega_n t} (1 - \eta\ \omega_n t) \right) \tag{3.40}$$

The shock isolation performance characteristics of the system, employing fixed orifice, the ideal tunable pressure limited, and the ideal semi-active 'on-off' dampers, are evaluated in terms of their responses to the rounded step input in the time domain and with respect to the shock severity parameter, respectively. The transient time history response characteristics of the system with these dampers are presented in terms of their displacement, velocity, acceleration and

relative displacement response ratios defined as:

$$\text{displacement response ratio} = x(t) \,/\, X_{max} \tag{3.41}$$

$$\text{velocity response ratio} = \dot{x}(t) \,/\, (X_{max}\, \omega_n) \tag{3.42}$$

$$\text{acceleration response ratio} = \ddot{x}(t) \,/\, (X_{max}\, \omega_n^2) \tag{3.43}$$

$$\text{relative displacement ratio} = z(t) \,/\, X_{max} \tag{3.44}$$

The transient response characteristics of the vibration isolator employing a tunable pressure limited damper to the rounded step displacement excitation with shock severity parameter η=10, are compared with those of the fixed orifice and the semi-active 'on-off' dampers, as shown in Figures 3.18 to 3.21, respectively. Figure 3.18 shows the displacement response ratios of the vibration isolator employing fixed orifice, tunable pressure limited, and two semi-active 'on-off' dampers. It is observed that the fixed orifice damper yields the largest peak displacement response value. While the displacement response of the tunable pressure limited damper is almost identical to that of the semi-active 'on-off' damper II and has the smallest peak value. The displacement response of 'on-off' damper I is improved as compared with that of the fixed orifice passive one and has a slightly larger peak value as compared with that of the tunable damper and 'on-off' damper II. The velocity and acceleration response ratios of those dampers are presented in Figure 3.19 and 3.20, respectively. A comparison of the response characteristics reveals that the tunable pressure limited and two semi-active 'on-off' dampers yield a superior performance to that of fixed orifice damper, in terms of peak response values. It is observed that the velocity and acceleration response ratios of the tunable

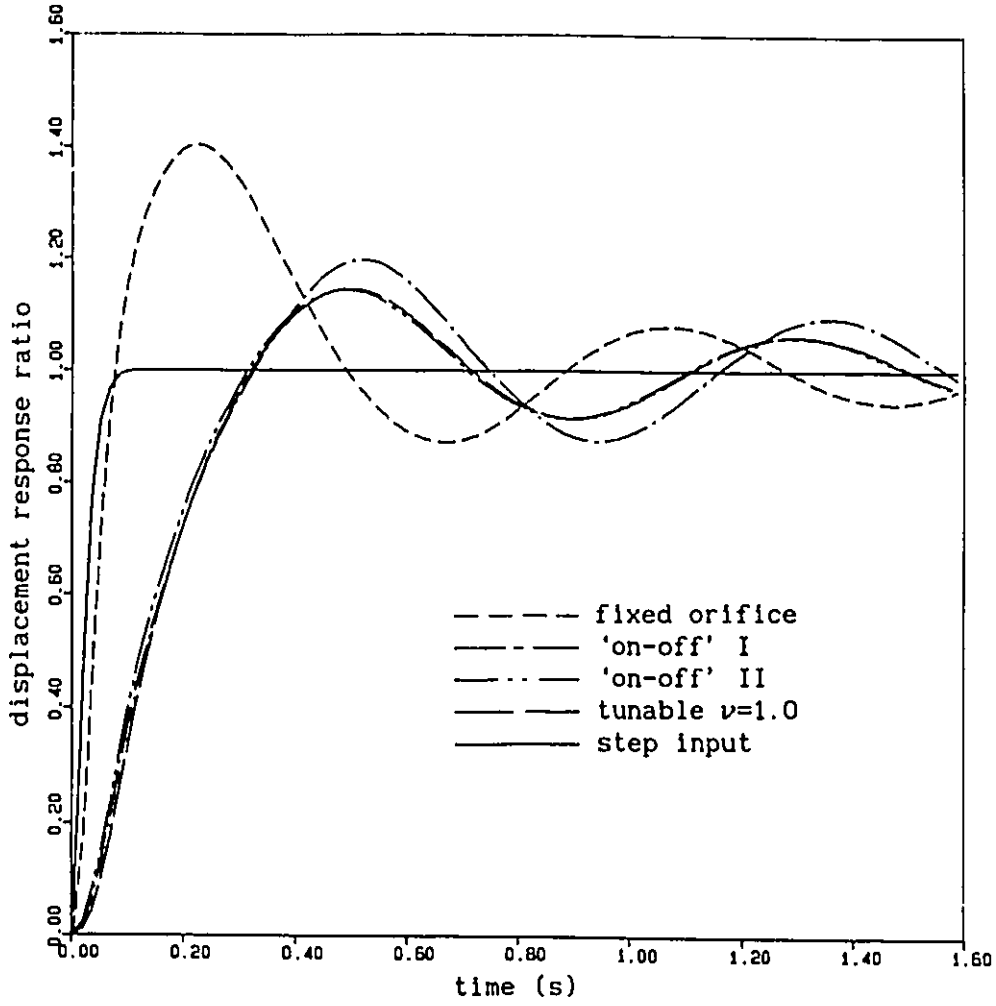

FIGURE 3.18 Displacement response of mass with tunable, semi-active 'on-off' and fixed orifice dampers to rounded step input (η=10)

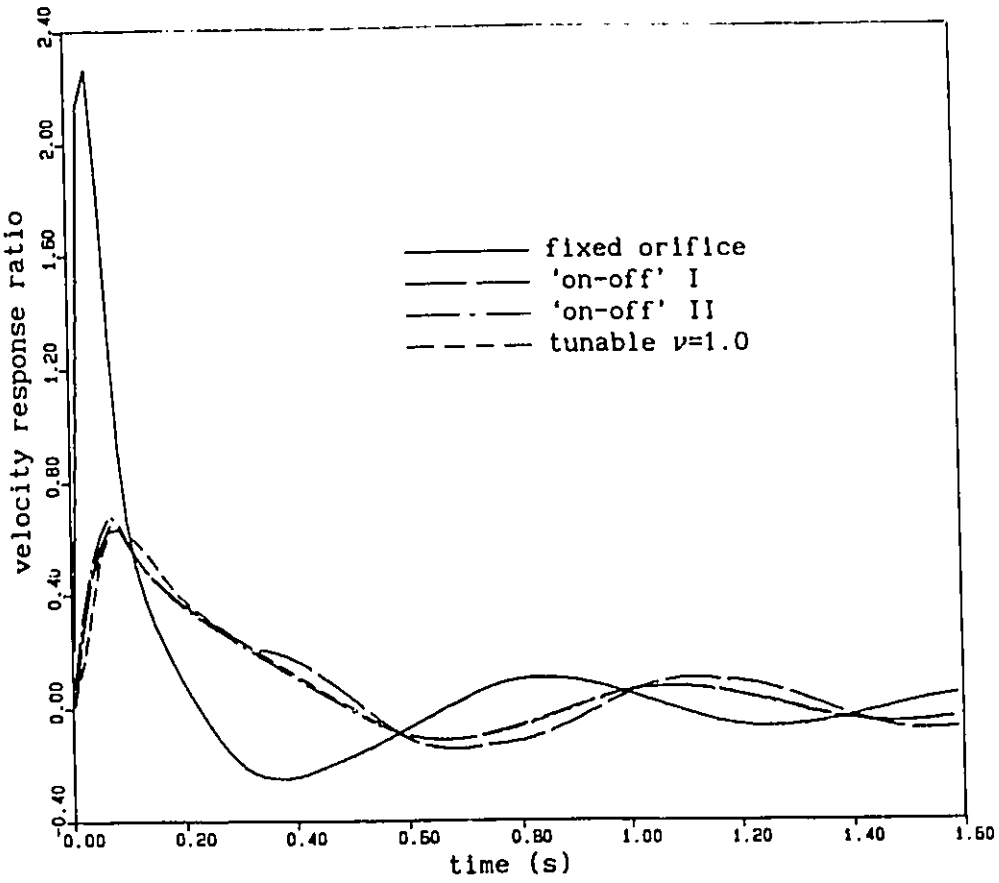

FIGURE 3.19 Velocity response of mass with tunable, semi-active 'on-off' and fixed orifice dampers to rounded step input (η=10)

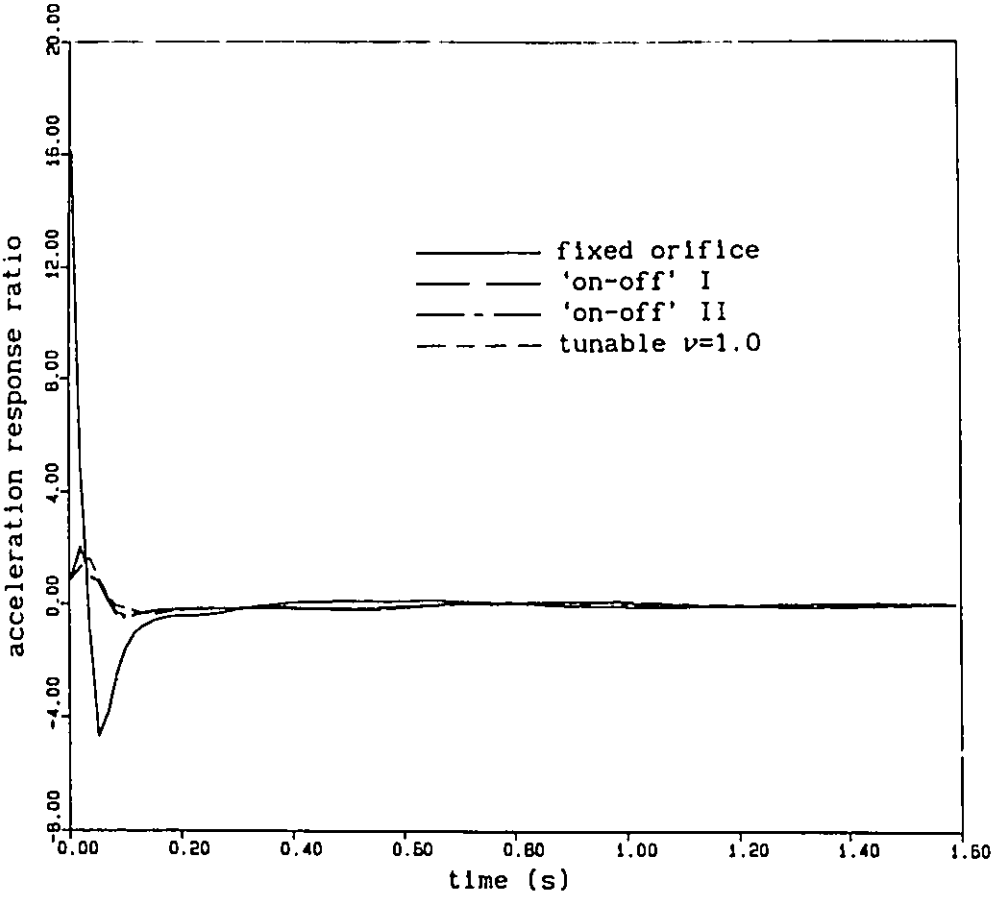

FIGURE 3.20 Acceleration response of mass with tunable, semi-active 'on-off' and fixed orifice dampers to rounded step input (η=10)

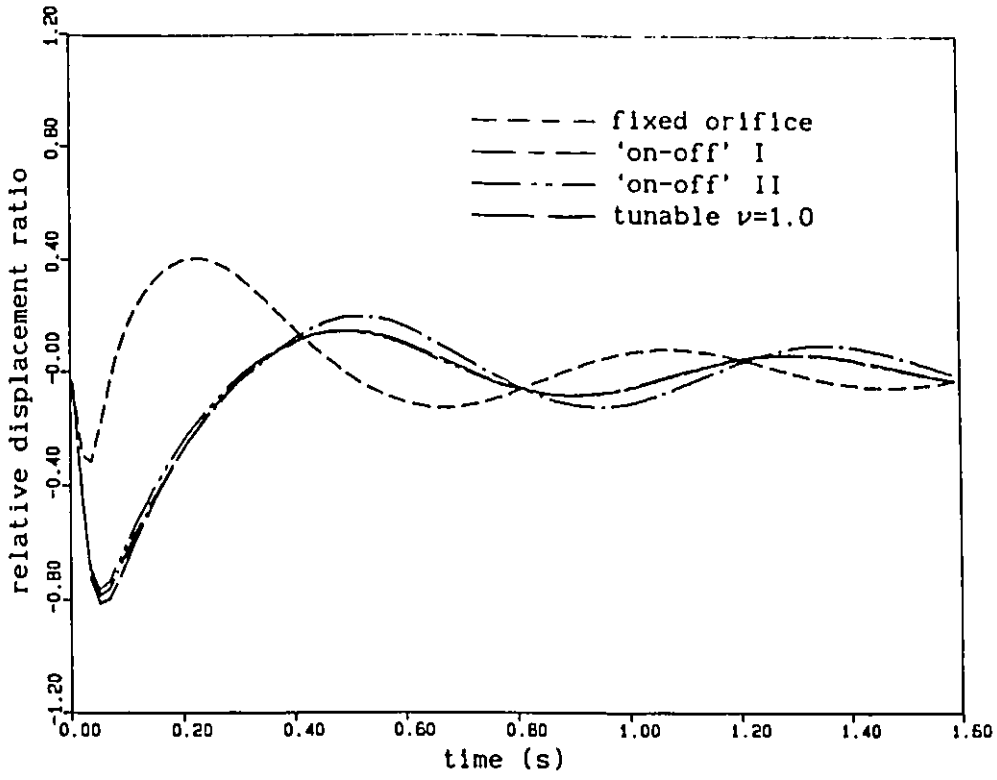

FIGURE 3.21 Relative displacement response of system employing tunable, semi-active 'on-off' and fixed orifice dampers to rounded step input (η=10)

pressure limited and the two 'on-off' dampers, to the rounded step excitation with severity parameter η=10, are almost identical. Figure 3.21 shows the relative displacement response of the tunable pressure limited damper as compared with that of the fixed orifice and two semi-active 'on-off' dampers. It can be seen that the fixed orifice damper yields the smallest valley point but the highest peak value of the relative response. On the other hand, the relative displacement response ratios of the tunable pressure limited and two 'on-off' dampers are almost identical and give deeper valley and smaller peak values, while the tunable damper produces the deepest valley value.

The influence of tuning factor ν of the tunable pressure limited damper on the transient response characteristics, to the rounded step displacement excitation with shock severity parameter η=10, are presented in Figures 3.22 and 3.23, respectively. Figure 3.22 shows the displacement response ratios of the vibration isolator employing tunable pressure limited for various values of tuning factor. It is observed that a low value of tuning factor (ν=0.7) yields a slightly high peak displacement response value. While a high value of tuning factor (ν=1.5) gives a displacement response almost identical to that of unit tuning factor (ν=1). The velocity response ratios of the vibration isolator employing tunable damper for various values of tuning factor are shown in Figure 3.23. It can be seen that a larger value of tuning factor yields a larger velocity peak response value. After the first peak response there is no significant difference in velocity response for various values of tuning factor within $0.7<\nu<1.5$.

The shock isolation performance characteristics of the vibration

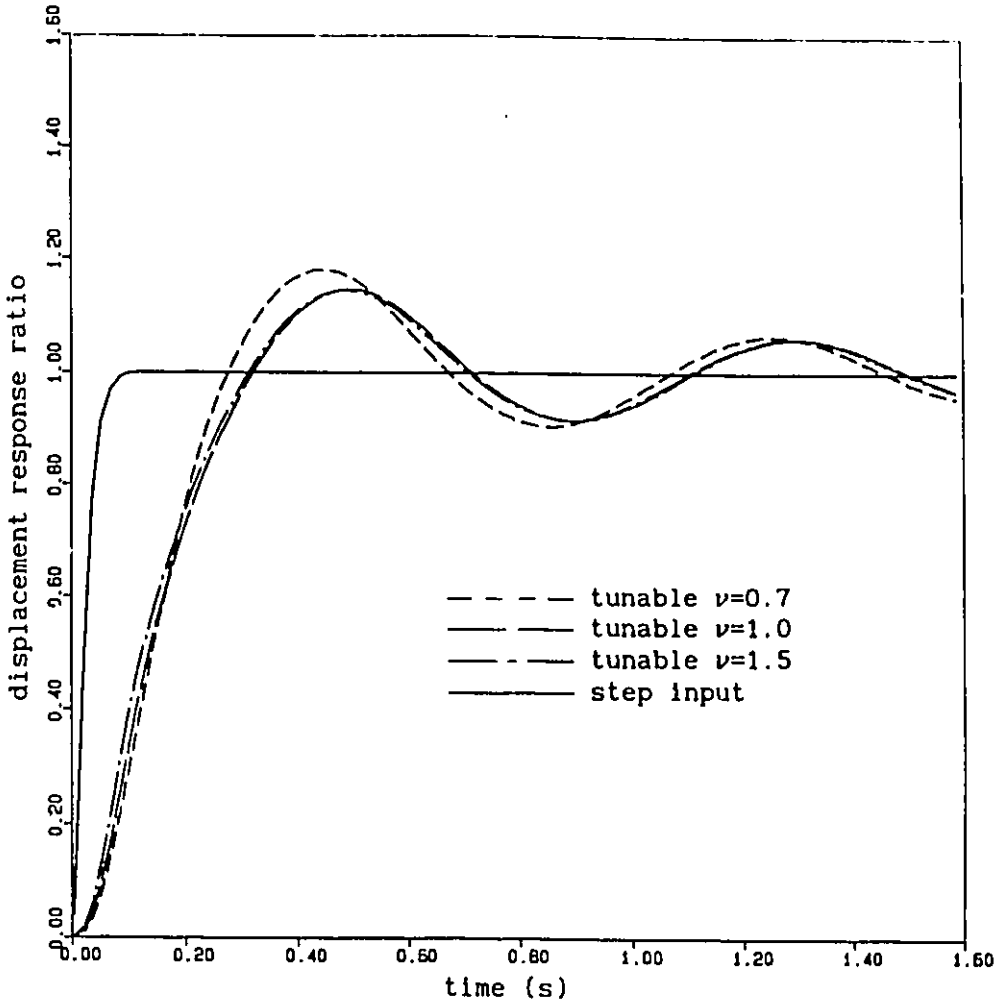

FIGURE 3.22 Displacement response of mass employing tunable damper for various values of tuning factor to rounded step input (η=10)

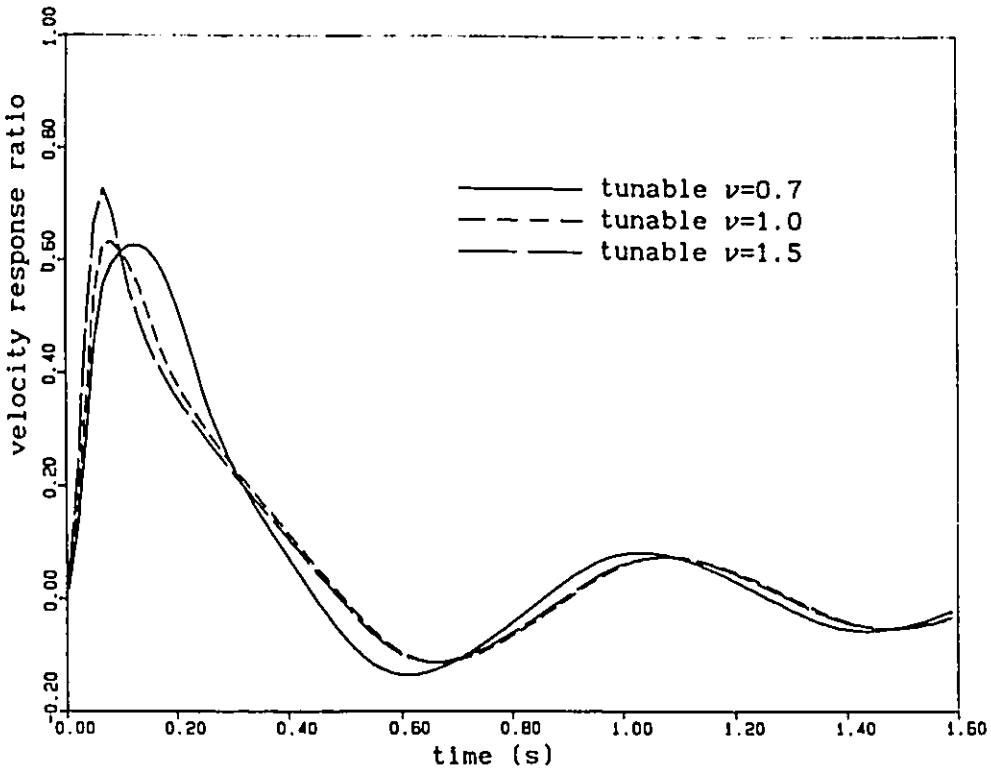

FIGURE 3.23 Velocity response of mass employing tunable damper for various values of tuning factor to rounded step input (η=10)

isolator employing fixed orifice, tunable pressure limited and two semi-active 'on-off' dampers are also evaluated with respect to shock severity parameter η in terms of the following response parameters:

$$\text{shock displacement ratio, SDR} = |x(t)|_{max} \,/\, |x_1(t)|_{max} \tag{3.45}$$

$$\text{shock velocity ratio, SVR} = |\dot{x}(t)|_{max} \,/\, |\dot{x}_1(t)|_{max} \tag{3.46}$$

$$\text{shock acceleration ratio, SAR} = |\ddot{x}(t)|_{max} \,/\, |\ddot{x}_1(t)|_{max} \tag{3.47}$$

$$\text{shock relative displacement ratio, RDR} = |z(t)|_{max} \,/\, |x_1(t)|_{max} \tag{3.48}$$

The SDR, SVR, SAR and RDR characteristics of the vibration isolator employing tunable pressure limited damper are compared with those of the fixed orifice and semi-active 'on-off' dampers for shock severity parameter ranging from 1 to 50, as shown in Figures 3.24 to 3.27. Shock displacement ratios of the system with a tunable damper as compared with those of the fixed orifice and two 'on-off' dampers are shown in Figure 3.24. It is apparent that the tunable and 'on-off' dampers offer improved SDR characteristics upon that of the fixed orifice damper. The tunable damper yields a SDR response almost identical to that of the 'on-off' damper II and the smallest value for shock severity parameter η > 10. Figure 3.25 shows the SVR characteristics of the vibration isolation system using fixed orifice, tunable and 'on-off' dampers. A comparison of the results reveals that at low shock severity parameter value there is not much difference in response among those dampers. However, as the shock severity parameter is increased, both tunable and 'on-off' dampers yield improved response, while the semi-active 'on-off' damper produces the lowest SVR value for η < 10 and the tunable damper gives the lowest value for η > 10. The shock acceleration ratio

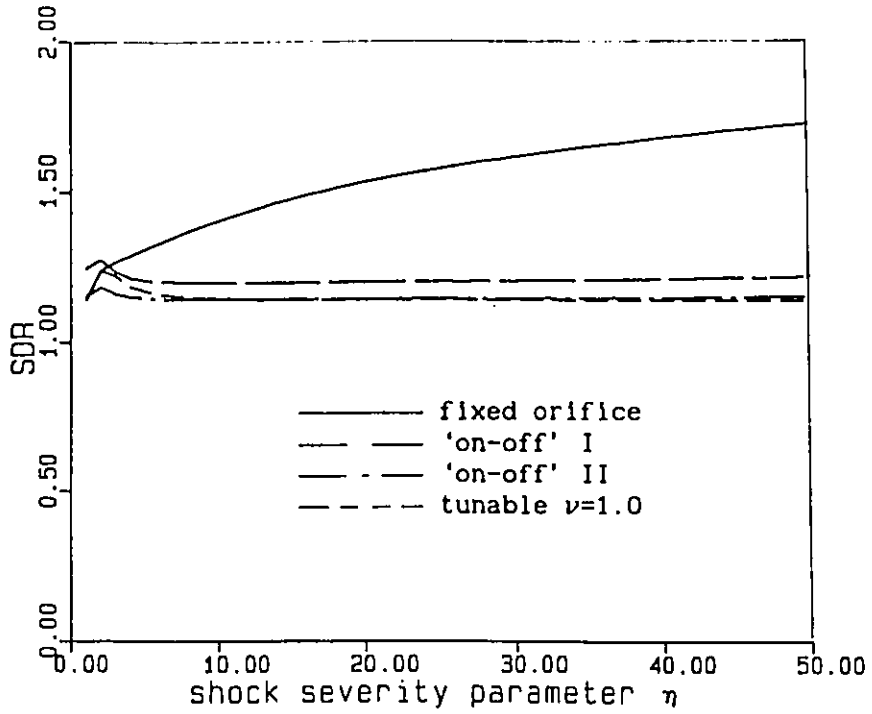

FIGURE 3.24 SDR response of mass employing tunable, semi-active, 'on-off' and fixed orifice dampers to rounded step input

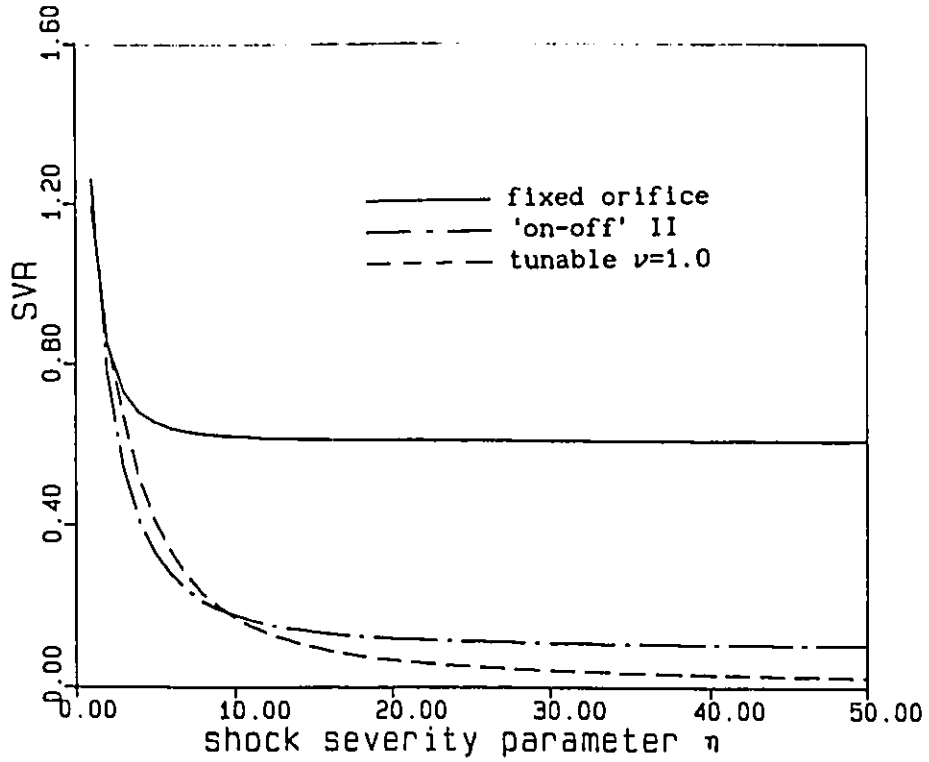

FIGURE 3.25 SVR response of mass employing tunable, semi-active, 'on-off' and fixed orifice dampers to rounded step input

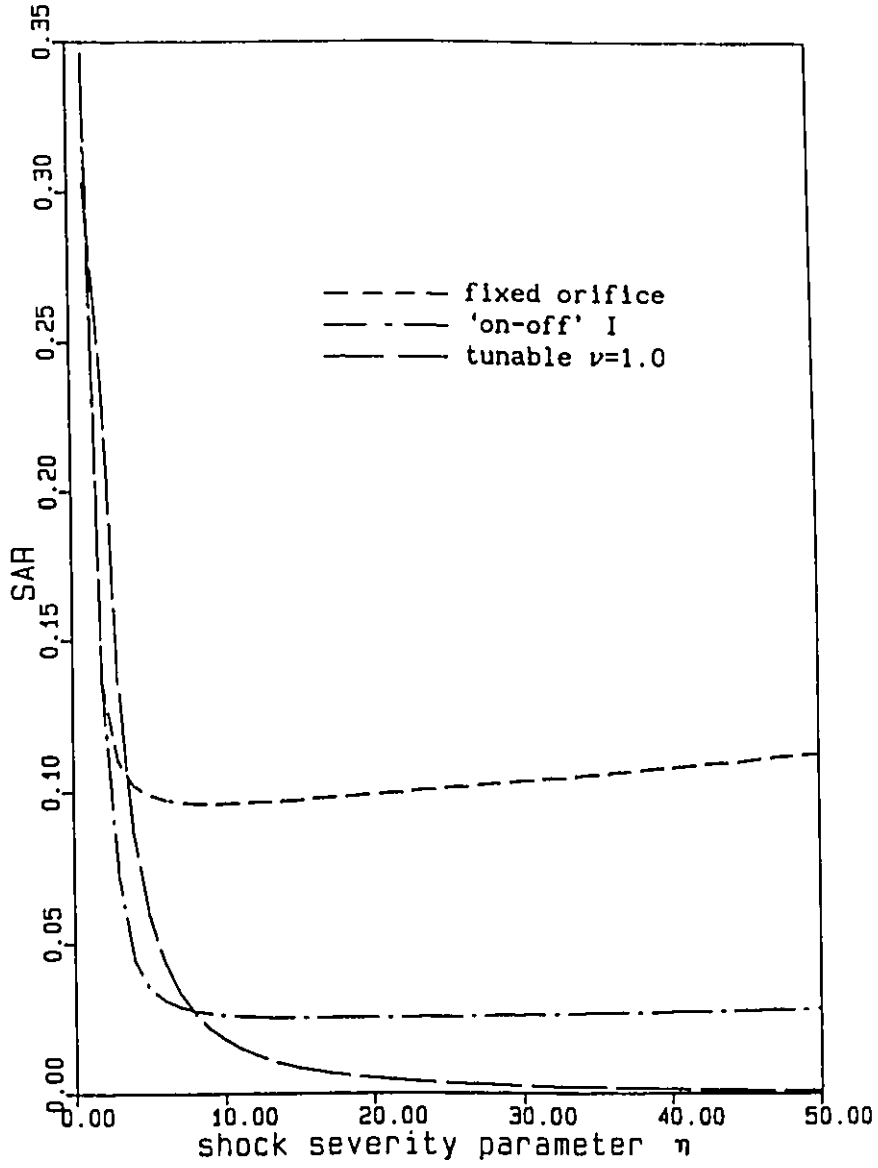

FIGURE 3.26 SAR response of mass employing tunable, semi-active 'on-off' and fixed orifice dampers to rounded step input

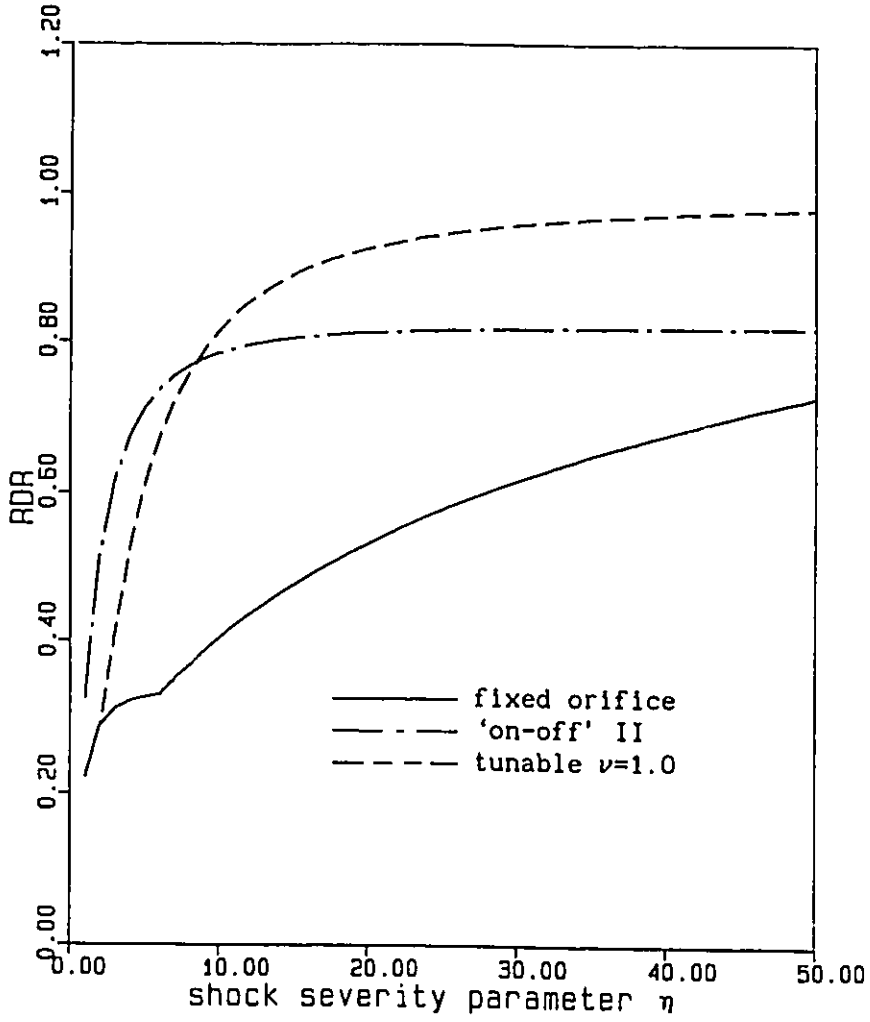

FIGURE 3.27 RDR response of system employing tunable, semi-active 'on-off' and fixed orifice dampers to rounded step input

characteristics of the isolator with fixed orifice, tunable and semi-active 'on-off' dampers are presented in Figure 3.26. It is observed that the fixed orifice damper yields largest SAR value, while both tunable and 'on-off' dampers result in improved SAR characteristics, as the shock severity parameter is increased. The SAR value of the system using tunable damper is larger than that of the semi-active 'on-off' damper for $\eta < 8$. However, the tunable damper yields superior SAR characteristics when the shock severity parameter is greater than 8 ($\eta > 8$). The RDR characteristics of vibration isolation system employing those dampers are compared in Figure 3.27. It is observed that the tunable damper yields largest RDR value for shock severity parameter $\eta > 10$. While the fixed orifice damper gives the smallest RDR response value.

3.9 Summary

In this chapter, a sequential damping mechanism is proposed using the concept of tunable pressure limiting modulation. The realization of such a sequential damping modulation is discussed through a tunable pressure limited hydraulic damper and a tuning methodology. Mathematical models of the vibration isolation systems employing fixed orifice damper, ideal semi-active 'on-off' dampers, and an ideal tunable passive pressure limited hydraulic damper, are developed. The vibration and shock isolation characteristics of the vibration isolation system employing tunable pressure limited damper are evaluated and compared with those of the fixed orifice and semi-active 'on-off' dampers. The simulation results demonstrate that the shock and vibration isolation performance of the system with tunable pressure limited damper is

superior to that of the fixed orifice damper, and is comparable to that of the ideal semi-active 'on-off' dampers. Moreover, the tunable hydraulic damper only limits the maximum value of the pressure differential and thus does not cause the discontinuity in damping force and acceleration response. The proposed tunable pressure limiting modulation does not require instrumentation and active control devices essential for active and semi-active vibration isolators. The influence of the dynamics of the pressure limiting mechanism, and the fluid and mechanical compliance on the shock and vibration isolation performance of the tunable pressure limited damper is investigated via analysis of a comprehensive mathematical model developed in the following chapter.

CHAPTER 4

ANALYSIS OF TUNABLE PRESSURE LIMITED DAMPER WITH FLUID AND MECHANICAL COMPLIANCE AND VALVE DYNAMICS

4.1 Introduction

The control forces, generated via passive, semi-active or active means, are often evaluated assuming ideal characteristics while the dynamics due to controller and force generating elements are considered insignificant [1, 32]. Various dual phase passive dampers have been investigated in view of their shock isolation performance assuming ideal characteristics [60, 61]. Vibration and shock isolation performance characteristics of 'on-off' dampers employing various semi-active control laws have been evaluated assuming ideal on-off damping characteristics [49, 51, 57]. The majority of the studies on active shock and vibration control systems have been conducted assuming ideal force generating elements [30, 31, 41].

Although it is well known that the control forces generated via semi-active or active control are strongly influenced by the dynamics associated with controller and the force generator, studies on semi-active and active vibration control systems incorporating these dynamics have been limited. Buzan and Hedrick [46] investigated the influence of the dynamics of a pneumatic actuator on the vibration isolation performance of an active vibration isolator. Klinger and Calzado [48] proposed an active control scheme which took into account the compensation for the dynamics of the force actuators. Margolis [55], and Sharp and Hassan [56] proposed a control scheme in semi-active 'on-off' isolators to compensate for the error caused by the measurement

of absolute velocity due to the signal processing system.

The damping characteristics of a tunable pressure limited damper, conceptually proposed in Chapter 3, are influenced by the dynamics associated with the pressure limiting mechanism. Shock and vibration isolation performance of the tunable damper are thus investigated via computer simulation of a mathematical model incorporating the dynamics of the tunable pressure relief valves. The tunable pressure limited hydraulic damper is represented by a higher order analytical model incorporating the fluid and mechanical compliance and, the dynamics of the tunable pressure limiting mechanism. Basic laws of dynamics, and fluid flow are employed, and the associated modeling methodology is presented. The pressure limiting mechanism is modeled as a second order dynamic system. The fluid flow through the pressure limiting mechanism is expressed as a function of the preset pressure, spool motion and port geometry. While the fluid and mechanical compliance of the hydraulic damper system is characterized in terms of effective bulk modulus.

The damping characteristics of the proposed tunable damper are investigated in view of the dynamics of the tunable pressure limiting mechanism and the effective bulk modulus. Parametric sensitivity analyses are carried out to establish the influence of the bulk modulus and the dynamics of the pressure limiting mechanism on shock and vibration isolation performance of the tunable pressure limited damper.

4.2 Development of Mathematical Model

The schematic of a vibration isolation system employing a tunable pressure limited hydraulic damper, subject to base excitation, is presented in Figure 4.1 (a). The tunable pressure limited hydraulic

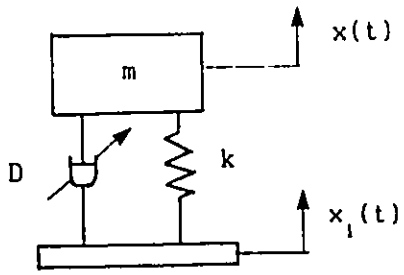

(a) tunable variable damping system

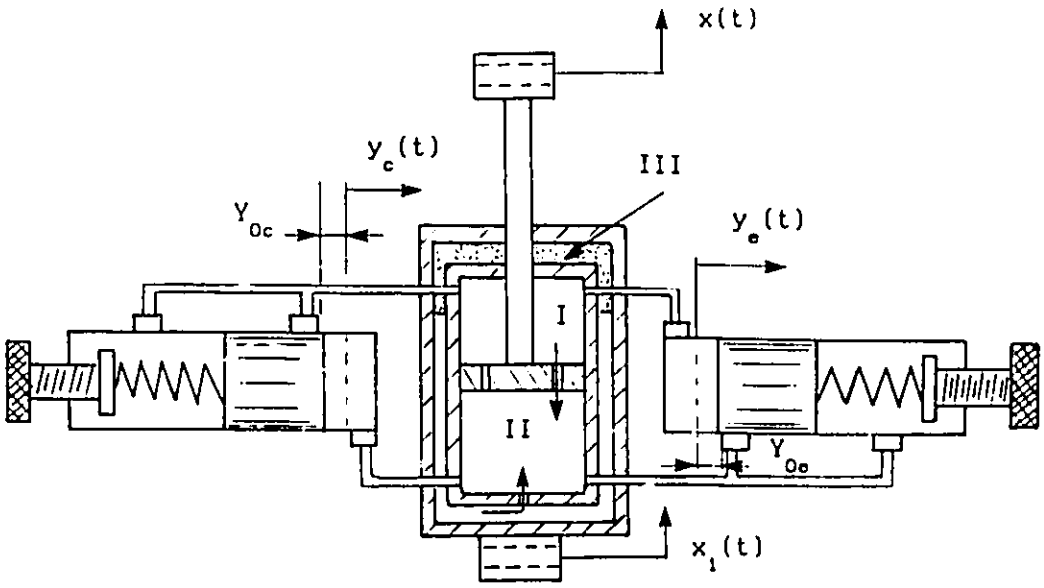

(b) tunable pressure limited damper

FIGURE 4.1 Schematic of vibration isolation system with tunable pressure limited hydraulic damper

damper is realized by implementing two pressure relief valves across chambers I and II, in order to limit the pressure differential during both compression and extension strokes, as shown in Figure 4.1 (b). The pressure relief valves can be tuned to limit the pressure differential across the piston to the desired preset value.

The static equilibrium equations of the tunable damper system are identical to that of the fixed orifice damper system, as presented in subsection 3.2.2.

4.2.1 Equations of Motion

The vibration isolation system employing tunable hydraulic damper with valve dynamics, shown in Figures 4.1 (a) and (b), comprises not only the main body mass but also two spool masses. The equations of motion are therefore derived with respect to the main body mass and spool masses, respectively.

Equation of Motion of System Main Body

Neglecting friction forces, the equation of motion of the main body mass subject to base excitation can be expressed as:

$$m\ddot{x}(t) + f_k(t) + f_{ds}(t) = 0 \tag{4.1}$$

where,

f_k = restoring force due to linear spring k (N), given by:

$$f_k(t) = k\, z(t) \tag{4.2}$$

z = $x - x_i$, relative displacement of main body mass with respect to the base (m)

f_{ds} = total dynamic force generated by tunable damper (N)

The total dynamic force of the tunable damper can be expressed as a combination of a gas-spring force and a damping force , based upon the

derivations presented in section 3.2:

$$f_{ds}(t) = f_a(t) + f_d(t) \tag{4.3}$$

where

f_a = restoring force due to gas-spring (N), given by:

$$f_a(t) = - p_{30} A_r \tag{4.4}$$

f_d = variable damping force due to the tunable damper (N), and is given by:

$$f_d(t) = p_{12} A_p + p_{32} A_r \tag{4.5}$$

The pressure differentials in equations (4.4) and (4.5) are derived from the flows through piston and cylinder orifices, pressure relief valves, and due to the compressibility of fluid. Flow through the relief valves is derived from dynamics of the spool mass, presented in the following subsections.

Equations of Motion of the Spools

The pressure relief valve, as shown in Figure 4.1 (b), comprises of a spool and an adjustable spring. Assuming viscous damping and linear spring characteristics, the equations of motion of the spool masses can be expressed as, respectively:

$$m_{rc}\ddot{y}_c(t) + c_{rc}\dot{y}_c(t) + k_{rc}y_c(t) = f_{rc}(t) \tag{4.6}$$

$$m_{re}\ddot{y}_e(t) + c_{re}\dot{y}_e(t) + k_{re}y_e(t) = f_{re}(t) \tag{4.7}$$

where,

m_{rc}, m_{re} = masses of spools of compression and extension valves, respectively (kg)

y_c, y_e = coordinates characterizing displacements of compression and extension spools, respectively (m)

c_{rc}, c_{re} = viscous damping coefficients of the compression and extension relief valves, respectively (N·s/m)

k_{rc}, k_{re} = stiffness coefficients of the compression and extension relief valves, respectively (N/m)

f_{rc}, f_{re} = forces acting on compression and extension spools, respectively (N), given by:

$$f_{rc}(t) = a_{rc}\, p_{12}(t) \tag{4.8}$$

$$f_{re}(t) = - a_{re}\, p_{12}(t) \tag{4.9}$$

a_{rc}, a_{re} = spool end areas of compression and extension valves respectively (m)

4.2.2 Flow Equations

The flow rates through orifices on the piston and the cylinder, and relief valves, and due to fluid compressibility are derived as functions of the piston movement, the motion of the spool masses and the effective bulk modulus. The leakage flows within the valves and damper are assumed to be negligible. The relationships among the fluid flows are established using the fluid continuity equation.

The total fluid flow between chambers I and II consists of the flows through the fixed orifices on the piston and the tunable relief valves expressed as:

$$Q_{12}(t) = Q_{or}(t) + Q_{re}(t) \tag{4.10}$$

where,

Q_{12} = volume flow rate of fluid from chamber I to II (m^3/s)

Q_{or} = volume flow rate through orifices from chamber I to II (m^3/s)

Q_{re} = volume flow rate through relief valves (m^3/s)

Assuming turbulent flows, the rate of fluid flow through the orifices on the piston is related to the pressure differential p_{12}

across the piston:

$$Q_{or} = \left(\sum_{i=1}^{n} C_{dii} a_{ii} \right) \sqrt{\frac{2\,|p_{12}|}{\rho}}\, \mathrm{sgn}(p_{12}) \qquad (4.11)$$

where,

n = number of orifice on the piston

C_{dii} = discharge coefficient of the ith orifice

a_{ii} = area of the ith orifice (m^2)

Assuming identical orifices on the piston, such that $C_{dii} = C_{di}$ and $a_{ii} = a_i$, equation (4.11) can be simplified as:

$$Q_{or} = n\, C_{di} a_i \sqrt{\frac{2\,|p_{12}|}{\rho}}\, \mathrm{sgn}(p_{12}) \qquad (4.12)$$

Assuming identical compression and extension relief valves of the tunable hydraulic damper $m_{rc} = m_{re} = m_r$; $k_{rc} = k_{re} = k_r$; $c_{rc} = c_{re} = c_r$; $a_{rc} = a_{re} = a_r$; $Y_{0c} = Y_{0e} = Y_0$, and symmetric damper characteristics, an identical motion of both spools is obtained :

$$y_c(t) = -\, y_e(t) = y(t) \qquad (4.13)$$

The total flow due to the relief valves consists of flow through valve openings and flow due to movements of valve spools. Assuming turbulent flow through the openings, the volume flow rate through the relief valves can, therefore, be expressed as:

$$Q_{re} = \begin{cases} 2\, a_r \dot{y}(t)\,, & |y| < Y_0 \\ C_{dr} a_e(y, Y_0) \sqrt{\dfrac{2\,|p_{12}|}{\rho}}\, \mathrm{sgn}(p_{12}) + 2\, a_r \dot{y}, & |y| \geq Y_0 \end{cases} \qquad (4.14)$$

C_{dr} = discharge coefficient of the valve opening

Y_0 = preset displacement overlap of the spools (m)

a_r = spool end area of relief valves (m^2)

a_o = area of the relief valve opening (m^2)

The spool overlap is related to the preset pressure limiting value $(p_{12})_0$ as the following:

$$Y_0 = (p_{12})_0 \, a_r \, / \, k_r \tag{4.15}$$

k_r = stiffness coefficient of the valves (N/m)

Assuming turbulent flows the fluid flow rate through the orifice on the cylinder is expressed as:

$$Q_{cy} = C_{d2} a_2 \sqrt{\frac{2 \, |p_{32}|}{\rho}} \, \mathrm{sgn}(p_{32}) \tag{4.16}$$

where,

Q_{cy} = volume flow rate through cylinder orifice (m^3/s)

C_{d2} = discharge coefficient of cylinder orifice

a_2 = area of cylinder orifice (m^2)

The rate of change of fluid volume in chamber I can be related to the relative velocity in the following manner:

$$Q_{m1}(t) = A_p \, \dot{z}(t) \tag{4.17}$$

Q_{m1} = rate of change of fluid volume in chamber I (m^3/s)

$\dot{z}$ = relative velocity of tunable damper (m/s)

The flow due to the effective bulk modulus is the rate of volume change due to the fluid compressibility and mechanical compliance of the damper cylinder. For chamber I, rate of change of fluid volume due to the fluid and mechanical compliance is expressed as:

$$Q_{e1}(t) = \frac{V_1}{\beta_{e1}} \frac{dp_1}{dt} \tag{4.18}$$

Q_{e1} = volume flow rate due to compliance in chamber I (m^3/s)

p_1 = instantaneous pressure in chamber I (Pa)

β_{e1} = effective bulk modulus of chamber I (Pa), given by

$$\frac{1}{\beta_{e1}} = \frac{1}{\beta_{c1}} + \frac{1}{\beta_l} \tag{4.19}$$

β_{c1} = bulk modulus of chamber I container (Pa)

β_l = bulk modulus of the fluid (Pa)

V_1 = instantaneous volume of chamber I (m^3), given by:

$$V_1(t) = [X_{st} - z(t)]\ A_p + V_{ro} + 2\ a_r\ y(t) \tag{4.20}$$

V_{ro} = equivalent volume due to connecting pipes (m^3)

Based on the law of conservation of mass, the flows in chamber I are related by the fluid continuity equation given as:

$$- Q_{or}(t) - Q_{re}(t) = - Q_{m1}(t) + Q_{e1}(t) \tag{4.21}$$

The rate of change of fluid volume in chamber II is related to the relative velocity of the damper in a similar manner:

$$Q_{m2}(t) = (A_p + A_r)\ \dot{z}(t) \tag{4.22}$$

Q_{m2} = rate of change of fluid volume in chamber II (m^3/s)

The rate of change volume in chamber II due to the effective modulus is caused by the mechanical and fluid compliance can be expressed:

$$Q_{e2}(t) = \frac{V_2}{\beta_{e2}} \frac{dp_2}{dt} \tag{4.23}$$

Q_{e2} = volume flow rate due to compliance in chamber II (m^3/s)

p_2 = instantaneous pressure in chamber II (Pa)

β_{e2} = effective bulk modulus in chamber II (Pa), given by

$$\frac{1}{\beta_{e2}} = \frac{1}{\beta_{c2}} + \frac{1}{\beta_l} \tag{4.24}$$

β_{c2} = bulk modulus of chamber II (Pa)

V_2 = instantaneous volume of chamber II (m^3), given by

$$V_2(t) = [(l - X_{st}) + z(t)] (A_p + A_r) + V_{ro} - 2 a_r y(t) \quad (4.25)$$

ℓ = length of the hydraulic damper stroke (m)

The fluid continuity equation yields the following relationship:

$$Q_{or}(t) + Q_{re}(t) + Q_{cy}(t) = Q_{m2}(t) + Q_{e2}(t) \quad (4.26)$$

In chamber III, the rate of change of gas volume can be expressed as:

$$Q_{m3}(t) = \frac{dV_3}{dt} \quad (4.27)$$

Q_{m3} = rate of change of gas volume in chamber III (m^3/s)

V_3 = instantaneous volume of gas in chamber III (m^3)

Assuming that the bulk modulus of the fluid is very high as compared with the compressibility of the gas, the volume change due to compressibility of the fluid in chamber III is thus negligible. The flow relationship for chamber III can be thus expressed as:

$$Q_{cy}(t) = Q_{m3}(t) \quad (4.28)$$

The instantaneous volume of gas in chamber III is given by:

$$V_3 = V_0 + V_{cy} \quad (4.29)$$

where

$$\frac{d V_{cy}}{d t} = Q_{cy}(t) \quad (4.30)$$

Opening Area of Relief Valve

The opening area of relief valves is a function of tunable preset displacement overlap, displacement of the spool and port geometry. In a

general case, the port geometry can be selected as shown in Figure 4.2. During the pressure limiting operation of the relief valve, the area of the opening can be derived from the following four spool positions:

(A) $0 < (|y| - Y_0) \leq R_r$:

$$a_e = \alpha_1 R_r^2 - x_1 x_2 \tag{4.31}$$

where,

R_r = radius of the port arc (m)

$$x_1 = R_r - (|y| - Y_0) \tag{4.32}$$

$$x_2 = \sqrt{R_r^2 - x_1^2} \tag{4.33}$$

$$\alpha_1 = \tan^{-1}\left(x_2 / x_1 \right) \tag{4.34}$$

(B) $R_r < (|y| - Y_0) \leq (L_r + R_r)$:

$$a_e = (\pi R_r^2 / 2) + 2 R_r \left((|y| - Y_0) - R_r \right) \tag{4.35}$$

where,

L_r = distance between two centers of the port arcs (m)

(C) $(L_r + R_r) < (|y| - Y_0) \leq (L_r + 2 R_r)$:

$$a_e = \pi R_r^2 - \left(\alpha_2 R_r^2 - x_3 x_4 \right) + 2 R_r L_r \tag{4.36}$$

where,

$$x_3 = (|y| - Y_0) - (L_r + R_r) \tag{4.37}$$

$$x_4 = \sqrt{R_r^2 - x_3^2} \tag{4.38}$$

$$\alpha_2 = \tan^{-1}\left(x_4 / x_3 \right) \tag{4.39}$$

(D) $(|y| - Y_0) > (L_r + 2 R_r)$:

$$a_e = \pi R_r^2 + 2 R_r L_r \tag{4.40}$$

It is apparent that circular and rectangular port shapes are only

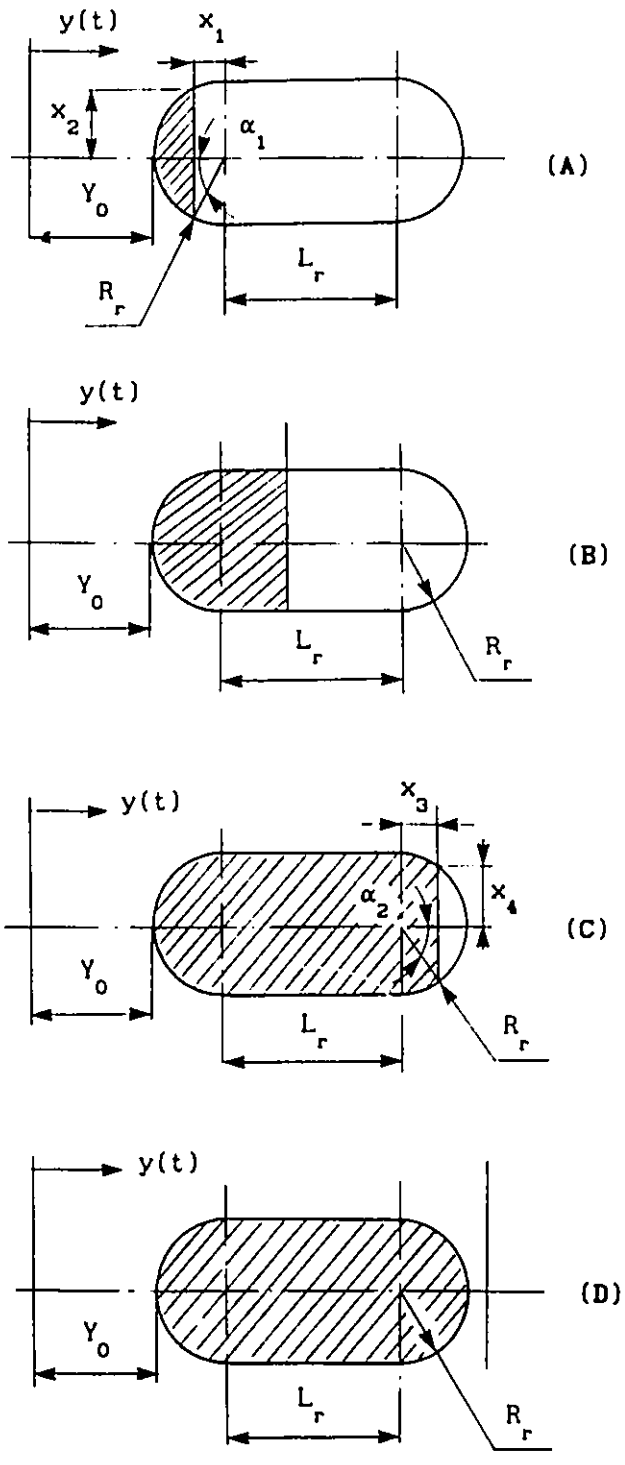

FIGURE 4.2 Schematic of a port configuration of pressure limiting valve

special cases of the above port shape. The above equations can be readily simplified to compute the relief valve opening for circular and rectangular ports.

4.2.3 Pressure Equations

The rate of change of fluid pressure in each chamber is related to compressibility of the fluid and fluid continuity equations. The rate of change of fluid pressure in chamber I, obtained from equations (4.18) and (4.21), is expressed as:

$$\frac{dp_1}{dt} = \frac{\beta_{e1}}{V_1}\left(Q_{m1}(t) - Q_{or}(t) - Q_{re}(t)\right) \tag{4.41}$$

where Q_{m1}, Q_{or} and Q_{re} are derived from equations (4.17), (4.12) and (4.14), respectively.

The rate of change of fluid pressure in chamber II is similarly established from equations (4.23) and (4.26) and expressed as:

$$\frac{dp_2}{dt} = \frac{\beta_{e2}}{V_2}\left(Q_{or}(t) + Q_{re}(t) + Q_{cy}(t) - Q_{m2}(t)\right) \tag{4.42}$$

where Q_{or}, Q_{re}, Q_{cy} and Q_{m2} are derived from equations (4.12), (4.14), (4.16) and (4.22), respectively.

The instantaneous pressure of the gas in chamber III is derived assuming polytropic process and expressed as:

$$p_3(t) = \frac{V_0^{\gamma}}{[V_0 + V_{cy}(t)]^{\gamma}} p_0 \tag{4.43}$$

p_3 = instantaneous pressure of gas in chamber III (Pa)

Solution of static equilibrium equation, presented in section 3.2.2, yields the static values of gas volume (V_0) and pressure (p_0). The

change in gas volume in chamber III due to fluid flow through the cylinder orifice (V_{cy}) is obtained from equation (4.30). The pressure differential, p_{30}, required to compute the gas spring force in (4.4) can be then derived from (4.43):

$$p_{30}(t) = - \frac{[V_0 + V_{cy}(t)]^{\gamma} - V_0^{\gamma}}{[V_0 + V_{cy}(t)]^{\gamma}} p_0 \qquad (4.44)$$

4.3 Dynamic Characteristics of Tunable Damper

The damping force, pressure differential, and shock and vibration isolation performance characteristics of the tunable damper are investigated in order to illustrate the significance of dynamics associated with the pressure relief valves and compliance of the damper. The system of nonlinear differential equations of the tunable pressure limited hydraulic damper incorporating the fluid and mechanical compliance, and the dynamics of the pressure limiting valves, developed in section 4.2, is solved using a numerical integration technique. The computer simulations are carried out for the parameters presented in Tables 4.1 and 4.2.

Damping characteristics of the tunable pressure limited damper are evaluated in terms of steady-state force-displacement Lissajous diagrams and compared with those of fixed orifice and ideal pressure limited dampers. The pressure differential characteristics of the tunable pressure limited damper are evaluated for constant amplitude harmonic excitations and compared with those of the fixed orifice and ideal pressure limited dampers. The influence of relief valve dynamics and variations in the effective bulk modulus on the damping characteristics

TABLE 4.1

Simulation Parameters of Tunable Pressure Limited Hydraulic Damper System

SYMBOL	DESCRIPTION	PARAMETER VALUE
m	Mass of the main body	365 kg
k	Stiffness coefficient	18730 N/m
ρ	Mass density of fluid	797 kg/m^3
A_p	Area of piston on rod side	2.5×10^{-3} m^2
A_r	Area of rod cross section	3.14×10^{-4} m^2
C_{d1}, C_{d2}	Discharge coefficient	0.7
a_1	Area of piston orifice	3.14×10^{-6} m^2
a_2	Area of cylinder orifice	6.28×10^{-6} m^2
γ	Polytropic exponent	1.4
p_{at}	Atmospheric pressure	101300 Pa
p_a	Initial charge pressure	15×10^5 Pa
V_a	Initial gas volume	3.0×10^{-4} m^3
n	Number of piston orifices	4
l	Damper stroke	0.4 m
X_i	Input amplitude	0.05 m

TABLE 4.2

Simulation Parameters of Tunable Pressure Limiting Valves

SYMBOL	DESCRIPTION	PARAMETER VALUE
m_r	Mass of the valve spool	0.056 kg
k_r	Stiffness coefficient of valve	2000 N/m
c_r	Viscous damping coefficient	8.5 N·s/m
β_{e1}, β_{e2}	Effective bulk moduli	6.9×10^{8}, 6.9×10^{8} Pa
a_r	Spool end area	2.0×10^{-4} m^2
R_r	Radius of the port arc	0.0025 m
L_r	Distance between the arc centers	0.02 m
C_{dr}	Discharge coefficient of valve	0.7
ρ	Mass density of fluid	797 kg/m^3
V_{ro}	Equivalent volumes due to pipes	5×10^{-6} m^3

of the tunable damper is discussed.

The dynamic force due to the hydraulic damper is non-dimensionalized with respect to the static damper force, given by:

$$F_0 = p_0 A_r \tag{4.45}$$

F_0 = damper force corresponding to static equilibrium position of the system (N)

The relative displacement response is non-dimensionalized with respect to the excitation amplitude X_1. Figure 4.3 presents the steady state non-dimensionalized force-displacement characteristics of the fixed orifice and tunable pressure limited hydraulic dampers for excitation

frequency ω/ω_n=2.0. The effective bulk modulus of the fluid in all chambers is assumed identical and β_e = 6.9×10^8 (Pa) is selected as recommended by Wahi [25] and Merritt [114]. The force-displacement characteristics, presented in Figure 4.3, clearly reveal that the tunable pressure limited hydraulic damper dissipates vibration energy in a different manner than that of the fixed orifice damper. Although, the amount of energy dissipated per cycle (area enclosed by the force-displacement curve) by the tunable damper is similar to that by the fixed orifice damper, the damping characteristics of the two dampers differ considerably. The fixed orifice hydraulic damper yields high damping force corresponding to maximum relative velocity response, while the magnitude of damping force generated by the tunable pressure limited damper is considerably smaller due to the pressure limiting modulation. The corresponding relative displacement response of the tunable damper is, however, larger than that of the fixed orifice damper, as shown in Figure 4.3.

The force-displacement characteristics of the tunable hydraulic damper incorporating pressure relief valve dynamics and effective bulk modulus (β_e = 6.9×10^8 (Pa)), referred to as "tunable (higher order)", are compared with that of an ideal tunable pressure limited damper, "tunable (ideal)", as shown in Figure 4.4, in order to illustrate the significance of relief valve dynamics and fluid compressibility. Figure 4.4 clearly illustrates that an ideal tunable pressure limited hydraulic damper limits the magnitude of damping force to a constant value corresponding to high relative velocity response. However, ideal pressure limiting and its corresponding damping characteristics can not

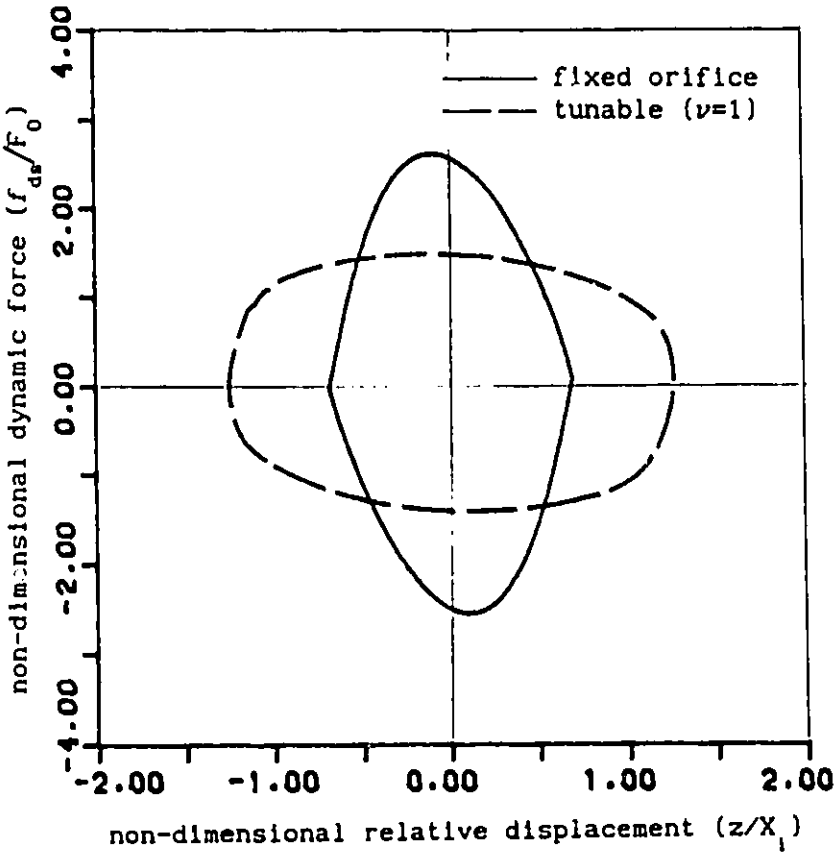

FIGURE 4.3 Force-displacement characteristics of vibration isolation system with fixed orifice and tunable dampers ($\beta_e = 6.9\times10^8$ (Pa), $\omega/\omega_n=2.0$)

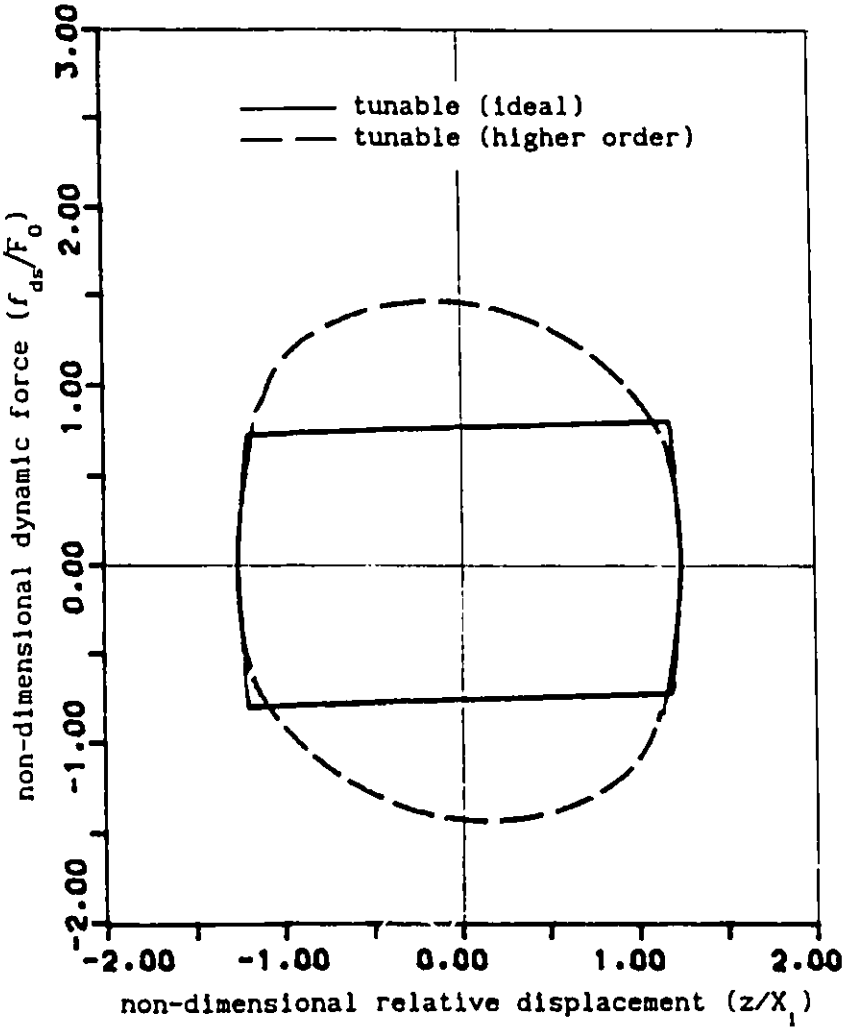

FIGURE 4.4 Force-displacement characteristics of tunable damper with ideal and higher order models (β_e=6.9x10^8 (Pa)), (ω/ω_n=2.0)

be achieved due to the dynamics associated with the relief valves. The magnitude of the damping force generated by the tunable damper, incorporating the relief valve dynamics, is considerably larger than that generated by the ideal tunable damper. A comparison of Figures 4.3 and 4.4 further reveals that the tunable hydraulic damper limits the magnitude of peak damping force to a great extent when compared with the magnitude of damping force due to a fixed orifice damper.

The area of valve opening required to modulate the fluid flow and limit the pressure differential across the piston is strongly related to the pressure differential itself. The pressure differential characteristics of the tunable pressure limited hydraulic damper incorporating the hydraulic and mechanical compliance, and relief valve dynamics are evaluated in the frequency range $0 \leq \omega/\omega_n \leq 5$, as shown in Figure 4.5. The pressure differential characteristics are compared with those of the ideal fixed orifice ($\beta_e = \infty$), fixed orifice with effective compliance and ideal tunable dampers in order to illustrate the influence of the valve dynamics and effective bulk modulus. The pressure differential is non-dimensionalized with respect to the static pressure p_0. Figure 4.5 reveals that the pressure differential across the piston of a fixed orifice damper increases as the excitation frequency is increased. The influence of hydraulic and mechanical compliance of the damper is insignificant for excitation frequencies below $2\omega_n$. However, the pressure differential response of the fixed orifice damper incorporating effective bulk modulus is larger than that of the ideal fixed orifice damper at high excitation frequencies, as shown in Figure 4.5. Response characteristics of the ideal tunable pressure limited

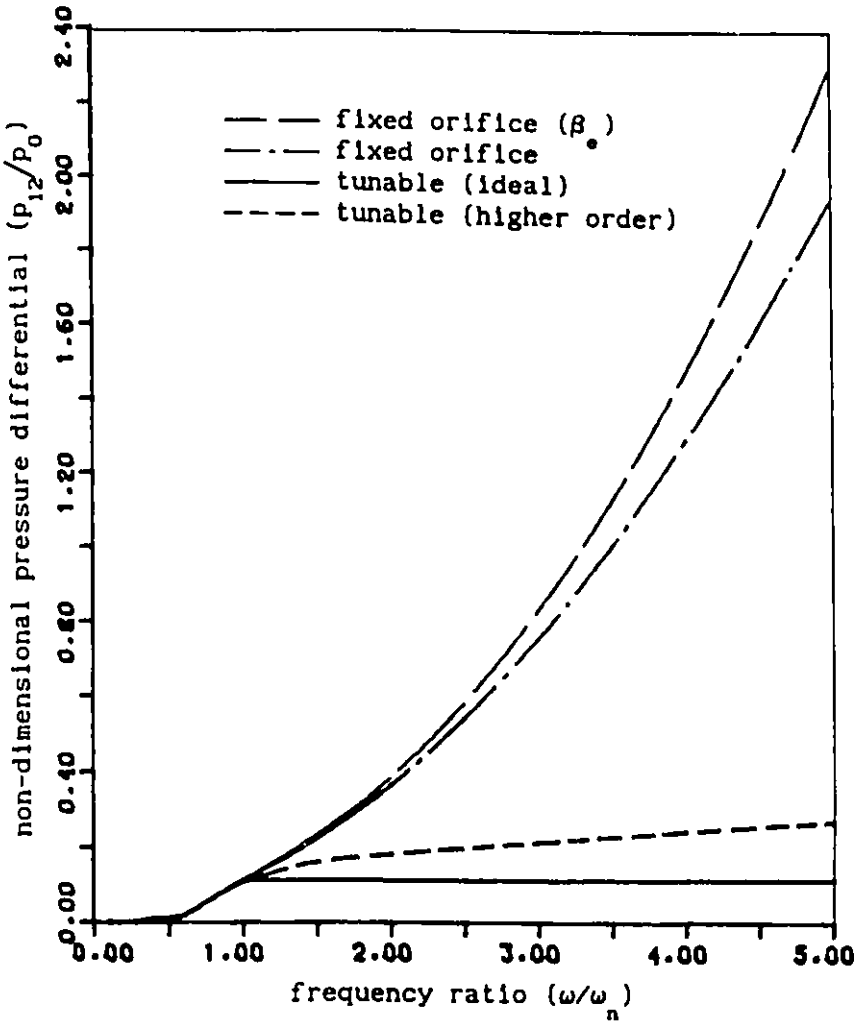

FIGURE 4.5 Pressure differential characteristics of tunable pressure limited damper system with respect to excitation frequency

damper (ν=1) reveal that the pressure differential is limited to a constant value at excitation frequencies beyond the resonant frequency. The response characteristics of the tunable pressure limited hydraulic damper, however, illustrate that the pressure differential can not be limited to a constant value due to dynamics of the pressure relief valve and fluid compliance. Although the pressure differential response of the tunable damper is larger than that of the ideal pressure limited damper, the magnitude of pressure differential is considerably smaller than that of the fixed orifice damper as shown in Figure 4.5.

Steady state damping force-displacement characteristics of tunable pressure limited hydraulic dampers are investigated for various values of the effective bulk modulus in order to demonstrate the influence of mechanical and fluid compliance on the damping characteristics. Figures 4.6 to 4.8 present the force-displacement characteristics of tunable damper corresponding to excitation frequency ω/ω_n = 0.5, 2.0 and 5.0, respectively. The effective bulk moduli used in the simulation are β_e = 6.9×10^8 (Pa), $\beta_e/16$ and $\beta_e/256$. Force-displacement characteristics reveal that the dynamic force due to the tunable damper is strongly influenced by the effective bulk modulus, especially at high excitation frequencies. At low excitation frequencies, the influence of effective bulk modulus is observed to be relatively insignificant, as shown in Figure 4.6. The magnitude of peak dynamic force increases slightly with reduced bulk modulus, while the energy dissipated per cycle remains almost similar. At higher excitation frequencies, the energy dissipated per cycle by the tunable damper, however, decreases considerably when the value of the effective bulk modulus is reduced, as shown in Figures

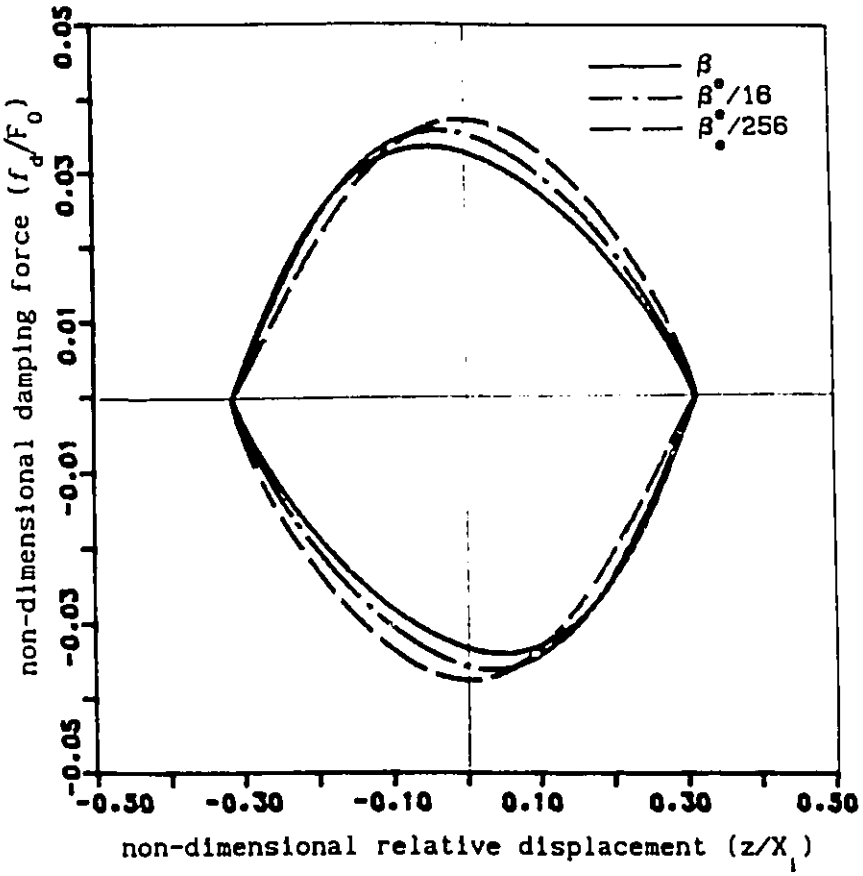

FIGURE 4.6 Damping force-displacement characteristics of tunable damper with various bulk moduli (β_e=6.9x10^8 (Pa), ω/ω_n=0.5)

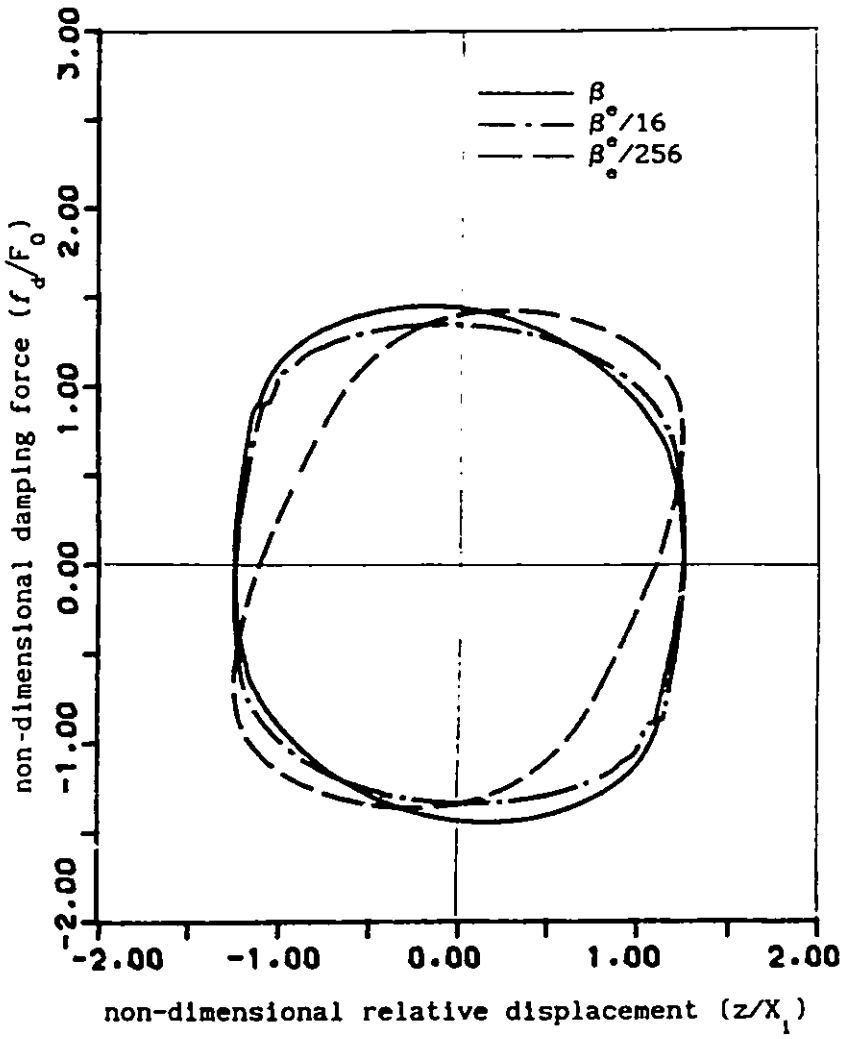

FIGURE 4.7 Damping force-displacement characteristics of tunable damper with various bulk moduli (β_e=6.9x10^8 (Pa), ω/ω_n=2.0)

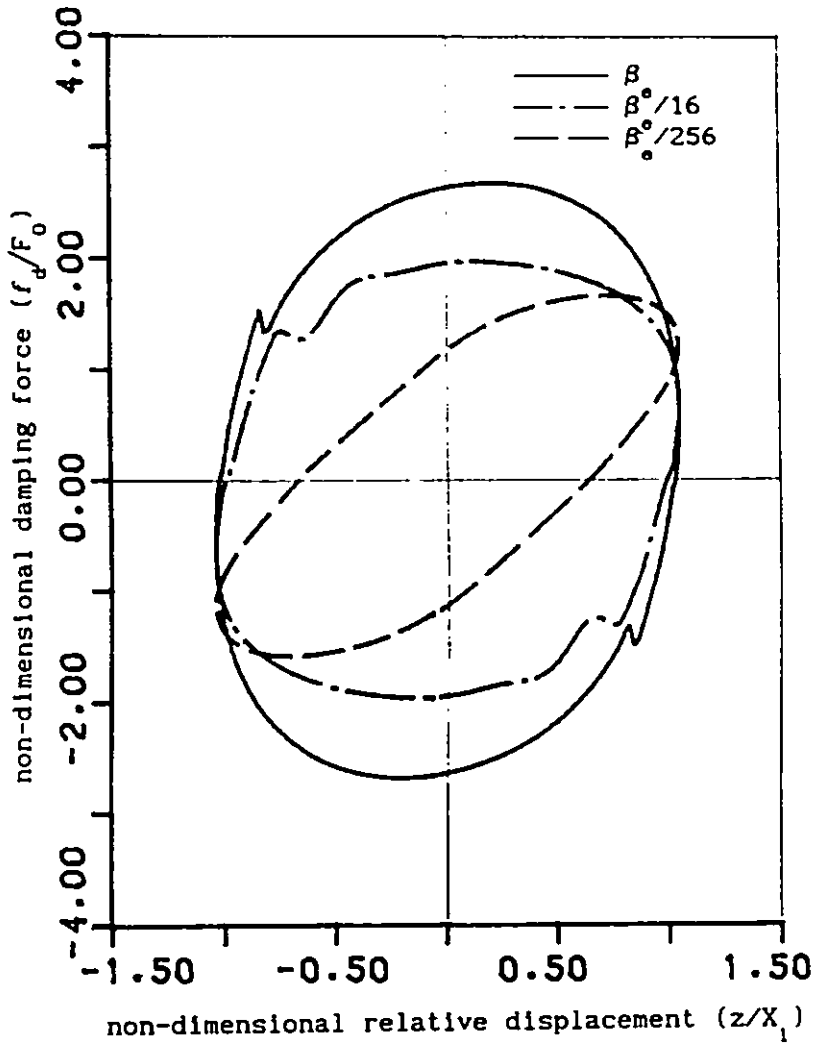

FIGURE 4.8 Damping force-displacement characteristics of tunable damper with various bulk moduli (β_e=6.9x10^8 (Pa), ω/ω_n=5.0)

4.7 and 4.8. The magnitude of peak damping force decreases considerably with reduced bulk modulus, as shown in Figure 4.8. At higher excitation frequencies, compliance due to the damper fluid gives rise to restoring force characteristics, as illustrated in Figure 4.8.

The restoring force due to the gas-spring of the pressure limited damper is computed from equations (4.4) and (4.44). The gas spring force-displacement characteristics of the tunable hydraulic damper incorporating valve dynamics and effective compliance are computed corresponding to excitation frequencies ω/ω_n = 0.5, 1.0 and 5.0, and compared with those of the ideal tunable pressure limited damper, as shown in Figures 4.9 to 4.11, respectively. It is observed that the force value due to the gas spring of the tunable pressure limited damper is shifted up , with respect to the gas spring force with incompressible fluid, when fluid compressibility is considered as shown in Figures 4.9 to 4.11. For the same load on the vibration isolation system, the effective bulk modulus results in a reduction in fluid volume within the damper. The compressed fluid volume thus introduces a further reduced gas volume in chamber III, which, in turn, shifts the gas spring force to a larger value. Furthermore, as the excitation frequency is increased the gas chamber within the tunable damper begins to dissipate a certain amount of vibration energy due to compressibility of the fluid and valve dynamics, as shown in Figure 4.10 and 4.11. The amount of energy dissipated per cycle due to the gas chamber increases as the excitation frequency is increased. An ideal tunable damper, however, provides only restoring force due to the gas chamber.

Figure 4.12 presents the total dynamic force-displacement

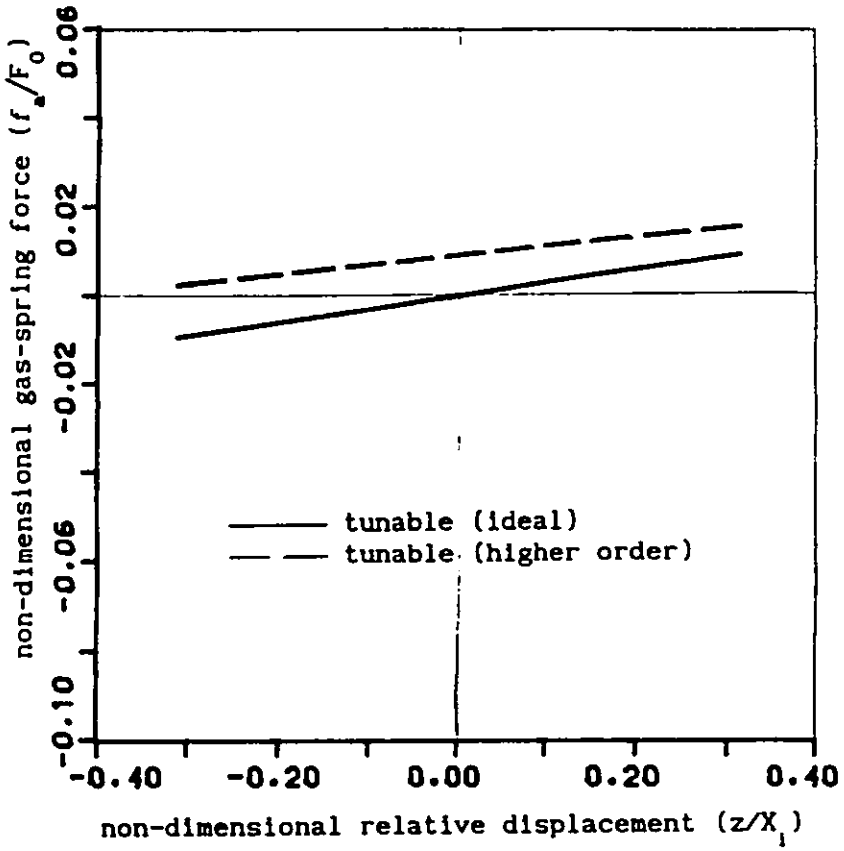

FIGURE 4.9 Force-displacement characteristics of gas-spring component with ideal and higher order models (β_e=6.9×10^8 (Pa)), (ω/ω_n=0.5)

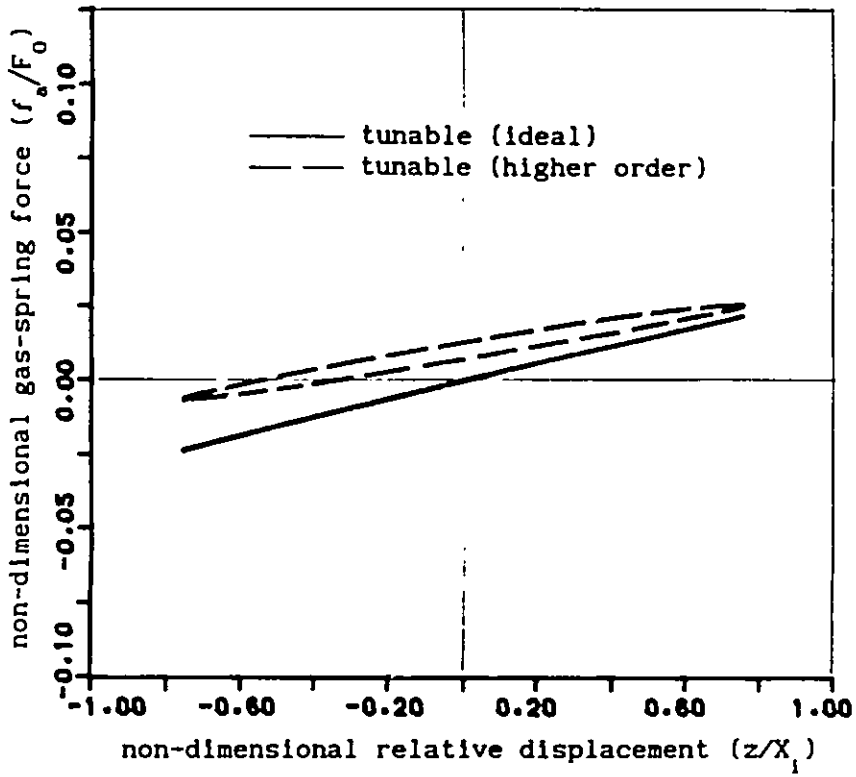

FIGURE 4.10 Force-displacement characteristics of gas-spring component with ideal and higher order models (β_e=6.9×10^8 (Pa)), (ω/ω_n=1.0)

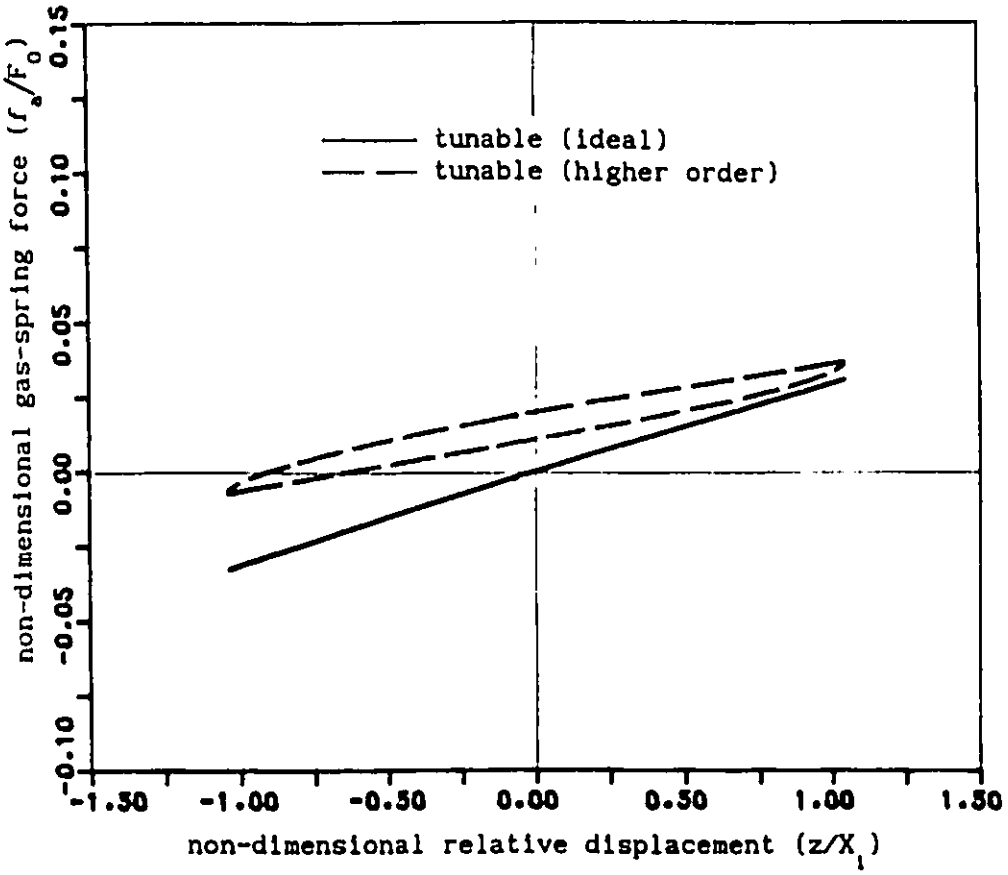

FIGURE 4.11 Force-displacement characteristics of gas-spring component with ideal and higher order models (β_e=6.9×10^8 (Pa)), (ω/ω_n=5.0)

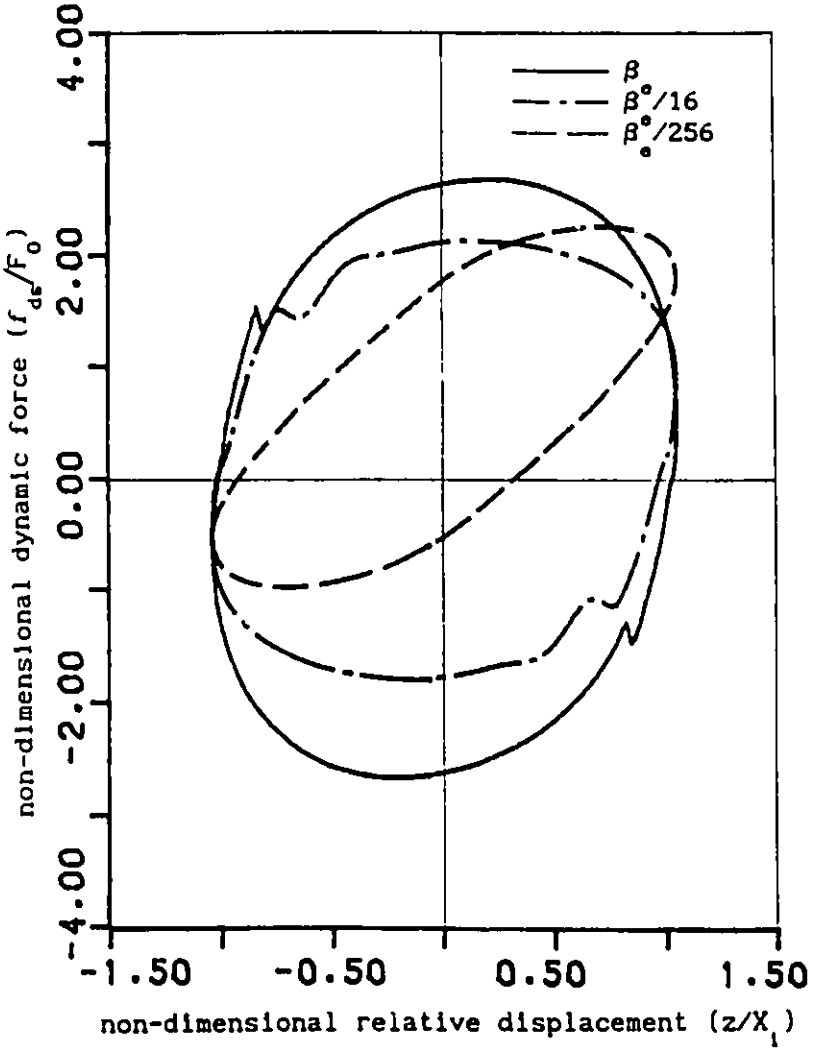

FIGURE 4.12 Total force-displacement characteristics of tunable damper with various bulk moduli (β_e=6.9x10^8 (Pa), ω/ω_n=5.0)

characteristics of the tunable pressure limited hydraulic damper, as function of the effective bulk modulus, corresponding to excitation frequency $\omega = 5\ \omega_n$. It is observed that the magnitude of peak damping force (corresponding to zero relative displacement) decreases considerably and orients towards a restoring force as well, when the value of bulk modulus is reduced. A lower value of effective bulk modulus yields a larger shifting of the total force component of the damper due to the increase in gas-spring force as shown in Figure 4.12.

A time history of the dynamic force of the tunable hydraulic damper with the ideal pressure limiting scheme and higher order models, corresponding to a rounded step excitation, is presented in Figure 4.13. It is observed that the magnitude of peak dynamic force due to the effective bulk modulus is increased, as compared with that of the ideal pressure limiting scheme. Figure 4.14 shows the dynamic force of tunable damper with various values of effective bulk modulus in time domain. A comparison of the results reveals that the magnitude of the peak dynamic force is reduced as the bulk modulus is decreased. Moreover, the steady state value of dynamic force of the tunable damper is increased due to the decrease of the effective bulk modulus and thus the increased gas spring force.

4.4 Vibration Isolation Performance

The system of equations derived in section 4.2 are solved to evaluate the vibration isolation performance of the system employing a tunable pressure limited damper in terms of vibration transmissibility. Vibration transmissibility characteristics of the system with a tunable

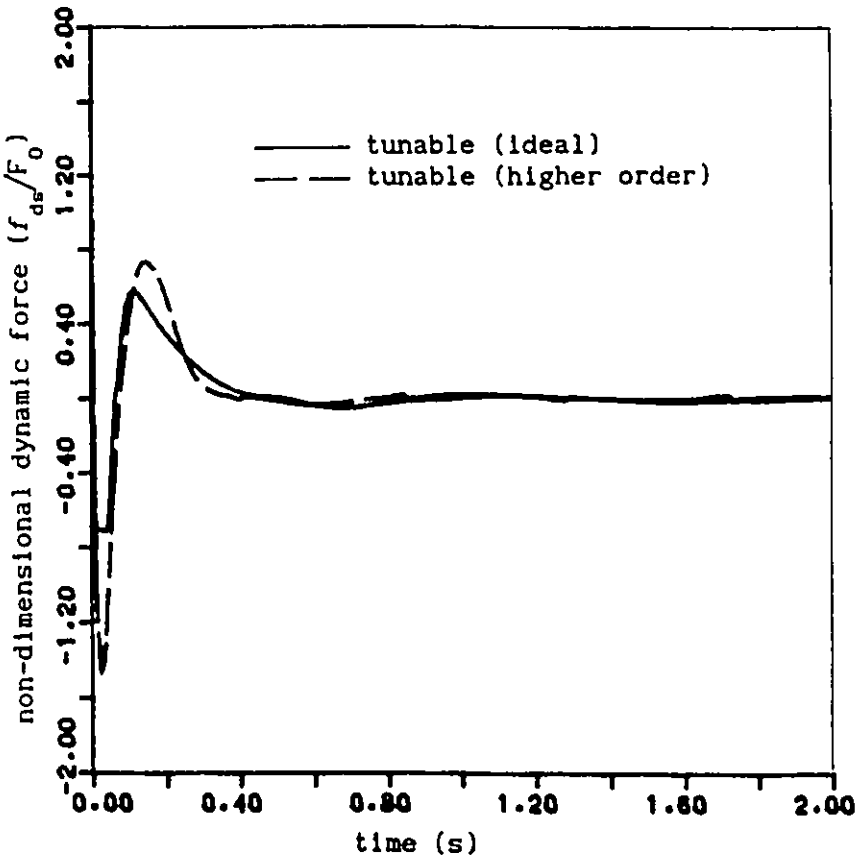

FIGURE 4.13 Transient force of tunable damper with ideal and higher order models (β_e=6.9x10^8 (Pa)) due to rounded step input (η=10)

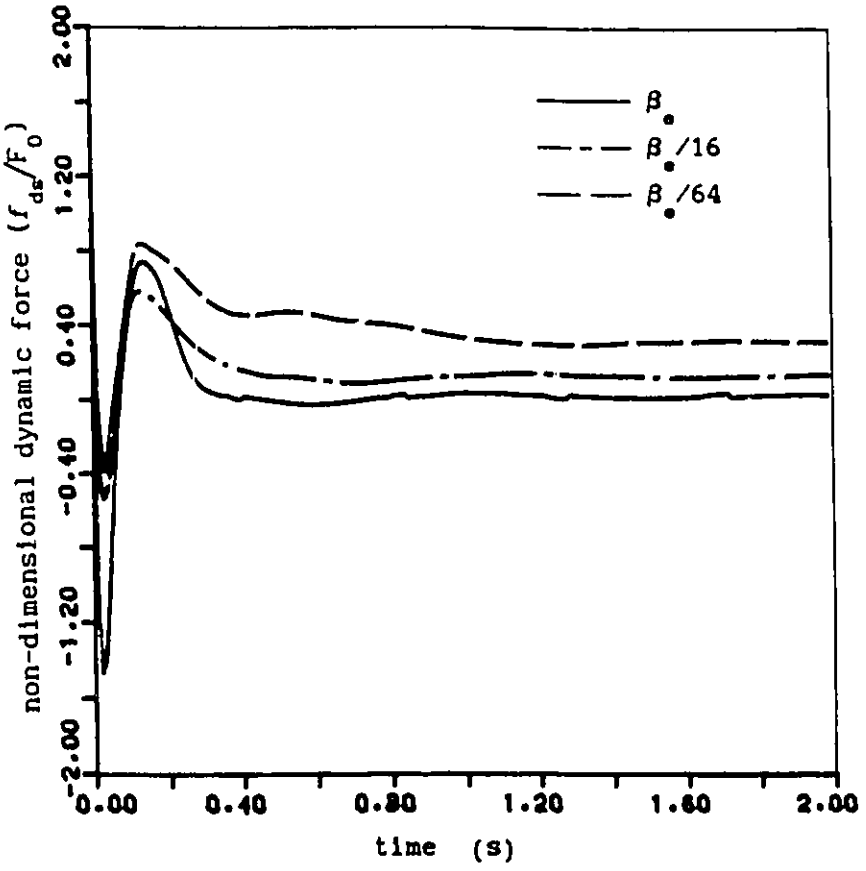

FIGURE 4.14 Transient force of tunable damper with various bulk moduli (β_o=6.9x10^8 (Pa)) due to rounded step input (η=10)

pressure limited damper are compared with those with an ideal tunable damper to demonstrate the influence of effective bulk modulus and valve dynamics. The vibration isolation characteristics of the system with a tunable pressure limited damper are further compared with those of the fixed orifice damper, incorporating the effect of fluid compliance, to illustrate the performance potentials of the proposed pressure limited hydraulic damper. The influence of variations in the tuning factor and effective bulk modulus on the vibration transmissibility characteristics is presented.

The displacement and velocity transmissibility characteristics of the vibration isolation system, employing a tunable pressure limited damper, are evaluated and compared with those of the isolator employing a fixed orifice hydraulic damper incorporating compliance of fluid, as shown in Figure 4.15 and 4.16, respectively. The effective bulk modulus for both dampers is selected as $\beta_e = 6.9 \times 10^8$ (Pa). It is observed that the displacement and velocity transmissibility response of the system with tunable damper (ν=1) is identical to that of the fixed orifice damper for excitation frequencies below the resonant frequency of the isolator. The resonant transmissibility response of the pressure limited hydraulic damper is slightly larger than that of the fixed orifice damper, as shown in Figures 4.15 and 4.16. The transmissibility characteristics of the pressure limited hydraulic damper continue to be larger than that of the isolator with fixed orifice damper corresponding to excitation frequencies above the resonant frequency. Dynamic motion of the spool within the pressure relief valves yields modulation of the fluid flow even before the pressure differential p_{12} approaches the

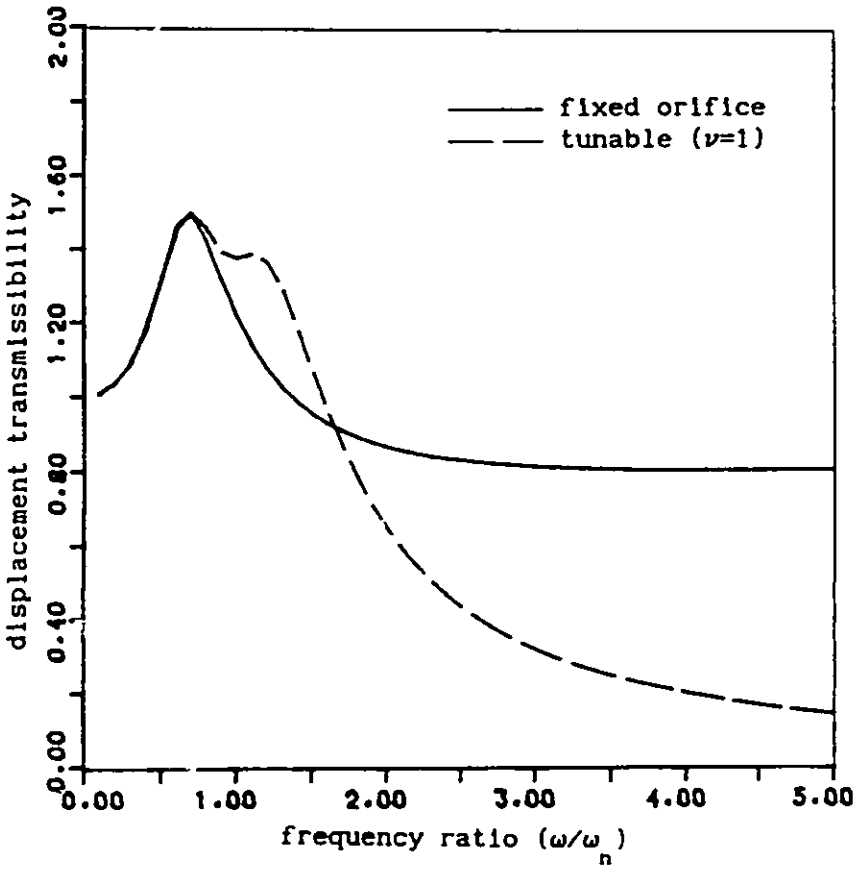

FIGURE 4.15 Displacement transmissibility of vibration isolation system employing fixed orifice and tunable dampers (β_e=6.9x10^8 (Pa))

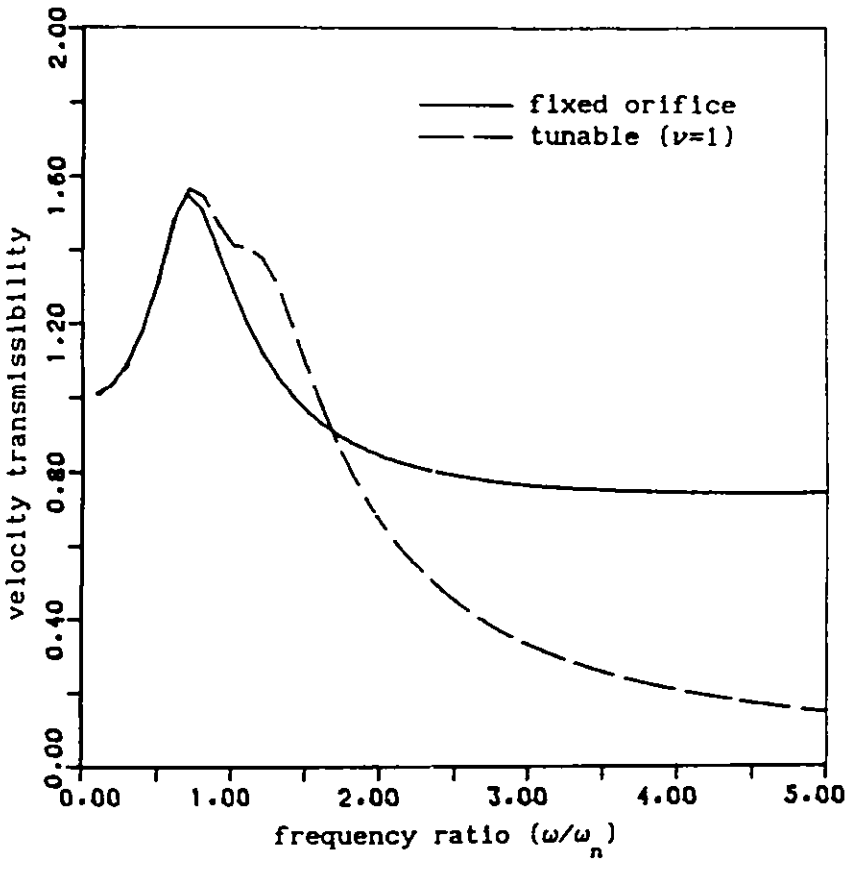

FIGURE 4.16 Velocity transmissibility of vibration isolation system employing fixed orifice and tunable dampers (β_e=6.9x10^8 (Pa))

preset value and thus provides poor transmissibility characteristics at excitation frequencies slightly larger than the resonant frequency. However, as the excitation frequency is further increased, the tunable pressure limited damper yields considerably superior vibration transmissibility characteristics when compared with those of the fixed orifice damper.

The influence of the dynamics of the pressure relief valve on the vibration isolation performance is further illustrated though comparison of the vibration transmissibility characteristics of the isolator with a higher order tunable damper system with those of an ideal tunable pressure limiting damper. Displacement, acceleration and relative displacement transmissibility characteristics of the pressure limited hydraulic damper are presented in Figures 4.17, 4.18 and 4.19, respectively. Transmissibility characteristics of the system employing ideal tunable pressure limited damper exhibit two peaks corresponding to the resonant frequency of the isolator and the frequency at which flow modulation occurs. Transmissibility characteristics of the system with a higher order tunable damper, incorporating the dynamics associated with relief valve and fluid compliance, also reveal two peaks similar to the ideal tunable damper, as shown in Figures 4.17 to 4.18. The magnitude of displacement transmissibility increases slightly, corresponding to excitation frequencies above the resonant frequency, when dynamics due to relief valve and fluid compliance are incorporated, as shown in Figure 4.17. The peak acceleration transmissibility, at the isolator's resonant frequency, also increases due to the dynamics of the relief valve, as shown in Figure 4.18. The acceleration transmissibility,

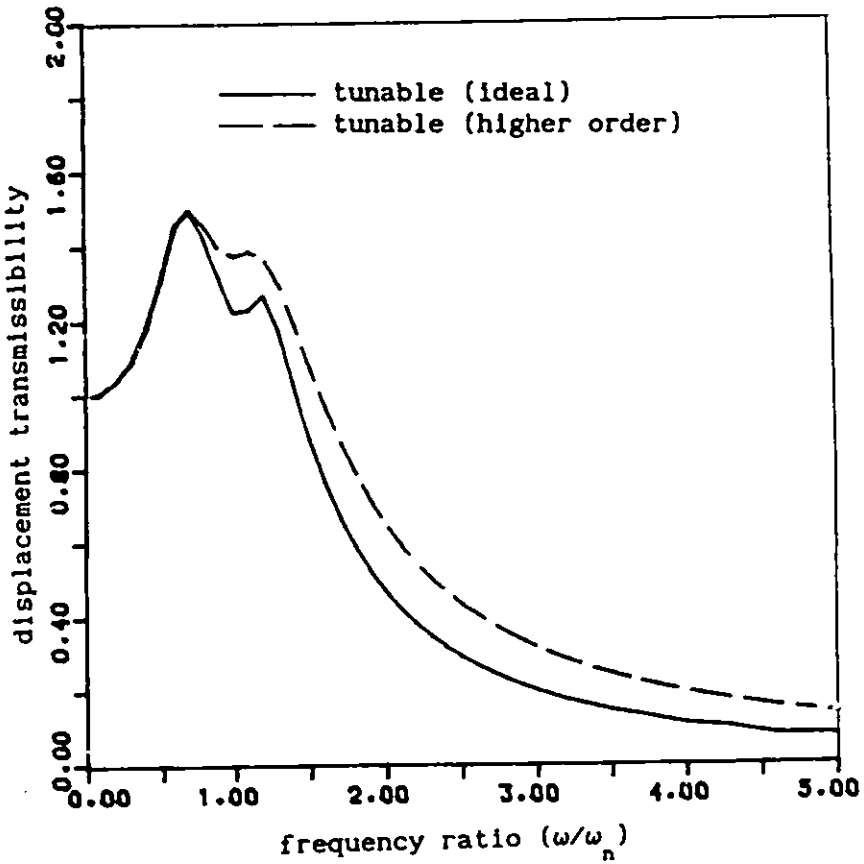

FIGURE 4.17 Displacement transmissibility of vibration isolation system employing tunable damper with ideal and higher order models (β_e=6.9x10^8 (Pa)), (ν=1)

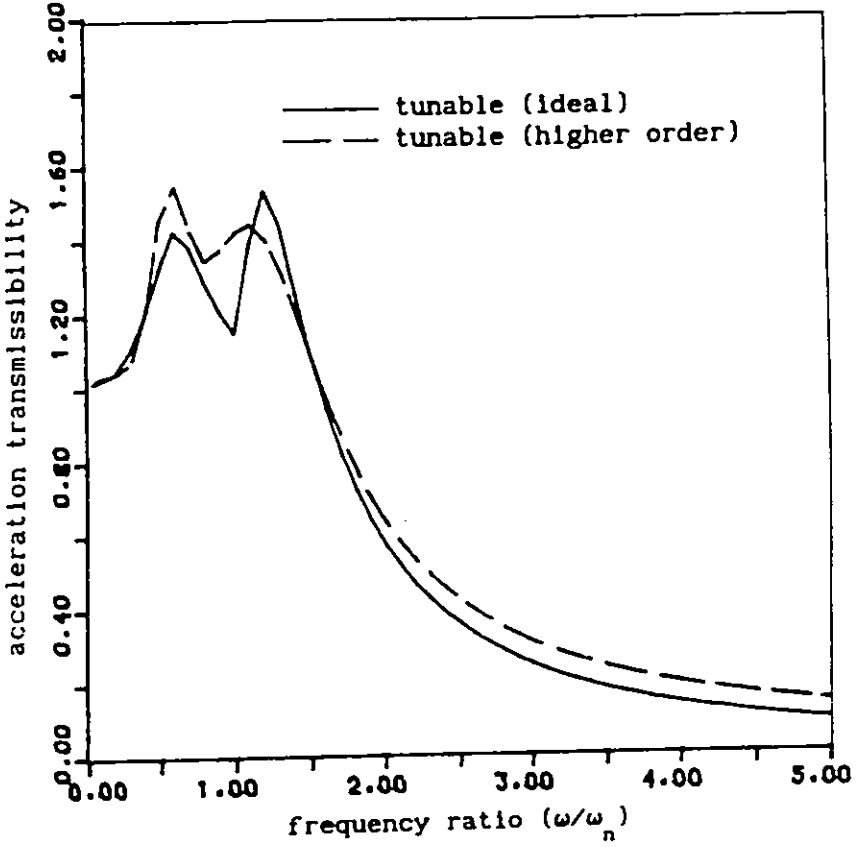

FIGURE 4.18 Acceleration transmissibility of vibration isolation system employing tunable damper with ideal and higher order models (β_e=6.9x10^8 (Pa)), (ν=1)

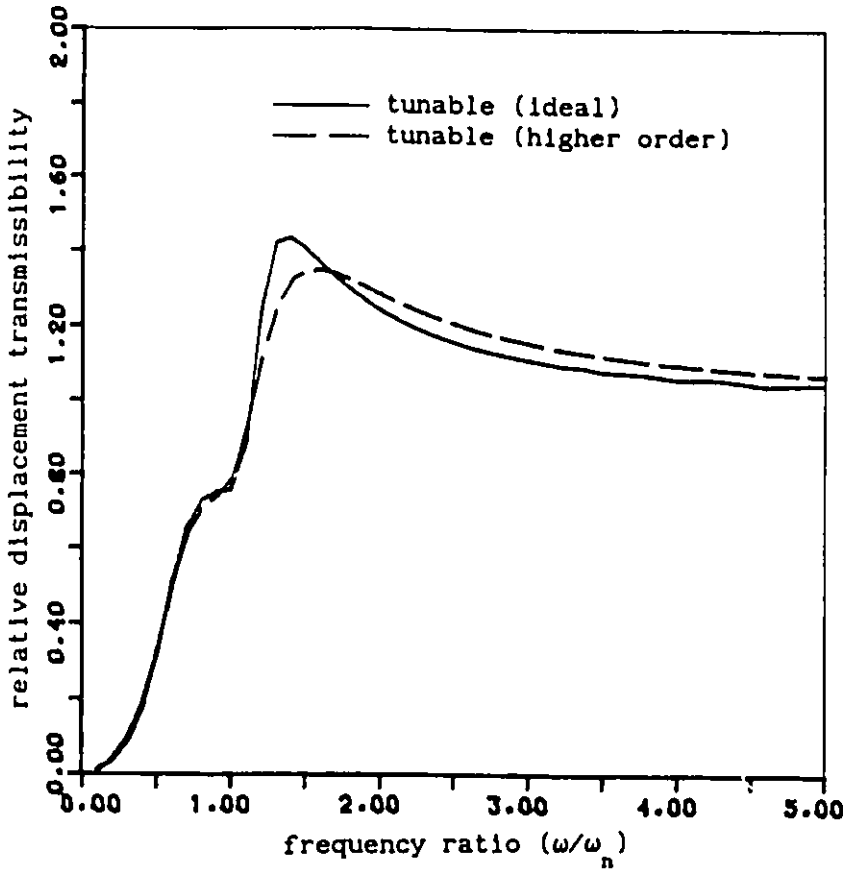

FIGURE 4.19 Relative displacement transmissibility of vibration isolation system employing tunable damper with ideal and higher order models (β_e=6.9x10^8 (Pa)), (ν=1)

corresponding to excitation frequency at which the pressure differential p_{12} approaches the preset value, however, decreases due to dynamics of the pressure relief valve. At higher excitation frequencies, pressure relief valve dynamics yields only insignificant influence on the acceleration transmissibility, as shown in Figure 4.18. Dynamic motion of the spools within the pressure relief valves yields improved relative displacement transmissibility corresponding to the excitation frequency at which pressure limiting occurs, as shown in Figure 4.19, due to gradual opening of the relief valve. However, the relative displacement response increases slightly due to the dynamics of the relief valves at higher excitation frequencies.

The influence of the effective bulk modulus on the displacement and velocity transmissibility characteristics of the vibration isolation system with a tunable pressure limited hydraulic damper are illustrated in Figures 4.20 and 4.21, respectively. In Figure 4.20 the displacement transmissibility characteristics are presented for various values of effective bulk moduli: $\beta_e = 6.9\times10^8$ (Pa), $\beta_e/4$ and $\beta_e/32$. It is observed that there is a moderate reduction in effective bulk modulus yields only a slight increase in displacement transmissibility, specifically around the excitation frequency at which pressure limiting takes place. However, an excessive reduction in the effective bulk modulus can yield significantly large peak transmissibility response, as shown in Figure 4.21 for various values of effective bulk moduli: $\beta_e = 6.9\times10^8$ (Pa), $\beta_e/16$, $\beta_e/128$ and $\beta_e/256$.

Vibration transmissibility characteristics of the vibration isolation system employing tunable pressure limited damper are strongly

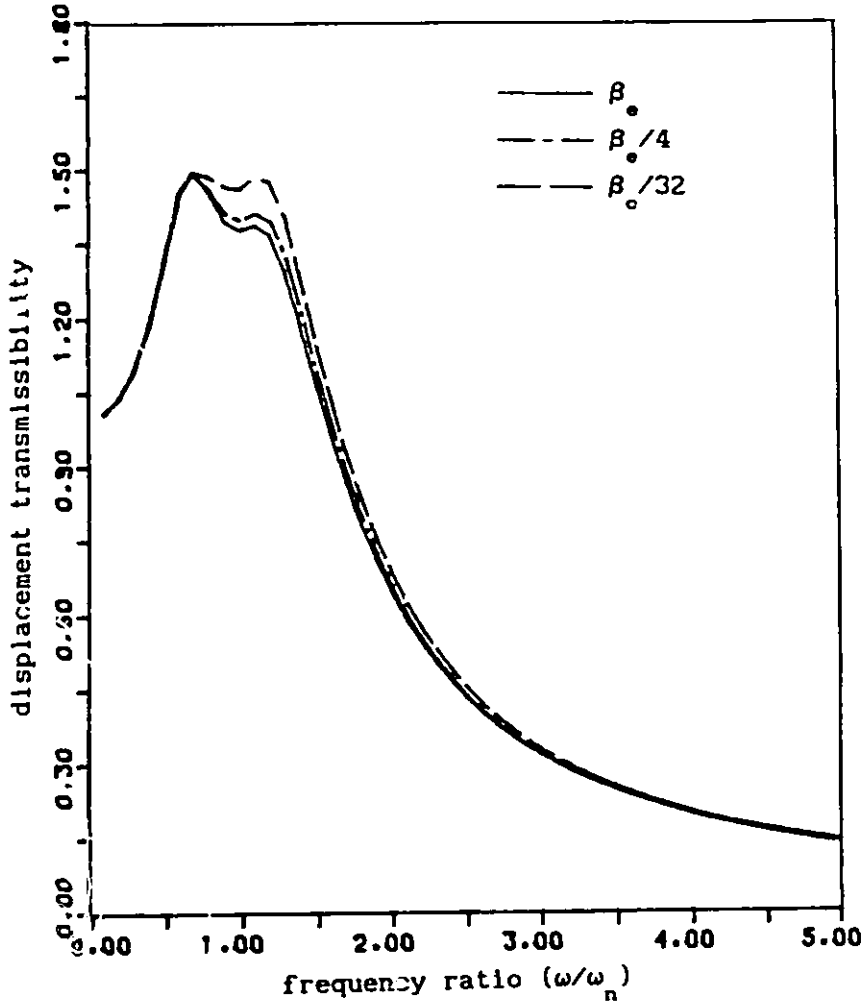

FIGURE 4.20 Displacement transmissibility of vibration isolation system employing tunable damper with various bulk moduli (β_e=6.9x10^8 (Pa)), (ν=1)

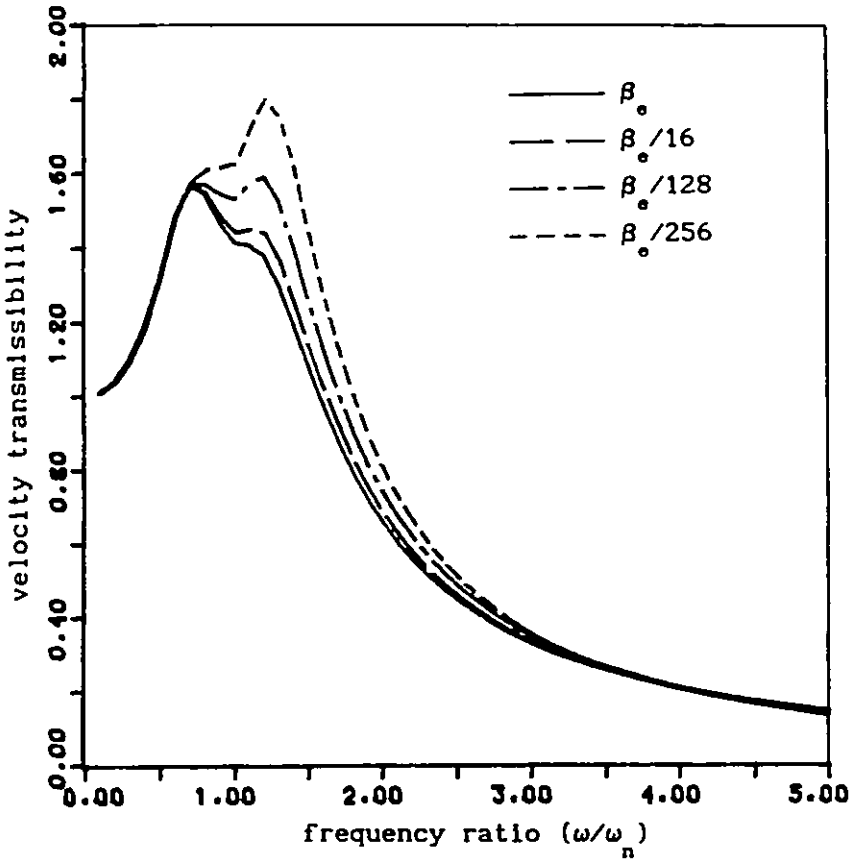

FIGURE 4.21 Velocity transmissibility of vibration isolation system employing tunable damper with various bulk moduli (β_e=6.9x10^8 (Pa)), (ν=1)

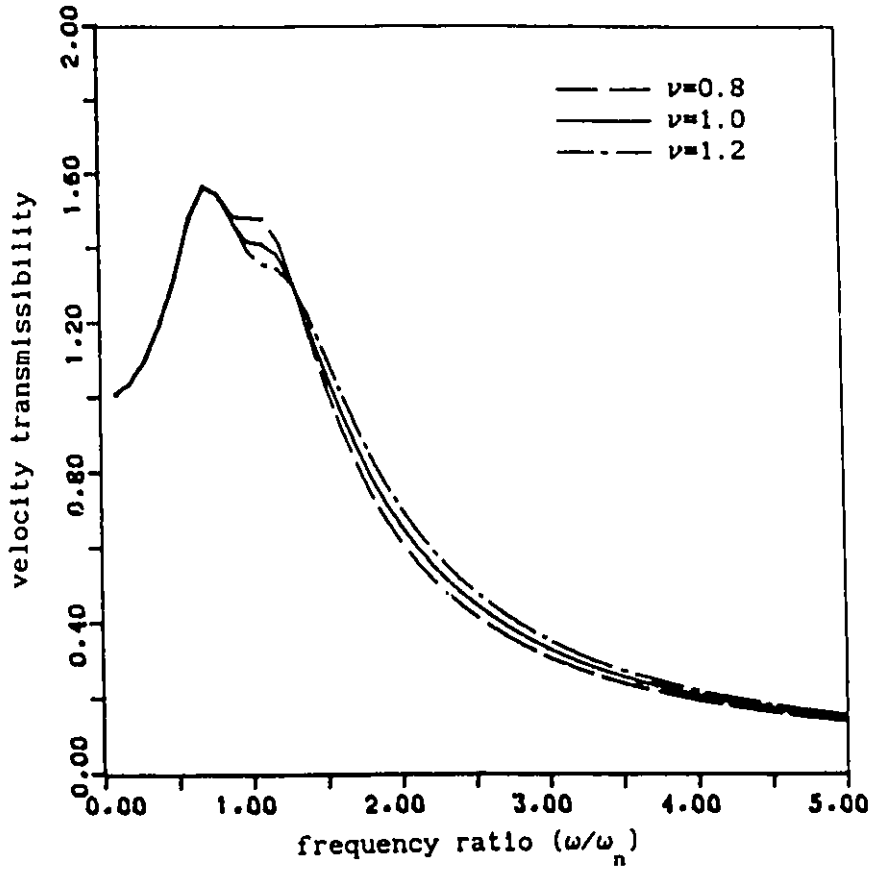

FIGURE 4.22 Velocity transmissibility of vibration isolation system employing tunable damper with various values of tuning factor (β_e=6.9x10^8 (Pa))

related to the tuning factor, ν, as shown in Figure 4.22. The vibration transmissibility characteristics at excitation frequencies near and above the resonant frequency are significantly influenced by the tuning factor. A lower value of tuning factor (ν=0.8) tends to limit the pressure differential at a lower excitation frequency and thus yields a larger transmissibility response near the resonance. Alternatively larger value of tuning factor can be selected to limit the pressure differential at a higher excitation frequency such that the transmissibility response near the resonant frequency can be reduced. However, larger tuning factor tends to limit the pressure differential to a higher preset value and thus yields slightly higher transmissibility response at higher excitation frequencies, as shown in Figure 4.22.

4.5 Shock Isolation Performance

The shock isolation performance of the system employing a tunable pressure limited hydraulic damper is also strongly related to the dynamics associated with the relief valve and the effective bulk modulus. Shock isolation characteristics are evaluated for a rounded step displacement excitation at the isolator's base in order to illustrate the significance of these parameters. The shock displacement and velocity responses are non-dimensionalized with respect to input magnitude X_{max} and $(\omega_n X_{max})$, respectively.

The transient displacement and velocity response characteristics of a shock isolation system, employing a fixed orifice hydraulic damper, are compared with those of the isolator employing a tunable damper

(ν=1.0) incorporating valve dynamics, as shown in Figures 4.23 and 4.24, respectively. Mechanical and fluid compliance is incorporated in both the dampers through an effective bulk modulus of $\beta_e = 6.9\times10^8$ (Pa). Figures 4.23 and 4.24 clearly reveal that the peak displacement and velocity responses of the tunable pressure limited damper are considerably lower than those of the fixed orifice damper.

Transient displacement and velocity response characteristics of the isolator with tunable pressure limited damper are further compared with those of an ideal pressure limited damper in order to illustrate the influence of relief valve dynamics, as shown in Figures 4.25 and 4.26, respectively. The shock displacement response, presented in Figure 4.25, reveals that the peak response and the corresponding settling time decrease slightly, when the relief valve dynamics and fluid compliance are incorporated in the higher order tunable damper model. However, the peak velocity response increases due to the dynamics associated with the relief valves. The settling time of the velocity response of the higher order tunable damper model associated valve dynamics and fluid compliance decreases as compared with that of the ideal tunable damper as shown in Figure 4.26.

Figure 4.27 illustrates the influence of the effective bulk modulus on the shock isolation performance of the tunable pressure limited damper, for relatively smaller reductions in effective bulk modulus ($\beta_e = 6.9\times10^8$ (Pa), $\beta_e/4$ and $\beta_e/16$). It is observed that the peak displacement response, the speed of response, and the steady state value of response decrease due to reduced effective bulk modulus of the fluid in the hydraulic damper.

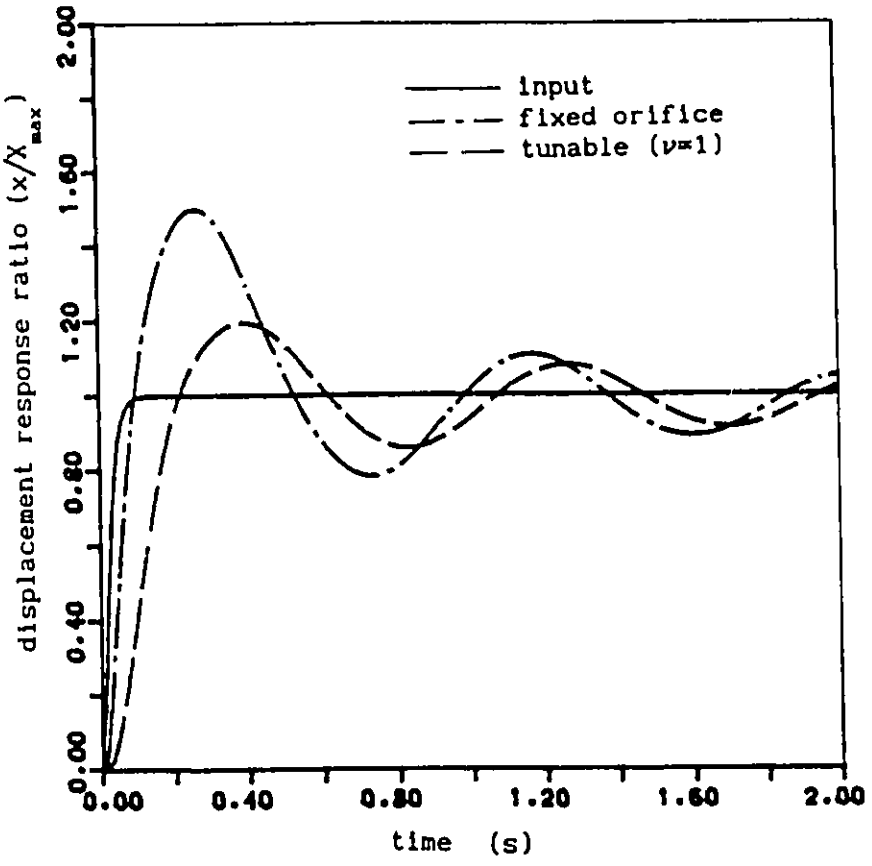

FIGURE 4.23 Transient displacement response of shock isolation system employing fixed orifice and tunable dampers (β_e=6.9x10^8 (Pa))

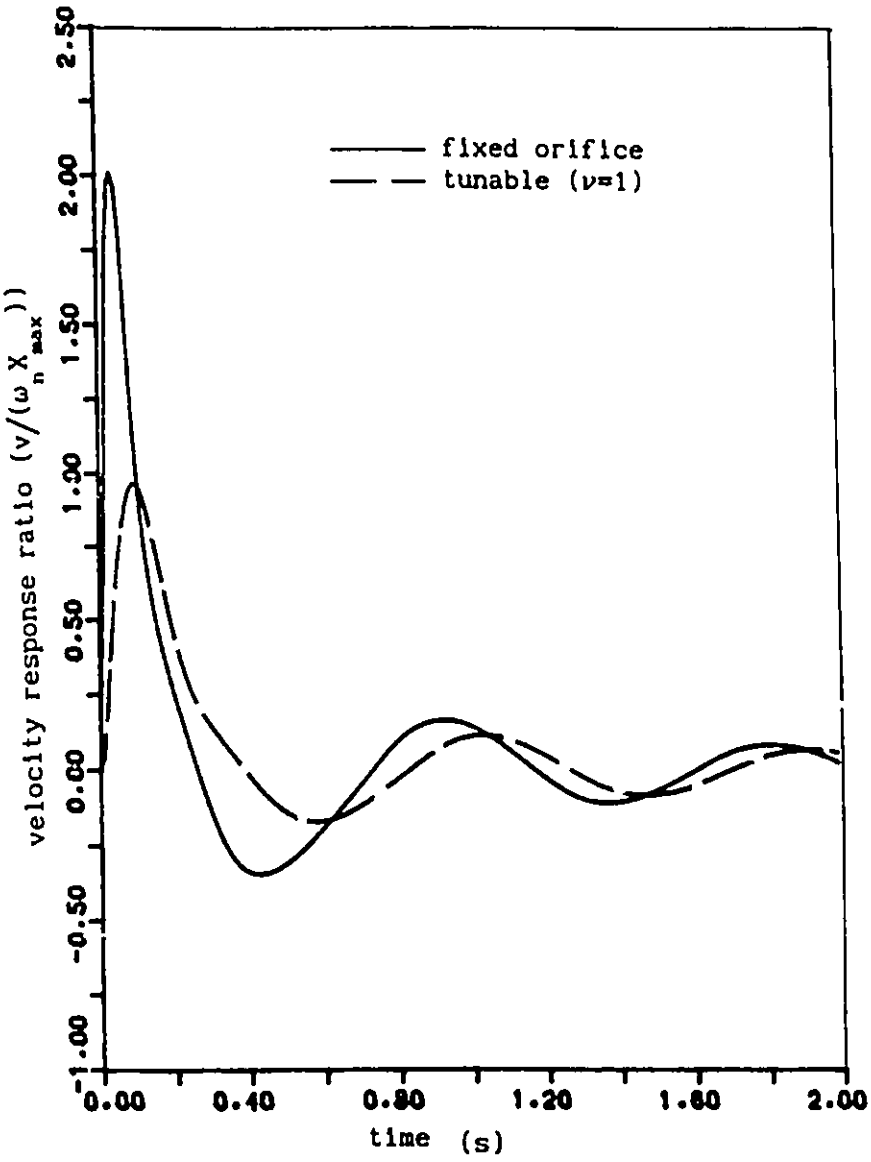

FIGURE 4.24 Transient velocity response of shock isolation system employing fixed orifice and tunable dampers (β_e=6.9x10^8 (Pa))

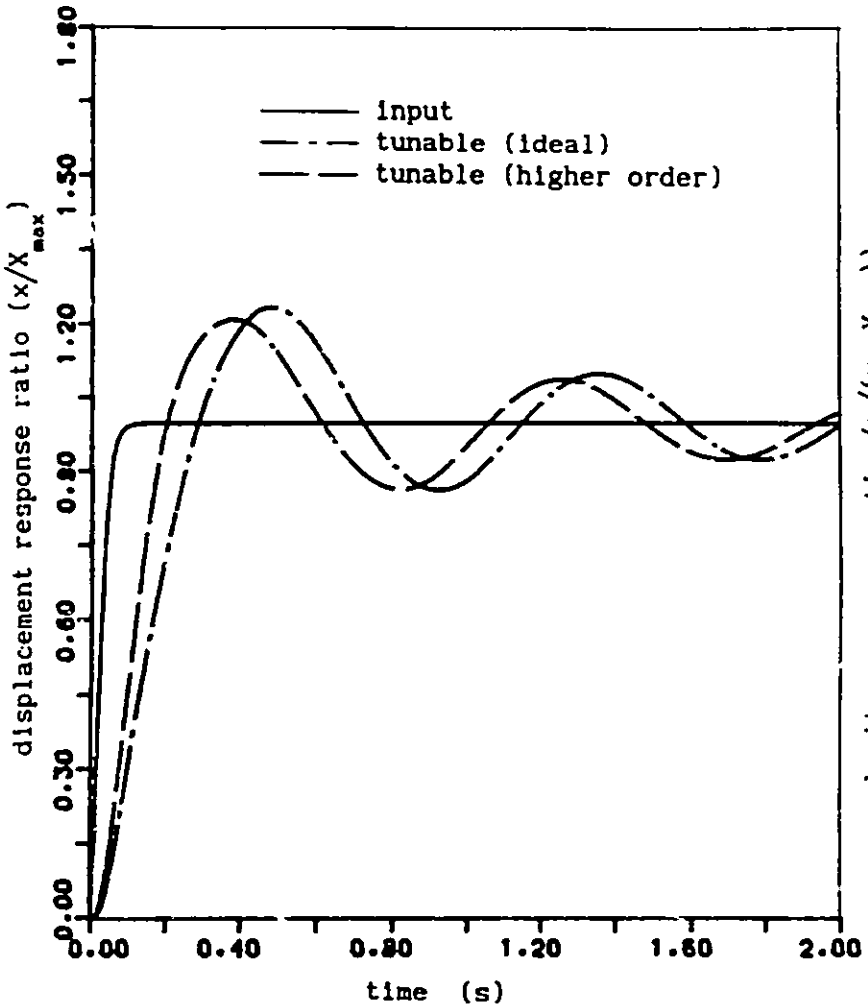

FIGURE 4.25 Transient displacement response of shock isolation system employing tunable damper with ideal and higher order models (β_e=6 9x10^8 (Pa)), (ν=1)

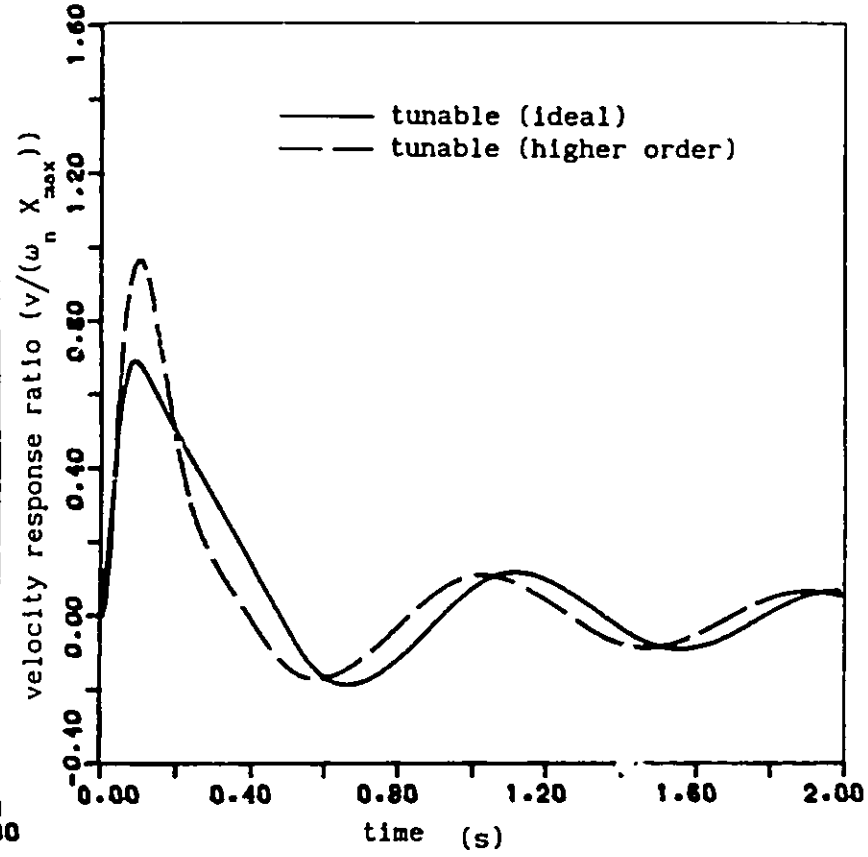

FIGURE 4.26 Transient velocity response of shock isolation system employing tunable damper with ideal and higher order models (β_e=6.9x10^8 (Pa)), (ν=1)

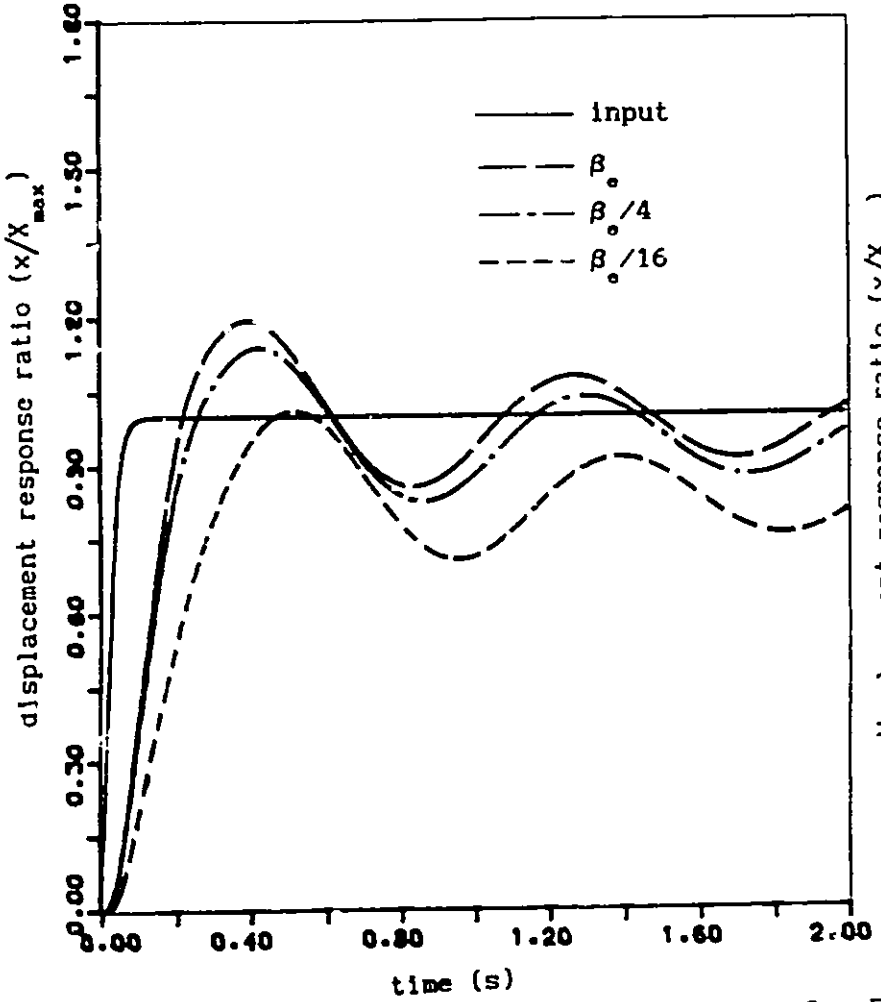

FIGURE 4.27 Transient displacement response of shock isolation system employing tunable damper with various bulk moduli (β_e=6.9x10^8 (Pa), (ν=1)

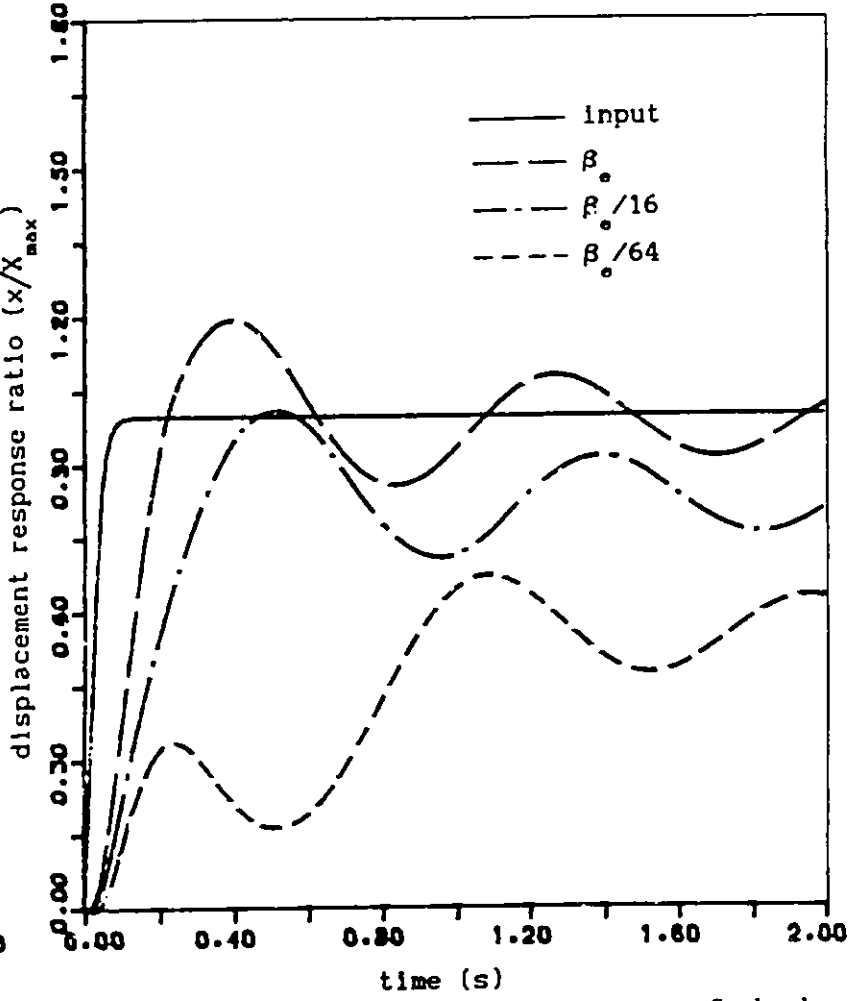

FIGURE 4.28 Transient displacement response of shock isolation system employing tunable damper with various bulk moduli (larger variation) (β_e=6.9x10^8 (Pa), (ν=1)

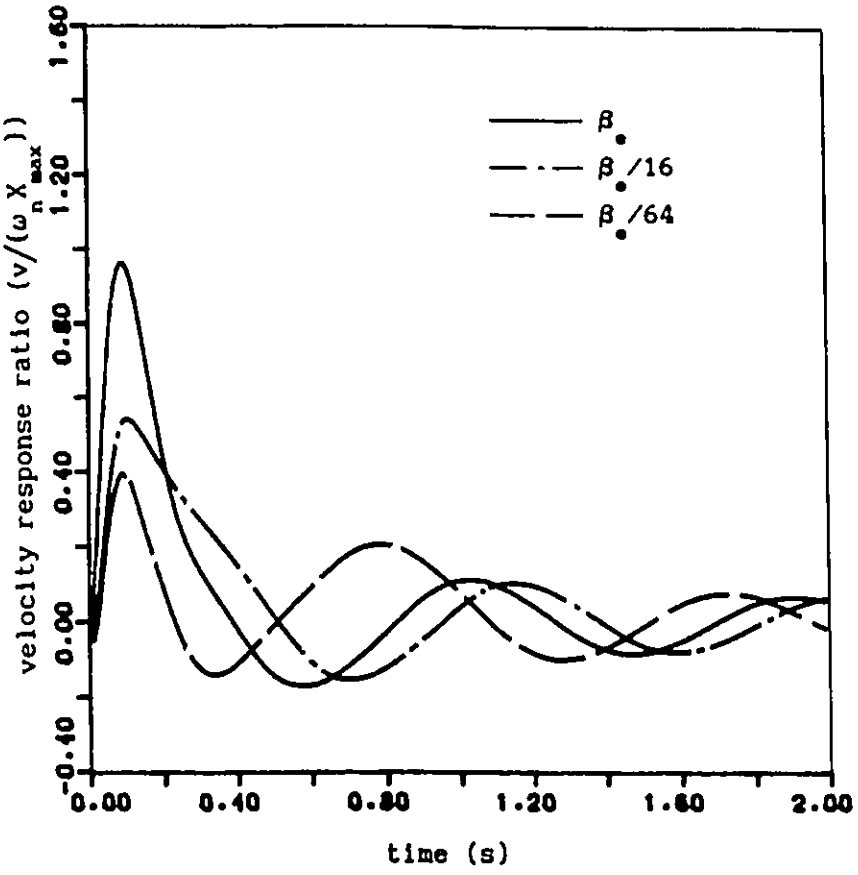

FIGURE 4.29 Transient velocity response of shock isolation system employing tunable damper with various bulk moduli (β_e=6.9×10^8 (Pa), (ν=1)

A further reduction in effective bulk modulus (β_e, $\beta_e/16$ and $\beta_e/64$) yields significant influence on the displacement and velocity response characteristics of the isolator as shown in Figures 4.28 and 4.29, respectively. The response speed of the tunable pressure limited hydraulic damper decreases considerably, when the value of the effective bulk modulus is further reduced. The fluid volume within the hydraulic damper decreases due to the reduced effective bulk modulus for the same load on the isolator and thus a further deflection of the hydraulic damper results with respect to the static equilibrium position. Therefore, the steady state value of displacement response of the isolator is further reduced with respect to the input displacement value, for a lower bulk modulus, as shown in Figure 4.28. When the value of effective bulk modulus is reduced and thus results in a softened damper, the peak value of velocity response of the system with tunable damper is also reduced, as shown in Figure 4.29.

4.6 Summary

A mathematical model of the tunable pressure limited hydraulic damper, incorporating the fluid and mechanical compliance, and the dynamics of pressure relief valves, is developed. Equations of motion and fluid flow are formulated for a general port geometry. The higher order analytical model of a tunable pressure limited hydraulic damper, incorporating fluid compliance and valve dynamics, is analyzed to determine the damping force, gas spring force, vibration transmissibility and shock response characteristics. The response characteristics of a tunable pressure limited damper are compared with

those of fixed orifice and ideal pressure limited dampers to demonstrate the significance of effective damper compliance and valve dynamics. The study demonstrates that the reduced effective bulk modulus can result in dynamic force changes which influence both shock and vibration isolation performance of hydraulic damper isolators considerably. The dynamics of the relief valves also have certain influence on the shock and vibration isolation characteristics of the isolator employing tunable pressure limited damper. The tunable damper incorporating valve dynamics and effective bulk modulus yields significantly improved shock and vibration isolation performance as compared with that of the fixed orifice damper.

CHAPTER 5

RIDE DYNAMIC ANALYSIS OF ROAD VEHICLES EMPLOYING TUNABLE PASSIVE SUSPENSION

5.1 Introduction

Ride comfort, handling and control performance of road vehicles pose conflicting requirements on primary vehicle suspensions. A soft vehicle suspension is required to effectively isolate the vehicle structure, cargo and driver from terrain induced excitations in order to achieve good ride quality. Directionally stable performance of the vehicle, however, requires the vehicle suspension to be relatively stiff. Design of vehicle suspensions thus involves the selection of appropriate spring and damping mechanisms to achieve a compromise among ride comfort, handling and control performance. A number of damping mechanisms have been proposed and investigated to achieve improved vehicle ride, while the suspension stiffness is selected to provide adequate handling and control performance. In view of the performance limitations of conventional passive vehicle suspensions, specifically due to the fixed damping, numerous semi-active, active and modified passive suspension systems have been proposed to achieve improved vehicle ride. Although active vehicle suspensions, with actively controlled damping and spring characteristics, provide superior vehicle ride quality, implementation of the active suspension has been limited due to requirements of external power source, feedback control devices, sensors and force generators [32]. Alternatively, semi-active suspensions, based on either continuous or sequential variations in damping, have been proposed to improve the dynamic ride performance of

road vehicles [49, 57]. Although the hardware requirements of a semi-active suspension are considerably simpler than that of an active suspension, a general use of the semi-active suspension is still prohibitive due to the requirements of instrumentation packages and feedback control devices, and the associated chatter problems [59].

In this chapter, the ride performance characteristics of road vehicles employing tunable pressure limited shock absorbers within the primary suspension are analytically investigated. Dynamic ride performance of a vehicle employing a tunable passive suspension is evaluated through deterministic and stochastic analyses. Two vehicle models, namely a quarter vehicle model and an in-plane vehicle model, are developed and investigated to demonstrate the ride performance potentials of tunable shock absorbers. The quarter vehicle model is first evaluated for deterministic excitations in the time and frequency domains. The dynamic ride performance of the quarter vehicle model is presented in terms of shock and vibration isolation characteristics. A generalized discrete harmonic linearization technique, based on frequency domain linearization methods is proposed to simulate nonlinear vehicle models for stochastic excitations. The equivalent linear stiffness and damping coefficients are derived as a function of excitation frequency and response amplitude to characterize the nonlinear restoring and damping elements. The stochastic response of an in-plane vehicle model with tunable passive shock absorbers is presented and discussed in terms of response power spectral density.

5.2 Development of Vehicle Models

The two vehicle models, namely a quarter vehicle model and an

in-plane vehicle model, are developed based on ideal tunable pressure limited shock absorber models, in order to simplify analysis of the dynamic ride performance potentials of the tunable vehicle suspensions. The bulk modulus of the fluid is also assumed to be high and its influence on ride performance is thus negligible.

5.2.1 A Quarter Vehicle Model

Shock and vibration isolation performance characteristics of a primary vehicle suspension, employing a tunable pressure limited shock absorber, are initially investigated through analysis of a simplified two-degrees-of-freedom vehicle model, often referred to as a "quarter vehicle model" [110], and is illustrated in Figure 5.1. The primary vehicle suspension is modeled as a parallel combination of a linear spring, k_s, and a tunable hydraulic shock absorber D. The tire is represented by a linear spring, k_t, assuming point contact with the terrain and negligible damping. Sprung mass, m_s, represents the portion of the mass of the vehicle supported on a single wheel suspension, while the mass due to wheel and axle assembly is modeled as an unsprung mass, m_u. The sprung and unsprung masses of the vehicle are constrained to move along the vertical axis alone. Assuming negligible friction, the total dynamic force generated by the tunable shock absorber includes a restoring force due to the gas-spring and a dissipative force due to orifice flows, as discussed earlier in Chapter 3. The equations of motion of the two-DOF vehicle model are expressed as:

$$m_s \ddot{x}(t) + k_s z(t) + f_a(t) + f_d(t) = 0 \quad . \qquad (5.1)$$

$$m_u \ddot{x}_u(t) - k_s z(t) - f_a(t) - f_d(t) + k_t x_u(t) = k_t x_i(t) \qquad (5.2)$$

where,

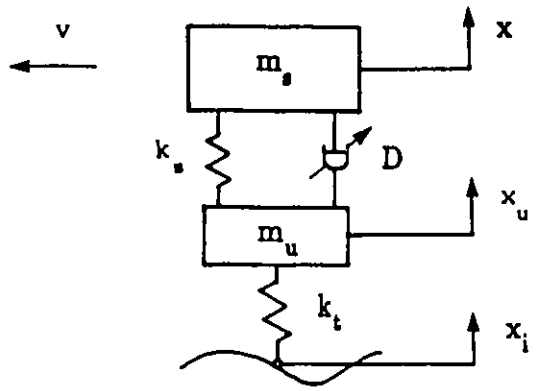

FIGURE 5.1 Schematic of a quarter vehicle model

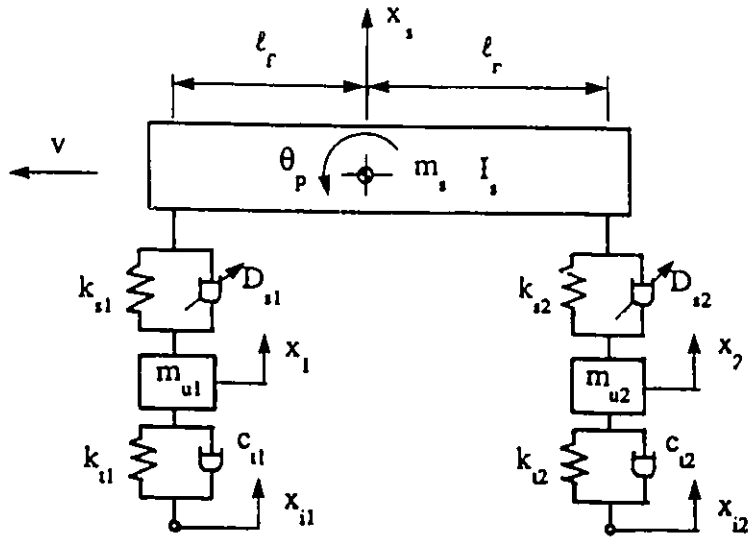

FIGURE 5.2 Schematic of an in-plane bounce and pitch vehicle model

x = vertical displacement coordinate of sprung mass (m)

x_u = vertical displacement coordinate of unsprung mass (m)

x_i = input displacement at tire-road interface (m)

z = $x - x_u$, relative displacement of suspension (m)

f_a = gas-spring force of shock absorber (N)

f_d = damping force due to tunable shock absorber (N)

The force due to gas spring, f_a, is determined from equation (3.24), while the tunable damping force, f_d, is defined in equations (3.17) and (3.31), letting $f_d = f_{d3}$.

5.2.2 An In-plane Vehicle Model

A two-axle road vehicle is modeled as an in-plane four-degree-of-freedom dynamic system, employing tunable pressure limited shock absorbers, as shown in Figure 5.2. The vehicle mass is characterized by sprung mass, m_s and pitch mass moment of inertia, I_s about its center of gravity. The front and rear axle assemblies are represented by unsprung masses, m_{u1} and m_{u2}, respectively. The vehicle mass is free to bounce (x_s) and pitch (θ_p), while each of the unsprung masses is constrained to translate along the heave axis. Each vehicle suspension is modeled as a combination of linear spring, and nonlinear gas-spring and nonlinear damping elements due to pressure limited shock absorber. The tires are represented by linear springs and viscous dampers, assuming point contact. Assuming a small attitude angle, the equations of motion of the in-plane vehicle model are expressed as follows:

Bounce motion of the sprung mass:

$$m_s \ddot{x}_s(t) + k_{s1} z_1 + k_{s2} z_2 + f_{s1}(z_1, \dot{z}_1, t) + f_{s2}(z_2, \dot{z}_2, t) = 0 \qquad (5.3)$$

Pitch motion of the sprung mass:

$$I_s \ddot{\theta}_p(t) - k_{s1}\,\ell_f\,z_1(t) + k_{s2}\,\ell_r\,z_2(t) - f_{s1}(z_1,\dot{z}_1,t)\,\ell_f + f_{s2}(z_2,\dot{z}_2,t)\,\ell_r = 0 \qquad (5.4)$$

Bounce motion of the front unsprung mass:

$$m_{u1}\ddot{x}_1(t) + c_{t1}\dot{x}_1(t) + k_{t1}x_1(t) - k_{s1}z_1(t) - f_{s1}(z_1,\dot{z}_1,t) = c_{t1}\dot{x}_{i1}(t) + k_{t1}x_{i1}(t) \qquad (5.5)$$

Bounce motion of the rear unsprung mass:

$$m_{u2}\ddot{x}_2(t) + c_{t2}\dot{x}_2(t) + k_{t2}x_2(t) - k_{s2}z_2(t) - f_{s2}(z_2,\dot{z}_2,t) = c_{t2}\dot{x}_{i2}(t) + k_{t2}x_{i2}(t) \qquad (5.6)$$

where,

m_s = sprung mass of the vehicle (kg)

I_s = pitch mass moment of inertia of the vehicle (kg·m^2)

m_{u1} = unsprung mass of front axle assembly (kg)

m_{u2} = unsprung mass of rear axle assembly (kg)

x_s = coordinate of bounce displacement of sprung mass (m)

θ_p = coordinate of pitch displacement of sprung mass (rad)

x_1, x_2 = coordinates of bounce displacements of front and rear unsprung masses, respectively (m)

x_{i1}, x_{i2} = input displacements at front and rear tire-road interfaces, respectively (m)

k_{s1}, k_{s2} = stiffness coefficients of front and rear suspension springs, respectively (N/m)

k_{t1}, k_{t2} = stiffness coefficients of front and rear tires, respectively (N/m)

c_{t1}, c_{t2} = damping coefficients of front and rear tires, respectively (N·s/m)

ℓ_f, ℓ_r = horizontal distances between sprung mass center and front and rear axles, respectively (m)

z_1, z_2 = relative displacements of front and rear suspension, respectively (m), given by:

$$z_1 = x_s - \ell_f \theta_p - x_1 \tag{5.7}$$

$$z_2 = x_s + \ell_r \theta_p - x_2 \tag{5.8}$$

f_{s1}, f_{s2} = total dynamic forces generated by the front and rear tunable shock absorbers, respectively (N)

The total dynamic force due to the ith tunable shock absorber is comprised of gas spring and damping forces, as discussed in Chapter 3:

$$f_{si} = f_{di}(\dot{z}_i, t) + f_{ai}(z_i, t), \quad i=1,2 \tag{5.9}$$

where,

f_{ai} = gas-spring force of ith shock absorber (N), as expressed in equation (3.24)

f_{di} = damping force due to tunable shock absorber (N), given in equations (3.17) and (3.31), letting $f_{di} = f_{d3}$.

5.3 Deterministic Analysis of Quarter Vehicle Model

The quarter vehicle model incorporating nonlinearities due to the gas-spring, orifice damping and tunable sequential damping is analyzed to determine the shock and vibration attenuation performance of a primary vehicle suspension employing a tunable pressure limited shock absorber. The differential equations of motion (5.1) and (5.2) are solved, in conjunction with (3.17), (3.24) and (3.31), for determined excitations via a numerical integration technique. The simulation parameters of the quarter vehicle model are illustrated in Table 5.1. Dynamic ride performance of the quarter vehicle model employing tunable

TABLE 5.1

Simulation Parameters of Quarter-Vehicle Model

SYMBOL	DESCRIPTION	PARAMETER VALUE
m_s	Sprung mass of the vehicle	240 kg
m_u	Unsprung mass of the vehicle	36 kg
k_s	Suspension spring stiffness	16000 N/m
k_t	Stiffness coefficient of tire	160000 N/m
ρ	Mass density of fluid	797 kg/m^3
A_p	Area of piston on rod side	2.51×10^{-3} m^2
A_r	Area of rod cross section	3.14×10^{-4} m^2
C_{d1}, C_{d2}	Discharge coefficients	0.7
a_1	Area of orifice on the piston	3.14×10^{-5} m^2
a_2	Area of cylinder orifice	3.14×10^{-5} m^2
γ	Polytropic exponent	1.4
p_{at}	Atmospheric pressure	101300 Pa
p_a	Initial charge pressure	14×10^5 Pa
V_a	Initial gas volume	1.9×10^{-4} m^3
n	Number of orifices on piston	2

suspension is presented in terms of vibration and shock isolation characteristics. The vibration isolation performance is evaluated through vibration transmissibility characteristics in the frequency domain, while the shock isolation performance of the tunable suspension is analyzed in terms of its transient response characteristics to a road bump input in the time domain.

5.3.1 Vibration Transmissibility Characteristics

The vibration isolation performance of the quarter vehicle model employing a tunable suspension is evaluated for harmonic displacement excitations at the tire-road interface. The vibration transmissibility is obtained by computing the ratio of steady state response amplitude to the excitation amplitude corresponding to excitation frequencies of interest. The steady state response amplitude corresponding to each excitation frequency is obtained by selecting the maximum value of the response after the response reaches the steady state in the simulation. The amplitude of displacement excitation is selected as 1.86×10^{-2} m.

The sprung mass velocity transmissibility characteristics of the vehicle model employing a tunable pressure limited shock absorber are compared with those of the vehicle model employing a fixed orifice shock absorber, as presented in Figure 5.3. Both the shock absorbers considered in the simulation are assumed to have two identical piston orifices, while a unit value of the tuning factor (ν=1) is selected for the tunable shock absorber. Figure 5.3 illustrates that velocity transmissibility response of the vehicle model with fixed orifice shock absorber yields two peaks corresponding to the resonant frequencies of the sprung mass (1.08 Hz) and unsprung mass (3.9 Hz) of the vehicle

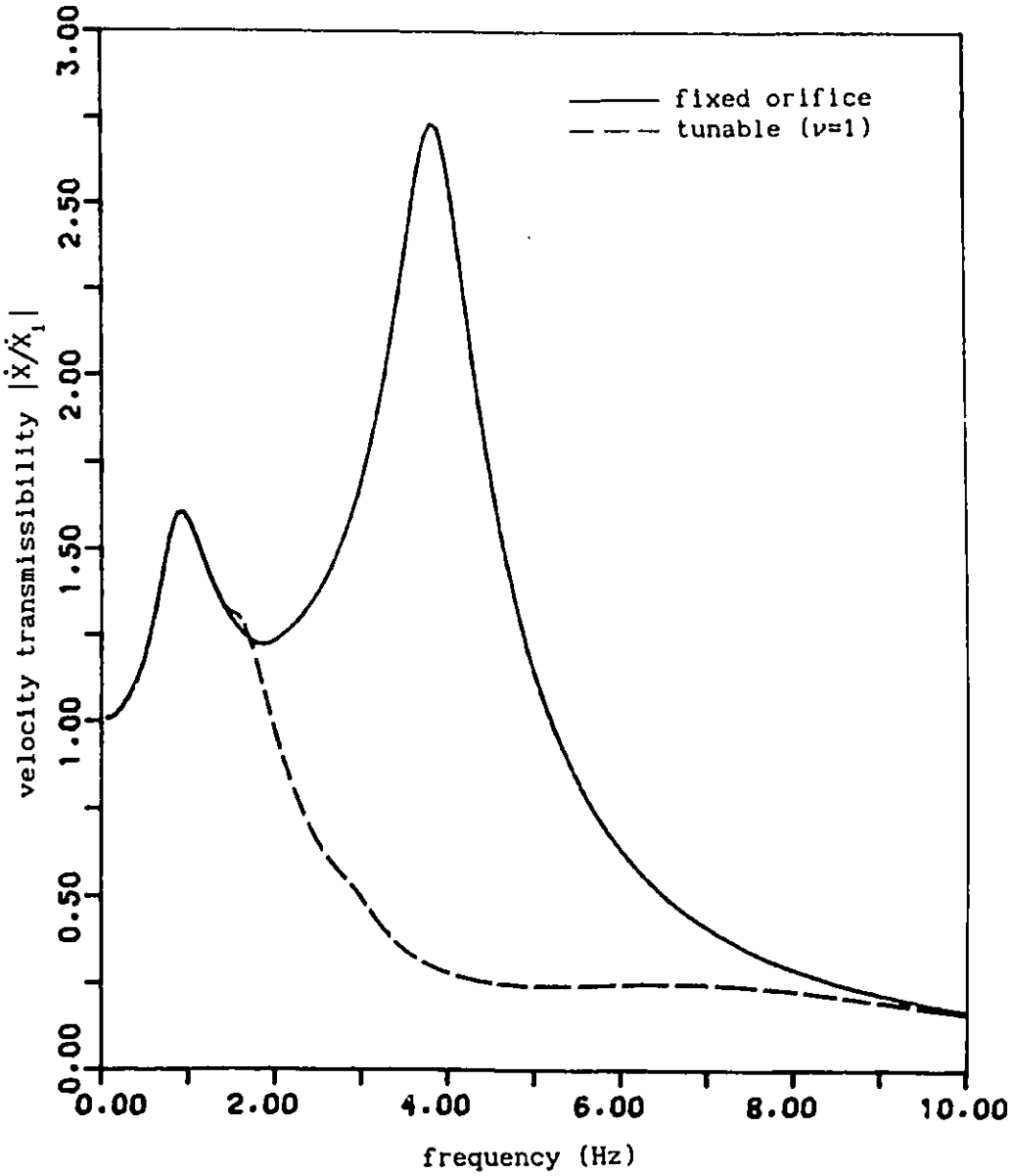

FIGURE 5.3 Velocity transmissibility of sprung mass of quarter vehicle model employing tunable and fixed orifice shock absorbers

model, respectively. The large transmissibility response corresponding to the resonance of the unsprung mass is attributed to the high value of the fixed orifice damping, primarily caused by flow through two piston orifices. The velocity transmissibility characteristics of the vehicle model employing tunable shock absorber are identical to that of the fixed orifice shock absorber at low excitation frequencies. The tunable shock absorber continues to dissipate vibration energy identically to that of the fixed orifice shock absorber around the first resonant frequency. However, as the excitation frequency and thus the relative velocity response across the primary suspension increases, the pressure differential across the piston increases. Flow modulation through the pressure limiting mechanism takes place when the pressure differential exceeds the preset value. The pressure differential is held around the preset value to limit the damping force due to the tunable pressure limited shock absorber. The magnitude of damping force developed by the tunable shock absorber is thus considerably smaller than that developed by the fixed orifice shock absorber. The velocity transmissibility peak corresponding to the unsprung mass resonance frequency is thus effectively attenuated by the tunable shock absorber, as shown in Figure 5.3. A comparison of response characteristics of the tunable and fixed orifice shock absorbers reveals that the vibration isolation performance of an adequately tuned pressure limited shock absorber is considerably superior to that of the fixed orifice system at excitation frequencies beyond the sprung mass resonant frequency.

The peak vibration transmissibility response of the vehicle model with a fixed orifice shock absorber can also be suppressed by reducing

the flow resistance and thus the effective damping. The displacement transmissibility characteristics of the sprung mass employing a lightly damped fixed orifice shock absorber (n=4) are compared with those of the heavily damped fixed orifice shock absorber (n=2) and the tunable shock absorber, as shown in Figure 5.4. Although, the lightly damped fixed orifice shock absorber effectively suppresses the peak corresponding to unsprung mass resonance, the peak transmissibility response, corresponding to the sprung mass resonance, increases considerably with light damping. A comparison of displacement transmissibility characteristics of the fixed orifice shock absorbers (n=2 and n=4) with those of the tunable shock absorber (n=2 and ν=1) reveals that the tunable shock absorber can provide an appropriate control of the peak responses corresponding to resonant frequencies of sprung and unsprung masses. Figure 5.4 further reveals that the tunable shock absorber can effectively attenuate terrain induced vibration at frequencies above the sprung mass resonant frequency.

The vibration isolation characteristics of the quarter vehicle model employing tunable pressure limited shock absorber are moderately related to the tuning factor. Figure 5.5 illustrates the influence of the tuning factor on the velocity transmissibility response of the sprung mass. A low value of tuning factor (ν=0.7) yields further reduction in the transmissibility response at higher excitation frequencies as shown in Figure 5.5. A lower value of the tuning factor, however, results in opening of the relief valves at relatively lower excitation frequency, that may produce a large transmissibility response near the sprung mass resonance due to insufficient damping at resonance.

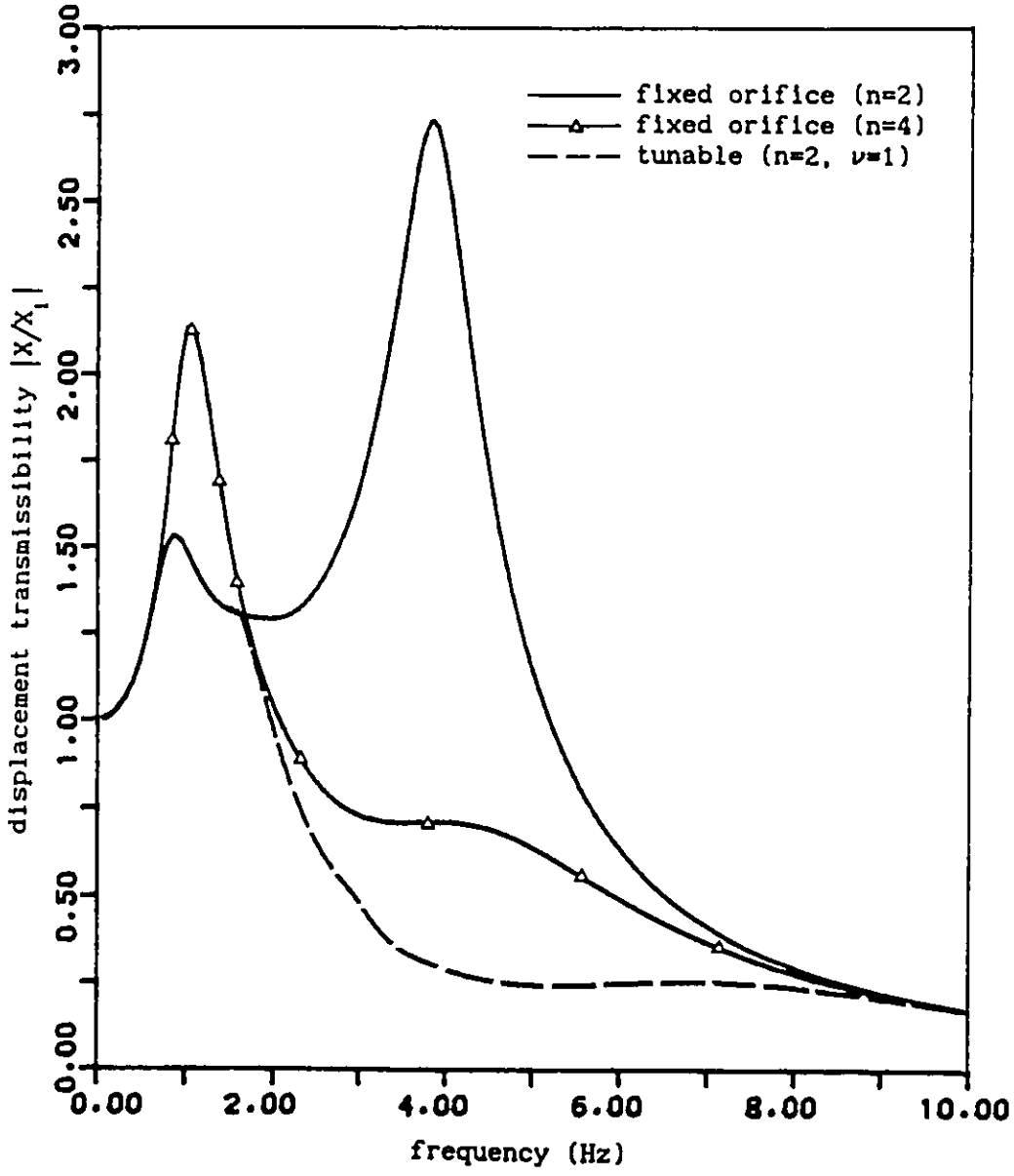

FIGURE 5.4 Displacement transmissibility of sprung mass of quarter vehicle model employing tunable and fixed orifice shock absorbers

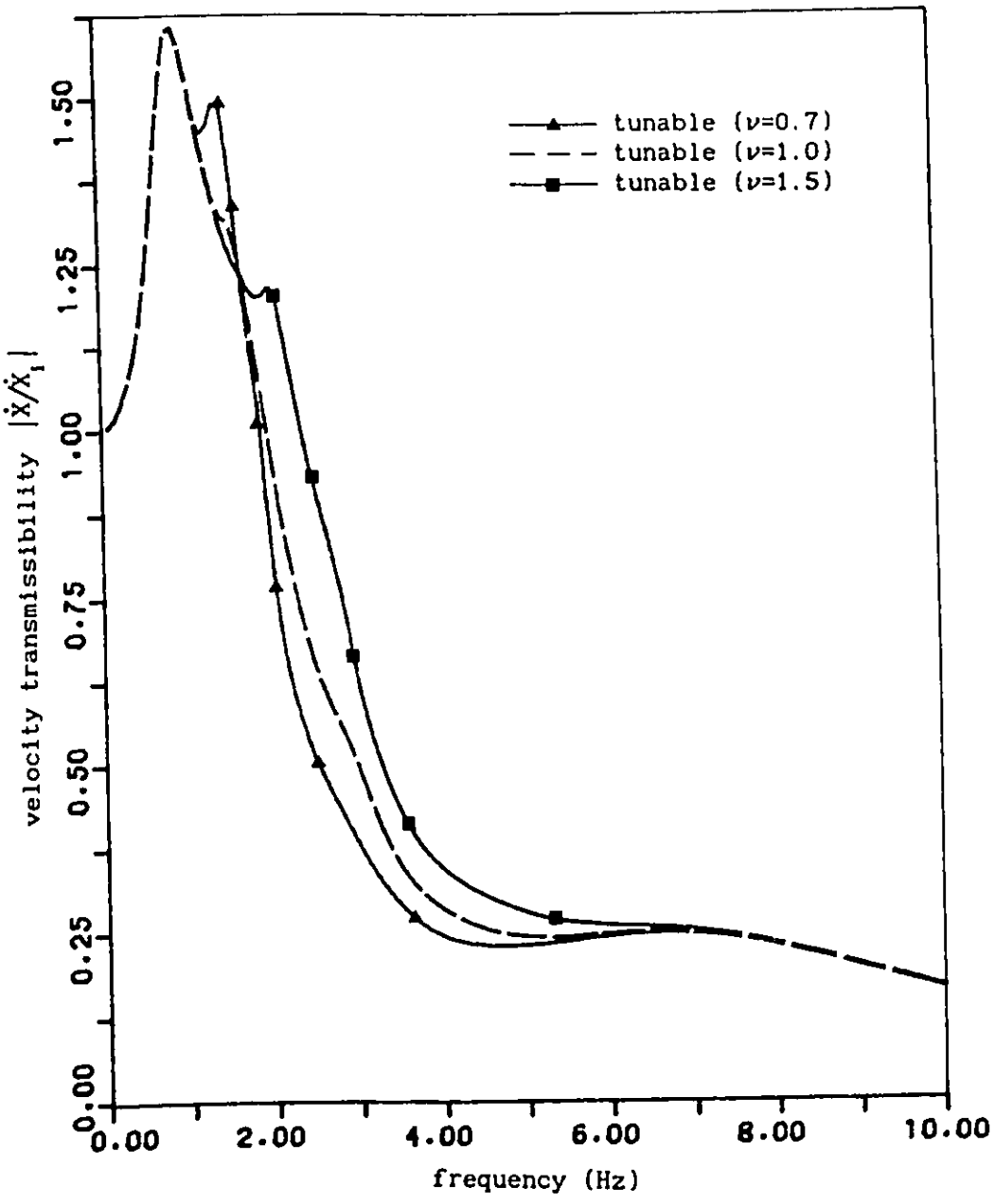

FIGURE 5.5 Velocity transmissibility of sprung mass of quarter vehicle model employing tunable shock absorber with various values of tuning factor

A higher value of the tuning factor (ν=1.5) results in opening of the relief valves at relatively higher excitation frequency and thus yields higher response values at higher excitation frequency. Figure 5.5 clearly demonstrates that a primary suspension system equipped with a tunable shock absorber with the pressure tunable factor range, $0.7<\nu<1.5$, offers considerable potential to achieve superior vibration isolation performance.

5.3.2 Transient Response Characteristics

Differential equations of motion (5.1) and (5.2) are solved for excitation arising from a road bump to determine the transient response characteristics of the quarter vehicle model employing fixed orifice and tunable pressure limited shock absorbers. A semi-circular road bump input is schematically presented in Figure 5.6. Assuming constant forward speed, the instantaneous horizontal location of the tire contact point with respect to center line of the bump can be expressed as a function of the vehicle speed

$$u(t) = u_0 + v\ t \tag{5.10}$$

where,

- u = instantaneous coordinate of the tire contact point (m)
- u_0 = initial position of vehicle away from the bump center (m)
- v = constant forward speed of vehicle (m/s)
- t = time (s)

The displacement excitation caused by a road bump of radius r, can be expressed as:

$$x_1(t) = \begin{cases} \sqrt{r^2 - u^2(t)}, & -r \le u(t) \le r \\ 0, & |u(t)| > r \end{cases} \tag{5.11}$$

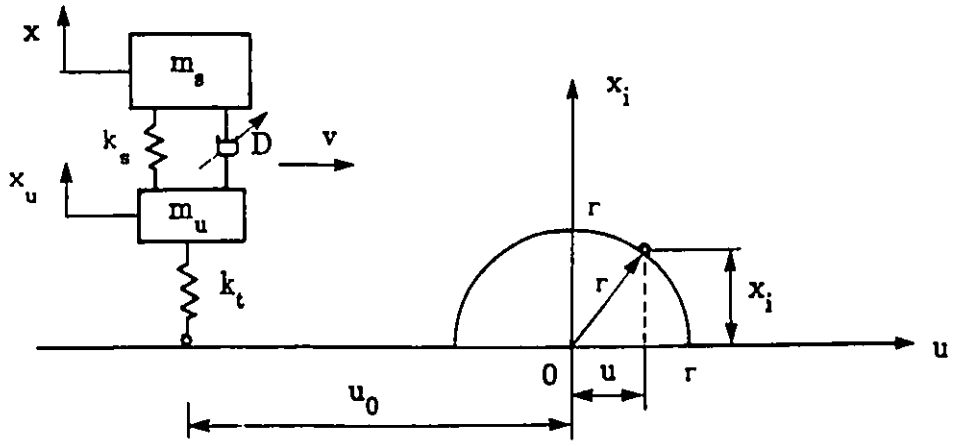

FIGURE 5.6 Representation of a bump road input

x_i = instantaneous input displacement of the bump (m)

r = radius of the road bump (m)

The transient response characteristics of the quarter vehicle model are evaluated for simulation parameters listed in Table 5.1, and r=0.1016 m, u_0= - 0.2524 m, and v = 10 m/s. The transient displacement response characteristics of sprung mass of the vehicle employing tunable and fixed orifice shock absorbers, together with the history of the input displacement, are presented in Figure 5.7. The total orifice areas of both shock absorbers are selected to be identical (n=2), and the tuning factor for the tunable shock absorber is selected as ν=1. The transient velocity response characteristics of the sprung mass of the quarter vehicle model with tunable and fixed orifice shock absorbers are presented in Figure 5.8. Figures 5.7 and 5.8 reveal that the peak displacement and velocity responses of the vehicle model employing a tunable shock absorber are considerably smaller than that of the fixed orifice shock absorber. For simulation parameters considered in this study, the fixed orifice shock absorber yields a peak sprung mass displacement of 0.036 m compared with 0.020 m caused by the tunable shock absorber. The peak sprung mass velocity response of the quarter vehicle model employing fixed orifice and tunable shock absorber is observed as 0.88 m/s and 0.36 m/s, respectively. Moreover, the transient response of the tunable absorber is less oscillatory than that of the fixed orifice one.

The transient displacement response of the unsprung mass, presented in Figure 5.9, reveals that the initial peak displacement response due to the tunable shock absorber is larger than that due to the fixed

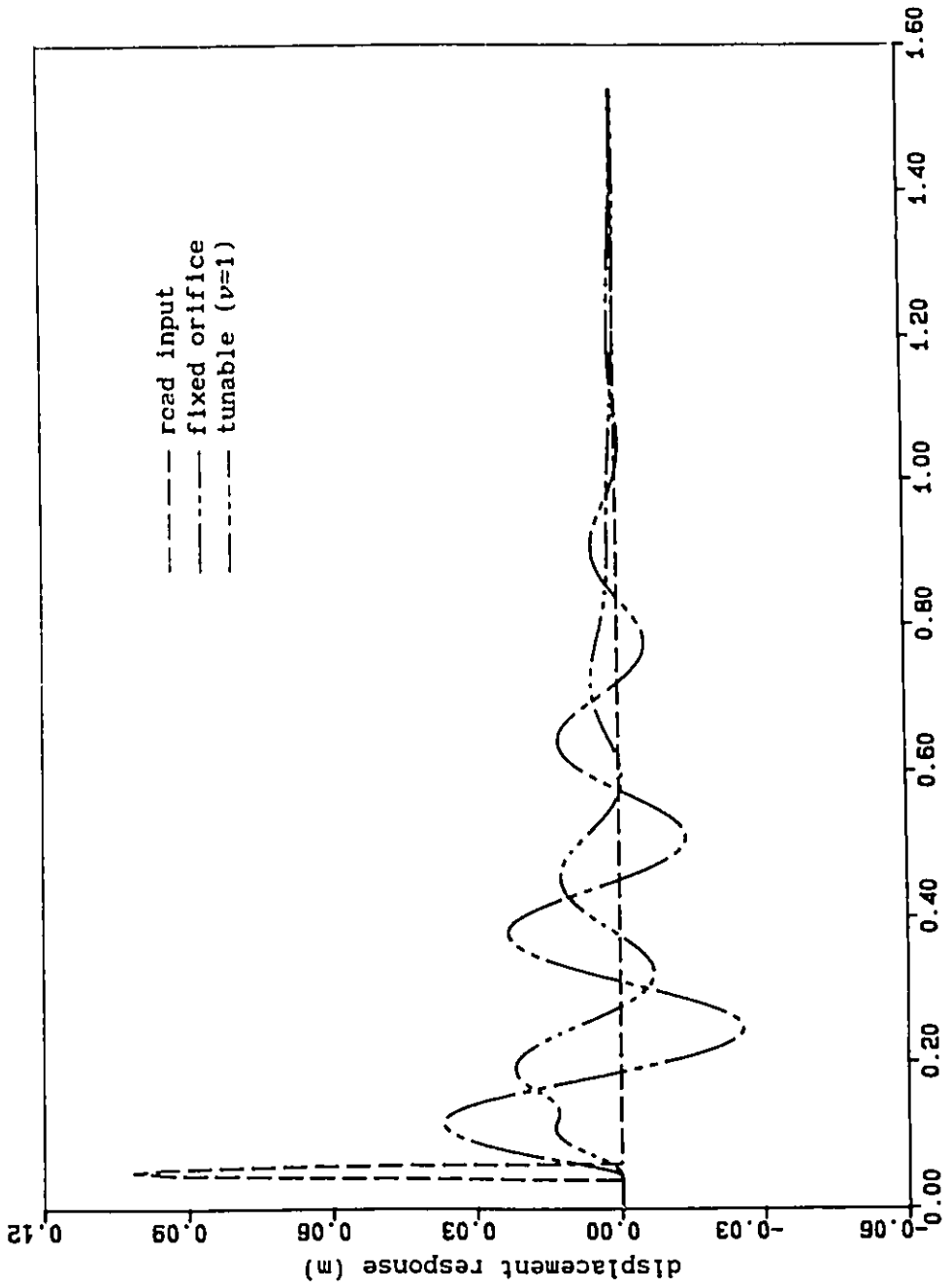

FIGURE 5.7 Transient displacement response of sprung mass of quarter vehicle model employing tunable and fixed orifice shock absorbers

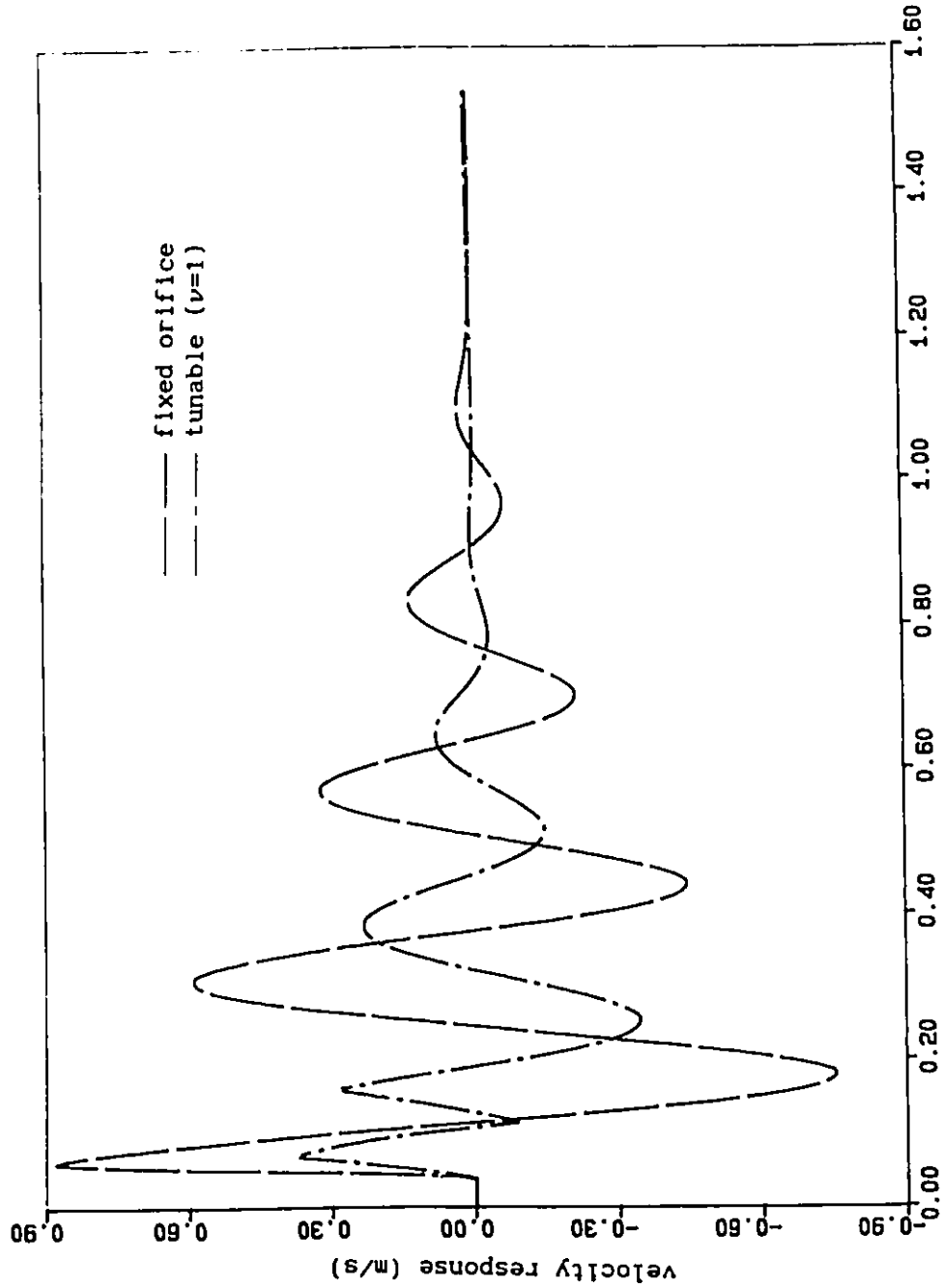

FIGURE 5.8 Transient velocity response of sprung mass of quarter vehicle model employing tunable and fixed orifice shock absorbers

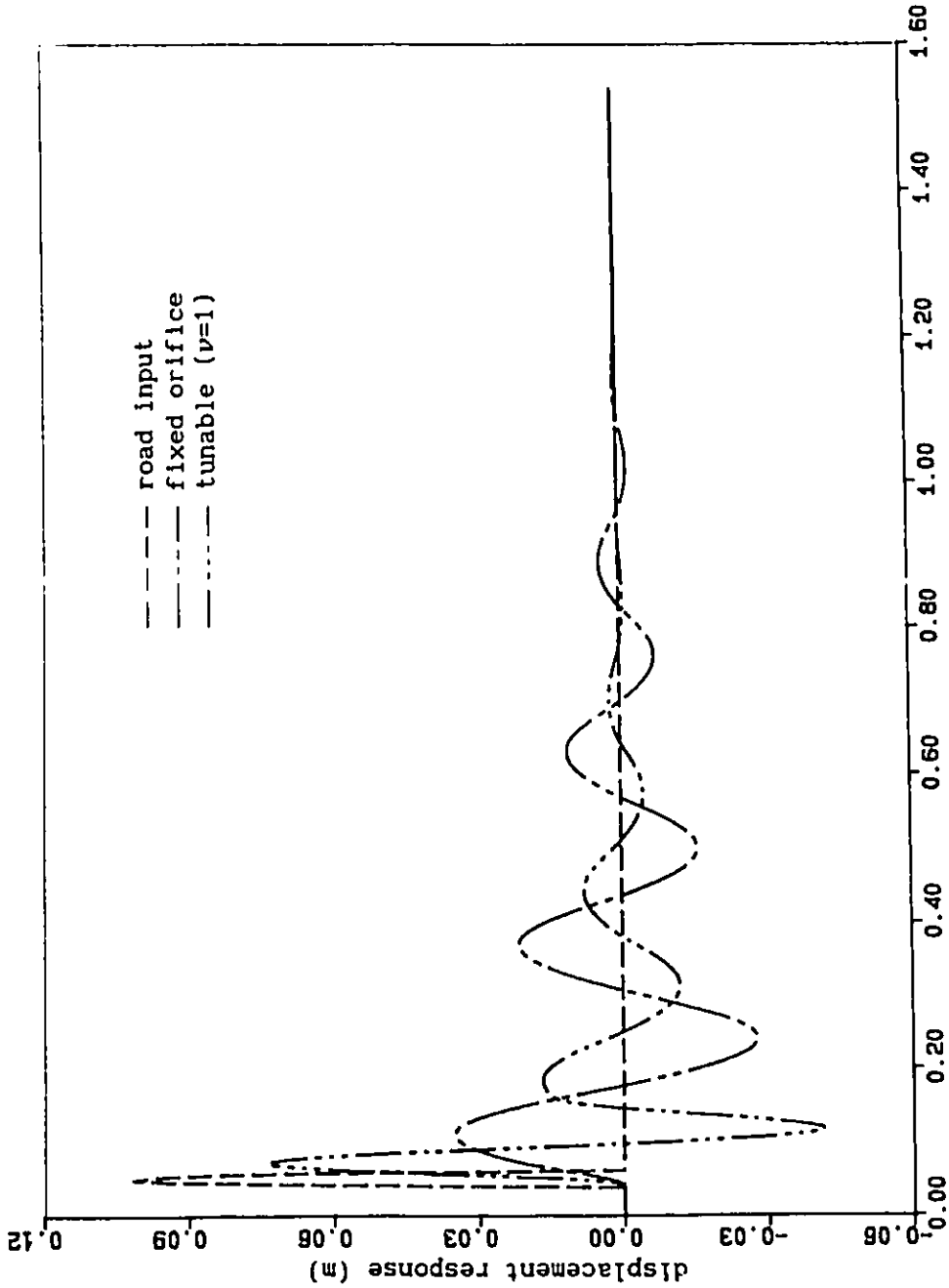

FIGURE 5.9 Transient displacement response of unsprung mass of quarter vehicle model employing tunable and fixed orifice shock absorbers

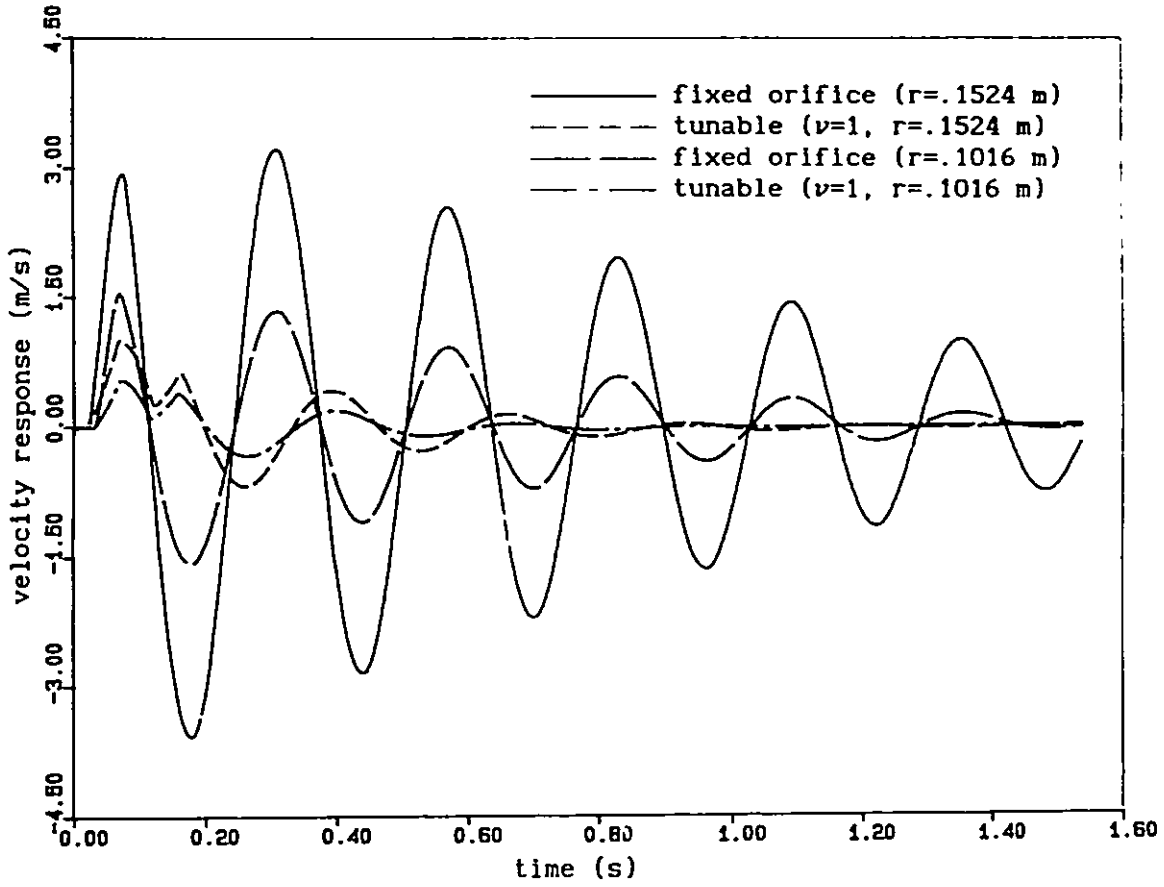

FIGURE 5.10 Transient velocity response of sprung mass of quarter vehicle model employing tunable and fixed orifice shock absorbers (v=5 m/s)

orifice one. However, the successive peak values of displacement response of the unsprung mass due to tunable shock absorber are smaller than those due to the fixed orifice. Moreover, the displacement response of the unsprung mass with tunable shock absorber is less oscillatory than that of the fixed orifice shock absorber.

The effectiveness of the tunable pressure limited shock absorber is further investigated for vehicle speed, v=5 m/s, and different bump heights (r=0.1016 m; r=0.1524 m). Figure 5.10 presents the transient velocity response of the sprung mass of the quarter vehicle model employing either fixed orifice or tunable shock absorbers. For the bump height r=0.1524 m, the peak values of sprung mass velocity response of the quarter vehicle model employing fixed orifice and tunable shock absorbers are observed to be 3.0 m/s and 0.9 m/s, respectively. For the bump height r=0.1016 m, the peak values of the velocity response due to fixed orifice and tunable shock absorbers are observed to be 1.5 m/s and 0.5 m/s, respectively. The response characteristics, presented in Figure 5.10, clearly demonstrate that an appropriately tuned pressure limited shock absorber continues to provide improved shock isolation performance for a wide range of vehicle speeds and excitation levels.

5.4 Development of A Generalized Discrete Harmonic Linearization Technique for Stochastic Analysis of Nonlinear Vehicle Models

Well established linear analytical tools provide a powerful and convenient approach to carry out stochastic analyses of either linear or linearized systems [103, 112]. Equivalent linearization techniques are frequently employed to evaluate the random response of nonlinear mechanical systems using linear analytical tools [75]. In equivalent

linearization techniques, a nonlinear system is replaced by a related appropriate linear system according to specified criteria such that the response characteristics of the linearized system do not deviate considerably from that of the nonlinear system [102].

A discrete harmonic linearization method, which is an extension of the frequency domain linearization, introduced by Thomson [107], for the stochastic analysis of nonlinear systems , was proposed by Rakheja et al. [109]. The discrete harmonic linearization technique, based upon balancing either average force or average energy dissipated per cycle, has been applied to simulate nonlinear systems with nonlinear coulomb and velocity squared damping mechanisms. Nonlinear damping mechanisms are characterized by an array of equivalent local damping coefficients, where each local constant is determined as a function of excitation frequency, excitation amplitude and the properties of the nonlinearity. Although, the discrete harmonic linearization technique provides a convenient tool to evaluate the random response of nonlinearly damped mechanical systems, treatment of nonlinear spring and variable damping mechanisms has not been addressed.

In this section, the discrete harmonic linearization technique is generalized to obtain linear representations of nonlinear conservative as well as dissipative elements, based on the principle of energy similarity of dynamic elements. The generalized discrete harmonic linearization technique is then applied to characterize the tunable shock absorber with nonlinear gas spring and variable orifice damping by local equivalent stiffness and damping coefficients, respectively. The stochastic response of a nonlinear vehicle model employing tunable

pressure limited shock absorber is then evaluated using linear stochastic analytical approach.

5.4.1 Principle of Energy Similarity of Dynamic Elements

It has been established that an equivalent viscous damping coefficient of a nonlinear damping element can be obtained by equating the dissipated energy per cycle due to the nonlinear dissipative element to that of a equivalent viscous damper [107]. A conservative restoring element, however, does not dissipate energy, it rather stores and releases energy during a vibration cycle. The energy stored by a conservative element during a vibration cycle is equal to the energy released. The total energy due to the restoring element is thus zero.

On the other hand, the total amount of energy processed by a conservative element in one complete cycle can be measured by summing the absolute values of both the stored and released energies, as described below.

Consider a dynamic element subjected to a harmonic excitation with period τ. Let $f(t)$ be the force function of the dynamic element, $z(t)$ be the relative displacement across the element, and $\dot{z}(t)$ be the derivative of z with respect to time t. The energy processed by the dynamic element can be determined using the following definitions.

Definition 1:

A function $f(t)$ is said to be in the same orientation in an interval $[t_{i-1}, t_i]$, if the sign of the product of $f(t)$ and $\dot{z}(t)$ remains the same for $t \in [t_{i-1}, t_i]$, where $|t_{i-1} - t_i| \leq \tau$.

Definition 2:

A processed energy E_p associated with a function $f(t)$ is the

sum of the absolute values of energy computed in all the same orientation intervals $[t_{i-1}, t_i]$ over the period τ, that is

$$E_p = \sum_{i=1}^{N} \left| \int_{t_{i-1}}^{t_i} f(t)\, \dot{z}\, dt \right| \tag{5.12}$$

where

$$\sum_{i=1}^{N} (t_{i-1} - t_i) = \tau \tag{5.13}$$

It is obvious that a dynamic element, whether dissipative or conservative, linear or nonlinear, can be characterized in terms of its processed energy. The discrete harmonic linearization technique can thus be generalized for simulation of nonlinear dissipative as well as conservative elements using the following principle of energy similarity of dynamic elements:

Principle of Energy Similarity of Dynamic Elements:

A dynamic element is considered to be equivalent to another dynamic element in a sense of energy similarity, if their force functions are of the same nature (dissipative or conservative) and their processed energies are identical.

A nonlinear mechanical system with nonlinear dissipative and/or conservative elements can be, therefore, replaced by an equivalent linear system, based on the above principle of energy similarity of dynamic elements such that the processed energy of elements within the linearized system does not deviate considerably from that of the elements within the nonlinear system. The generalized discrete harmonic linearization technique can thus be employed for simulation of nonlinear

systems containing dissipative as well as conservative nonlinear elements using the above principle.

5.4.2 Computation of Equivalent Linear Coefficients

Nonlinear dynamic elements within a mechanical system are represented by their equivalent linear elements, using the generalized discrete harmonic linearization technique. Coefficients of equivalent linear elements are obtained by equating the processed energy of nonlinear dynamic elements to that of equivalent linear elements of the same nature (dissipative or conservative).

Assuming harmonic motion across a nonlinear dynamic element, the nonlinear force, $f(z,\dot{z},t)$, due to the nonlinear element can be approximated by local equivalent stiffness and damping coefficients, where each local coefficient is valid in the vicinity of a selected excitation frequency and excitation amplitude. The nonlinear force can thus be approximated as:

$$f_j(z,\dot{z},t) = c_{eq}(\omega_j,Z)\ \dot{z}(t) + k_{eq}(\omega_j,Z)\ z(t), \quad j = 1,\ldots N \qquad (5.14)$$

where $z(t)$ is the harmonic motion across the element at a discrete excitation frequency ω_j, given by

$$z(t) = Z \sin(\omega_j t) \qquad (5.15)$$

Z is the amplitude of displacement across the element and N is the total number of excitation frequencies. $c_{eq}(\omega_j,z)$ and $k_{eq}(\omega_j,z)$ are the local equivalent damping and stiffness coefficients, respectively, corresponding to discrete frequency ω_j and relative displacement amplitude Z.

The local equivalent coefficients are established by equating the

processed energy of the nonlinear element to that of an equivalent linear element of the same nature, at a discrete excitation frequency such that each local coefficient is valid around the vicinity of a selected excitation frequency and amplitude.

Vehicle models, presented in section 5.2, exhibit suspension nonlinearities due to orifice damping, damping modulation caused by a pressure limiting mechanism, and a gas-spring. These suspension nonlinearities are expressed by their local equivalent stiffness and damping coefficients, using the generalized discrete harmonic linearization technique. The detailed methodology associated with derivation of local equivalent coefficients is presented below.

Fixed Orifice Damper

Since the sign of the product of the orifice damping force and relative velocity is always positive for a complete vibration cycle, the damping force is in the same orientation interval for $t \in [0, 2\pi/\omega_j]$. The processed energy of an fixed orifice damper is then the energy dissipated by the element per cycle and can thus be expressed by:

$$E_d(\omega_j, Z) = \int_0^{2\pi/\omega_j} f_d(t)\, \dot{z} dt \qquad (5.16)$$

where $f_d(t)$, the nonlinear damping force due to orifice flow, is expressed in equation (3.23). The local equivalent damping coefficient is then obtained by equating the dissipated energy to that of a viscous damper [107]:

$$c_{eq}(\omega_j, Z) = 8c_2\omega_j\, Z/\, 3\pi \qquad (5.17)$$

where c_2 is the nonlinear damping coefficient of the orifice damper

given by:

$$c_2 = \frac{\rho}{2\, n^2 C_{d1}^2} \left(\frac{A_p}{a_1}\right)^2 \alpha \qquad (5.18)$$

and

$$\alpha = A_p + \left(\frac{C_{d1}}{C_{d2}}\right)^2 \left(\frac{na_1}{a_2}\right)^2 \left(\frac{A_r}{A_p}\right)^2 A_r \qquad (5.19)$$

Tunable Pressure Limited Damper

The tunable pressure limited damper is also an orifice damper, however the orifice damping varies due to flow modulation through the pressure limiting mechanism. A tunable pressure limited damper can be treated as a fixed orifice damper for a part of the vibration cycle when the magnitude of the damping force, expressed in equation (3.31), is below the limiting force given by:

$$F_0 = \alpha(p_{12})_0$$

The damping force due to tunable pressure limited damper, however, is held to around F_0 during the remaining part of the cycle due to flow modulation though the pressure limiting mechanism. Assuming a harmonic response across the tunable damper, the damping force due to the pressure limited hydraulic damper is illustrated in Figure 5.11. The magnitude of damping force initially increases proportional to the square of the relative velocity, as described by equations (3.17) and (3.31). As the magnitude of damping force approaches the limiting value F_0, the damping force is held constant as the relative velocity response increases. The time, when the damping force approaches the limiting value F_0, at t_0, can be expressed as:

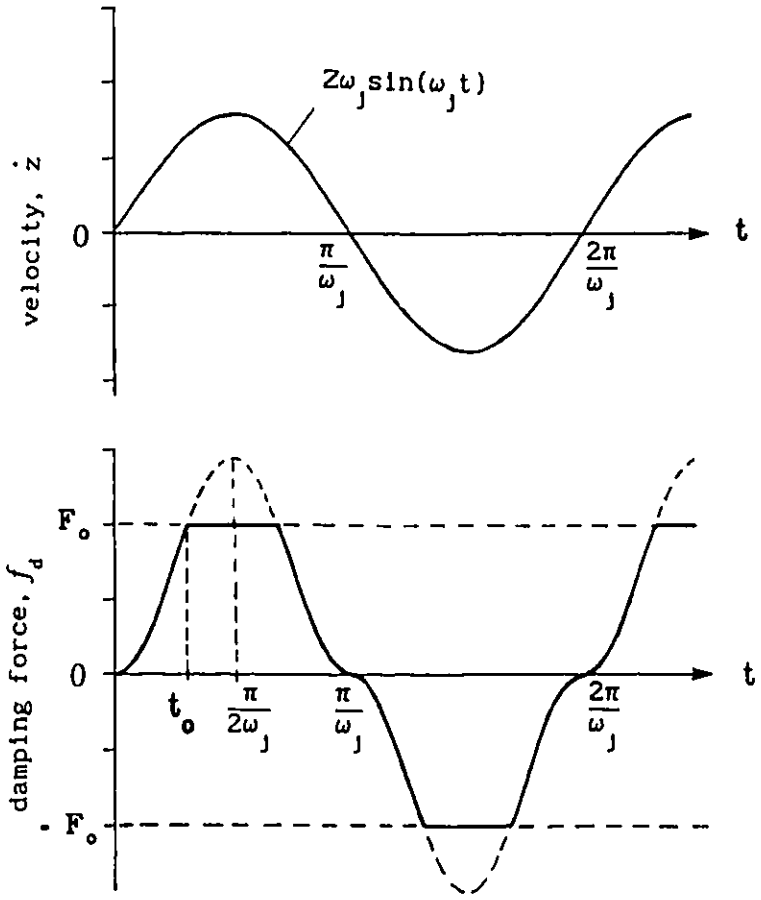

FIGURE 5.11 Damping force of a tunable shock absorber

$$t_o = \frac{1}{\omega_j} \sin^{-1}\left(\frac{1}{Z\omega_j}\sqrt{\frac{F_o}{c_2}}\right) \tag{5.20}$$

The damping force is then held equal to F_o until the decrease in relative velocity response yields a damping force less than the limiting value, as shown in Figure 5.11. The processed energy, which is the total energy dissipated by the tunable pressure limited shock absorber per cycle, can thus be expressed as:

$$E_d(\omega_j,Z) = 4\left[\int_0^{t_o} c_2\,\dot{z}^3\,dt + \int_{t_o}^{\pi/2\omega_j} F_o\,\dot{z}\,dt\right] \tag{5.21}$$

The local equivalent damping coefficient is then obtained by equating the processed energy to that of a linear viscous damper:

$$c_{eq}(\omega_j,Z) = \begin{cases} 8c_2\omega_j\,Z\,/\,3\pi\,, & |f_d| < F_o \\ \frac{4}{\pi\omega_j Z}\left[c_2 Z^3\omega_j^2\left(\frac{2}{3} - \cos\omega_j t_o + \frac{1}{3}\cos^3\omega_j t_o\right) + F_o Z\cos\omega_j t_o\right], & \text{otherwise} \end{cases} \tag{5.22}$$

Gas-spring

The nonlinear restoring force $f_a(z,t)$, expressed in equation (3.24), due to the gas-spring within the shock absorber is expressed by an array of local stiffness coefficients by equating the processed energy of the nonlinear restoring element to that of a linear spring. The processed energy of a linear spring is first determined, as illustrated below.

The force function f_k due to a linear spring with stiffness coefficient k is given by:

$$f_k(z,t) = k\,z(t) \tag{5.23}$$

Since the linear force f_k is an odd function of displacement z and the sign of product of displacement z and velocity $\dot{z}$ changes four times during each harmonic cycle, there exist, according to **Definition 1** presented in section 5.4.1, four same orientation intervals associated with the linear restoring force within a vibration cycle $\tau=2\pi/\omega_j$, namely $[0,\ \pi/2\omega_j]$, $[\pi/2\omega_j,\ \pi/\omega_j]$, $[\pi/\omega_j,\ 3\pi/2\omega_j]$, and $[3\pi/2\omega_j,\ 2\pi/\omega_j]$. The processed energy of the linear spring, based on **Definition 2** in section 5.4.1, is then expressed by:

$$E_k(\omega_j,Z) = \left| \int_0^{\pi/2\omega_j} f_k(z,t)\ \dot{z}\ dt \right| + \left| \int_{\pi/2\omega_j}^{\pi/\omega_j} f_k(z,t)\ \dot{z}\ dt \right| + \left| \int_{\pi/\omega_j}^{3\pi/2\omega_j} f_k(z,t)\ \dot{z}\ dt \right| + \left| \int_{3\pi/2\omega_j}^{2\pi/\omega_j} f_k(z,t)\ \dot{z}\ dt \right| \qquad (5.24)$$

Integration of equation (5.24) yields

$$E_k = 2\ k\ Z^2 \qquad (5.25)$$

Equation (5.25) reveals that the processed energy of the linear spring is a function of the spring stiffness coefficient, k, and amplitude of displacement across the spring, Z.

It is apparent, from equation (3.24), that dynamic nonlinear force f_a due to a gas-spring is an asymmetric function of the relative displacement across the gas-spring, as shown in Figure 5.12. Since the nonlinear restoring force of gas-spring has the same sign as that of the relative displacement, as shown in Figure 5.12, the vibration cycle can also be divided into the four same orientation intervals as in the case of a linear spring. The processed energy of a gas-spring can, therefore,

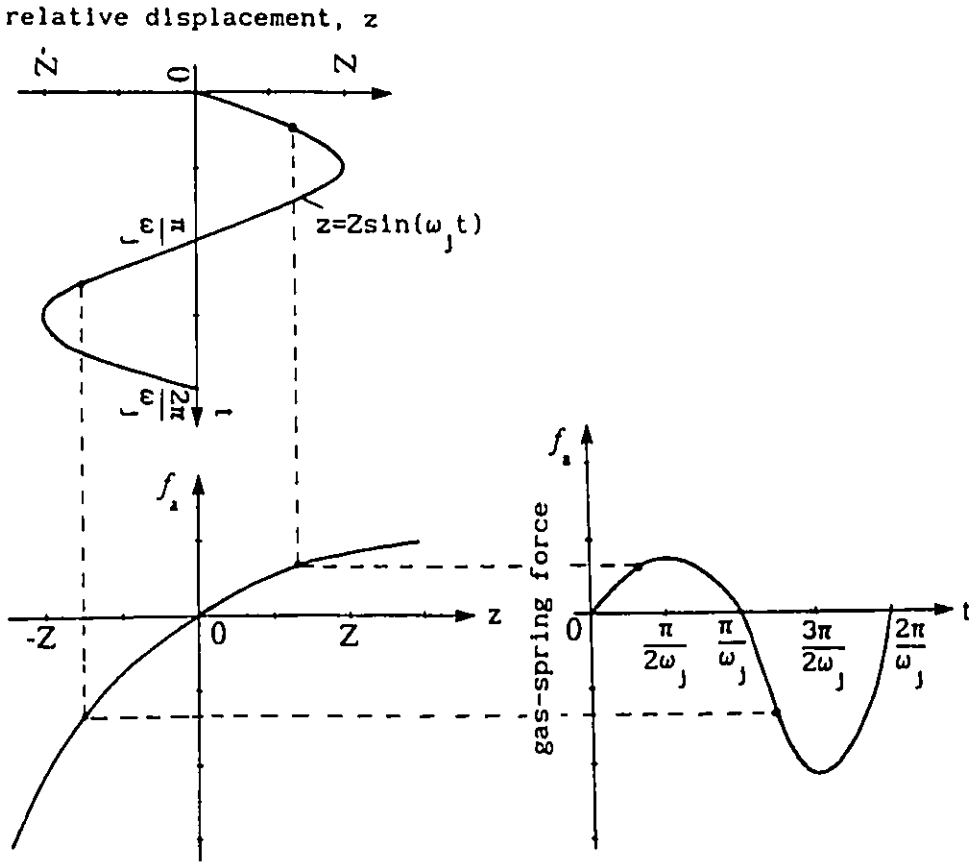

FIGURE 5.12 Gas-spring force of a shock absorber

be established by computing the absolute values of the energy stored and released over each the same orientation interval, using the definitions presented in section 5.4.1:

$$E_k(\omega_j,z) = \left| \int_0^{\pi/2\omega_j} f_a(z,t)\ \dot{z}\ dt \right| + \left| \int_{\pi/2\omega_j}^{\pi/\omega_j} f_a(z,t)\ \dot{z}\ dt \right| + \left| \int_{\pi/\omega_j}^{3\pi/2\omega_j} f_a(z,t)\ \dot{z}\ dt \right| + \left| \int_{3\pi/2\omega_j}^{2\pi/\omega_j} f_a(z,t)\ \dot{z}\ dt \right| \qquad (5.26)$$

where force function f_a is expressed in equation (3.24). Considering two cases of polytropic exponent for $\gamma=1$ and $\gamma\neq1$, the magnitude of the processed energy of the gas-spring is obtained by integration of equation (5.26), as given by:

$$E_k = \begin{cases} 2p_0V_0\left[-\ln\left(1 + \frac{A_rZ}{V_0}\right) -\ln\left(1 - \frac{A_rZ}{V_0}\right)\right] & , \quad \text{for } \gamma=1 \\ \frac{2p_0V_0}{1-\gamma}\left[2 -\left(1 + \frac{A_rZ}{V_0}\right)^{1-\gamma} -\left(1 - \frac{A_rZ}{V_0}\right)^{1-\gamma}\right], & \text{for } \gamma\neq1 \end{cases} \qquad (5.27)$$

Based on the principle of energy similarity of dynamic elements, the local equivalent linear stiffness coefficient is then obtained by equating the processed energy of the gas-spring, expressed in equation (5.27), to that of a linear spring, in equation (5.25):

$$k_{eq}(\omega_j,Z) = \begin{cases} \frac{p_0V_0}{Z^2}\left[-\ln\left(1 + \frac{A_rZ}{V_0}\right) - \ln\left(1 - \frac{A_rZ}{V_0}\right)\right] & , \text{ for } \gamma=1 \\ \frac{p_0V_0}{Z^2(1-\gamma)}\left[2 -\left(1 + \frac{A_rZ}{V_0}\right)^{1-\gamma} -\left(1 - \frac{A_rZ}{V_0}\right)^{1-\gamma}\right], & \text{for } \gamma\neq1 \end{cases} \qquad (5.28)$$

5.4.3 Random Response Analysis

A random road surface is often characterized by its power spectral density (PSD), and the road vehicle by its complex frequency response function. The complex frequency response function of the vehicle is used as a transfer function operating on the road spectrum to derive the spectrum of vibration response of the vehicle moving at a specified speed. Linear vehicle models are conveniently expressed by their frequency response functions in order to carry out random response analyses. Nonlinear vehicle models, however, are described by frequency response functions of their linear equivalent models such that convenient linear analytical tools can be applied to evaluate random responses of nonlinear vehicle models. The generalized discrete harmonic linearization technique can be applied to express the nonlinear vehicle model by an array of local equivalent linear models, where each locally equivalent model describes the nonlinear model's behavior in the vicinity of a discrete frequency. The complex frequency response function of the local equivalent model can thus be generated to be used as the transfer function operating on the road spectrum.

Local equivalent representation of nonlinear vehicle models is achieved through computation of local equivalent stiffness and damping coefficients, using equations (5.16) through (5.28). Determination of local equivalent constants, however, requires prior knowledge of the relative response quantities across the nonlinear elements corresponding to a selected excitation frequency. Since these relative response quantities are dependent upon excitation amplitude, an iterative algorithm is developed to compute the relative displacement response and

thus the local constants corresponding to a specific excitation frequency.

The iterative methodology initially assumes the values of the local equivalent coefficients in order to formulate a linear model at a selected excitation frequency. The random road spectrum is discretized to yield the excitation amplitude corresponding to the selected excitation frequency. An input amplitude vector is estimated from the input power spectral density in the following manner [105]:

$$X_i(\omega_j) = \psi \left[\int_{\omega_j-\Delta\omega/2}^{\omega_j+\Delta\omega/2} s_i(\omega)\, d\omega \right]^{1/2} \tag{5.29}$$

where $X_i(\omega_j)$ is the excitation amplitude corresponding to the excitation frequency ω_j, $s_i(\omega)$ is the input power spectral density, $\Delta\omega$ is a small frequency band around the center frequency ω_j and ψ is a constant. A time history, $x_i(t)$ is then synthesized using sine series approximation:

$$x_i(t) = \sum_{j=1}^{N} (-1)^j X_i(\omega_j) \sin(\omega_j t) \tag{5.30}$$

where N is the total number of the discretized excitation frequencies.

The assumed linear system is then solved to compute the relative response quantities using the estimated amplitude vector $X_i(\omega_j)$. Equations (5.16) through (5.28) are solved to determine local equivalent coefficients corresponding to selected frequency ω_j. For each nonlinear dynamic element, an error vector between the assumed and computed values of local equivalent coefficients is evaluated as:

$$\bar{\varepsilon} = \begin{bmatrix} c^{\circ}_{eq}(\omega_j, Z) - c_{eq}(\omega_j, Z) \\ k^{\circ}_{eq}(\omega_j, Z) - k_{eq}(\omega_j, Z) \end{bmatrix} \tag{5.31}$$

where c°_{eq} and k°_{eq} are the initially assumed local equivalent coefficients, and c_{eq} and k_{eq} are the local coefficients established from equations (5.16) through (5.28). The assumed local equivalent coefficients are updated and the iterative process is continued until convergence is achieved. The iterative process is repeated for each discrete excitation frequency to generate a complete array of local equivalent linear systems.

Although the nonlinear vehicle model is characterized by its local equivalent linear models using a deterministic approach, the generalized discrete harmonic linearization can provide an accurate estimate of the frequency response function as a function of discrete excitation frequency and amplitude [109]. The estimated frequency response function can then be used to determine the random response in the following manner [116]:

$$[s_x(\omega_j)] = [H(\omega_j)]^{*} \; [s_i(\omega_j)] \; [H(\omega_j)]^{T} \tag{5.32}$$

where $s_x(\omega_j)$ is the response spectral density and $H(\omega_j)$ is the complex frequency response function at discrete excitation frequency ω_j. '*' and 'T' denote complex conjugate and transpose, respectively. Equation (5.32) illustrates that random response is evaluated from the spectral density of road roughness and the frequency response characteristics of the equivalent system corresponding to a local frequency ω_j. Thus a deterministic excitation is assumed only to determine the frequency

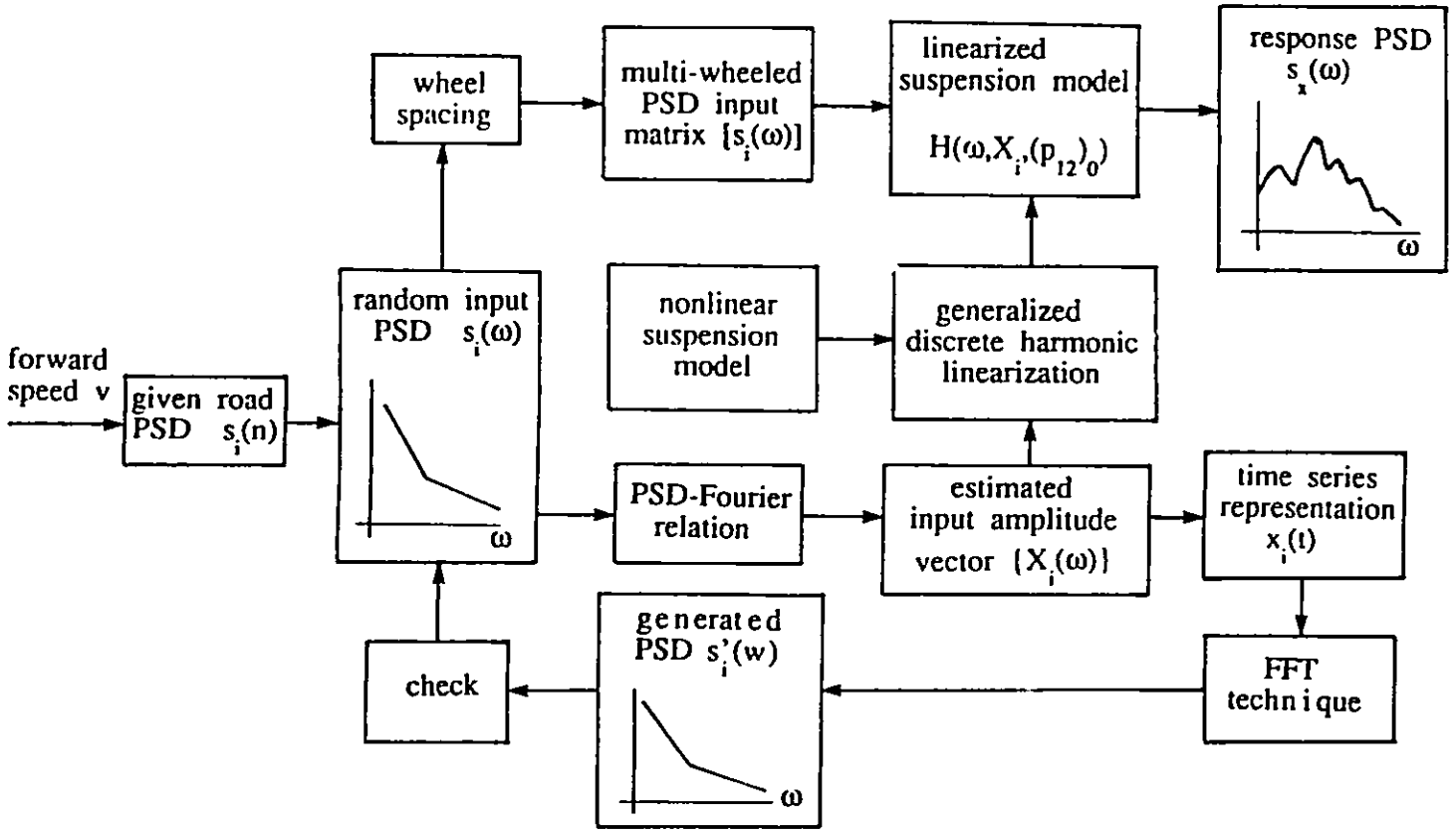

FIGURE 5.13 A flow diagram of simulation procedure for random response of nonlinear vehicle models

response characteristics of the nonlinear system. A flow diagram of the simulation procedure is illustrated in Figure 5.13.

5.5 Stochastic Analysis of In-plane Vehicle Model

The differential equations of motion, from (5.3) to (5.6), describing the ride dynamics of a two-axle vehicle employing tunable pressure limited shock absorbers, are solved for stochastic excitations originating from the randomly distributed road roughness. The stochastic response of the in-plane model a of two-axle vehicle is evaluated using the generalized harmonic linearization technique and the corresponding simulation parameters are listed in Table 5.2. Random road roughness is expressed by auto- and cross-spectral densities, assuming an undeformable road. The response characteristics of the vehicle model are presented and discussed in terms of response power spectral densities.

5.5.1 Random Road Excitation

Road surfaces traversed by vehicles are random in nature. It has been established that most road surface irregularities are normally distributed and may be accurately described by a stationary random process [117, 118]. The PSD of road roughness provides the essential profile characteristics distributed over the frequency range of interest and is thus suitable for analysis of the dynamic behavior of vehicle systems. Spectral densities of road surfaces that closely approximate available experimental data are described by [119]:

$$s(\mu) = \begin{cases} s(\mu_0)(\mu/\mu_0)^{-w_1}, & \mu \le \mu_0 \\ s(\mu_0)(\mu/\mu_0)^{-w_2}, & \mu > \mu_0 \end{cases} \tag{5.33}$$

TABLE 5.2

Simulation Parameters of Tunable
In-plane Two Axle Vehicle Suspension

SYMBOL	DESCRIPTION	PARAMETER VALUE
m_s	Sprung mass of the vehicle	1460 kg
I_s	Pitch mass moment of inertia of the suspension	2460 kg·m^2
m_{u1}	Unsprung mass of front axle assembly	80 kg
m_{u2}	Unsprung mass of rear axle assembly	71 kg
k_{s1},k_{s2}	Stiffness coefficients of front and rear suspension springs	39920, 35500 N/m
k_{t1},k_{t2}	Stiffness coefficients of front and rear tires	351000, 351000 N/m
c_{t1},c_{t2}	Damping coefficients of front and rear tires	800, 800 N·s/m
ℓ_f	Horizontal distance between front axle and sprung mass cg	1.01 m
ℓ_r	Horizontal distance between rear axle and sprung mass cg	1.803 m
A_p	Area of piston on rod side	2.51×10^{-3} m^2
A_r	Area of rod cross section	3.14×10^{-4} m^2
C_{d1},C_{d2}	Discharge coefficients	0.7
a_1	Area of piston orifice	3.14×10^{-5} m^2
a_2	Area of cylinder orifice	3.14×10^{-5} m^2
γ	Polytropic exponent	1.4
p_a	Initial charge pressure	14×10^5 Pa
V_a	Initial gas volume	1.9×10^{-4} m^3
n	Number of piston orifices	2

where,

$s(\mu)$ = spatial spectral density of road roughness (m^3/cycle)

μ = spatial frequency (cycles/m)

$s(\mu_0)$ = roughness coefficient and amplitude of the spectral density at reference spatial frequency μ_0 (m^3/cycle)

μ_0 = $1/2\pi$, reference spatial frequency (cycles/m)

w_1, w_2 = constants characterizing road waviness

Assuming a constant forward speed v, the temporal spectral density of road excitations can be expressed as [120]:

$$s(f) = s(\mu)/\, v \tag{5.34}$$

where,

$s(f)$ = temporal spectral density of road roughness (m^2/Hz)

v = constant forward speed of vehicle (m/s)

f = μ v, temporal frequency (Hz)

The vehicle model, shown in Figure 5.2, is subjected to two vertical excitations at the front and rear tire-terrain interfaces, respectively. Assuming that the rear wheel follows the same profile as the front one, the cross-spectral density of road input can be then expressed in terms of a time delay function:

$$s_{fr}(f) = s(f)\, \exp(-i\, 2\pi\, f\, \tau) \tag{5.35}$$

$s_{fr}(f)$= cross-spectral density of road input (m^2/Hz)

τ = time delay between the front and rear wheels (s), given by:

$$\tau = \ell_{fr} \,/\, v \tag{5.36}$$

ℓ_{fr} = vehicle wheelbase (m)

and

TABLE 5.3

Data of Random Road Input

SYMBOL	DESCRIPTION	PARAMETER VALUE
$s(\mu_0)$	Roughness coefficient of road	252.8×10^{-6} m^3/cycle
w_1	Road waviness constant one	2.1
w_2	Road waviness constant two	1.4
v	Vehicle travel speed	20 m/s

$$s_{rf}(f) = s^{*}_{fr}(f) \tag{5.37}$$

$s^{*}_{rf}(f)$ = complex conjugate of $s_{fr}(f)$ (m^2/Hz)

The temporal displacement spectral density matrix can be, therefore, established and expressed as:

$$[s_{x1}(f)] = \frac{s(\mu)}{v}\begin{bmatrix} 1 & e^{-i2\pi f\tau} \\ e^{i2\pi f\tau} & 1 \end{bmatrix} \tag{5.38}$$

where $[s_{x1}(f)]$ is the temporal displacement spectral density matrix of the road excitation. Figure 5.14 illustrates the temporal displacement PSD of the random road excitation, used for the response evaluation of the vehicle model, and the corresponding parameters are presented in Table 5.3. The road spectrum is discretized to yield the excitation amplitude vector using equation (5.29). A synthesized time history is generated based on the estimated input amplitude vector using equation (5.30). The temporal power spectral density of synthesized time history is estimated using a fast Fourier transform (FFT) and compared with the displacement PSD of road roughness, as shown in Figure 5.14. It can be

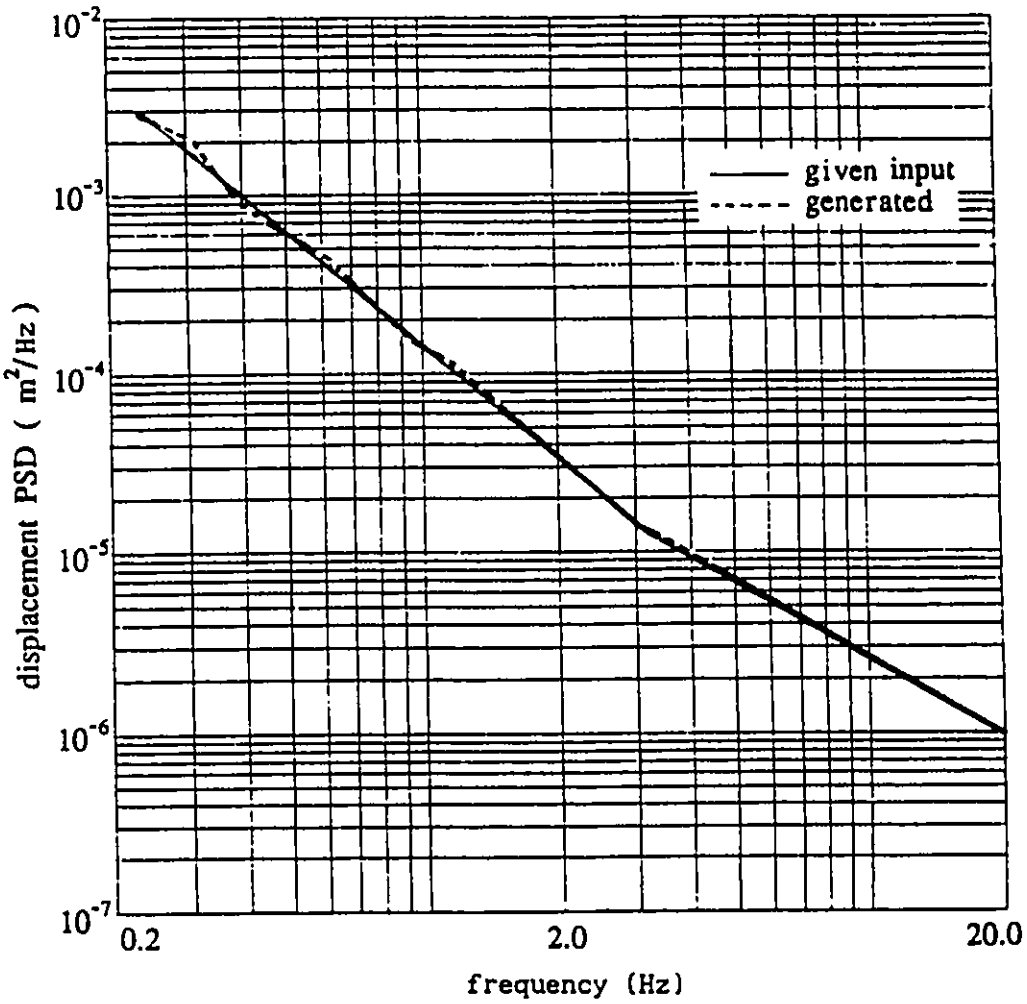

FIGURE 5.14 Displacement PSD of a random road input (v=20 m/s)

observed that the estimated displacement PSD correlates quite well with displacement PSD of the road.

5.5.2 Dynamic Analysis of In-plane Vehicle Model

The dynamic response of a nonlinear in-plane vehicle model, employing tunable shock absorbers, is evaluated using the generalized discrete harmonic linearization technique. The nonlinearities associated with the gas-spring, orifice flow and the pressure limiting mechanism are expressed by local equivalent stiffness and damping coefficients. The complex frequency response function matrix of the nonlinear vehicle model is thus established as a function of local excitation frequency and amplitude, as well as the preset limiting pressure value:

$$[H(\omega_j, X_1, (p_{12})_0)]_{nxm} = \left([k_{eq}] - \omega_j^2[m] + i\omega_j[c_{eq}]\right)^{-1}_{nxn} \left([k_t] + i\omega_j[c_t]\right)_{nxm} \qquad (5.39)$$

where,

n = number of degrees of freedom of the vehicle model

m = number of input variables

[H] = complex frequency response function matrix

i = $\sqrt{-1}$, unit imaginary number

[m] is the mass matrix, $[k_{eq}]$ and $[c_{eq}]$ are nxn matrices of equivalent stiffness and damping coefficients, respectively. $[k_t]$ and $[c_t]$ are nxm matrices of stiffness and damping properties of the tires, respectively. The PSD of the response variables is then computed for the random road excitations in the following manner [116]:

$$[s_x(\omega_j)]_{nxn} = [H(\omega_j, X_1, (p_{12})_0)]_{nxm}\ [s_1(\omega_j)]_{mxm}\ [H^*(\omega_j, X_1, (p_{12})_0)]^T_{mxn} \qquad (5.40)$$

where $[s_x]$ is the response PSD matrix. The dynamic ride performance of

the tunable vehicle suspension is evaluated through power spectral density characteristics of the vehicle response. The response characteristics are expressed and discussed in terms of the bounce and pitch acceleration spectra of the sprung mass, and the vertical acceleration spectra of the front and rear unsprung masses, respectively.

The PSD of the vertical and pitch acceleration response of the vehicle sprung mass is computed for the tunable and fixed orifice shock absorbers as shown in Figures 5.15 and 5.16, respectively. Identical orifice sizes (n=2) have been selected for both tunable and fixed orifice shock absorbers to demonstrate the effectiveness of the tunable pressure limiting modulation. The pressure limiting factors of the front and rear tunable shock absorbers are selected to be identical and unit (ν=1). Figures 5.15 and 5.16 reveal that bounce and pitch acceleration response of the vehicle with tunable suspension is identical to that of the vehicle with fixed orifice shock absorbers at low excitation frequencies. Since the relative velocity response and thus the pressure differential across the piston is small at low frequencies, the tunable shock absorber acts as the fixed one due to closed relief valves. However, the relief valves open when the relative velocity response increases at higher excitation frequencies. The pressure differential across the shock absorber is then held around the preset pressure $(p_{12})_0$ by the pressure relief mechanism, and the corresponding damping force generated by the tunable shock absorber is reduced. The peak bounce and pitch acceleration response of the vehicle sprung mass with tunable shock absorbers is, therefore, considerably lower than that of the vehicle with fixed orifice shock absorbers.

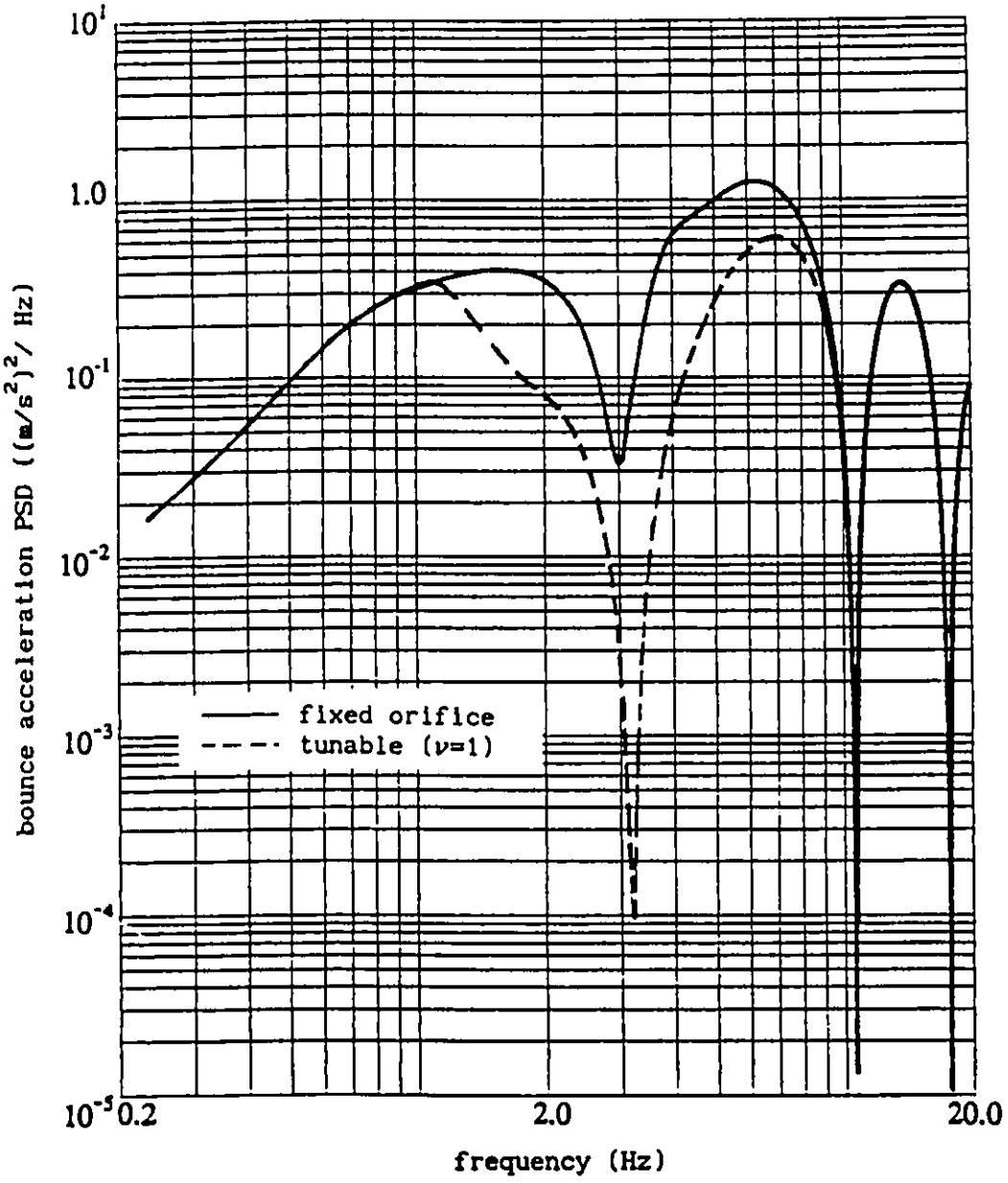

FIGURE 5.15 Bounce acceleration PSD of vehicle sprung mass with tunable and fixed orifice shock absorbers

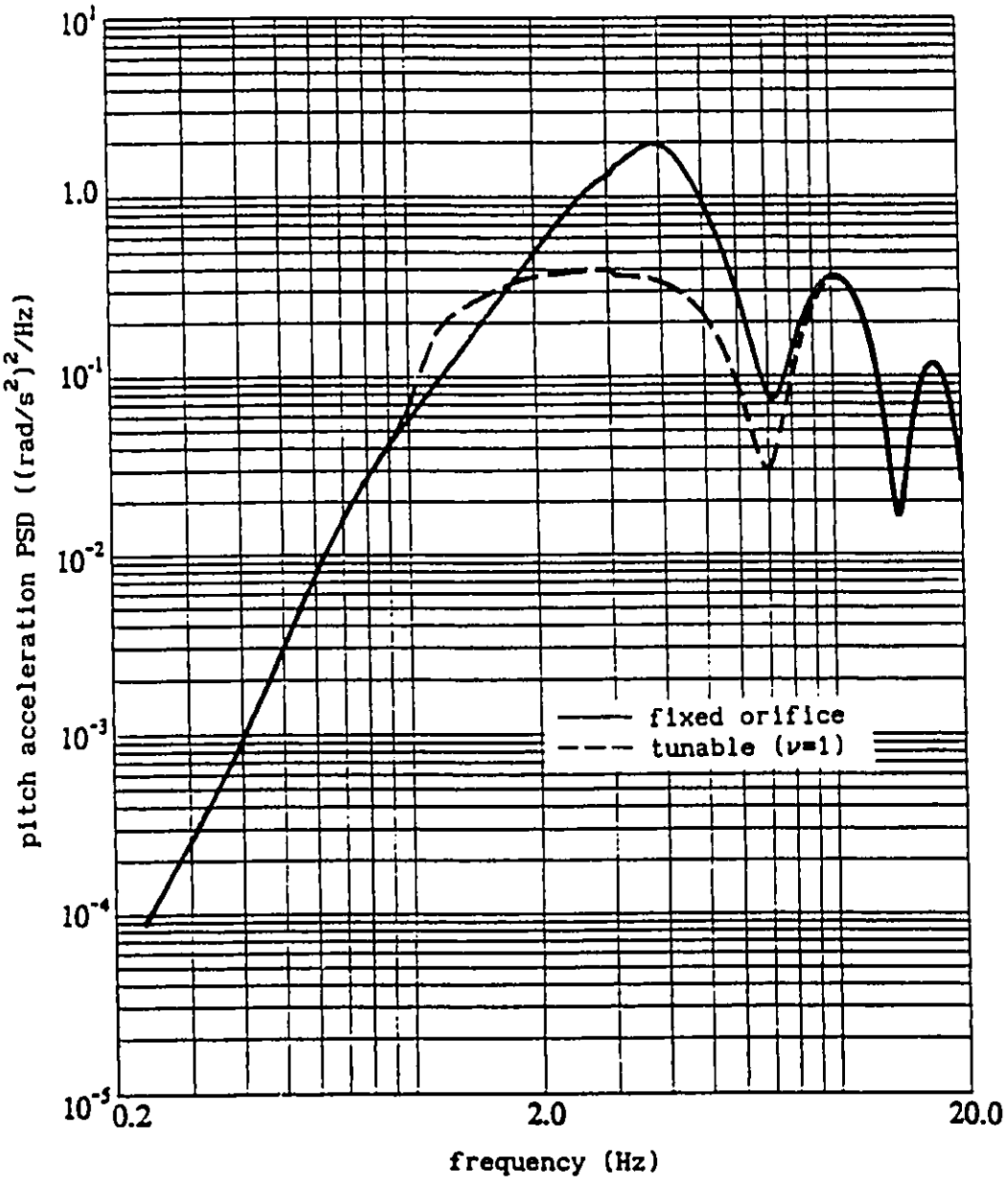

FIGURE 5.16 Pitch acceleration PSD of vehicle sprung mass with tunable and fixed orifice shock absorbers

A comparison of the bounce and pitch acceleration PSD of the vehicle model employing the tunable suspension with that of the fixed orifice suspension reveals that the ride performance of the vehicle can be improved considerably via the tunable shock absorbers in the frequency range 1 to 10 Hz, which is known to be the frequency range to which human body is most fatigue sensitive [111]. The pressure differential approaches a low value due to almost insignificant road excitation corresponding to frequencies above 10 Hz, as illustrated in Figure 5.14. The fixed orifice and tunable shock absorbers, therefore, yield identical vehicle ride response at higher frequencies, as shown in Figures 5.15 and 5.16.

The PSD of the vertical acceleration response of the front and rear unsprung masses is presented in Figures 5.17 and 5.18, respectively. The tunable pressure limited shock absorbers tend to reduce the vertical acceleration response of sprung as well as unsprung masses at excitation frequencies above 1.1 Hz, where pressure limiting occurs, as shown in Figures 5.15 and 5.17. Figures 5.17 and 5.18 clearly reveal that vertical acceleration response of unsprung masses with tunable shock absorbers is smaller than that of axles with fixed orifice shock absorbers. The reduced damping due to pressure limiting shock absorbers, however, can not suppress the unsprung mass resonance and thus yield larger acceleration PSD peaks around 9.5 Hz.

The vehicle ride response is strongly influenced by preset value of the limiting pressure $(p_{12})_0$. The influence of the preset pressure on the vehicle ride response is investigated by varying the value of the tuning factor ν of the tunable pressure limited shock absorber. The PSD

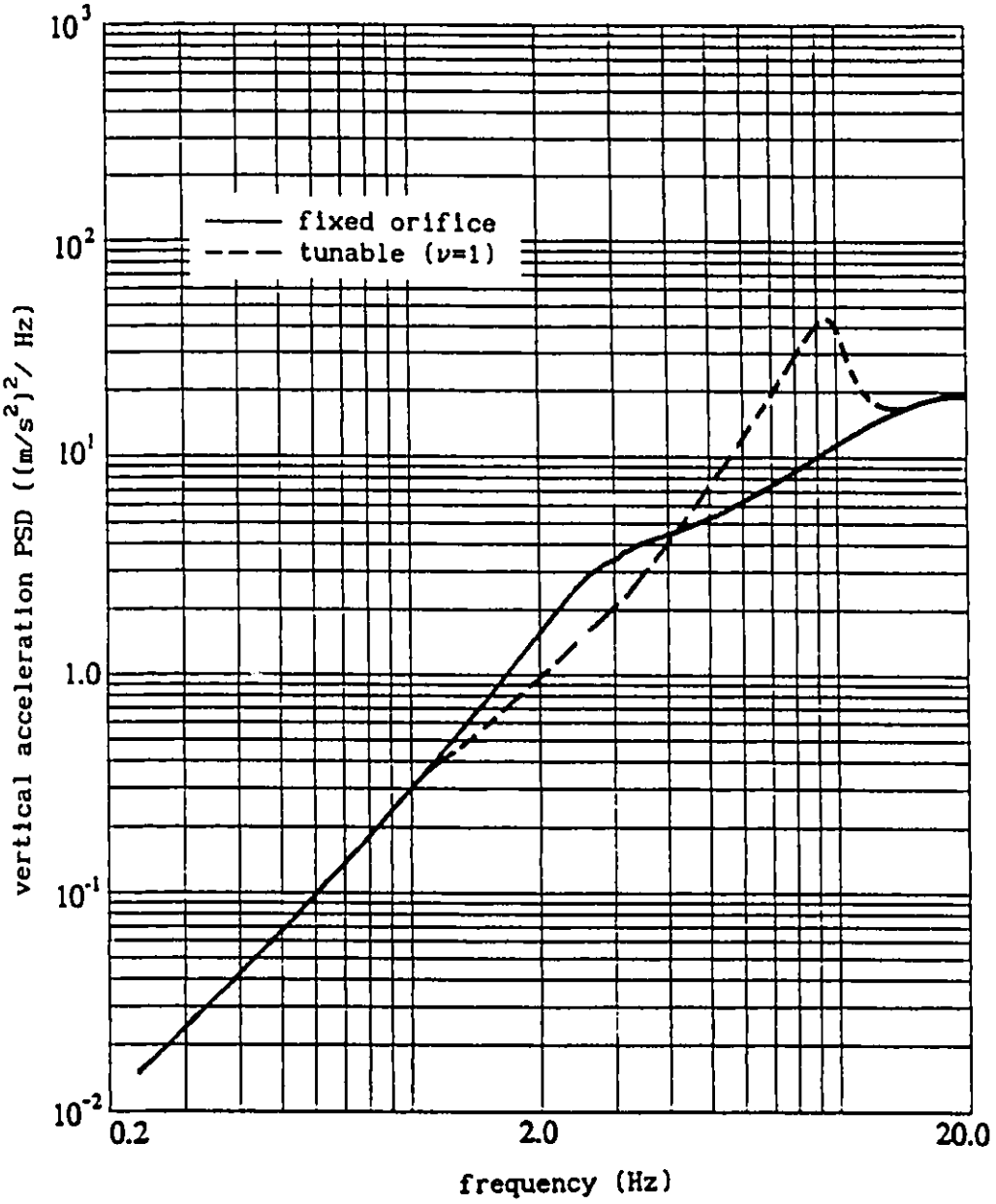

FIGURE 5.17 Vertical acceleration PSD of front unsprung mass with tunable and fixed orifice shock absorbers

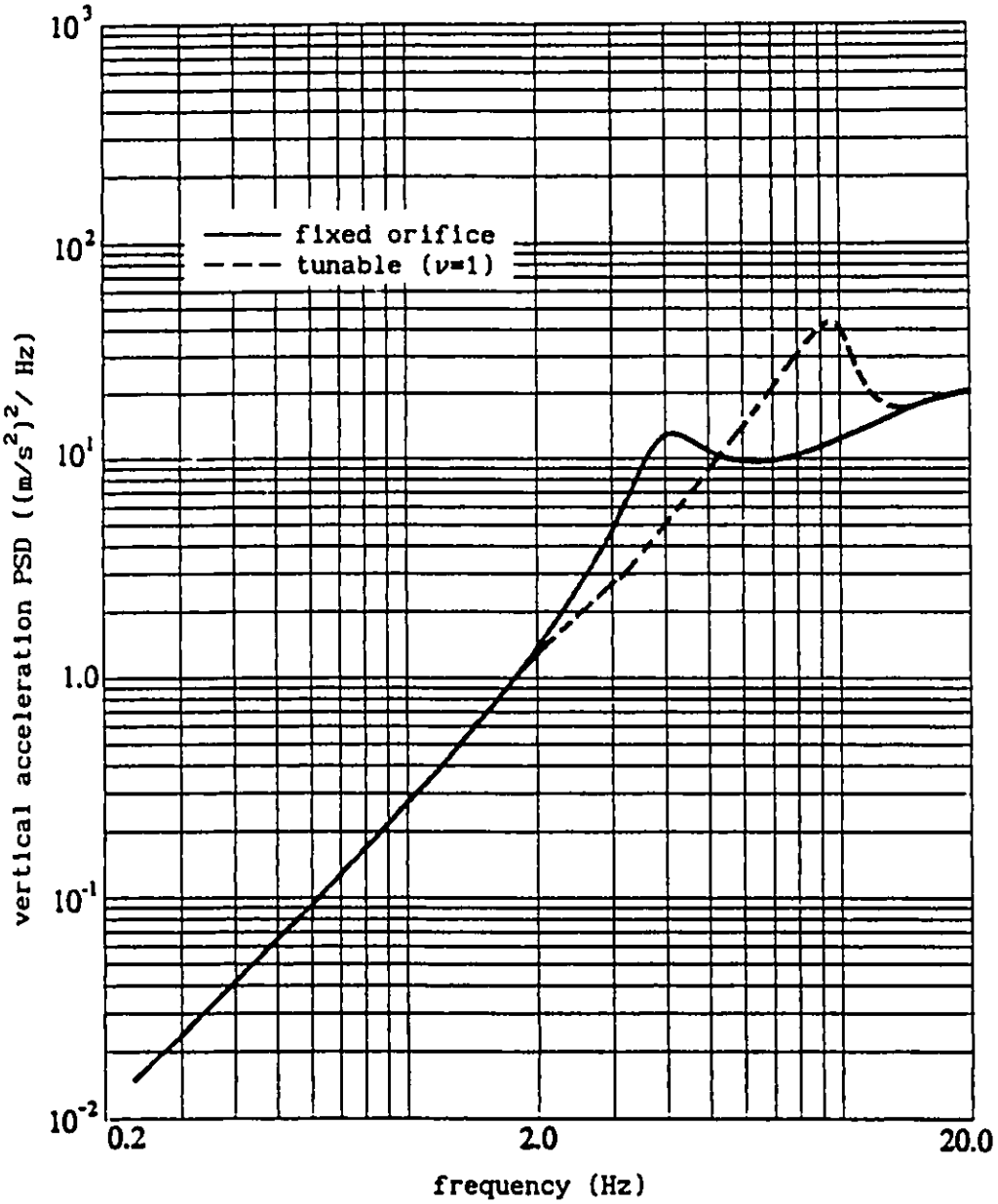

FIGURE 5.18 Vertical acceleration PSD of rear unsprung mass with tunable and fixed orifice shock absorbers

of the bounce and pitch acceleration response of the sprung mass is presented in Figures 5.19 and 5.20, respectively, for various values of the tuning factor. A low value of pressure tuning factor (ν=0.8) yields a further reduction of both bounce and pitch acceleration response in the frequency range 1.5 – 10 Hz. However, a lower value of pressure tuning factor induces a large resonant peak, around 1 Hz, due to reduced suspension damping. A high value of the pressure limiting factor (ν=1.2) yields poor vertical and pitch ride when compared with the vehicle response for a lower value of the tuning factor. However, a high value of the tuning factor suppresses the resonant peak caused by the suspension system with lower preset pressure. A comparison of the response characteristics of the tunable shock absorber with that of the fixed orifice shock absorber reveals that a higher value of the limiting factor can still provide a considerable improvement in vehicle ride performance, in the frequency range 1 to 10 Hz.

The random response characteristics of the vehicle are influenced not only by the input power spectral density but also by cross coupling between the axles. The coupling effects may be altered by varying the suspension parameters. A further improvement in vehicle ride response may be realized by appropriately tuning of the front and rear suspensions. The influence of front and rear suspension parameters on the vehicle ride quality is investigated for three shock absorber configurations: fixed orifice; identically tuned front and rear shock absorbers (ν_f=ν_r=1); and front and rear shock absorbers with different preset pressure (ν_f=1, ν_r=0.7). The bounce and pitch acceleration PSD response characteristics of the vehicle sprung mass with the above three

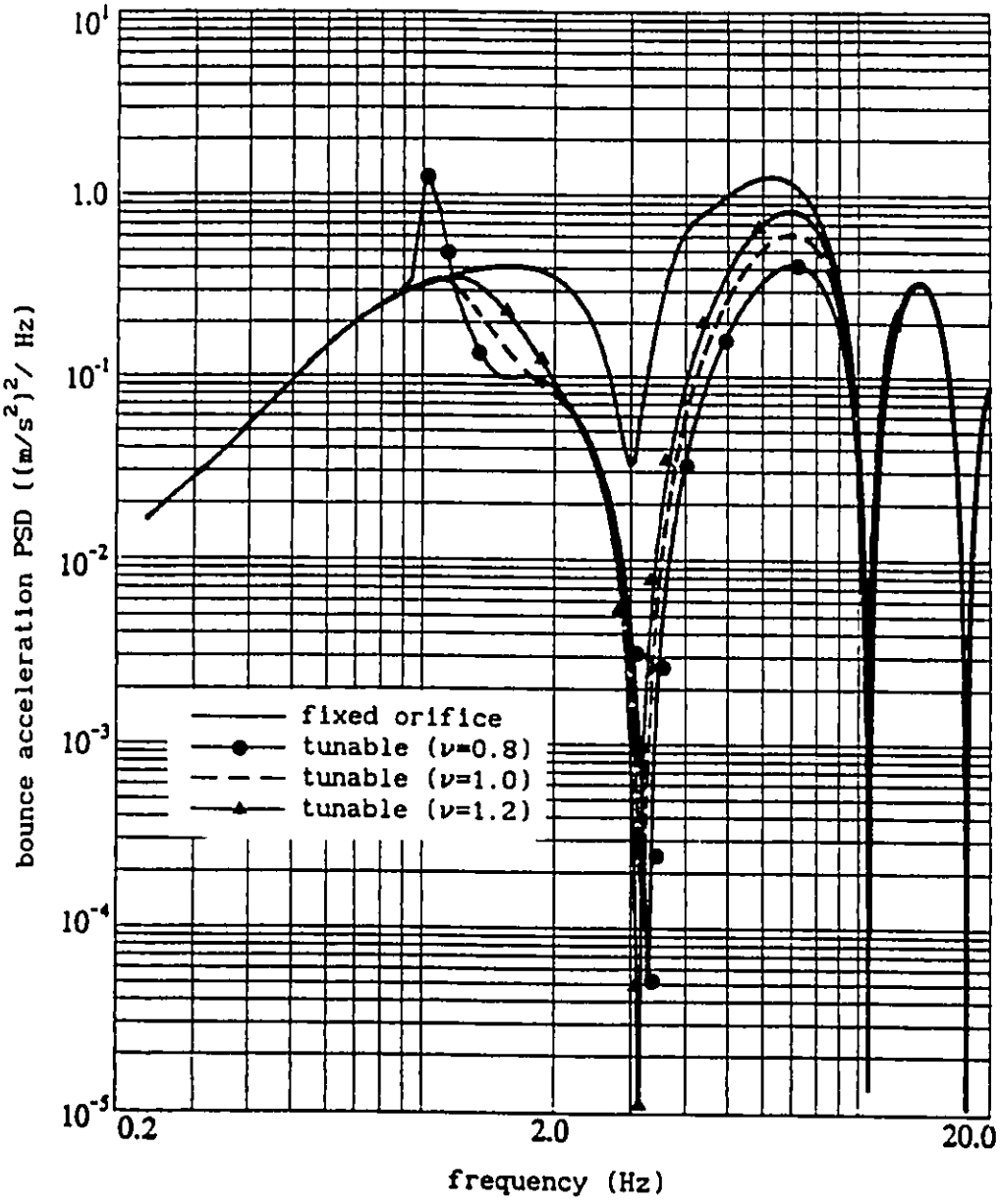

FIGURE 5.19 Bounce acceleration PSD of vehicle sprung mass with tunable shock absorber for various values of tuning factor

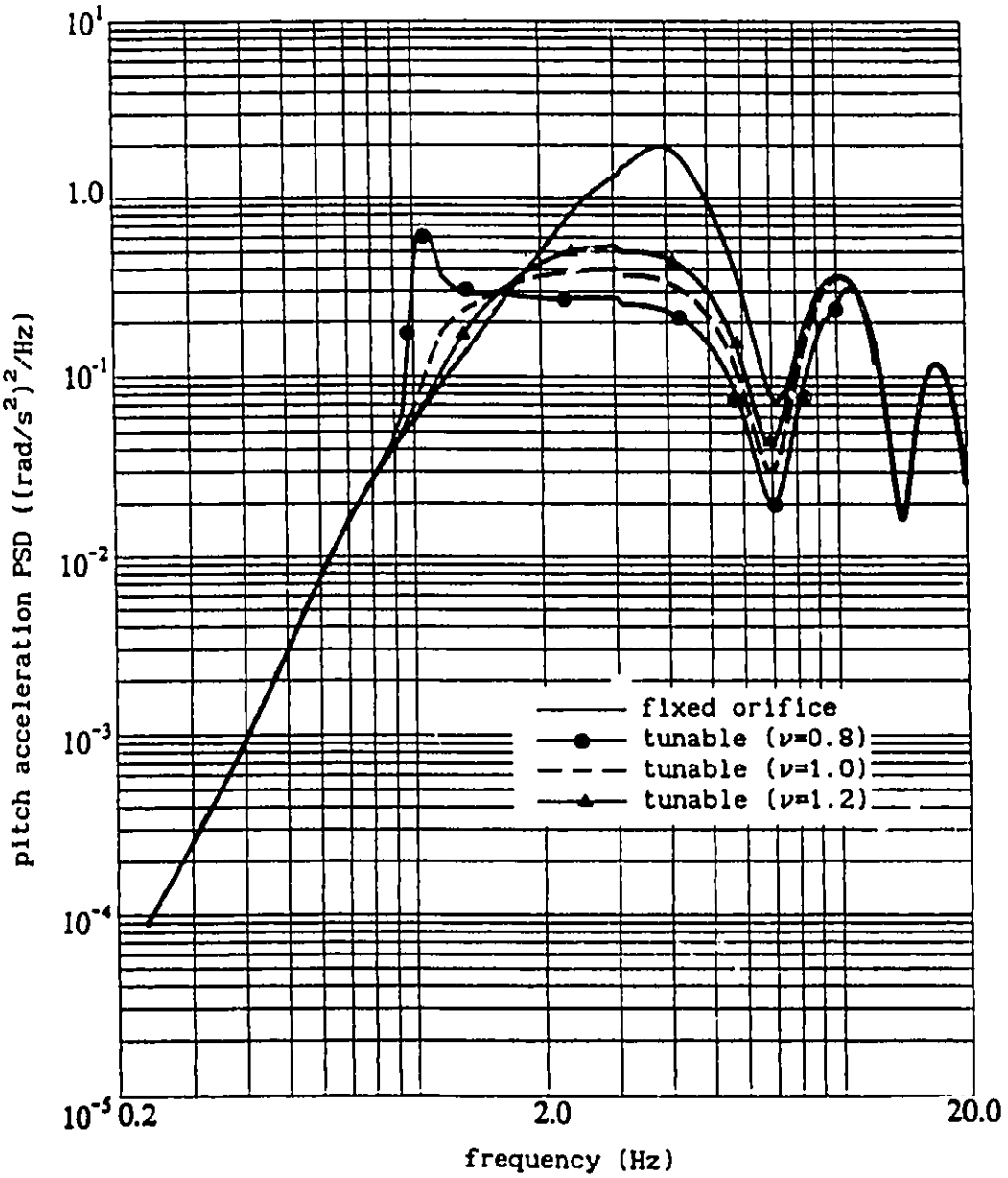

FIGURE 5.20 Pitch acceleration PSD of vehicle sprung mass with tunable shock absorber for various values of tuning factor

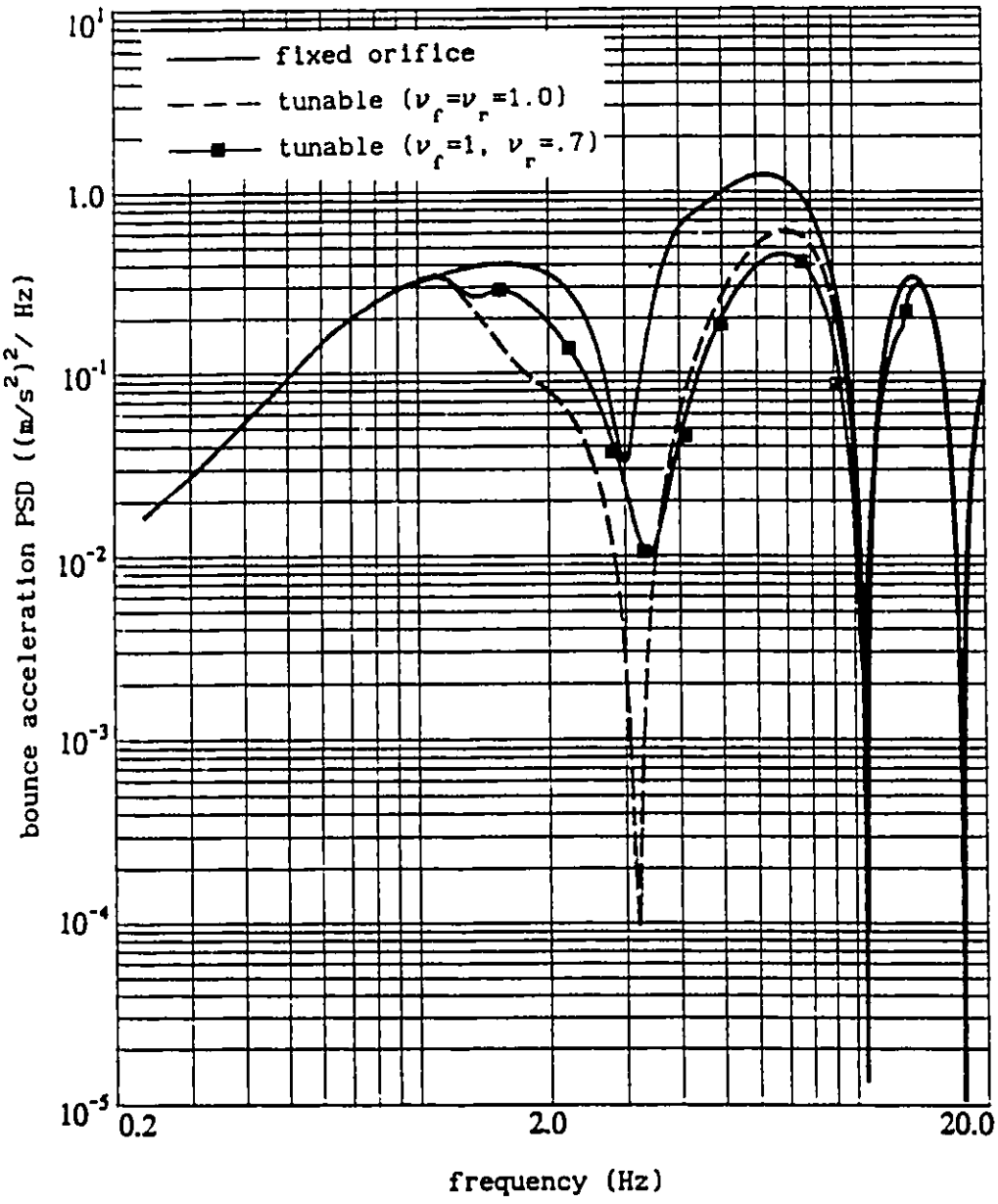

FIGURE 5.21 Bounce acceleration PSD of vehicle sprung mass with fixed orifice and tunable shock absorbers (various ν_f and ν_r)

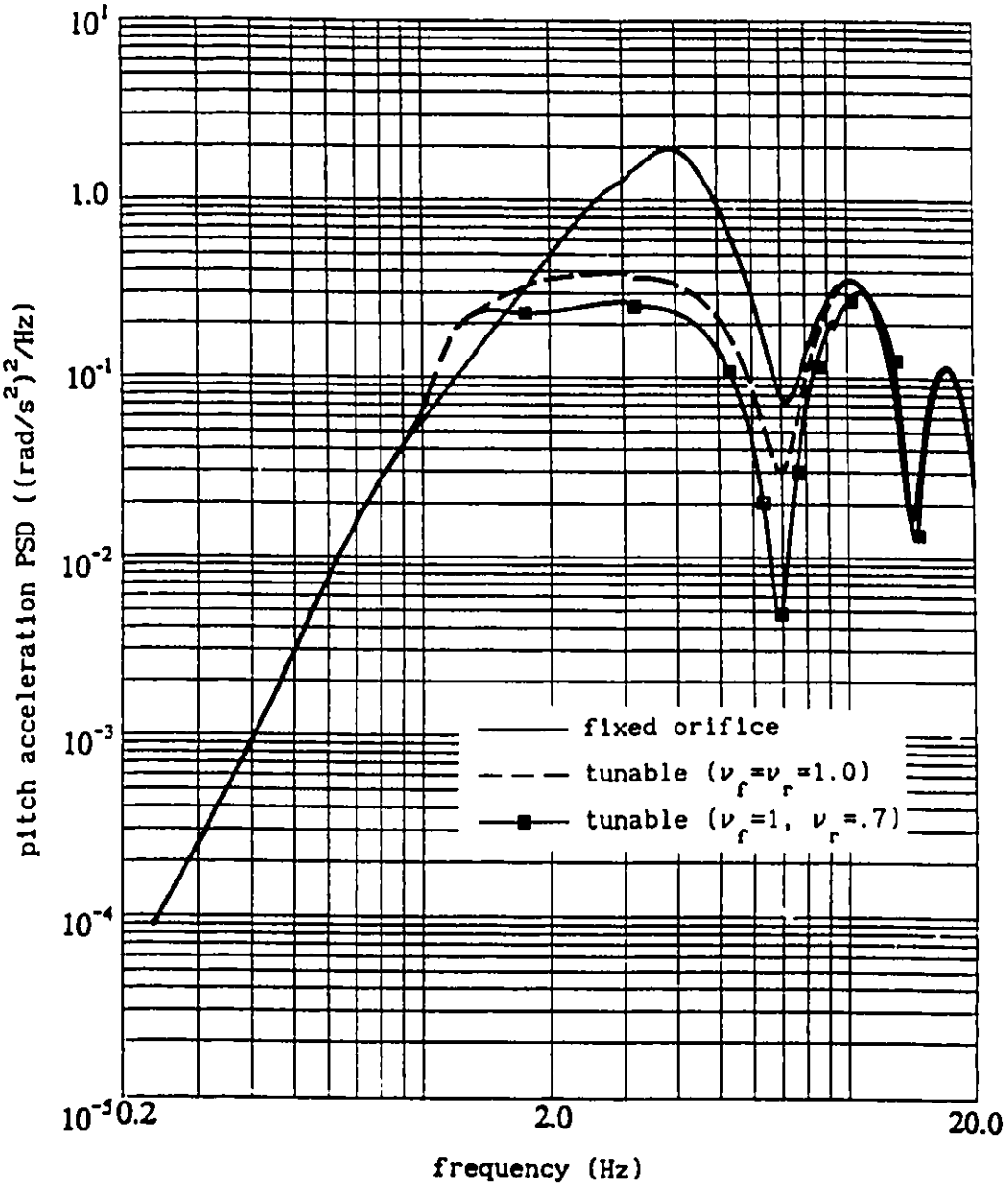

FIGURE 5.22 Pitch acceleration PSD of vehicle sprung mass with fixed orifice and tunable shock absorbers (various ν_f and ν_r)

configurations are presented in Figures 5.21 and 5.22, respectively. A comparison of both bounce and pitch acceleration PSD response shows that the tunable shock absorber with identical pressure limiting factor yields improved ride response as compared with the fixed one in the frequency range from 1 to 10 Hz. The PSD of the vertical acceleration response, shown in Figure 5.21, reveals that the selected tuning parameters (ν_f=1, ν_r=0.7) yield poor bounce ride at lower frequencies, while the vertical ride of the vehicle is improved around the higher frequencies. The pitch acceleration PSD response of the tunable vehicle suspension, however, can be improved in the frequency range 1 to 10 Hz by selecting different tuning parameters, as shown in Figure 5.22.

5.6 Summary

Dynamic analyses of two vehicle models, employing tunable pressure limited shock absorbers, are carried out for deterministic and stochastic excitations. The quarter vehicle model is first evaluated for deterministic analysis in the time and frequency domains. The ride dynamics of the quarter vehicle model are presented in terms of shock and vibration isolation characteristics to demonstrate the performance benefits of tunable pressure limited shock absorbers. A generalized discrete harmonic linearization technique is proposed, based on the principle of energy similarity of dynamic elements, to carry out stochastic analysis of a nonlinear vehicle model. The equivalent linear coefficients of the nonlinear vehicle model are derived for the nonlinear restoring as well as damping elements, using the generalized discrete harmonic linearization technique. The stochastic response characteristics of an in-plane vehicle model with tunable pressure

limited shock absorbers are evaluated and compared with those of the vehicle model with fixed orifice shock absorbers. The results presented in this chapter reveal that the vehicle ride in the frequency range 1 - 10 Hz can be improved considerably by using tunable pressure limited shock absorbers.

CHAPTER 6

ANALYSIS OF AN INTERCONNECTED SUSPENSION WITH TUNABLE DAMPING CONTROL

6.1 Introduction

Handling, control and ride quality of road vehicles pose conflict requirements on vehicle suspensions. A comfortable ride demands a suspension system that can provide effective shock and vibration isolation performance. Effective isolation of shock and vibration, induced by road surface irregularities, requires not only a soft suspension but also appropriate variable damping characteristics. Adequate directional control and handling performance of road vehicles require a stiffer suspension to reduce roll angle at the wheel liftoff condition. An stiffer suspension is essential to enhance the rollover threshold value and thus static roll stability of road vehicles [121]. Vehicle suspension designs are thus carried out to achieve a compromise between ride quality and handling and control performance of road vehicles. Auxiliary roll stiffness mechanisms are often introduced to increase effective roll stiffness and thus a vehicle's rollover threshold value. Addition of roll stiffness, however, deteriorates the vehicle ride quality.

Interconnected passive and active vehicle suspensions have been proposed to achieve improved vehicle ride as well as handling and control performance. Interconnected suspension systems are configured via fluid coupling between the hydraulic struts of suspensions, either within an axle or on front and rear axles [65, 66]. Felez and Vera [65] investigated interconnected passive and active hydro-pneumatic

suspension systems for their ride and roll response characteristics. The study demonstrated an improved vehicle handling and control performance of the interconnected suspensions. Moulton and Best [66] proposed an interconnected suspension system with rubber springs, and demonstrated an improved load distribution control of the vehicle. Horton and Crolla [69] investigated interconnected suspensions incorporating active and semi-active feedback mechanisms. A mechanical linkage mechanism was used to control the hydraulic servo valve and thus the stiffness and damping characteristics of the suspension. The study indicated improved ride comfort and attitude control of the vehicle. It has been established that the effective roll stiffness and rollover threshold value of vehicles can be improved via an interconnected vehicle suspension, while the improved ride quality can be achieved by variable damping characteristics via active or semi-active means. Therefore, improvement in vehicle ride can also be achieved via damping control using a tunable pressure limiting mechanism. The interconnections between hydraulic suspension struts provide an enhanced anti-roll capability and thus static roll stability, while the tunable pressure limiting mechanism between the strut and accumulator of the suspension offers sequential damping to improve shock and vibration isolation performance of road vehicles.

In this chapter, an interconnected hydro-pneumatic suspension with tunable passive pressure limiting mechanism is investigated to achieve overall suspension performance. A roll plane model of a road vehicle, incorporating hydraulically interconnected suspension struts within a beam axle, is developed. Ride quality and static roll stability

performance potentials of two interconnected suspension struts, located at the right and left tracks of the vehicle, are investigated via computer simulations. Performance characteristics of the interconnected vehicle suspension with tunable damping control are compared with those of an interconnected suspension with fixed orifice damping valves and an independent strut suspension.

Roll plane models of vehicles, employing independent and interconnected suspensions with a beam axle, are first analyzed assuming a high fluid bulk modulus. Fundamental characteristics of an interconnected suspension are derived; specifically the influence of fluid coupling and feedback effects are discussed through analysis of these simplified models. A comprehensive analytical model of a modified tunable interconnected hydro-pneumatic suspension is developed, incorporating the dynamics of the pressure limiting mechanism, as well as fluid and mechanical compliance.

The static roll stability and the ride performance of the interconnected hydro-pneumatic suspension are analyzed through computer simulation. The roll stability of the suspension systems is evaluated in terms of the roll response of the sprung mass during constant radius turns. Ride performance is established in terms of shock and vibration isolation characteristics of the suspension subject to road excitations. The influence of effective bulk modulus and the dynamics of the tunable relief valves on the dynamic performance of the modified tunable interconnected suspension is presented and discussed.

6.2 Development of Roll Plane Vehicle Model

The roll plane model of a road vehicle, consisting of a beam axle,

is presented in Figure 6.1. The primary vehicle suspension is represented by nonlinear springs ($k_{s\ell}$ and k_{sr})and dampers ($c_{s\ell}$ and c_{sr}). The tires are represented by linear spring and damper elements ($k_{t\ell}$, k_{tr}, $c_{t\ell}$ and c_{tr}), assuming point contact in the roll plane. Excitations to the roll plane model include vertical excitation at the tire-terrain interface due to road roughness and a roll moment $T_{\phi}(t)$ of the sprung mass caused by centrifugal forces about the roll center during a turning maneuver.

Assuming small vibration of the roll plane vehicle model and a fixed height of the roll center of the sprung mass, the equations of motion of the roll plane model can be derived as follows:

Bounce motion of the sprung mass:

$$m_1\ddot{x}_s(t) + f_{k\ell}(z_\ell,t) + f_{d\ell}(\dot{z}_\ell,t) + f_{kr}(z_r,t) + f_{dr}(\dot{z}_r,t) = 0 \qquad (6.1)$$

Roll motion of the sprung mass:

$$I_1\ddot{\phi}_s(t) - [f_{k\ell}(z_\ell,t) + f_{d\ell}(\dot{z}_\ell,t)]\,\ell_\ell + [f_{kr}(z_r,t) + f_{dr}(\dot{z}_r,t)]\ell_r = T_{\phi}(t) \qquad (6.2)$$

Bounce motion of the unsprung mass:

$$m_2\ddot{x}_u(t) - [f_{k\ell}(z_\ell,t) + f_{d\ell}(\dot{z}_\ell,t)] - [f_{kr}(z_r,t) + f_{dr}(\dot{z}_r,t)] = -[k_{t\ell}z_{1\ell}(t) + c_{t\ell}\dot{z}_{1\ell}(t)] - [k_{tr}z_{1r}(t) + c_{tr}\dot{z}_{1r}(t)] \qquad (6.3)$$

Roll motion of the unsprung mass:

$$I_2\ddot{\phi}_u(t) + [f_{k\ell}(z_\ell,t) + f_{d\ell}(\dot{z}_\ell,t)]\,\ell_\ell - [f_{kr}(z_r,t) + f_{dr}(\dot{z}_r,t)]\,\ell_r = [k_{t\ell}z_{1\ell}(t) + c_{t\ell}\dot{z}_{1\ell}(t)]\,\ell_{w\ell} - [k_{tr}z_{1r}(t) + c_{tr}\dot{z}_{1r}(t)]\,\ell_{wr} \qquad (6.4)$$

where,

m_1 = sprung mass of the vehicle (kg)

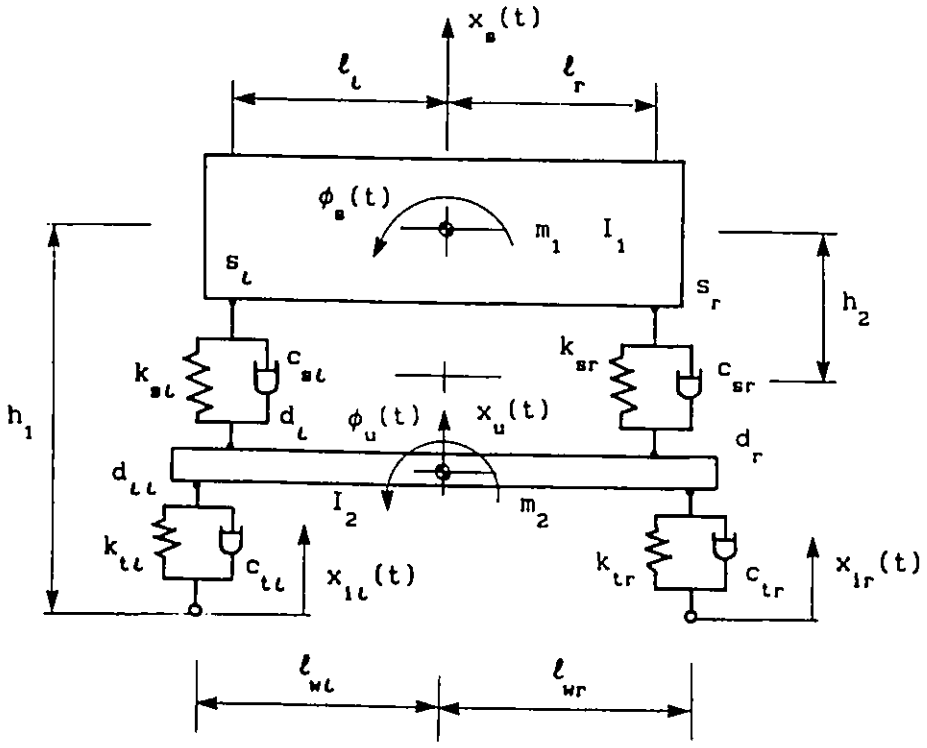

FIGURE 6.1 Representation of roll plane model of a road vehicle

I_1 = roll mass moment of inertia of sprung mass about the roll center ($kg \cdot m^2$)

m_2 = unsprung mass of the beam axle assembly (kg)

I_2 = roll mass moment of inertia of the beam axle assembly ($kg \cdot m^2$)

x_s, x_u = general coordinates characterizing bounce displacements of the sprung and unsprung masses, respectively (m)

ϕ_s, ϕ_u = general coordinates characterizing roll angles of the sprung and unsprung masses, respectively (rad)

$f_{k\ell}, f_{kr}$ = restoring forces due to the left and right suspension struts, respectively (N)

$f_{d\ell}, f_{dr}$ = damping forces due to the left and right suspension struts, respectively (N)

$T_{s\phi}$ = total external moment acting on sprung mass (N·m)

$k_{t\ell}, k_{tr}$ = stiffness coefficients of the tires (N/m)

$c_{t\ell}, c_{tr}$ = damping coefficients of the tires (N·s/m)

ℓ_ℓ, ℓ_r = lateral distances from the struts to the center of gravity of the sprung mass (m)

$\ell_{w\ell}, \ell_{wr}$ = lateral distances from the tires to the center of gravity of the unsprung mass (m)

and

$$z_\ell = (x_s - \ell_\ell \phi_s) - (x_u - \ell_r \phi_u)$$

$$z_r = (x_s + \ell_r \phi_s) - (x_u + \ell_r \phi_u)$$

$$z_{i\ell} = (x_u - \ell_{w\ell} \phi_u) - x_{i\ell}$$

$$z_{ir} = (x_u + \ell_{wr} \phi_u) - x_{ir}$$

The simulation parameters of the roll plane model of the vehicle are presented in Table 6.1.

The generalized coordinates and excitations can be expressed by

TABLE 6.1

Simulation Parameters of
the Roll Plane Vehicle Model

SYMBOL	DESCRIPTION	PARAMETER VALUE
m_1	Sprung mass	1460 kg
m_2	Unsprung mass of beam axle assembly	120 kg
I_1	Roll mass moment of inertia of sprung mass about roll centre	2020 $kg \cdot m^2$
I_2	Roll mass moment of inertia of beam axle assembly	140 $kg \cdot m^2$
ℓ_l, ℓ_r	Lateral distances from left and right struts to sprung mass cg.	0.6, 0.6 m
ℓ_{wl}, ℓ_{wr}	Lateral distances from tires to unsprung mass cg.	1.25, 1.25 m
k_{tl}, k_{tr}	Stiffness coefficients of left and right tires	451000, 451000 N/m
c_{tl}, c_{tr}	Damping coefficients of left and right tires	200, 200 N·s/m
h_1	Height of sprung mass center above the ground	1.2 m
h_2	Height of sprung mass center with respect to roll center	1.4 m

the following vectors:

$$\{x\} = [x_s \; x_u \; \phi_s \; \phi_u]^T \tag{6.5}$$

$$\{x_i\} = [x_{il} \; x_{ir}]^T \tag{6.6}$$

where T denotes transpose. The relative displacements vectors:

$$\{z\} = \begin{Bmatrix} z_l \\ z_r \end{Bmatrix} \quad \text{and} \quad \{z_i\} = \begin{Bmatrix} z_{il} \\ z_{ir} \end{Bmatrix} \tag{6.7}$$

can be expressed in terms of general coordinate and input vectors by:

$$\{z\} = [TZM] \; \{x\} \tag{6.8}$$

$$\{z_i\} = [TZM1] \; \{x\} + [TZM2] \; \{x_i\} \tag{6.9}$$

where [TZM], [TZM1] and [TZM2] are coordinate transformation matrices given by:

$$[TZM] = \begin{bmatrix} 1 & -1 & -\ell_l & \ell_l \\ 1 & -1 & \ell_r & -\ell_r \end{bmatrix} \tag{6.10}$$

$$[TZM1] = \begin{bmatrix} 0 & 1 & 0 & -\ell_{wl} \\ 0 & 1 & 0 & \ell_{wr} \end{bmatrix} \tag{6.11}$$

and

$$[TZM2] = \begin{bmatrix} -1 & 0 \\ 0 & -1 \end{bmatrix} \tag{6.12}$$

Equations (6.1) through (6.4), in general, describe the dynamics of a vehicle in the roll plane. While the equations of motion for the roll plane model are retained in the same form, the suspension forces can be considerably different for varying types of suspensions and associated modeling assumptions. Independent, interconnected and tunable interconnected hydro-pneumatic vehicle suspensions are systematically modeled in the following sections in order to derive their respective forces.

6.3 Modeling of Independent Hydro-pneumatic Suspension

The schematic diagram of a hydro-pneumatic shock absorber, comprising a hydraulic strut, an accumulator and a damping restriction, is shown in Figure 6.2. The chamber I of the hydraulic strut is assumed to be open to atmosphere, while chamber II contains pressurized hydraulic fluid. The accumulator, chamber III, includes a separator to prevent the gas from diffusing into the fluid. Elastic diaphragms or floating pistons are often used in the accumulator to separate the gas from the hydraulic fluid. The roll plane model of the vehicle incorporating independent hydro-pneumatic suspension with a beam axle is presented in Figure 6.3. Simulation parameters of the hydro-pneumatic suspension employed in the vehicle model are listed in Table 6.2.

6.3.1 Static Equilibrium Equations

The internal pressure of the hydro-pneumatic suspension, with respect to atmospheric pressure p_{at}, corresponding to the static equilibrium, is determined from the static load transferred to the suspension. Assuming negligible mass due to the separator, the internal static pressure can be expressed as:

$$p_{oj} = W_j / A_{cj} , \quad (j = \ell, r) \tag{6.13}$$

where,

ℓ, r = subscripts referring to left and right suspension units, respectively

p_{oj} = static internal pressure of suspension strut j (Pa)

A_{cj} = piston area of suspension strut j (m^2)

W_j = static load acting on suspension strut j (N)

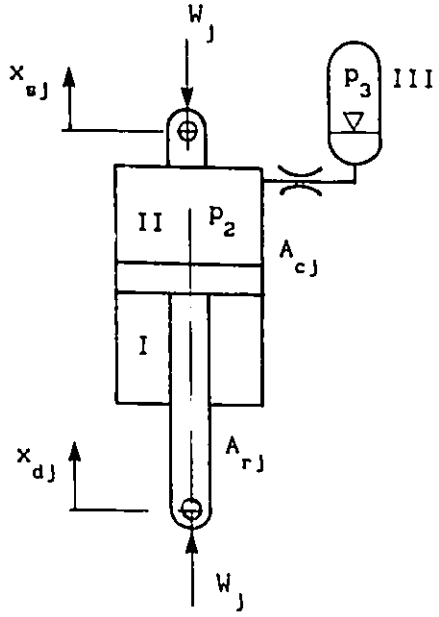

FIGURE 6.2 Schematic of hydro-pneumatic shock absorber

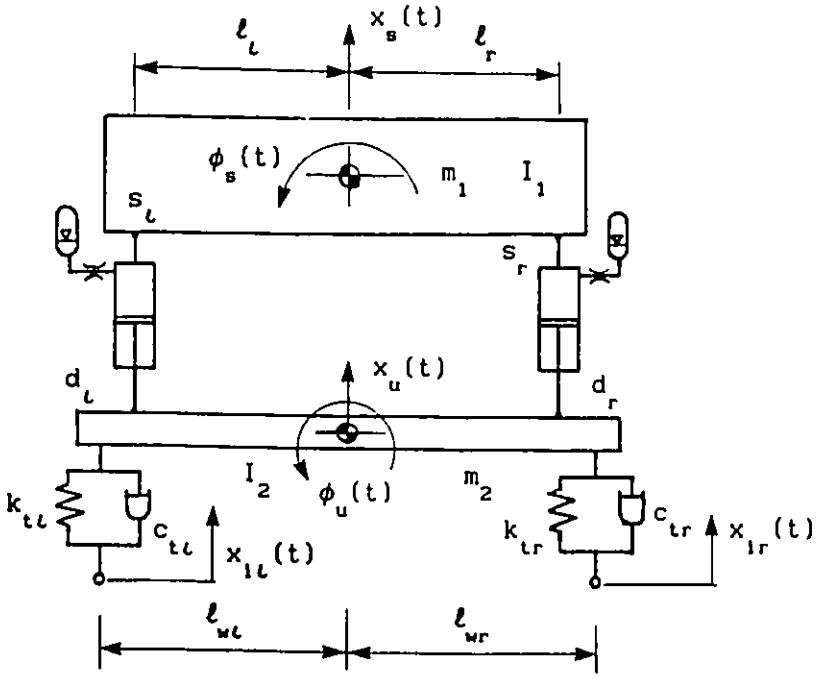

FIGURE 6.3 Schematic of roll plane model of vehicle employing independent hydro-pneumatic suspension

TABLE 6.2

Simulation Parameters of Hydro-pneumatic Suspension

SYMBOL	DESCRIPTION	PARAMETER VALUE
ρ	Mass density of fluid	797 kg/m^3
C_d	Discharge coefficient	0.7
γ	polytropic exponent	1.4
p_{at}	Atmospheric pressure	101300 Pa
A_{cl}, A_{cr}	Piston areas	9.5×10^{-3}, 9.5×10^{-3} m^2
a_{1l}, a_{1r}	Orifice areas	5.1×10^{-5}, 5.1×10^{-5} m^2
p_{al}, p_{ar}	Initial charge pressure	12.0×10^{5}, 12.0×10^{5} Pa
V_{al}, V_{ar}	Initial gas volume	1.5×10^{-3}, 1.5×10^{-3} m^3

and

$$W_\ell = \frac{m_1 g \ell_r}{\ell_\ell + \ell_r} \quad \text{and} \quad W_r = \frac{m_1 g \ell_\ell}{\ell_\ell + \ell_r} \tag{6.14}$$

Assuming a polytropic process, the static pressure can be related to the initial charge pressure of the accumulator:

$$p_{0j} V_{0j}^{\gamma} = p_{aj} V_{aj}^{\gamma} , \quad (j = \ell, r) \tag{6.15}$$

where,

V_{0j} = static volume of gas chamber (m^3)

p_{aj} = initial charge pressure (Pa)

V_{aj} = initial volume of gas chamber (m^3)

γ = polytropic exponent, $1 \leq \gamma \leq 1.4$, γ=1 for an isothermal process, and γ=1.4 for an adiabatic process

The static deflection, X_{stj} of the suspension strut is then derived as:

$$X_{stj} = (V_{aj} - V_{0j}) / A_{cj} , \quad (j = \ell, r) \tag{6.16}$$

Simultaneous solution to equations (6.13) to (6.16) yields static values of the pressure, volume and deflection of the hydro-pneumatic suspension, corresponding to the static equilibrium position.

6.3.2 Fluid Flow Equations

The rate of change of fluid volume in chamber II, caused by relative motion across the hydro-pneumatic suspension is given by:

$$Q_{m2j} = A_{cj} \dot{z}_j , \quad (j = \ell, r) \tag{6.17}$$

where,

Q_{m2j} = rate of change of fluid volume in chamber II of suspension strut j (m^3/s)

$\dot{z}_j$ = relative velocity across suspension strut j (m/s)

Assuming turbulent fluid flow, flow through the orifice between the strut and the accumulator can be expressed in the following manner:

$$Q_{23j} = C_d\, a_{1j} \sqrt{\frac{2\,|p_{23j}|}{\rho}}\ \mathrm{sgn}(p_{23j}) \ , \quad (j = \ell,\ r) \tag{6.18}$$

where,

Q_{23j} = volume flow rate through the orifice between chambers II to III (m^3/s)

C_d = discharge coefficient

a_{1j} = orifice area (m^2)

ρ = mass density of fluid (kg/m^3)

p_{abj} = $p_{aj} - p_{bj}$, pressure differential between chambers a and b of suspension strut j (Pa)

$$\mathrm{sgn}(\cdot) = \begin{cases} +1 \ , & (\cdot) \geq 0 \\ -1 \ , & (\cdot) < 0 \end{cases}$$

Assuming incompressible fluid, the fluid continuity equation is given by:

$$-Q_{23j} = Q_{m2j} \ , \quad (j = \ell,\ r) \tag{6.19}$$

6.3.3 Pressure Equations

Equations (6.17) to (6.19) yield the pressure differential due to the orifice restriction:

$$p_{23j} = \frac{\rho}{2} \left(\frac{A_{cj}\, \dot{z}_j}{C_d\, a_{1j}} \right)^2 \mathrm{sgn}(\dot{z}_j) \ , \quad (j = \ell,\ r) \tag{6.20}$$

Assuming a polytropic process, the instantaneous pressure and volume of the gas are related to the static values:

$$p_{3j}\, V_{3j}^{\gamma} = p_{0j}\, V_{0j}^{\gamma} \ , \quad (j = \ell,\ r) \tag{6.21}$$

where,

p_{3j} = instantaneous pressure of gas in chamber III (Pa)

V_{3j} = instantaneous volume of gas in chamber III (m^3), given by

$$V_{3j} = V_{0j} + A_{cj}\, z_j \,, \quad (j = \ell,\ r) \tag{6.22}$$

From equations (6.21) and (6.22), the gas pressure can be related to relative displacement across the suspension system:

$$p_{3j} = \left(\frac{V_{0j}}{V_{0j} + A_{cj} z_j} \right)^{\gamma} p_{0j} \,, \quad (j = \ell,\ r) \tag{6.23}$$

and the pressure differential, p_{30j}, is expressed as:

$$p_{30j} = \left(\frac{V_{0j}^{\gamma} - (V_{0j} + A_{cj} z_j)^{\gamma}}{(V_{0j} + A_{cj} z_j)^{\gamma}} \right) p_{0j} \,, \quad (j = \ell,\ r) \tag{6.24}$$

6.3.4 Dynamic Forces of Independent Suspension

The total dynamic force generated by the independent strut hydro-pneumatic suspension, with respect to the static equilibrium position, is established from the fluid pressure acting upon the piston:

$$f_{dsj} = (p_{2j} - p_{0j})\, A_{cj} \,, \quad (j = \ell,\ r) \tag{6.25}$$

where,

f_{dsj} = total dynamic force of suspension strut j (N)

p_{2j} = instantaneous fluid pressure in chamber II (Pa)

Equation (6.25) can be expressed in terms of pressure differentials, through simple manipulations:

$$f_{dsj} = p_{23j}\, A_{cj} + p_{30j}\, A_{cj} \,, \quad (j = \ell,\ r) \tag{6.26}$$

Substituting for p_{23j} and p_{30j} from equations (6.20) and (6.24) yields:

$$f_{daj}(z_j,\ \dot{z}_j,\ t) = f_{dj}(\dot{z}_j,\ t) + f_{aj}(z_j,\ t)\ ,\quad (j = \ell,\ r) \qquad (6.27)$$

where $f_{aj}(z_j,\ t)$ and $f_{dj}(\dot{z}_j,\ t)$ are restoring and damping forces, respectively, given by:

$$f_{aj}(z_j,\ t) = \left(\frac{V_{oj}^{\gamma} - (V_{oj} + A_{cj} z_j)^{\gamma}}{(V_{oj} + A_{cj} z_j)^{\gamma}} \right) p_{oj} A_{cj}\ ,\quad (j = \ell,\ r) \qquad (6.28)$$

$$f_{dj}(\dot{z}_j,\ t) = \frac{\rho}{2} \left(\frac{A_{cj}\ \dot{z}_j}{C_d\ a_{1j}} \right)^2 A_{cj}\ \mathrm{sgn}(\dot{z}_j)\ ,\quad (j = \ell,\ r) \qquad (6.29)$$

Equations (6.27) to (6.29) reveal that the total dynamic force generated due to the hydro-pneumatic suspension comprises a restoring force due to the gas chamber and a damping force caused by orifice flows. The restoring and damping forces are nonlinear functions of the relative displacement and velocity, respectively, across the hydro-pneumatic suspension. Equations of motion of the roll plane model of the vehicle employing independent hydro-pneumatic suspension can then be obtained by substituting for stiffness ($f_{kj} = f_{aj}$) and damping forces, equations (6.28) and (6.29), into equations (6.1) to (6.4).

6.4 Modeling of Interconnected Hydro-pneumatic Suspension

The roll plane model of an interconnected hydro-pneumatic suspension is presented in Figure 6.4. Two hydraulic suspension struts are linked via connecting pipes, as illustrated in Figure 6.4. The upper chamber of hydraulic strut located on the left side of the axle (chamber II_ℓ) is connected to lower chamber of hydraulic strut located on the right side of the axle (chamber I_r). The lower chamber of the left strut (I_ℓ) is connected to the upper chamber of the right strut (II_r). Fluid

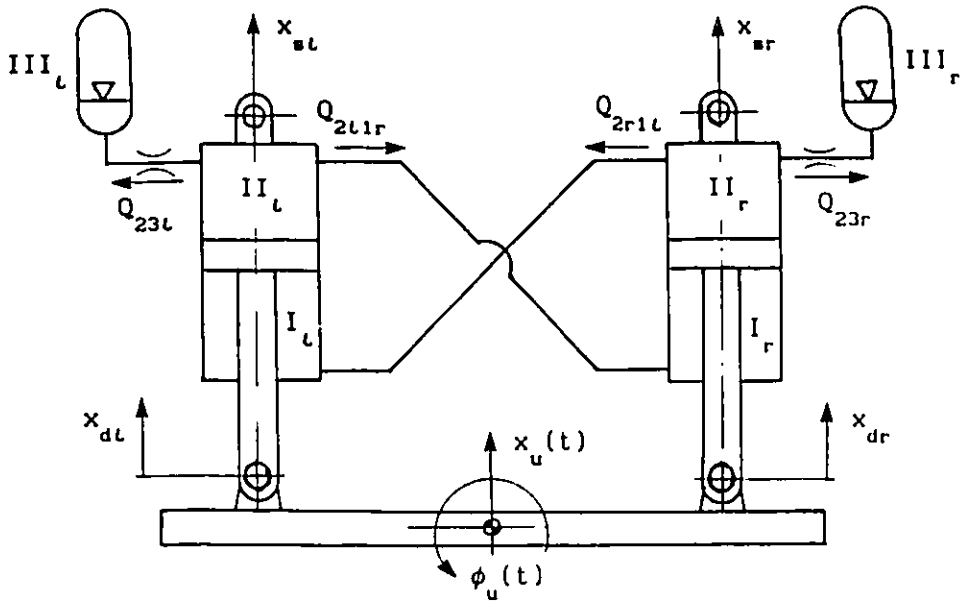

FIGURE 6.4 Schematic of roll plane model of interconnected hydro-pneumatic suspension

couplings between right and left hydraulic suspension struts yield a fluid feedback effect that influences both static and dynamic characteristics of the interconnected suspension. An analytical model of the suspension is thus developed to include the static and dynamic effects of the overall interconnected system. Simulation parameters of the interconnected hydro-pneumatic suspension are listed in Table 6.3.

6.4.1 Static Equilibrium Equations

Static loads acting upon the left and right suspension struts are balanced by the reaction forces established from internal pressures in all the chambers. The force balancing equations for the interconnected hydro-pneumatic suspension are expressed by:

$$p_{2\ell 0} A_{c\ell} - p_{1\ell 0}(A_{c\ell} - A_{r\ell}) = W_{\ell} \tag{6.30}$$

$$p_{2r0} A_{cr} - p_{1r0}(A_{cr} - A_{rr}) = W_{r} \tag{6.31}$$

where,

$p_{1\ell 0}$, $p_{2\ell 0}$ = static pressures in chambers I_{ℓ} and II_{ℓ} of left suspension strut, respectively (Pa)

p_{1r0}, p_{2r0} = static pressures in chambers I_{r} and II_{r} of right suspension strut, respectively (Pa)

$A_{c\ell}$, A_{cr} = piston areas of left and right suspension struts, respectively (m^2)

$A_{r\ell}$, A_{rr} = rod cross section areas of left and right suspension struts, respectively (m^2)

W_{ℓ}, W_{r} = static loads on left and right suspension struts (N), as expressed in equation (6.14)

In view of the connections between the right and left suspension struts, the static pressures in the connected chambers should be identical

TABLE 6.3

Simulation Parameters of Interconnected Hydro-pneumatic Suspension

SYMBOL	DESCRIPTION	PARAMETER VALUE
ρ	Mass density of fluid	797 kg/m^3
μ	Absolute viscosity of fluid	0.006 $N \cdot s/m^2$
D	Inside diameter of pipe	0.02 m
L	Length of connecting pipe	1.2 m
C_d	Discharge coefficient	0.7
γ	Polytropic exponent	1.4
p_{at}	Atmospheric pressure	101300 Pa
$A_{c\ell}$, A_{cr}	Piston areas	9.5×10^{-3}, 9.5×10^{-3} m^2
$A_{r\ell}$, A_{rr}	Cross section area of rod	5.0×10^{-3}, 5.0×10^{-3} m^2
$a_{2\ell}$, a_{2r}	Orifice areas	5.1×10^{-5}, 5.1×10^{-5} m^2
$p_{a\ell}$, p_{ar}	Initial charge pressure	12.0×10^{5}, 12.0×10^{5} Pa
$V_{a\ell}$, V_{ar}	Initial gas volume	1.5×10^{-3}, 1.5×10^{-3} m^3

[113]. The following constraint equations are thus derived corresponding to the static equilibrium position:

$$p_{2\ell 0} = p_{3\ell 0} = p_{1r0} \tag{6.32}$$

$$p_{2r0} = p_{3r0} = p_{1\ell 0} \tag{6.33}$$

Assuming a polytropic process, the static value of fluid pressure can be related to the initial gas charge pressure:

$$p_{3\ell 0}\, V_{0\ell}^{\gamma} = p_{a\ell}\, V_{a\ell}^{\gamma} \tag{6.34}$$

$$p_{3r0}\, V_{0r}^{\gamma} = p_{ar}\, V_{ar}^{\gamma} \tag{6.35}$$

where,

$V_{0\ell}$, V_{0r} = static volumes of gas chambers (m^3)

$p_{a\ell}$, p_{ar} = initial charge pressures (Pa)

$V_{a\ell}$, V_{ar} = initial volumes of gas chambers (m^3)

The static deflections of the suspension struts are derived as functions of the volume changes of the gas chambers and are given by:

$$A_{c\ell}\, X_{st\ell} - (A_{cr} - A_{rr})\, X_{str} = (V_{a\ell} - V_{0\ell}) \tag{6.36}$$

$$-(A_{c\ell} - A_{r\ell})\, X_{st\ell} + A_{cr}\, X_{str} = (V_{ar} - V_{0r}) \tag{6.37}$$

where $X_{st\ell}$ and X_{str}, static deflections of left and right suspension struts respectively, are derived from equations (6.36) and (6.37):

$$X_{st\ell} = \frac{(V_{a\ell} - V_{0\ell})\, A_{cr} + (V_{ar} - V_{0r})(A_{cr} - A_{rr})}{A_{c\ell}\, A_{cr} - (A_{c\ell} - A_{r\ell})(A_{cr} - A_{rr})} \tag{6.38}$$

$$X_{str} = \frac{(V_{ar} - V_{0r})\, A_{c\ell} + (V_{a\ell} - V_{0\ell})(A_{c\ell} - A_{r\ell})}{A_{c\ell}\, A_{cr} - (A_{c\ell} - A_{r\ell})(A_{cr} - A_{rr})} \tag{6.39}$$

Simultaneous solution to the nonlinear algebraic equations (6.30) to (6.39), by using an iteration method, yields the static values of

pressure, volume and deflection of the interconnected hydro-pneumatic suspension corresponding to the static equilibrium position.

6.4.2 Fluid Flow Equations

The fluid flows within the interconnected suspension include the flows through orifices, flows through connecting pipes and flows due to piston movements. Assuming a high bulk modulus of fluid, the fluid flows due to fluid compressibility are neglected. The relationships among the various volume flow rates are established from fluid continuity equations, based on the law of conservation of mass.

Assuming turbulent flows through the orifice restrictions between the struts and the accumulators, the volume flow rates through the orifices in the left and right suspension units are related to pressure differentials across the orifices, in the following manner:

$$Q_{23\ell} = C_d\, a_{2\ell} \sqrt{\frac{2\,|p_{23\ell}|}{\rho}}\ \mathrm{sgn}(p_{23\ell})\ , \tag{6.40}$$

$$Q_{23r} = C_d\, a_{2r} \sqrt{\frac{2\,|p_{23r}|}{\rho}}\ \mathrm{sgn}(p_{23r})\ , \tag{6.41}$$

where,

$Q_{23\ell}$, Q_{23r} = flow rates through orifices between Chambers II_ℓ and III_ℓ and between II_r and III_r, respectively (m^3/s)

$a_{2\ell}$, a_{2r} = orifice areas of left and right suspension units, respectively (m^2)

Assuming laminar fluid flow through interconnecting pipes, volume flow rates through the pipes are expressed, for two identical interconnecting pipes in length L and diameter D, as follows [114]:

$$Q_{2\ell 1r} = \frac{\pi D^4}{128 \mu L} p_{2\ell 1r} \tag{6.42}$$

$$Q_{2r1\ell} = \frac{\pi D^4}{128 \mu L} p_{2r1\ell} \tag{6.43}$$

$Q_{2\ell 1r}$ = flow rate from chamber II_ℓ to chamber I_r (m^3/s)

$Q_{2r1\ell}$ = flow rate from chamber II_r to chamber I_ℓ (m^3/s)

μ = absolute viscosity of fluid ($N \cdot s/m^2$)

$p_{2\ell 1r}$ = $p_{2\ell} - p_{1r}$, pressure differential (Pa)

$p_{2r1\ell}$ = $p_{2r} - p_{1\ell}$, pressure differential (Pa)

The laminar fluid assumption is verified by computing the Reynolds number, R, by using the following equation [114]:

$$R = \frac{4 \rho Q}{\pi \mu D} \tag{6.44}$$

Since the diameters of the interconnecting pipes are much larger than that of the orifices, it is found that the Reynolds number is much less than 2000 for the simulations in this study. The assumption of laminar flow in the connecting pipes can therefore be justified.

The rates of change of fluid volume in chambers I of the left and right suspension struts are related to their relative velocities as expressed by, respectively,

$$Q_{m1\ell} = (A_{c\ell} - A_{r\ell}) \dot{z}_\ell(t) \tag{6.45}$$

$$Q_{m1r} = (A_{cr} - A_{rr}) \dot{z}_r(t) \tag{6.46}$$

$Q_{m1\ell}$ = rate of change of fluid volume in chamber I_ℓ (m^3/s)

Q_{m1r} = rate of change of fluid volume in chamber I_r (m^3/s)

Assuming incompressible fluid, the fluid continuity yields the following flows equations for chambers I_ℓ and I_r:

$$Q_{m1\ell} + Q_{2r1\ell} = 0 \tag{6.47}$$

$$Q_{m1r} + Q_{2\ell 1r} = 0 \tag{6.48}$$

where $Q_{m1\ell}$, $Q_{2r1\ell}$, Q_{m1r} and $Q_{2\ell 1r}$ are expressed in equations (6.45), (6.43), (6.46) and (6.42), respectively.

The respective rates of change of fluid volumes in chambers II of the left and right suspension struts, related to their piston movement, are expressed as:

$$Q_{m2\ell} = A_{c\ell} \dot{z}_{\ell}(t) \tag{6.49}$$

$$Q_{m2r} = A_{cr} \dot{z}_{r}(t) \tag{6.50}$$

$Q_{m2\ell}$ = rate of change of fluid volume in chamber II_{ℓ} (m^3/s)

Q_{m2r} = rate of change of fluid volume in chamber II_{r} (m^3/s)

The flow rates related to chambers II_{ℓ} and II_{r} are constrained by the fluid continuity equation expressed as, respectively:

$$Q_{m2\ell} + Q_{2\ell 1r} + Q_{23\ell} = 0 \tag{6.51}$$

$$Q_{m2r} + Q_{2r1\ell} + Q_{23r} = 0 \tag{6.52}$$

where $Q_{m2\ell}$, $Q_{2\ell 1r}$ and $Q_{23\ell}$ are expressed in Equations (6.49), (6.42) and (6.40), and Q_{m2r}, $Q_{2r1\ell}$ and Q_{23r} in (6.50), (6.43) and (6.41), respectively.

The rates of change of gas volumes in chambers III_{ℓ} and III_{r} are expressed, respectively, by

$$Q_{m3\ell} = \frac{dV_{3\ell}}{dt} \tag{6.53}$$

$$Q_{m3r} = \frac{dV_{3r}}{dt} \tag{6.54}$$

where,

$Q_{m3\ell}$ = rate of change of gas volume in chamber III_{ℓ} (m^3/s)

Q_{m3r} = rate of change of gas volume in chamber III_{r} (m^3/s)

$V_{3\ell}$ = instantaneous gas volume in chamber III_{ℓ} (m^3)

V_{3r} = instantaneous gas volume in chamber III_{r} (m^3)

The rates of change of gas volumes are further related to volume flow rates through the orifices, respectively:

$$Q_{23\ell} = Q_{m3\ell} \tag{6.55}$$

$$Q_{23r} = Q_{m3r} \tag{6.56}$$

where $Q_{23\ell}$ and $Q_{m3\ell}$ are expressed in equations (6.40) and (6.53), and Q_{23r} and Q_{m3r} in equations (6.41) and (6.54), respectively.

6.4.3 Pressure Equations

The fluid pressures in various chambers of the interconnected hydro-pneumatic suspension are derived in terms of pressure differentials due to orifice and pipe flows. The pressure differentials due to orifice flows in the left and right suspension units are obtained from equations (6.40) and (6.41), respectively, as:

$$p_{23\ell} = \frac{\rho}{2}\left(\frac{Q_{23\ell}}{C_d\, a_{2\ell}}\right)^2 \mathrm{sgn}(Q_{23\ell}) \tag{6.57}$$

$$p_{23r} = \frac{\rho}{2}\left(\frac{Q_{23r}}{C_d\, a_{2r}}\right)^2 \mathrm{sgn}(Q_{23r}) \tag{6.58}$$

where volume flow rate, $Q_{23\ell}$, is derived from equations (6.51), (6.46), (6.48) and (6.49):

$$Q_{23\ell} = -A_{c\ell}\,\dot{z}_{\ell}(t) + (A_{cr} - A_{rr})\,\dot{z}_{r}(t) \tag{6.59}$$

Volume flow rate, Q_{23r}, is similarly derived from equation (6.52), (6.45), (6.47) and (6.50):

$$Q_{23r} = - A_{cr} \dot{z}_r(t) + (A_{c\ell} - A_{r\ell}) \dot{z}_\ell(t) \tag{6.60}$$

The pressure differentials due to laminar flows through the connecting pipes are obtained from equations (6.42) and (6.43), respectively, as:

$$p_{2\ell 1r} = \frac{128 \mu L}{\pi D^4} Q_{2\ell 1r} \tag{6.61}$$

$$p_{2r1\ell} = \frac{128 \mu L}{\pi D^4} Q_{2r1\ell} \tag{6.62}$$

where volume flow rates, $Q_{2\ell 1r}$ and $Q_{2r1\ell}$, derived from equations (6.48) and (6.46), and (6.47) and (6.45), respectively, are expressed as:

$$Q_{2\ell 1r} = - (A_{cr} - A_{rr}) \dot{z}_r(t) \tag{6.63}$$

$$Q_{2r1\ell} = - (A_{c\ell} - A_{r\ell}) \dot{z}_\ell(t) \tag{6.64}$$

Instantaneous gas pressures in the accumulators are established, assuming polytropic processes. For the left and right accumulators, the pressures in chamber III_ℓ and III_r are expressed as follows:

$$p_{3\ell} = p_{3\ell 0} \left(\frac{V_{0\ell}}{V_{3\ell}} \right)^\gamma \tag{6.65}$$

$$p_{3r} = p_{3r0} \left(\frac{V_{0r}}{V_{3r}} \right)^\gamma \tag{6.66}$$

where,

$p_{3\ell}$, p_{3r} = instantaneous pressures in chambers III_ℓ and III_r, respectively (Pa)

$p_{3\ell 0}$, p_{3r0} = static pressures in chambers III_ℓ and III_r, respectively (Pa)

$V_{0\ell}$, V_{0r} = static gas volumes in chambers III_ℓ and III_r, respectively (Pa)

$V_{3\ell}$, V_{3r} = instantaneous gas volumes in chamber III_ℓ and III_r, respectively (m^3), given by:

$$V_{3\ell} = V_{0\ell} - V_{23\ell} \tag{6.67}$$

$$V_{3r} = V_{0r} - V_{23r} \tag{6.68}$$

where volumes, $V_{23\ell}$ and V_{23r}, are defined using equations (6.53) and (6.55), and (6.54) and (6.56), respectively:

$$\frac{dV_{23\ell}}{dt} = Q_{23\ell} \; ; \qquad \frac{dV_{23r}}{dt} = Q_{23r} \tag{6.69}$$

From equations (6.65) to (6.68) the instantaneous pressures in Chambers III_ℓ and III_r are expressed as:

$$p_{3\ell} = \left(\frac{V_{0\ell}}{V_{0\ell} - V_{23\ell}} \right)^{\gamma} p_{3\ell 0} \tag{6.70}$$

$$p_{3r} = \left(\frac{V_{0r}}{V_{0r} - V_{23r}} \right)^{\gamma} p_{3r0} \tag{6.71}$$

The pressure differentials, $p_{30\ell}$ and p_{30r} are expressed in the following manner:

$$p_{30\ell} = \left(\frac{V_{0\ell}^{\gamma} - (V_{0\ell} - V_{23\ell})^{\gamma}}{(V_{0\ell} - V_{23\ell})^{\gamma}} \right) p_{3\ell 0} \tag{6.72}$$

$$p_{30r} = \left(\frac{V_{0r}^{\gamma} - (V_{0r} - V_{23r})^{\gamma}}{(V_{0r} - V_{23r})^{\gamma}} \right) p_{3r0} \tag{6.73}$$

The pressure differentials $p_{21\ell}$ and p_{21r}, needed for computing the dynamic forces, are defined, respectively, by:

$$p_{21\ell} = p_{20\ell} - p_{1\ell 0r} \tag{6.74}$$

$$p_{21r} = p_{20r} - p_{1r0\ell} \tag{6.75}$$

where,

$$p_{20\ell} = p_{2\ell} - p_{2\ell 0} \quad ; \quad p_{20r} = p_{2r} - p_{2r0}$$

$$p_{1\ell 0r} = p_{1\ell} - p_{2r0} \quad ; \quad p_{1r0\ell} = p_{1r} - p_{2\ell 0}$$

Since chambers I_ℓ and II_r, and I_r and II_ℓ, are connected through pipes, the desired pressure differentials can then be expressed in terms of the following already derived pressure differentials:

$$p_{21\ell} = p_{23\ell} + p_{30\ell} + p_{2r1\ell} - p_{23r} - p_{30r} \tag{6.76}$$

$$p_{21r} = p_{23r} + p_{30r} + p_{2\ell 1r} - p_{23\ell} - p_{30\ell} \tag{6.77}$$

6.4.4 Dynamic Forces of Interconnected Suspension

The dynamic forces, generated by the interconnected hydro-pneumatic suspension, are established by considering the pressures acting upon the pistons, with respect to the static equilibrium position. The respective total dynamic forces of the left and right suspension units are given by:

$$f_{ds\ell} = (p_{2\ell} - p_{2\ell 0})A_{c\ell} - (p_{1\ell} - p_{1\ell 0})(A_{c\ell} - A_{r\ell}) \tag{6.78}$$

$$f_{dsr} = (p_{2r} - p_{2r0})A_{cr} - (p_{1r} - p_{1r0})(A_{cr} - A_{rr}) \tag{6.79}$$

where,

$f_{ds\ell}$ = total dynamic force of left suspension unit (N)

f_{dsr} = total dynamic force of right suspension unit (N)

The total dynamic forces can be expressed in terms of pressure differentials, using simple manipulation:

$$f_{ds\ell} = p_{21\ell}\,(A_{c\ell} - A_{r\ell}) + p_{23\ell}\,A_{r\ell} + p_{30\ell}A_{r\ell} \tag{6.80}$$

$$f_{dsr} = p_{21r} (A_{cr} - A_{rr}) + p_{23r} A_{rr} + p_{30r} A_{rr} \tag{6.81}$$

Substituting equations (6.76) and (6.77) into above equations yields:

$$f_{dsl} = (p_{23l} + p_{30l}) A_{cl} + p_{2r1l}(A_{cl} - A_{rl}) - (p_{23r} + p_{30r}) (A_{cl} - A_{rl}) \tag{6.82}$$

$$f_{dsr} = (p_{23r} + p_{30r}) A_{cr} + p_{2l1r}(A_{cr} - A_{rr}) - (p_{23l} + p_{30l}) (A_{cr} - A_{rr}) \tag{6.83}$$

where pressure differentials p_{23l}, p_{23r}, p_{2l1r}, p_{2r1l}, p_{30l} and p_{30r} are given in equations (6.57), (6.58), (6.61), (6.62), (6.72) and (6.73), respectively. Equations (6.82) and (6.83) reveal that the connecting pipes between two cylinders produce fluid feedback effects within the interconnected suspension. The total dynamic force generated by one suspension unit consists of the following three components:

(i) Damping and restoring forces due to flows within the same suspension unit:

$(p_{23l} + p_{30l}) A_{cl}$ —— left suspension unit

$(p_{23r} + p_{30r}) A_{cr}$ —— right suspension unit

(ii) Damping forces due to flow through the pipes connecting the two suspension units:

$p_{2r1l}(A_{cl} - A_{rl})$ —— left suspension unit

$p_{2l1r}(A_{cr} - A_{rr})$ —— right suspension unit

(iii) Negative feedback damping and restoring forces due to flows within the other suspension unit:

$- (p_{23r} + p_{30r}) (A_{cl} - A_{rl})$ —— left suspension unit

$- (p_{23l} + p_{30l}) (A_{cr} - A_{rr})$ —— right suspension unit

The equations of motion of the roll plane model of the vehicle

employing interconnected hydro-pneumatic suspension are then obtained by substituting the following into equations (6.1) to (6.4):

$$f_{k\ell}(z,\ t) + f_{d\ell}(\dot{z},\ t) = f_{d\ell}(z,\ \dot{z},\ t) \tag{6.84}$$

$$f_{kr}(z,\ t) + f_{dr}(\dot{z},\ t) = f_{dr}(z,\ \dot{z},\ t) \tag{6.85}$$

6.5 Modeling of Tunable Interconnected Hydro-pneumatic Suspension

The damping forces in an interconnected vehicle suspension, presented in section 6.4, are primarily generated due to fluid flows through fixed area orifices and interconnecting pipes. The damping force due to fixed area orifices deteriorates vibration isolation performance at excitation frequencies beyond the sprung mass resonant frequencies. Shock and vibration isolation performance of mechanical systems with variable damping characteristics can be improved considerably, as discussed in chapters 3 and 4. Vibration isolation and thus ride performance of interconnected vehicle suspension can be further improved via variable damping. Variable damping in an interconnected suspension can be conveniently achieved by introducing pressure limiting valves between the strut and the accumulator of each suspension unit. Such an interconnected vehicle suspension can thus offer tunable damping characteristics to improve ride performance potentials of the vehicle, while the suspension continues to provide good handling and control characteristics of the vehicle due to the interconnections.

A tunable pressure limiting mechanism is introduced between the strut and accumulator of each suspension unit to achieve variable damping characteristics. The roll plane model of an interconnected vehicle suspension is presented in Figure 6.5. The fluid flows through

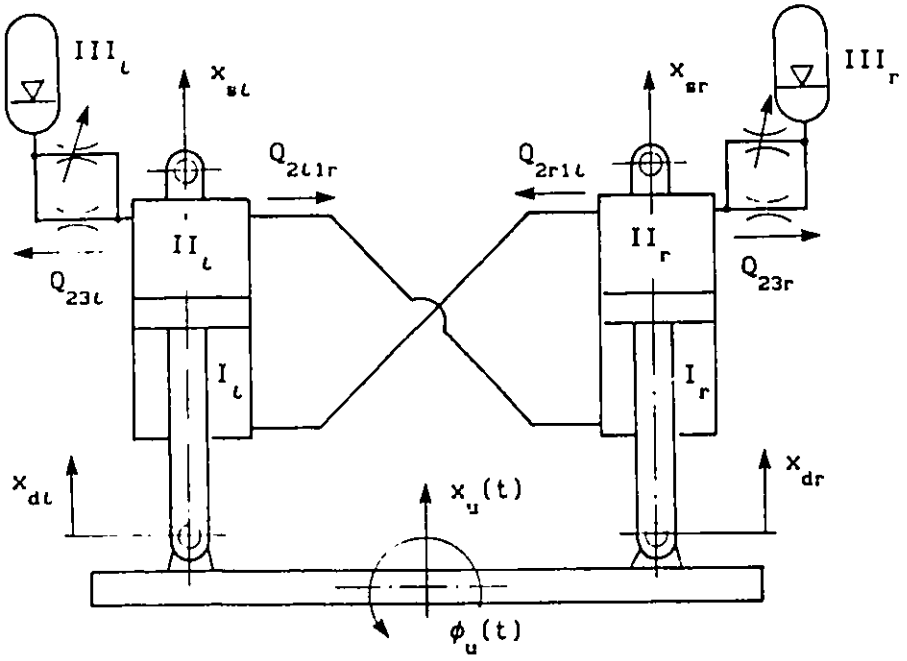

(a) Tunable interconnected suspension

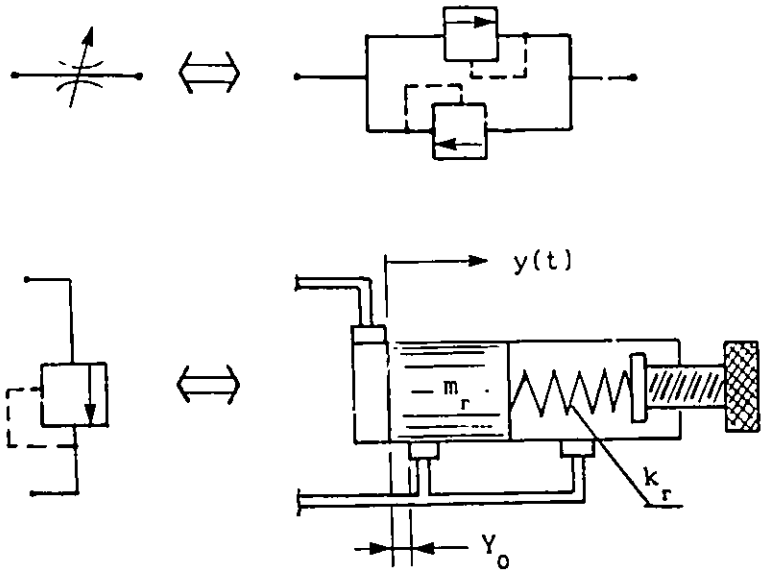

(b) Pressure relief valve

FIGURE 6.5 Schematic of roll plane model of tunable interconnected hydro-pneumatic suspension

the orifices between chambers II_ℓ and III_ℓ, and II_r and III_r, are modulated by a pressure limiting mechanism to achieve tunable passive sequential damping in an interconnected suspension. The tunable interconnected vehicle suspension is modeled incorporating hydraulic and mechanical compliance, and t' dynamics associated with pressure limiting relief valves. While the simulation parameters of the tunable interconnected suspension are identical to those listed in Table 6.3, parameters related to the pressure relief valves and fluid compliance are presented in Table 6.4.

The static equilibrium equations of the tunable interconnected suspension have the same form as that of the interconnected hydro-pneumatic suspension, equations (6.30) to (6.39) in section 6.4.1.

6.5.1 Fluid Flow Equations

Since the tunable relief valves provide additional flow passages between the strut and the accumulator of each hydro-pneumatic suspension unit, the fluid flows between chambers II_ℓ and III_ℓ, and II_r and III_r, consist of not only the flows through the fixed orifices but also the flows through the tunable relief valves. The respective volume flow rates in left and right suspension units are, therefore, expressed as:

$$Q_{23\ell} = Q_{or\ell} + Q_{re\ell} \tag{6.86}$$

$$Q_{23r} = Q_{orr} + Q_{rer} \tag{6.87}$$

where,

$Q_{23\ell}$, Q_{23r} = total volume flow rates from chambers II_ℓ to III_ℓ, and II_r to III_r, respectively (m^3/s)

$Q_{or\ell}$, Q_{orr} = volume flow rates through fixed orifices in left and right suspension units, respectively (m^3/s)

TABLE 6.4

Simulation Parameters of Tunable Interconnected Hydro-pneumatic Suspension

SYMBOL	DESCRIPTION	PARAMETER VALUE
β_e	Effective bulk modulus	6.9×10^{8} Pa
ρ	Mass density of fluid	797 kg/m^3
μ	Absolute viscosity of fluid	0.006 N·s/m^2
a_{rl}, a_{rr}	Spool end areas	5.5×10^{-4}, 5.5×10^{-4} m^2
m_{rl}, m_{rr}	Masses of valve spools	0.05, 0.05 kg
k_{rl}, k_{rr}	Stiffness coefficients of valves	3000, 3000 N/m
c_{rl}, c_{rr}	Viscous damping coefficients	9.7, 9.7 N·s/m
V_{ro1l}, V_{ro2l}	Equivalent volumes due to pipes	5×10^{-5}, 5×10^{-5} m^3
V_{ro1r}, V_{ro2r}	Equivalent volumes due to pipes	5×10^{-5}, 5×10^{-5} m^3
ℓ_{1l}, ℓ_{1r}	Strokes of chambers I	0.25, 0.25 m
ℓ_{2l}, ℓ_{2r}	Strokes of chambers II	0.25, 0.25 m

Q_{rel}, Q_{rer} = volume flow rates through relief valves in left and right suspension units, respectively (m^3/s)

Assuming turbulent flow through the orifices, volume flow rates Q_{23l} and Q_{23r} are expressed as:

$$Q_{orl} = C_{dl} a_{2l} \sqrt{\frac{2|p_{23l}|}{\rho}} \; sgn(p_{23l}) \tag{6.88}$$

$$Q_{orr} = C_{dr} a_{2r} \sqrt{\frac{2|p_{23r}|}{\rho}} \; sgn(p_{23r}) \tag{6.89}$$

where a_{2l} and a_{2r} are areas of orifices in left and right orifice suspension units, respectively. Assuming turbulent flows through valve openings, volume flow rates due to spool movements and valve openings, Q_{rel} and Q_{rer} are expressed as:

$$Q_{rel} = \begin{cases} 2\, a_{rl}\, \dot{y}_l(t) & , \; |y_l| \le Y_{0l} \\ C_d\, a_{el}(y_l, Y_{0l}) \sqrt{\frac{2|p_{23l}|}{\rho}} \; sgn(p_{23l}) + 2\, a_{rl} \dot{y}_l & , \; |y_l| > Y_{0l} \end{cases} \tag{6.90}$$

$$Q_{rer} = \begin{cases} 2\, a_{rr}\, \dot{y}_r(t) & , \; |y_r| \le Y_{0r} \\ C_d\, a_{er}(y_r, Y_{0r}) \sqrt{\frac{2|p_{23r}|}{\rho}} \; sgn(p_{23r}) + 2\, a_{rr} \dot{y}_r & , \; |y_r| > Y_{0r} \end{cases} \tag{6.91}$$

where,

y_l, y_r = displacements of spools in left and right suspension units, respectively (m)

Y_{0l}, Y_{0r} = preset displacements of relief valves (m)

a_{rl}, a_{rr} = spool end areas of relief valves (m^2)

a_{el}, a_{er} = opening areas of relief valves.

The opening area of a relief valve is a function of the spool's

displacement and preset position, as discussed earlier in section 3.2.2.

The flows through the connecting pipes between the two cylinders are assumed to be laminar flows and expressed as:

$$Q_{2\ell 1r} = \frac{\pi D^4}{128 \mu L} p_{2\ell 1r} \tag{6.92}$$

$$Q_{2r1\ell} = \frac{\pi D^4}{128 \mu L} p_{2r1\ell} \tag{6.93}$$

Rates of change of fluid volumes in chamber I of the left and right suspension units, $Q_{m1\ell}$ and Q_{m1r}, are related to their relative velocities of the struts, respectively, given by:

$$Q_{m1\ell} = (A_{c\ell} - A_{r\ell}) \dot{z}_\ell(t) \tag{6.94}$$

$$Q_{m1r} = (A_{cr} - A_{rr}) \dot{z}_r(t) \tag{6.95}$$

The rates of change of volume due to fluid compressibility and mechanical compliance of the cylinder, in chamber I of left and right suspension units, respectively, are expressed as:

$$Q_{e1\ell} = \frac{V_{1\ell}}{\beta_e} \frac{dp_{1\ell}}{dt} \tag{6.96}$$

$$Q_{e1r} = \frac{V_{1r}}{\beta_e} \frac{dp_{1r}}{dt} \tag{6.97}$$

where,

$Q_{e1\ell}$, Q_{e1r} = rates of change of volumes due to compliance in chambers I_ℓ and I_r, respectively (m^3/s)

$p_{1\ell}$, p_{1r} = instantaneous pressures in chambers I_ℓ and I_r (Pa)

β_e = effective bulk modulus (Pa), given by:

$$\frac{1}{\beta_e} = \frac{1}{\beta_c} + \frac{1}{\beta_\ell} \tag{6.98}$$

β_c = bulk modulus of strut chamber (Pa)

β_ℓ = bulk modulus of liquid fluid (Pa)

$V_{1\ell}$, V_{1r} = instantaneous volumes of chambers I_ℓ and I_r, respectively (m^3), given by:

$$V_{1\ell} = [\ell_{1\ell} + X_{st\ell} - z_\ell(t)]\ (A_{c\ell} - A_{r\ell}) + V_{r01\ell} \tag{6.99}$$

$$V_{1r} = [\ell_{1r} + X_{str} - z_r(t)]\ (A_{cr} - A_{rr}) + V_{r01r} \tag{6.100}$$

$\ell_{1\ell}$, ℓ_{1r} = strokes of chambers I_r and I_ℓ (m)

$V_{r01\ell}$, V_{r01r} = equivalent volumes due to connection pipes (m^3)

Applying the law of conservation of mass, the fluid flows in chambers I_ℓ and I_r are related by the fluid continuity equation, respectively:

$$Q_{2r1\ell} = - Q_{m1\ell} + Q_{e1\ell} \tag{6.101}$$

$$Q_{2\ell 1r} = - Q_{m1r} + Q_{e1r} \tag{6.102}$$

where $Q_{2r1\ell}$, $Q_{m1\ell}$ and $Q_{e1\ell}$ are expressed in equations (6.93), (6.94) and (6.96), and $Q_{2\ell 1r}$, Q_{m1r} and Q_{e1r} in (6.92), (6.95) and (6.97), respectively.

Rates of change of the fluid volume in chamber II of the left and right suspension units, $Q_{m2\ell}$ and Q_{m2r}, related to their piston movements, respectively, are expressed as:

$$Q_{m2\ell} = A_{c\ell}\ \dot{z}_\ell(t) \tag{6.103}$$

$$Q_{m2r} = A_{cr}\ \dot{z}_r(t) \tag{6.104}$$

The rates of change of volumes due to the effective bulk modulus, in chamber II of the left and right suspension units, respectively, are

derived for fluid and mechanical compliance and expressed as:

$$Q_{e2\ell} = \frac{V_{2\ell}}{\beta_e} \frac{dp_{2\ell}}{dt} \tag{6.105}$$

$$Q_{e2r} = \frac{V_{2r}}{\beta_e} \frac{dp_{2r}}{dt} \tag{6.106}$$

$Q_{e2\ell}$, Q_{e2r} = rates of change of volumes due to compliance in chamber II of left and right suspension units (m^3/s)

$p_{2\ell}$, p_{2r} = instantaneous pressures in chambers II_ℓ and II_r (Pa)

$V_{2\ell}$, V_{2r} = instantaneous volumes of chambers II_ℓ and II_r, respectively (m^3), given by:

$$V_{2\ell} = [\ell_{2\ell} - X_{st\ell} + z_\ell(t)]\ A_{c\ell} + V_{r02\ell} - 2\ a_{r\ell}\ y_\ell \tag{6.107}$$

$$V_{2r} = [\ell_{2r} - X_{str} + z_r(t)]\ A_{cr} + V_{r02r} - 2\ a_{rr}\ y_r \tag{6.108}$$

$\ell_{2\ell}$, ℓ_{2r} = strokes of chambers II_ℓ and II_r (m)

$V_{r02\ell}$, V_{r02r} = equivalent volumes due to connection pipes (m^3)

The fluid continuity in chambers II_ℓ and II_r establishes the following flows equations as:

$$-Q_{or\ell} - Q_{re\ell} - Q_{2\ell 1r} = Q_{m2\ell} + Q_{e2\ell} \tag{6.109}$$

$$-Q_{orr} - Q_{rer} - Q_{2r1\ell} = Q_{m2r} + Q_{e2r} \tag{6.110}$$

where $Q_{or\ell}$, $Q_{re\ell}$, $Q_{2\ell 1r}$, $Q_{m2\ell}$ and $Q_{e2\ell}$ are expressed in equations (6.88), (6.90), (6.92), (6.103) and (6.105), and Q_{orr}, Q_{rer}, $Q_{2r1\ell}$, Q_{m2r} and Q_{e2r} are given in equations (6.89), (6.91), (6.93), (6.104) and (6.106), respectively.

Rates of change of gas volumes in chamber III of the left and right suspension units, $Q_{m3\ell}$ and Q_{m3r}, respectively, are expressed as:

$$Q_{m3\ell} = \frac{dV_{3\ell}}{dt} \tag{6.111}$$

$$Q_{m3r} = \frac{dV_{3r}}{dt} \tag{6.112}$$

$V_{3\ell}$, $V_{3\ell}$ = instantaneous gas volumes in chambers III_ℓ and III_r (m^3)

The flow equations in Chambers III_ℓ and III_r are expressed as:

$$Q_{or\ell} + Q_{re\ell} = - Q_{m3\ell} \tag{6.113}$$

$$Q_{orr} + Q_{rer} = - Q_{m3r} \tag{6.114}$$

where $Q_{or\ell}$, $Q_{re\ell}$ and $Q_{m3\ell}$ are expressed in (6.88), (6.90) and (6.111), and Q_{orr}, Q_{rer} and Q_{m3r} are given in (6.89), (6.91) and (6.112), respectively.

6.5.2 Pressure Equations

The rate of change of fluid pressure is related to the compressibility of the fluid volume and is derived from the fluid continuity equation. The pressure change rates in chamber I of the left and right suspension units are then obtained from equations (6.96) and (6.101), and (6.97) and (6.102), respectively:

$$\frac{dp_{1\ell}}{dt} = \frac{\beta_e}{V_{1\ell}} (Q_{2r1\ell} + Q_{m1\ell}) \tag{6.115}$$

$$\frac{dp_{1r}}{dt} = \frac{\beta_e}{V_{1r}} (Q_{2\ell 1r} + Q_{m1r}) \tag{6.116}$$

where $Q_{2\ell 1r}$ and Q_{m1r} are expressed in equations (6.92) and (6.95), and $Q_{2r1\ell}$ and $Q_{m1\ell}$ are given in equations (6.93) and (6.94), respectively.

Pressure change rates in chamber II of the left and right suspension units, established from equations (6.105) and (6.109), and (6.106) and (6.110), respectively, are expressed as:

$$\frac{dp_{2\ell}}{dt} = -\frac{\beta_e}{V_{2\ell}} (Q_{or\ell} + Q_{re\ell} + Q_{2\ell 1r} + Q_{m2\ell}) \tag{6.117}$$

$$\frac{dp_{2r}}{dt} = -\frac{\beta_e}{V_{2r}} (Q_{orr} + Q_{rer} + Q_{2r1\ell} + Q_{m2r}) \tag{6.118}$$

where $Q_{or\ell}$, $Q_{re\ell}$, $Q_{2\ell 1r}$ and $Q_{m2\ell}$ are expressed in equations (6.88), (6.90), (6.92) and (6.103), and Q_{orr}, Q_{rer}, $Q_{2r1\ell}$ and Q_{m2r} are given in equations (6.89), (6.91), (6.93) and (6.104), respectively.

Assuming a polytropic process, the instantaneous pressures in gas chamber III of the left and right suspension units are, respectively, expressed as:

$$p_{3\ell} = \left(\frac{V_{0\ell}}{V_{0\ell} - V_{23\ell}} \right)^{\gamma} p_{3\ell 0} \tag{6.119}$$

$$p_{3r} = \left(\frac{V_{0r}}{V_{0r} - V_{23r}} \right)^{\gamma} p_{3r0} \tag{6.120}$$

where $V_{23\ell}$ and V_{23r}, the gas change volumes due to flows from Chambers II to III of the left and right units, respectively, are expressed as:

$$\frac{dV_{23\ell}}{dt} = Q_{or\ell} + Q_{re\ell} \tag{6.121}$$

$$\frac{dV_{23r}}{dt} = Q_{orr} + Q_{rer} \tag{6.122}$$

where $Q_{or\ell}$ and $Q_{re\ell}$ are expressed in equations (6.88) and (6.90), and Q_{orr} and Q_{rer} in (6.89) and (6.91), respectively.

The pressure differentials, $p_{30\ell}$ and p_{30r}, are expressed as:

$$p_{30\ell} = \left(\frac{V_{0\ell}^{\gamma} - (V_{0\ell} - V_{23\ell})^{\gamma}}{(V_{0\ell} - V_{23\ell})^{\gamma}} \right) p_{3\ell 0} \tag{6.123}$$

$$p_{30r} = \left(\frac{V_{0r}^{\gamma} - (V_{0r} - V_{23r})^{\gamma}}{(V_{0r} - V_{23r})^{\gamma}} \right) p_{3r0} \qquad (6.124)$$

6.5.3 Dynamic Forces of Tunable Interconnected Suspension

The dynamic forces of suspension units in the modified interconnected configuration are established from the pressures equations presented in section 6.5.2. The total dynamic forces of both suspension units, derived by considering various pressures acting on the pistons, can be expressed as:

$$f_{dsl} = (p_{2l} - p_{1l})\ (A_{cl} - A_{rl}) + (p_{2l} - p_{3l})\ A_{rl} + p_{3l}\ A_{rl} \qquad (6.125)$$

$$f_{dsr} = (p_{2r} - p_{1r})\ (A_{cr} - A_{rr}) + (p_{2r} - p_{3r})\ A_{rr} + p_{3r}\ A_{rr} \qquad (6.126)$$

where,

f_{dsl} = total dynamic force of left suspension unit (N)

f_{dsr} = total dynamic force of right suspension unit (N)

The instantaneous pressures, p_{1l}, p_{2l}, p_{3l}, p_{1r}, p_{2r} and p_{3r}, are computed from equations (6.115) to (6.120), respectively.

The equations of motion of the roll plane model of the vehicle, employing tunable interconnected hydro-pneumatic suspension can be obtained by substituting the following into equations (6.1) to (6.4):

$$f_{kl}(z,\ t) + f_{dl}(\dot{z},\ t) = f_{dsl}(t) \qquad (6.127)$$

$$f_{kr}(z,\ t) + f_{dr}(\dot{z},\ t) = f_{dsr}(t) \qquad (6.128)$$

6.5.4 Equations of Motion of Valve Spools

The spool in a tunable relief valve is subjected to forces due to the pressure differential between the strut and accumulator. Assuming viscous damping, the equations of motion of the spools within the left

and right suspension units are expressed as:

$$m_{r\ell}\,\ddot{y}_{\ell}(t) + c_{r\ell}\,\dot{y}_{\ell}(t) + k_{r\ell}\,y_{\ell}(t) = f_{r\ell}(t) \qquad (6.129)$$

$$m_{rr}\,\ddot{y}_{r}(t) + c_{rr}\,\dot{y}_{r}(t) + k_{rr}\,y_{r}(t) = f_{rr}(t) \qquad (6.130)$$

where,

$m_{r\ell}$, m_{rr} = masses of spools of left and right valves (kg)

$c_{r\ell}$, c_{rr} = viscous damping coefficients of dynamic spool subsystems (N·s/m)

$k_{r\ell}$, k_{rr} = stiffness coefficients of valve springs (N/m)

$f_{r\ell}$, f_{rr} = forces acting on left and right spools, respectively, given by:

$$f_{r\ell} = a_{r\ell}\,p_{23\ell} \qquad (6.131)$$

$$f_{rr} = a_{rr}\,p_{23r} \qquad (6.132)$$

The system of nonlinear differential equations of the roll plane model of the vehicle employing independent, interconnected and tunable interconnected suspensions, developed in sections 6.2 to 6.5, is solved using the numerical integration technique. Roll response characteristics and ride performance of the roll plane model of the vehicle employing the various types of suspensions are analyzed via computer simulation. The roll response characteristics of the vehicle model are evaluated in terms of the roll response of the sprung mass during a steady turning maneuver. The ride performance is illustrated in terms of the shock and vibration isolation characteristics of the roll plane vehicle model subject to road excitations. The influences of effective bulk modulus and the dynamics of pressure limiting mechanism on the dynamic ride performance of a vehicle employing the tunable interconnected suspension are also discussed.

6.6 Analysis of Vehicle Roll During Steady Turning

The roll response characteristics of a vehicle, employing independent, interconnected and tunable interconnected suspensions are evaluated via computer simulation of the roll plane vehicle model. The static roll stability of the three suspension models are evaluated in terms of the roll response of the sprung mass to an external roll moment caused by centrifugal forces during a steady turning maneuver.

6.6.1 External Roll Moments

The sprung mass of a vehicle experiences roll angle and centrifugal acceleration during steady turning. Centrifugal acceleration gives rise to an overturning moment, while the sprung mass roll yields a roll moment due to lateral displacement of the sprung mass, as shown in Figure 6.6. Thus the total external roll moment, acting on a vehicle during steady turning, can be expressed as:

$$T_{s\phi}(t) = T_{p\phi}(t) + T_{\iota\phi}(t) \tag{6.133}$$

where $T_{s\phi}$ is the total roll moment acting on the vehicle, presented in equation (6.2), $T_{p\phi}$ is the primary overturning moment due to lateral acceleration and $T_{\iota\phi}$ is the roll moment due to lateral displacement of the sprung mass.

Assuming constant forward vehicle speed and turn radius, the centrifugal force due to lateral acceleration of the vehicle, encountered during steady turning maneuver can be expressed as:

$$f_c(t) = a_\iota(t)\, m_1 \tag{6.134}$$

where f_c is the centrifugal force, and $a_\iota = v^2 / R$ is the vehicle lateral

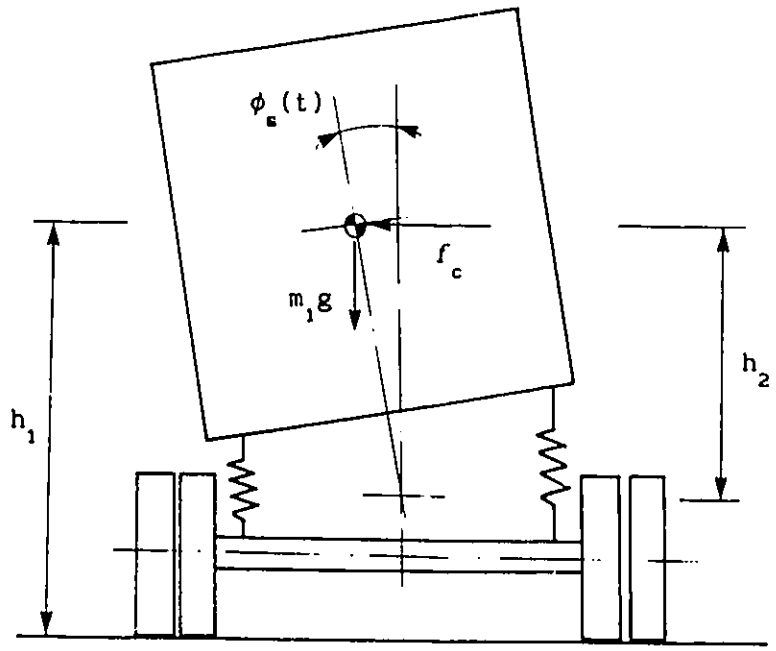

FIGURE 6.6 External roll moments acting upon sprung mass

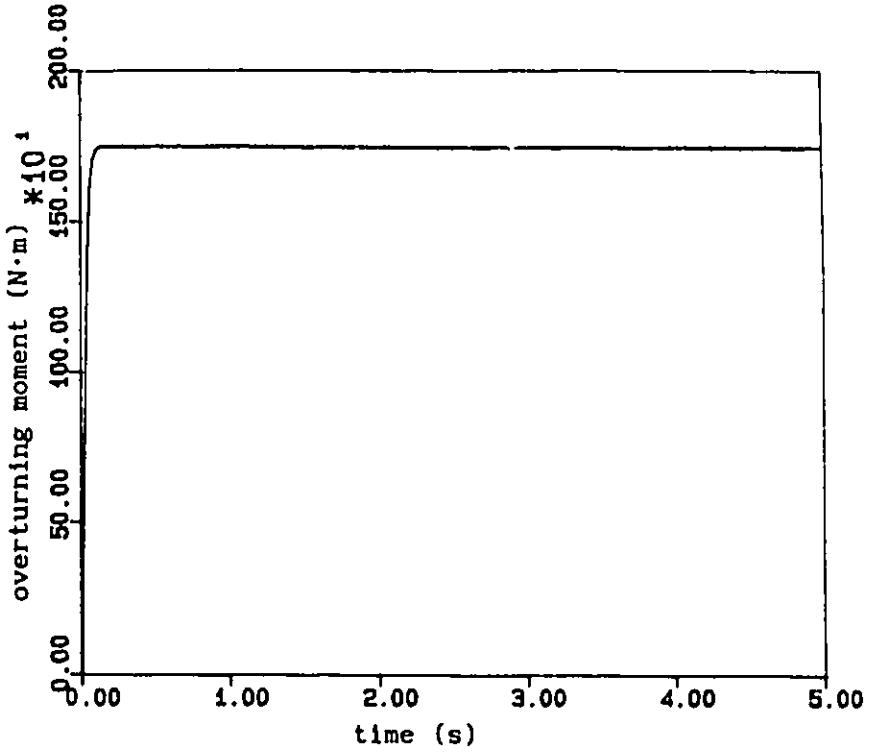

FIGURE 6.7 A rounded step overturning moment acting on vehicles during steady turning

acceleration encountered during negotiating a turn of constant radius R at a constant forward speed v. Assuming small roll angles, roll moments caused by lateral acceleration and lateral displacement of the sprung mass can be expressed as:

$$T_{p\phi}(t) = m_1 \, a_\ell \, h_2 \tag{6.135}$$

$$T_{\ell\phi}(t) = m_1 \, g \, h_2 \, \phi_s(t) \tag{6.136}$$

where g is the acceleration of gravity and h_2 is the height of the sprung mass center with respect to the roll center. Equation (6.136) clearly reveals that a large sprung mass roll response, caused by a soft vehicle suspension, will yield large roll moment due to the lateral displacement of sprung mass. The effective roll stiffness can be increased via a stiff suspension, so that the magnitude of the roll angle and lateral displacement moment can be reduced.

6.6.2 Roll Response of Vehicle Model

The roll angle response characteristics of the sprung mass of the vehicle, employing independent, interconnected and tunable interconnected hydro-pneumatic suspensions, are evaluated for constant lateral acceleration excitation. The primary overturning roll moment imposed on the vehicle is characterized by a rounded step with steep rise, as shown in Figure 6.7.

The roll angle response characteristics of the sprung mass of the vehicle employing independent and interconnected suspension, subject to constant lateral acceleration, $a_\ell = 0.5$ m/s^2, are illustrated in Figure 6.8. Independent vehicle suspension yields high amplitude roll response, as compared with that of the interconnected vehicle suspension. Roll

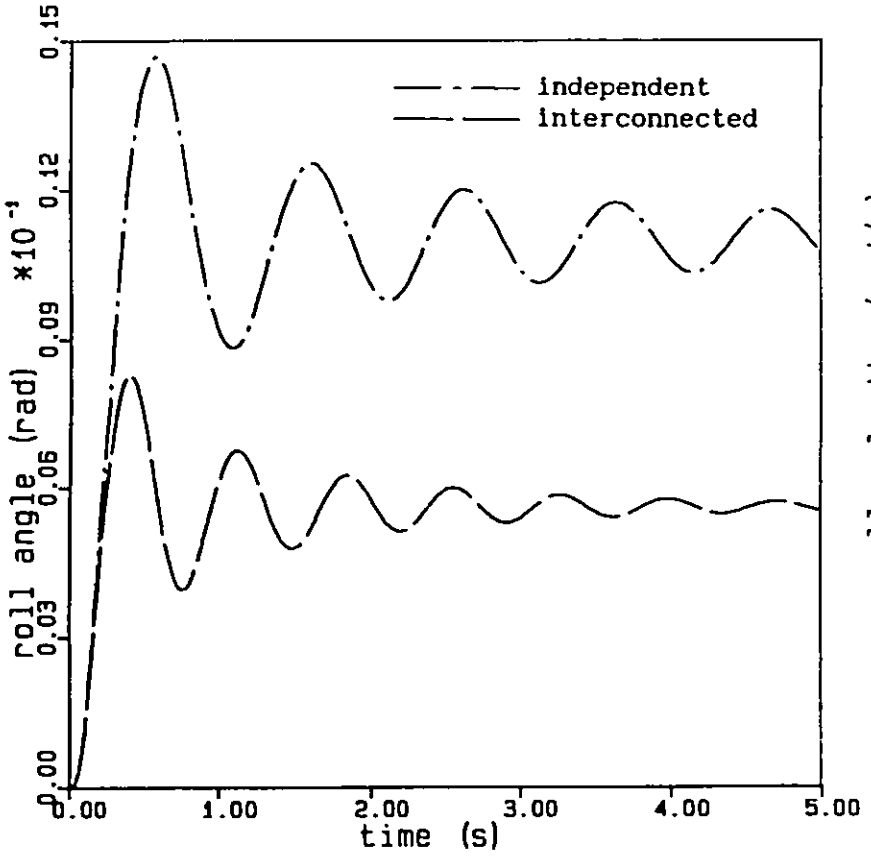

FIGURE 6.8 Transient roll angle response of sprung mass of vehicle employing independent and interconnected suspensions for a_t=0.5 m/s^2

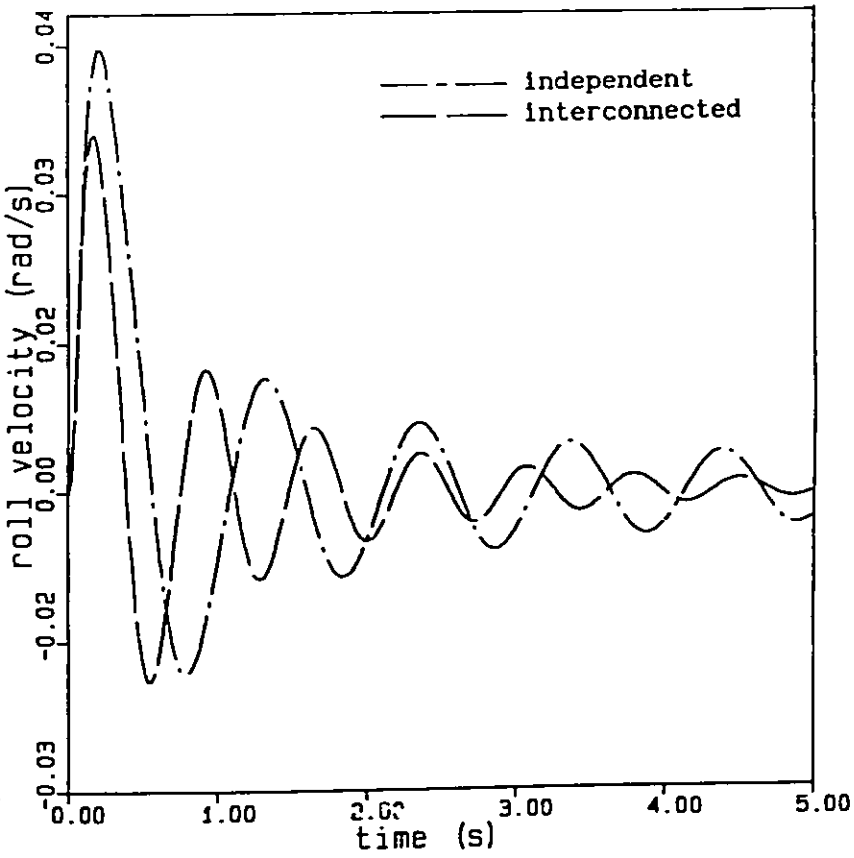

FIGURE 6.9 Transient roll angle velocity response of sprung mass of vehicle employing independent and interconnected suspensions for a_t=0.5 m/s^2

angular response of the sprung mass reveals oscillation occurring at 1.0 and 1.4 Hz, for independent and interconnected vehicle suspensions, respectively. Comparison of the oscillation frequencies clearly illustrates that interconnection between two suspension units increases the effective roll stiffness of the vehicle, and thus reduces the amplitude of roll oscillation. The roll angle of the sprung mass approaches steady value of 1.1×10^{-2} and 0.6×10^{-2} rad, respectively, for independent and interconnected suspensions. Comparison of these steady state values further demonstrates the increased effective roll stiffness and thus enhanced static roll stability of the interconnected suspension. The roll velocity response of sprung mass of the vehicle, illustrated in Figure 6.9, reveals that the sprung mass roll rate can be considerably reduced via an interconnected suspension. The roll velocity response of the sprung mass employing an interconnected suspension also clearly reveals a higher oscillation frequency and thus a higher roll stiffness than that of the independent suspension.

Figures 6.10 and 6.11 show the roll angle and roll velocity response characteristics of sprung mass, using interconnected and tunable interconnected suspensions, respectively. The vehicle is subjected to a constant lateral acceleration, $a_y = 1.0$ m/s^2. The results show that the tunable interconnected suspension yields a sprung mass roll response identical to that of interconnected suspension, when the tuning factor, $\nu > 0.35$. Figures 6.10 and 6.11 clearly reveal that variable damping achieved via tunable relief valves does not affect the roll response characteristics. The roll response of a vehicle with a tunable interconnected suspension tends to increase, when the tuning

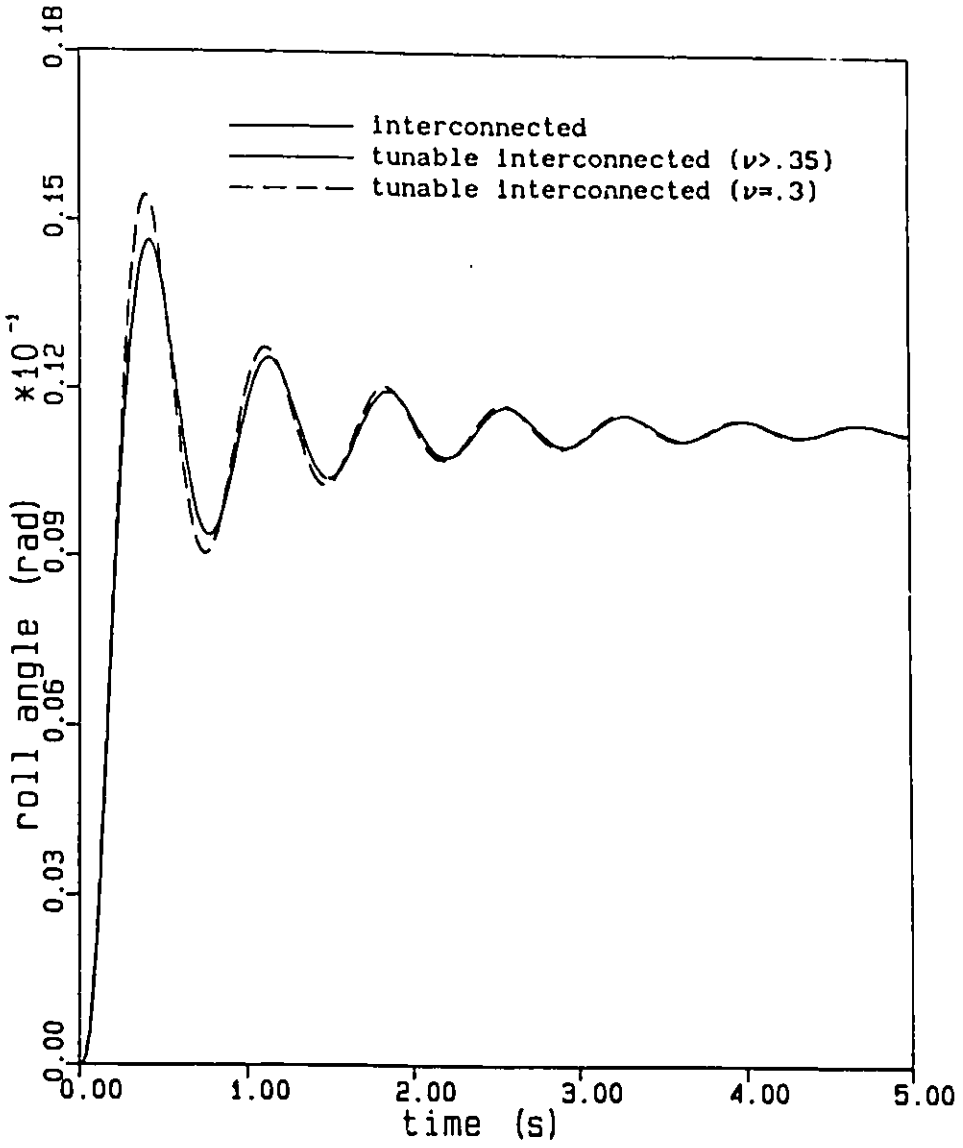

FIGURE 6.10 Transient roll angle response of sprung mass of vehicle employing interconnected and tunable interconnected (ν=0.3) suspensions for a_t=1.0 m/s^2

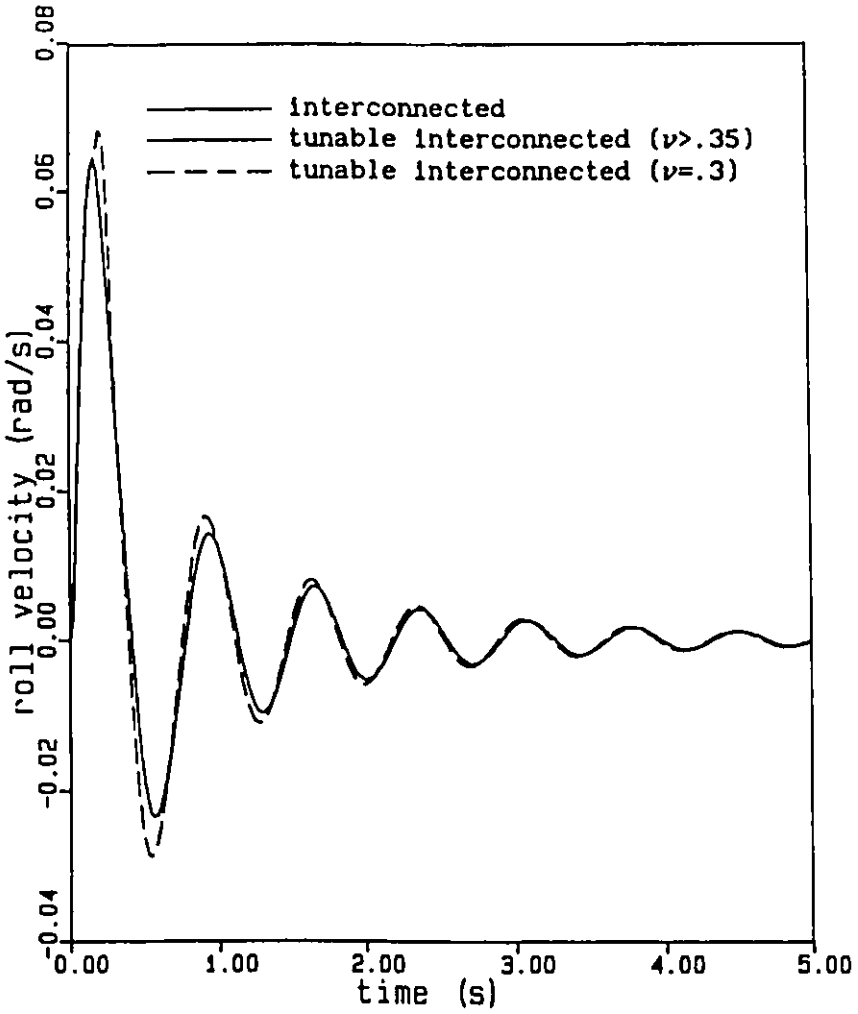

FIGURE 6.11 Transient roll angle velocity response of sprung mass of vehicle employing interconnected and tunable interconnected (ν=0.3) suspensions for a_t=1.0 m/s^2

factor is selected at a very low value ($\nu \leq 0.35$). The roll response of a vehicle employing a tunable interconnected suspension ($\nu = 0.3$) exhibits a slightly larger peak due to the extremely low preset tuning factor. However, the steady state value of roll response of vehicle employing tunable suspension is identical to that employing the simple interconnected suspension. The roll oscillation of both types of suspensions reveals almost identical frequencies, as shown in Figures 6.10 and 6.11. The static roll stability of the vehicle thus remains unaffected by the tunable pressure limiting valves.

A comparison of the roll response of a vehicle with three types of suspensions, for lateral acceleration excitation $a_t = 1.0$ m/s^2, is illustrated in Figure 6.12. The steady state values of sprung mass roll angle are obtained as 1.1×10^{-2} rad for the interconnected and tunable interconnected suspensions, and 2.55×10^{-2} rad for the independent vehicle suspension, respectively. It shows that the effective roll stiffness of both interconnected and tunable interconnected vehicle suspensions is much higher than that of the independent suspension. Furthermore the independent vehicle suspension yields excessive roll oscillation, as shown in Figure 6.12.

The roll angle response characteristics of the unsprung mass of the vehicle employing independent and interconnected suspensions are presented in Figure 6.13, for $a_t = 0.5$ m/s^2. The roll angle response of the unsprung mass is smaller than that of sprung mass due to high value of tire stiffness. It is clear that the peak roll angle response of the unsprung mass, with the independent suspension, is slightly less than that with the interconnected one. The roll angle response of the

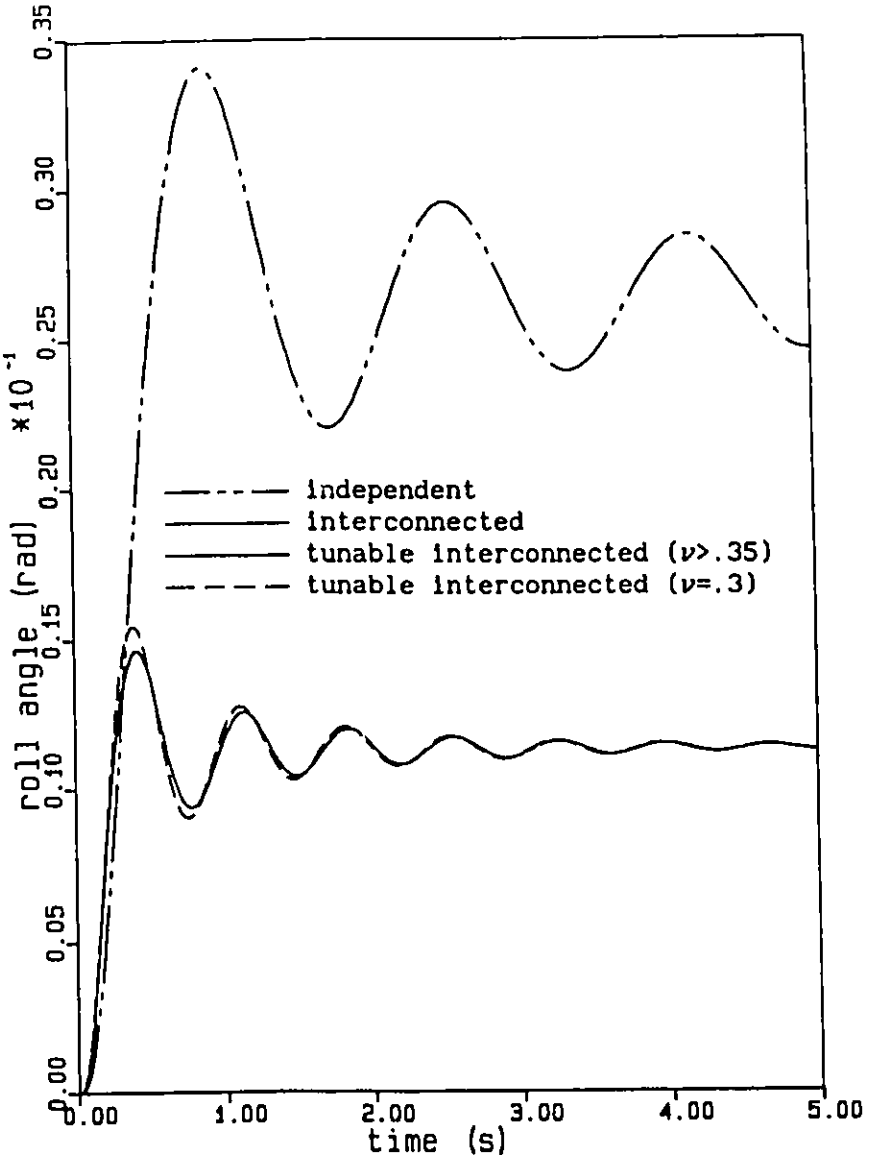

FIGURE 6.12 Transient roll angle response of sprung mass of vehicle employing independent, interconnected and tunable interconnected (ν=0.3) suspensions for a_t=1.0 m/s^2

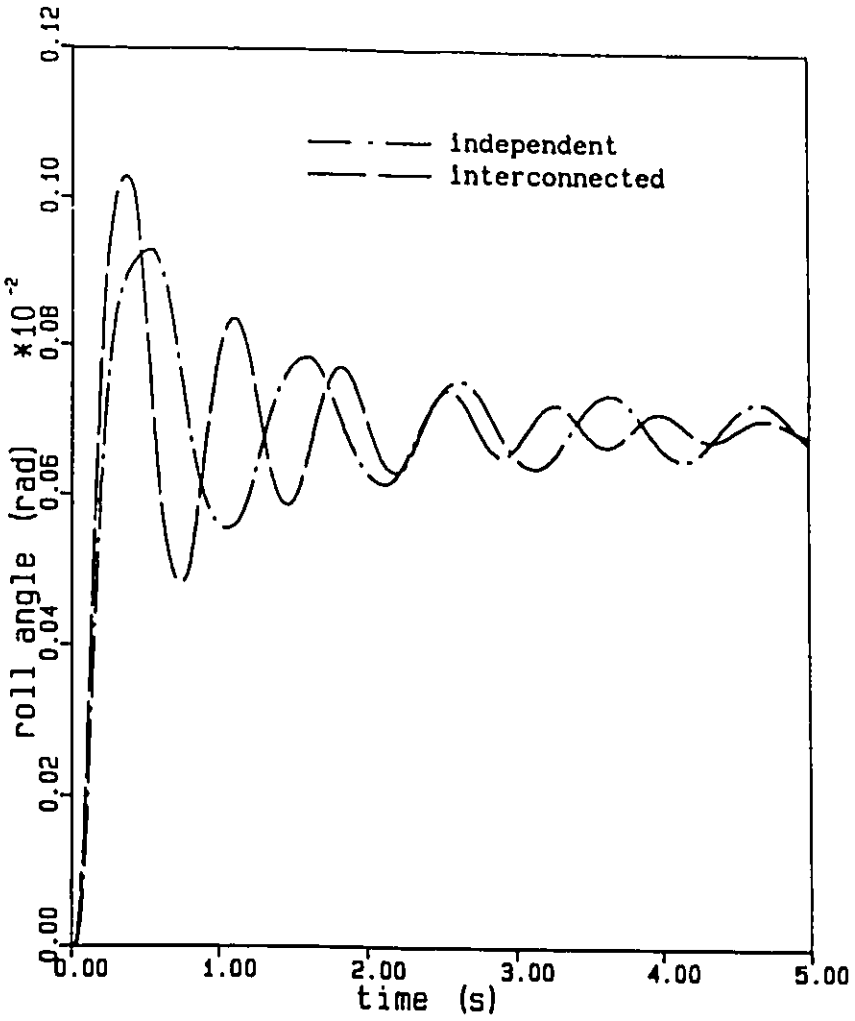

FIGURE 6.13 Transient roll angle response of unsprung mass of vehicle employing independent and interconnected suspensions for a_t=0.5 m/s^2

unsprung mass, however, approaches the identical steady state value for both independent and interconnected suspensions. It can be further observed that the amplitude of roll oscillation of the unsprung mass with interconnected suspension decays at a faster rate than that with the independent one. The frequencies of roll oscillation are 0.97 Hz and 1.37 Hz for the independent and interconnected ones, respectively.

Figure 6.14 presents the vertical displacement response of the sprung mass, caused by a lateral acceleration excitation (0.5 m/s^2). The amplitudes of vertical displacement oscillation of the sprung mass of a vehicle employing the independent suspension are considerably larger than that of the vehicle employing the interconnected one. The steady state displacement response of interconnected suspension approaches a considerable lower value than that of the independent one, due to the higher effective roll stiffness of the interconnected suspension. The displacement response oscillation of the vehicle's sprung mass employing the interconnected suspension exhibits a higher decay rate as compared with that of the vehicle employing the independent one. The vertical displacement response of the vehicle's sprung mass, employing the tunable interconnected suspension, is compared with that of the vehicle employing the interconnected suspension, as shown in Figure 6.15. Computer simulations, carried out for a lateral acceleration excitation, a_t= 1.0 m/s^2, reveal that the tunable interconnected suspension with a tuning factor ν>0.35 yields vertical displacement response characteristics identical to those of the interconnected suspension, as shown in Figure 6.15. A low value of tuning factor (ν=0.3), however, yields a large negative peak due to the sudden opening of the pressure

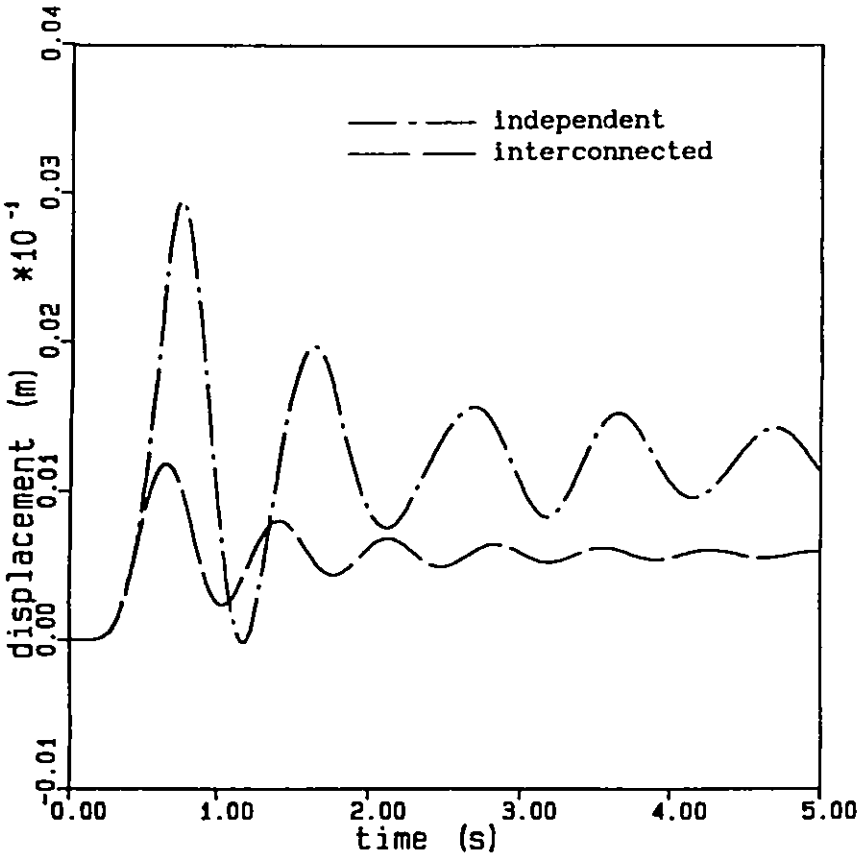

FIGURE 6.14 Transient displacement response of sprung mass of vehicle employing independent and interconnected suspensions for a_t=0.5 m/s^2

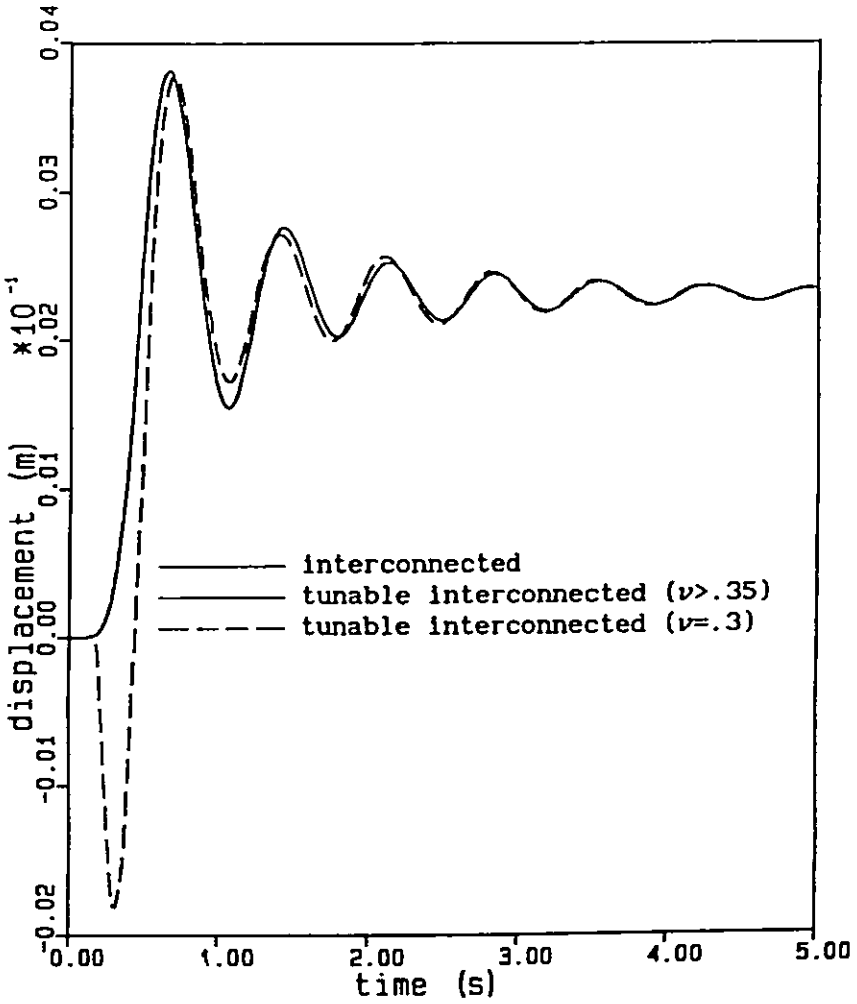

FIGURE 6.15 Transient displacement response of sprung mass of vehicle employing interconnected and tunable interconnected (ν=0.3) suspensions for a_t=1.0 m/s^2

relief valves corresponding to a relatively low value of the pressure differential between chambers II and III. The displacement characteristics, after the initial peak, however, are similar to the response behavior of the non-tunable and tunable (ν>0.35) interconnected suspensions, as illustrated in Figure 6.15. Identical steady state amplitude as well as frequency of oscillation of the sprung mass displacement response are obtained for both suspensions.

6.7 Dynamic Ride Performance Evaluation

Dynamic ride performance characteristics of the vehicle employing independent, interconnected and tunable interconnected hydro-pneumatic suspensions are analyzed via computer simulations for transient as well as harmonic excitation. The ride dynamics of three types of suspensions, evaluated in terms of their shock and vibration isolation characteristics, are compared to illustrate the ride performance potential of the tunable interconnected suspension. The effects of effective bulk modulus of the fluid and the dynamics of the relief valves on the shock and vibration isolation performance of the tunable interconnected suspension is also investigated and discussed.

6.7.1 Transient Response Characteristics

The ride performance characteristics of the vehicle model in the roll plane are investigated for a rounded step displacement excitation. The transient response characteristics are evaluated, assuming that only the right tire is subjected to a rounded step displacement excitation of amplitude, X_{ir}=0.025 m. Bounce and roll response characteristics of various suspensions can thus be evaluated. Figure 6.16 illustrates the vehicle model and corresponding rounded step displacement excitation

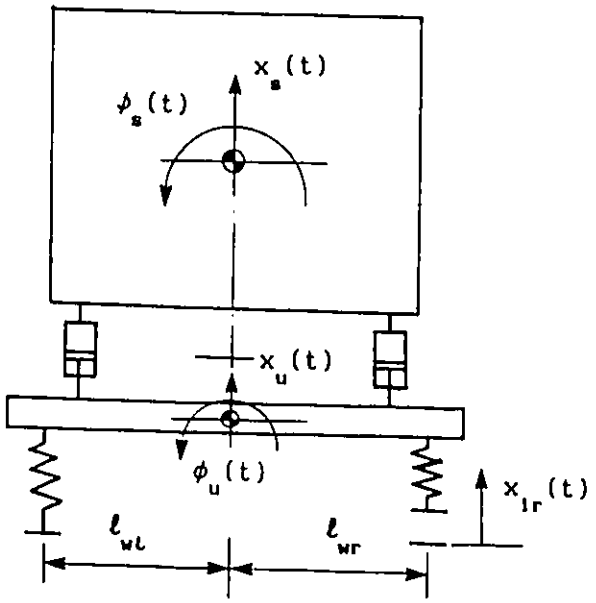

(a) Displacement road input to right tire

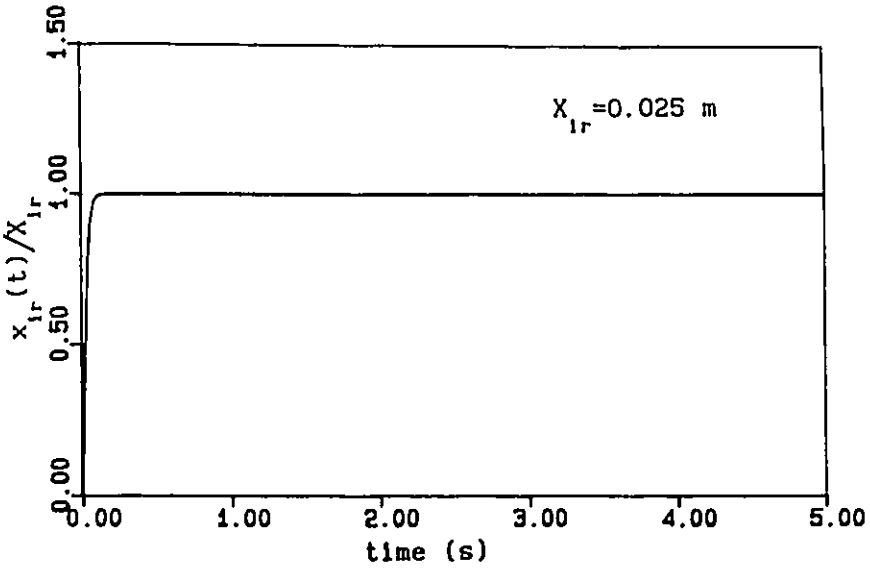

(b) A rounded step displacement input

FIGURE 6.16 Schematic of road input to roll plane model of a road vehicle

imposed at the right tires. The transient response variables of the vehicle employing various suspensions are non-dimensionalized with respect to the equivalent excitation amplitudes and their corresponding constants. The amplitude of equivalent roll excitation is computed as, assuming small roll angle:

$$\phi_{ie} = \frac{X_{ir}}{\ell_{wl} + \ell_{wr}} \tag{6.137}$$

where X_{ir} is the amplitude of step displacement excitation at the right tire-road interface, and Φ_{ie} is the amplitude of equivalent roll excitation. The corresponding vertical excitation at the center of the vehicle track is computed as:

$$X_{ie} = \frac{X_{ir}\ \ell_{wl}}{\ell_{wl} + \ell_{wr}} \tag{6.138}$$

where X_{ie} is the amplitude of vertical excitation at the center of the vehicle track. The shock isolation characteristics are thus expressed by the following response ratios:

displacement response ratio of sprung mass = $x_s(t)/X_{ie}$

velocity response ratio of sprung mass = $\dot{x}_s(t)/(X_{ie}\cdot\omega_{n0})$

roll response ratio of sprung mass = $\phi_s(t)/\phi_{ie}$

roll velocity ratio of sprung mass = $\dot{\phi}_s(t)/(\phi_{ie}\cdot\omega_{n0})$

displacement response ratio of unsprung mass = $x_u(t)/X_{ie}$

roll response ratio of unsprung mass = $\phi_u(t)/\phi_{ie}$

where $\omega_{n0} = \sqrt{g/X_{st}}$ and X_{st} is the static deflection of the suspension.

The vertical displacement and velocity, and roll angle response characteristics of the sprung mass of the vehicle employing three different types of suspensions, with incompressible fluid and ideal

tunable valves, are illustrated in Figures 6.17, 6.18 and 6.19, respectively. The vehicle with independent suspension yields a large displacement peak and the oscillation frequency is obtained near 1.48 Hz. The resonant frequency, however, reduces to near 1 Hz, when the independent suspension units within the axle are interconnected. The interconnected suspension configuration also reduces the peak amplitude of vertical displacement, as shown in Figure 6.17. The vertical displacement response of the sprung mass with interconnected suspension approaches the steady state value at a much quicker rate than that with independent suspension. The frequency of vertical oscillation increases slightly to 1.05 Hz, when tunable pressure relief valves are introduced between chambers II and III. The corresponding peak amplitude of vertical displacement of the sprung mass decreases considerably with tunable interconnected vehicle suspension. Comparison of the vertical displacement response characteristics thus reveals that an interconnected vehicle suspension tends to reduce the peak amplitude response as well as bounce resonant frequency of the sprung mass. The vertical velocity response of the sprung mass, presented in Figure 6.18, also reveals that the bounce resonant frequency and the peak velocity response of an independent suspension are considerably larger than those of the interconnected suspension. A tunable interconnected suspension yields considerably superior response of the sprung mass when compared with that of the interconnected as well as the independent suspensions.

The roll angle response of the sprung mass, caused by transient excitation at the right tires, is presented in Figure 6.19. A comparison of roll angle response characteristics of the sprung mass with three

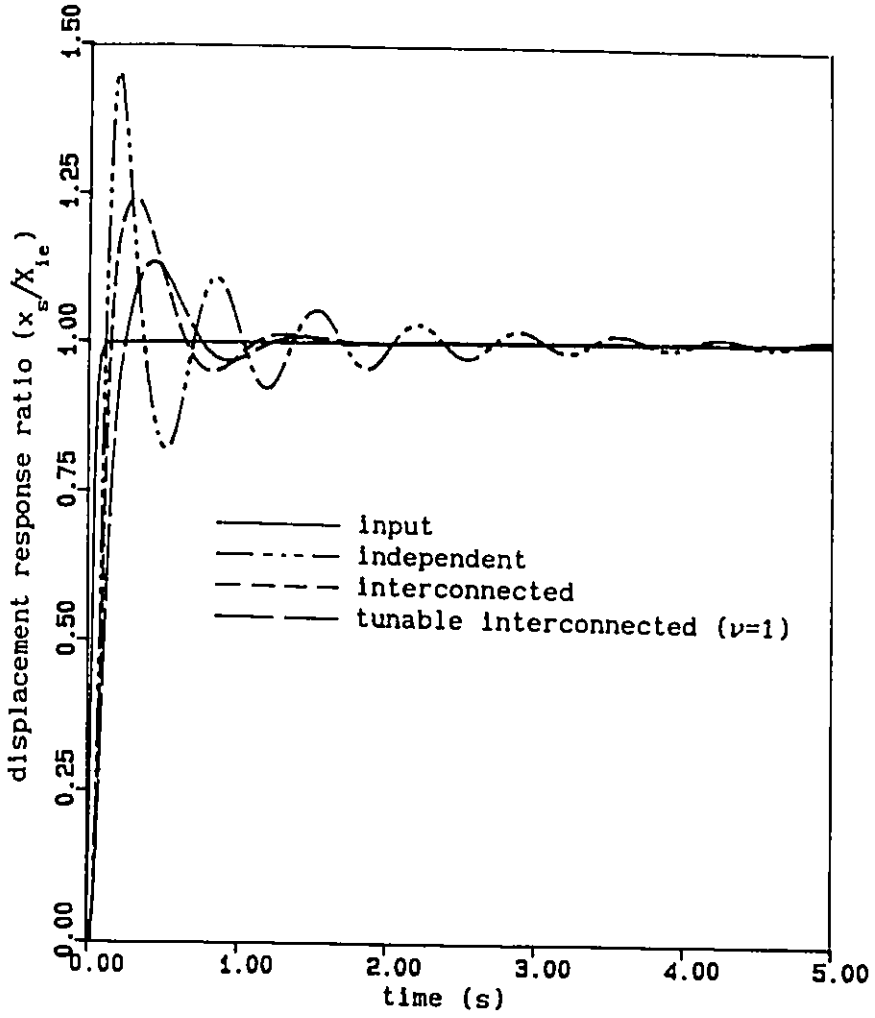

FIGURE 6.17 Transient displacement response of sprung mass of vehicle employing independent, interconnected and tunable interconnected (ν=1) suspensions

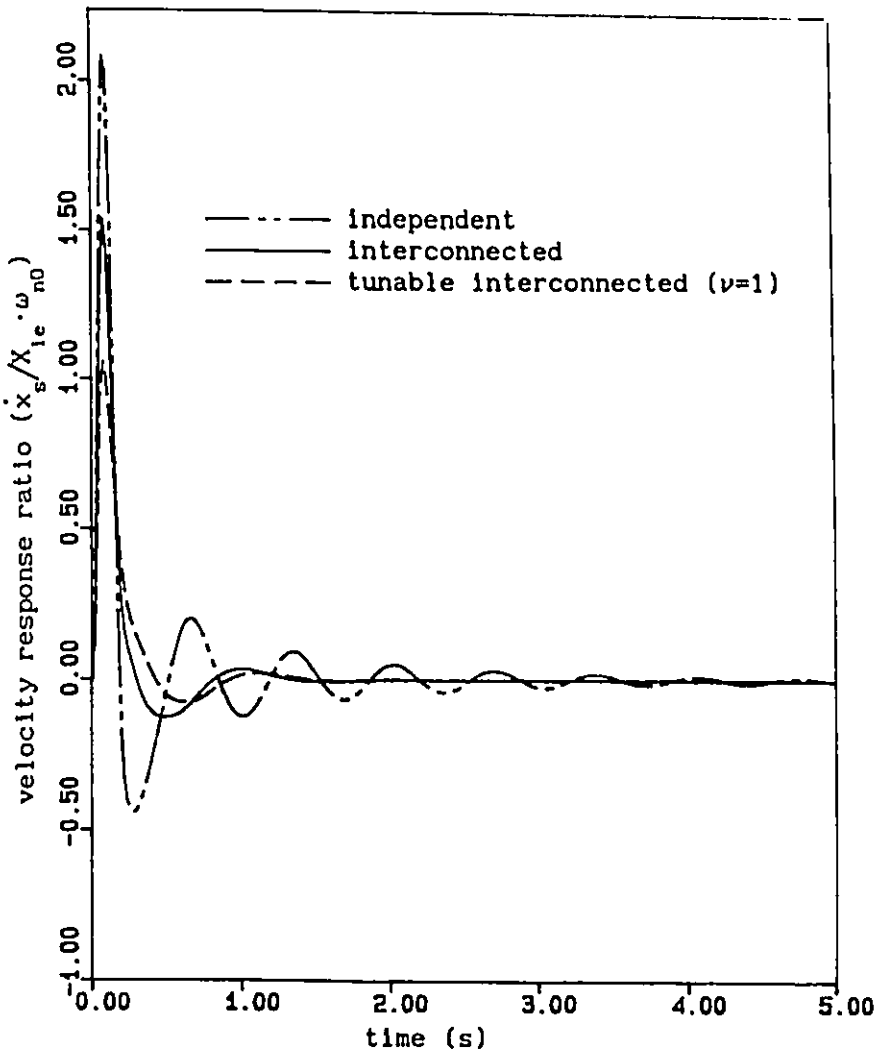

FIGURE 6.18 Transient velocity response of sprung mass of vehicle employing independent, interconnected and tunable interconnected (ν=1) suspensions

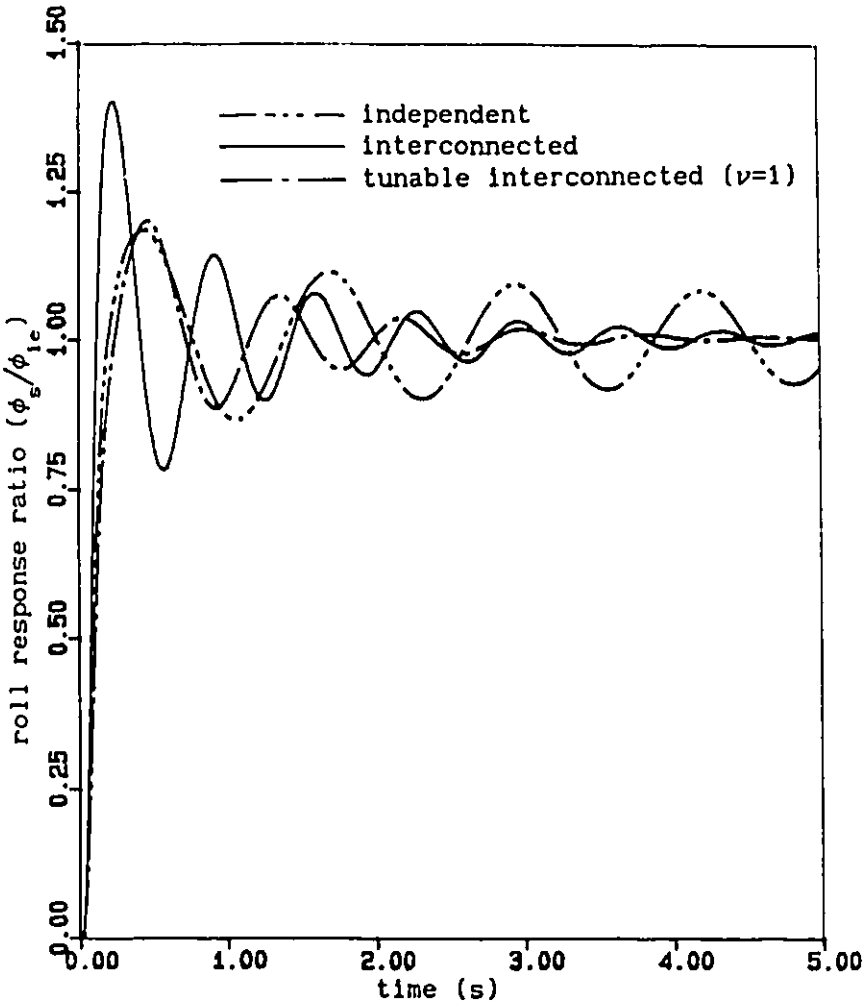

FIGURE 6.19 Transient roll angle response of sprung mass of vehicle employing independent, interconnected and tunable interconnected (ν=1) suspensions

different types of suspensions clearly reveals that the interconnected suspension yields the highest resonant frequency in the roll mode. The resonant frequencies associated with the sprung mass roll mode are obtained as 1.4 Hz and 0.8 Hz, respectively, for interconnected and independent suspensions. Figure 6.19 further reveals that the peak roll angle response of the sprung mass with the interconnected is considerably larger than that with independent one. The peak amplitudes of subsequent roll oscillations of the sprung mass with the interconnected suspension, however, decrease rapidly, while the roll response of the independent one continues to exhibit high amplitude oscillation. Comparison of the response characteristics of the independent and interconnected suspensions to those of a tunable interconnected one reveals that the tunable interconnected suspension provides the best of both: that is the high roll resonant frequency of the interconnected and the low peak response of the independent, as shown in Figure 6.19. The roll resonant frequency of the tunable suspension (1.2 Hz) is slightly less than that of the interconnected one (1.4 Hz). The peak roll response of the tunable interconnected suspension, however, is quite close to that of the independent one. Furthermore, the roll response of the sprung mass with the tunable interconnected suspension decays at a faster rate than that of the independent and interconnected ones. Figures 6.17 through 6.19 clearly illustrate the performance potential of the tunable suspension for transient excitations, in view of both peak response and settling time.

The transient response characteristics of the roll plane vehicle model, employing interconnected and tunable interconnected suspensions,

are further evaluated, while the dynamics due to fluid compliance and the relief valves are appropriately incorporated, as presented in Figures 6.20 through 6.25. A comparison of vertical displacement and velocity of the sprung mass, employing interconnected and tunable interconnected suspensions, is presented in Figures 6.20 and 6.21. These figures clearly illustrate that the transient response of the sprung mass can be improved considerably via the tunable interconnected suspension. Roll angle and rate response characteristics of the sprung mass of the vehicle, employing interconnected and tunable interconnected suspensions, illustrated in Figures 6.22 and 6.23, clearly show that the peak roll angle as well as rate response can be suppressed considerably via the tunable interconnected suspension. Furthermore, the roll resonant frequency of sprung mass with the tunable interconnected suspension (1.1 Hz) is almost identical to that with the interconnected one. A tunable interconnected suspension not only suppresses the peak response of the sprung mass, but also yields lower response of the unsprung mass, as illustrated by the bounce and roll displacement response of the unsprung mass of the vehicle shown in Figures 6.24 and 6.25.

The shock and vibration isolation performance characteristics of the vehicle model employing the tunable interconnected suspension are strongly related to the effective fluid bulk modulus and valve dynamics. Figures 6.26 through 6.29 present a comparison of the sprung mass vertical displacement and velocity, and roll angle and velocity response characteristics of the vehicle employing an ideal model of the tunable interconnected suspension to those of a higher order one incorporating

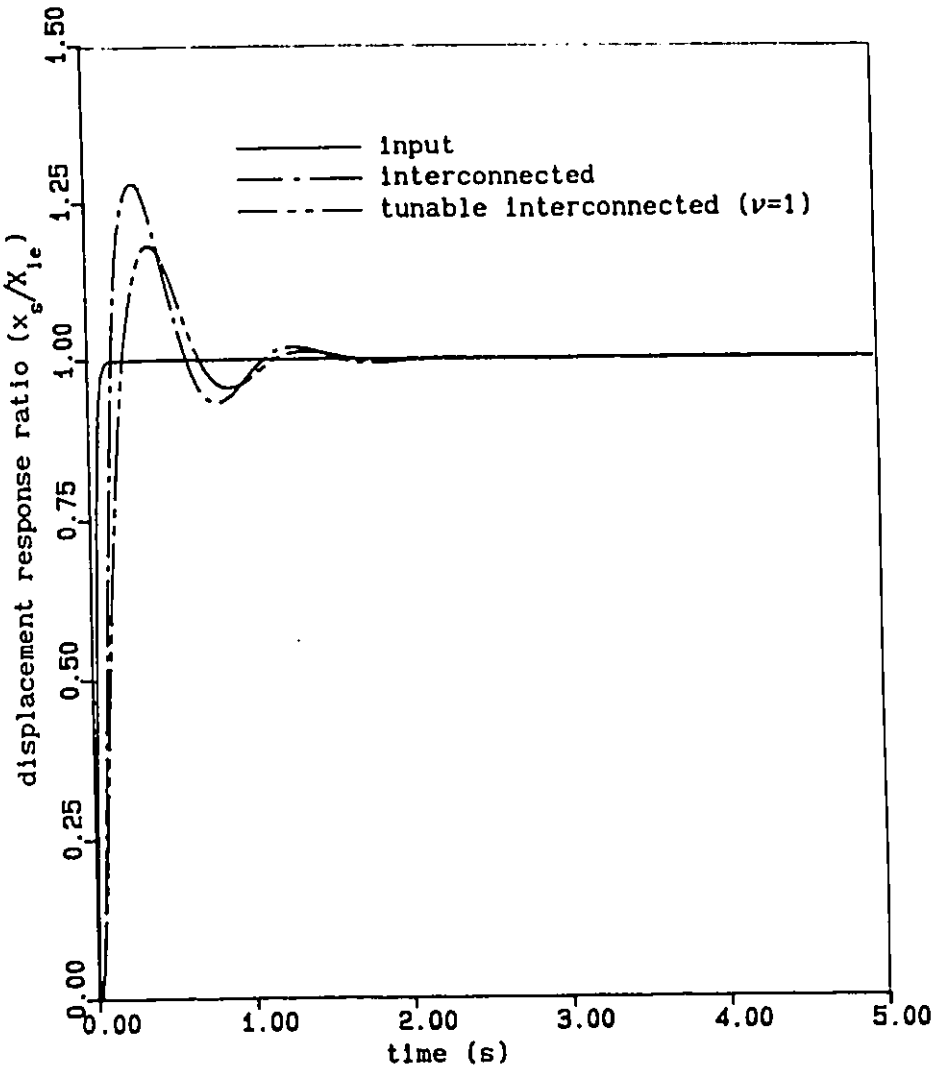

FIGURE 6.20 Transient displacement response of sprung mass of vehicle employing interconnected and tunable interconnected (ν=1) suspensions (β_o=6.9x10^8 (Pa))

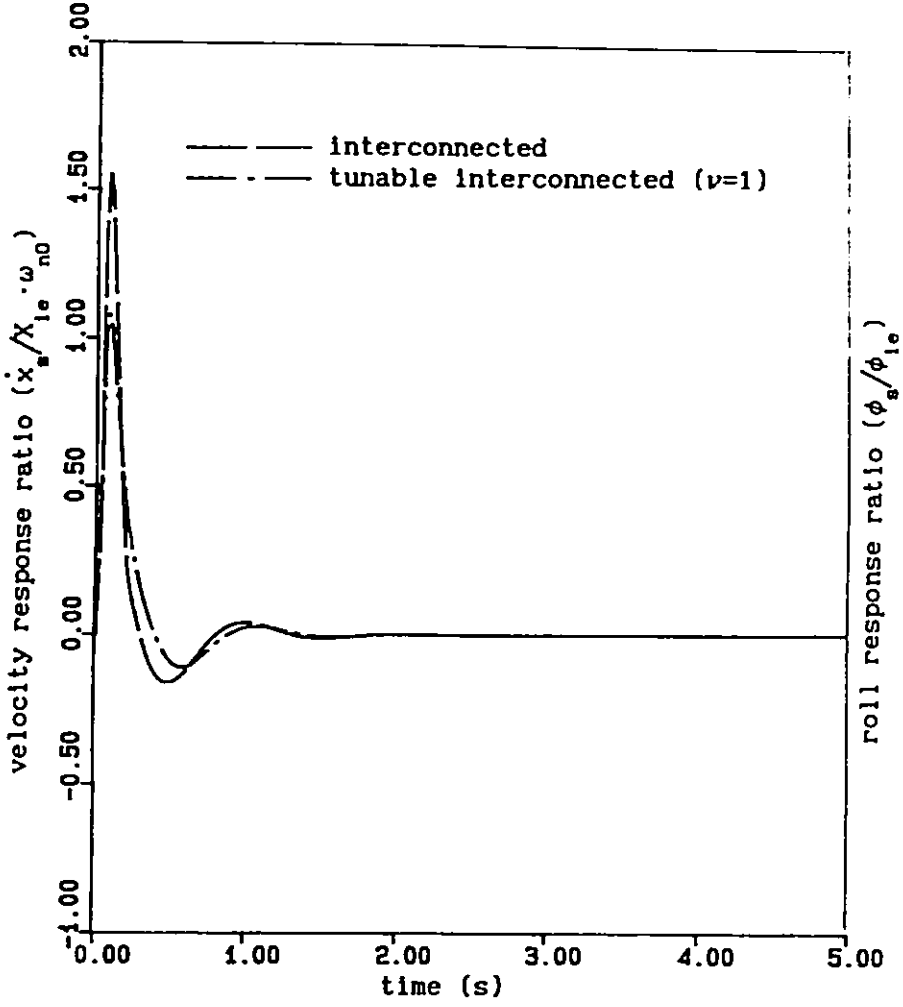

FIGURE 6.21 Transient velocity response of sprung mass of vehicle employing interconnected and tunable interconnected (ν=1) suspensions (β_e=6.9x10^8 (Pa))

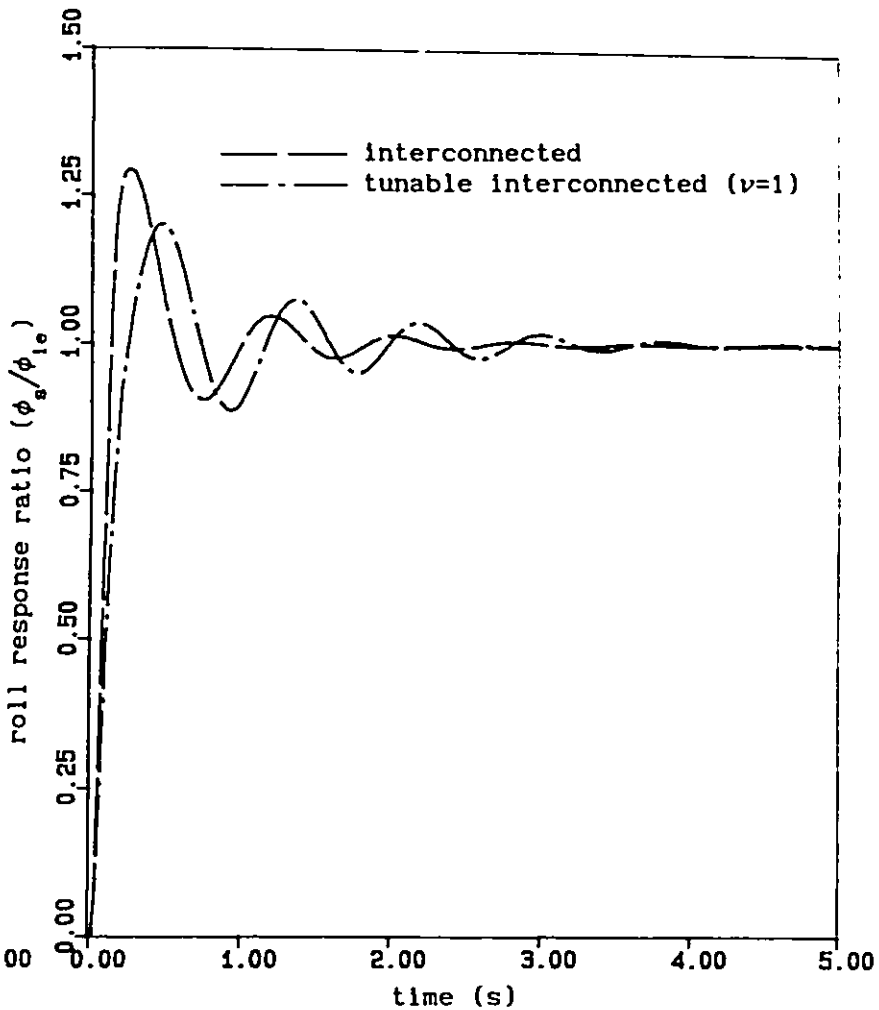

FIGURE 6.22 Transient roll angle response of sprung mass of vehicle employing interconnected and tunable interconnected (ν=1) suspensions (β_e=6.9x10^8 (Pa))

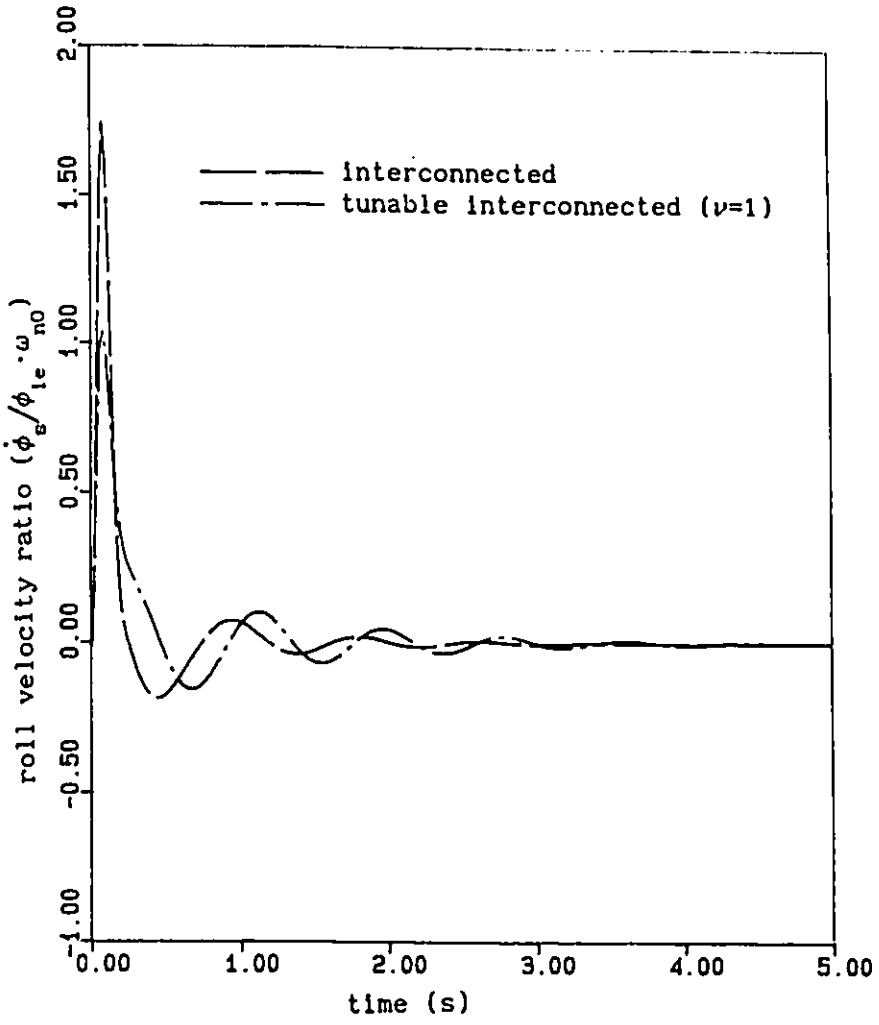

FIGURE 6.23 Transient roll velocity response of sprung mass of vehicle employing interconnected and tunable interconnected (ν=1) suspensions (β_o=6.9x10^8 (Pa))

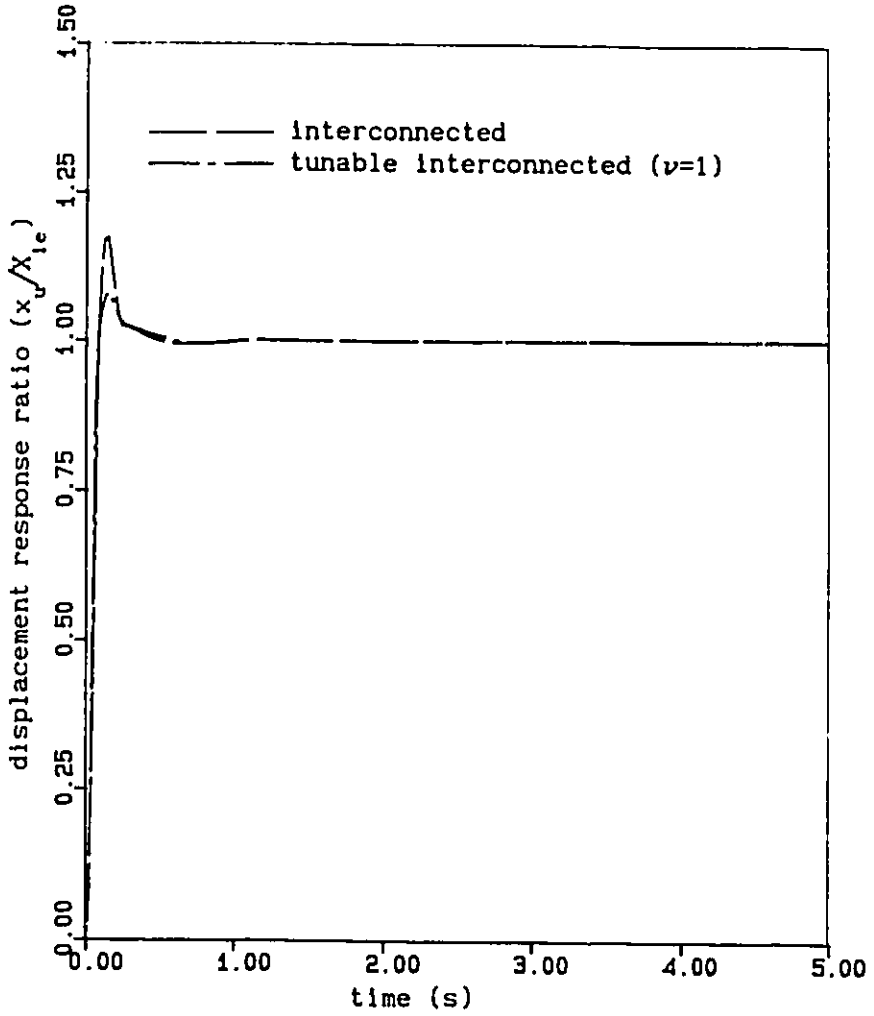

FIGURE 6.24 Transient displacement response of unsprung mass of vehicle employing interconnected and tunable interconnected (ν=1) suspensions (β_e=6.9x10^8 (Pa))

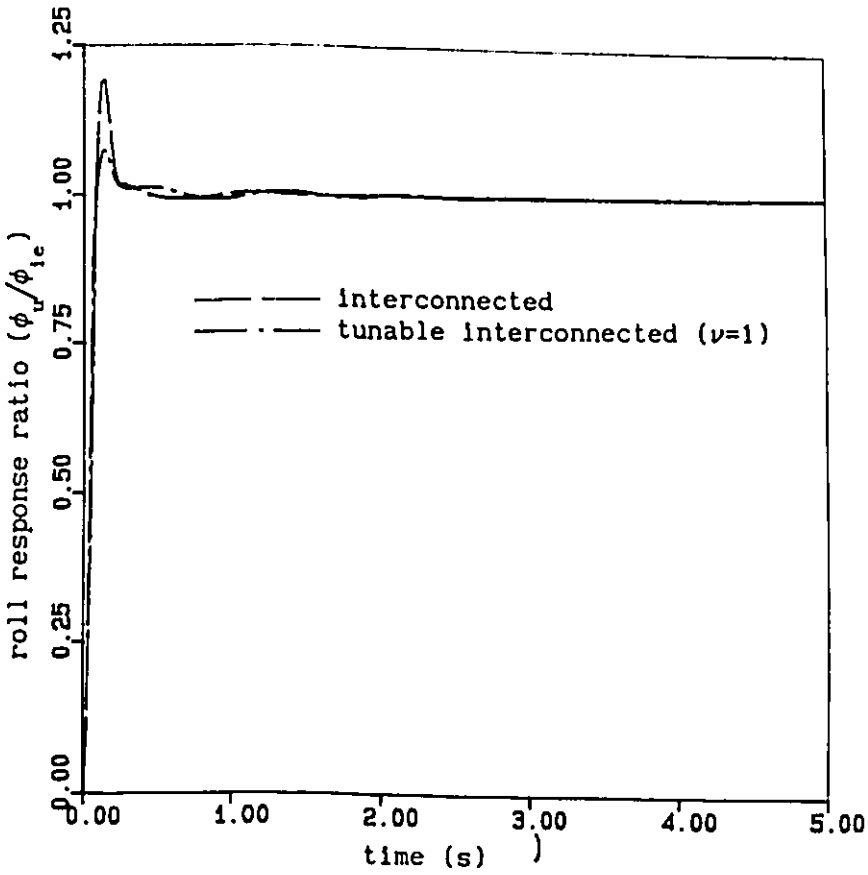

FIGURE 6.25 Transient roll angle response of unsprung mass of vehicle employing interconnected and tunable interconnected (ν=1) suspensions (β_e=6.9x10^8 (Pa))

the valve dynamics and fluid compliance. The response characteristics of the higher order of tunable interconnected suspension including the dynamics due to fluid compressibility and pressure relief valves are referred to as "TIC (higher order)". Comparison of the response characteristics, presented in Figure 6.26, reveals that peak vertical displacement response of higher order model of tunable interconnected suspension is slightly deteriorated when the effects of valve dynamics and fluid compressibility are considered. However, the response characteristics of higher order tunable interconnected suspension remain superior to those of an interconnected suspension, as shown in Figure 6.26. The vertical velocity response characteristics, presented in Figure 6.27, reveals that the vertical velocity response of higher order tunable interconnected suspension, is almost identical to that of the ideal tunable interconnected suspension. Figures 6.28 and 6.29 show the transient roll angle and roll rate response of the two tunable interconnected suspension models, respectively. Comparison of the roll response characteristics of the ideal and higher order models of tunable interconnected suspensions reveals that the peak roll angle and roll rate response of the sprung mass decrease with consideration of the effective bulk modulus and valve dynamics. Furthermore, the roll angle and roll rate response of the higher order tunable interconnected suspension model approaches steady state values at a faster rate.

6.7.2 Frequency Response Characteristics

The frequency response characteristics of the roll plane vehicle model employing the interconnected and tunable interconnected suspensions are evaluated to determine their relative vibration

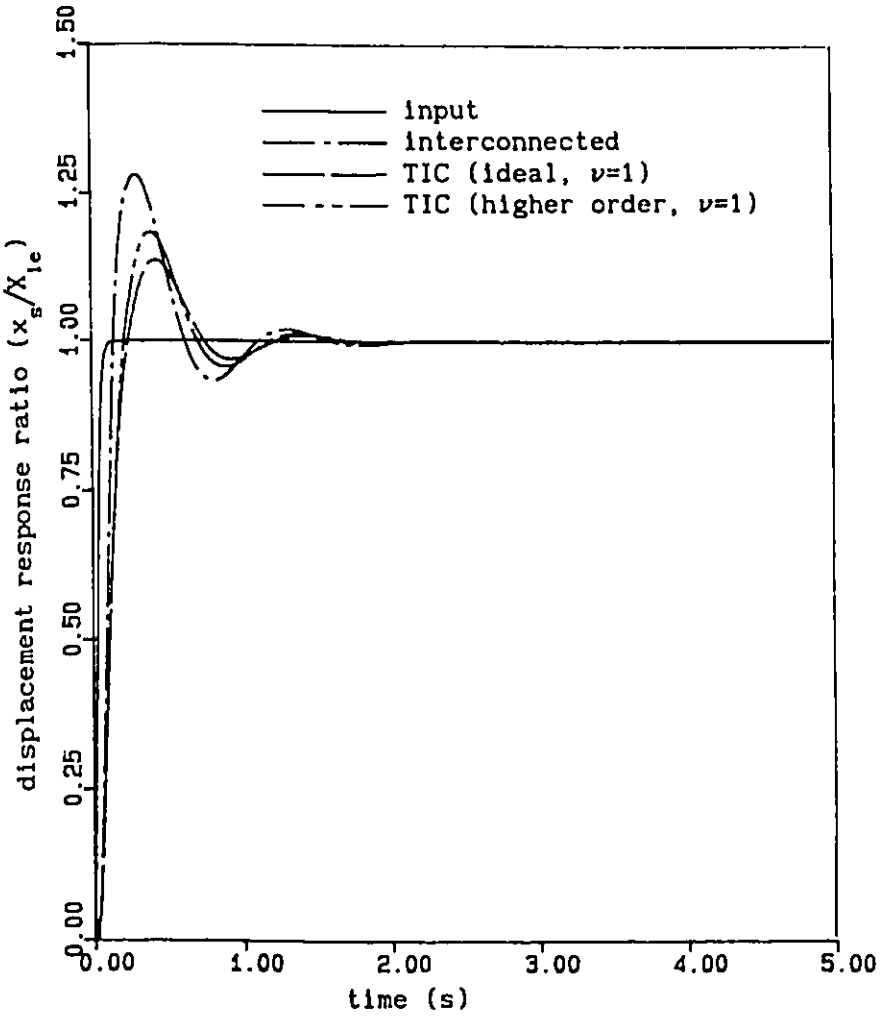

FIGURE 6.26 Transient displacement response of sprung mass of vehicle employing interconnected, and higher order and ideal tunable interconnected suspensions

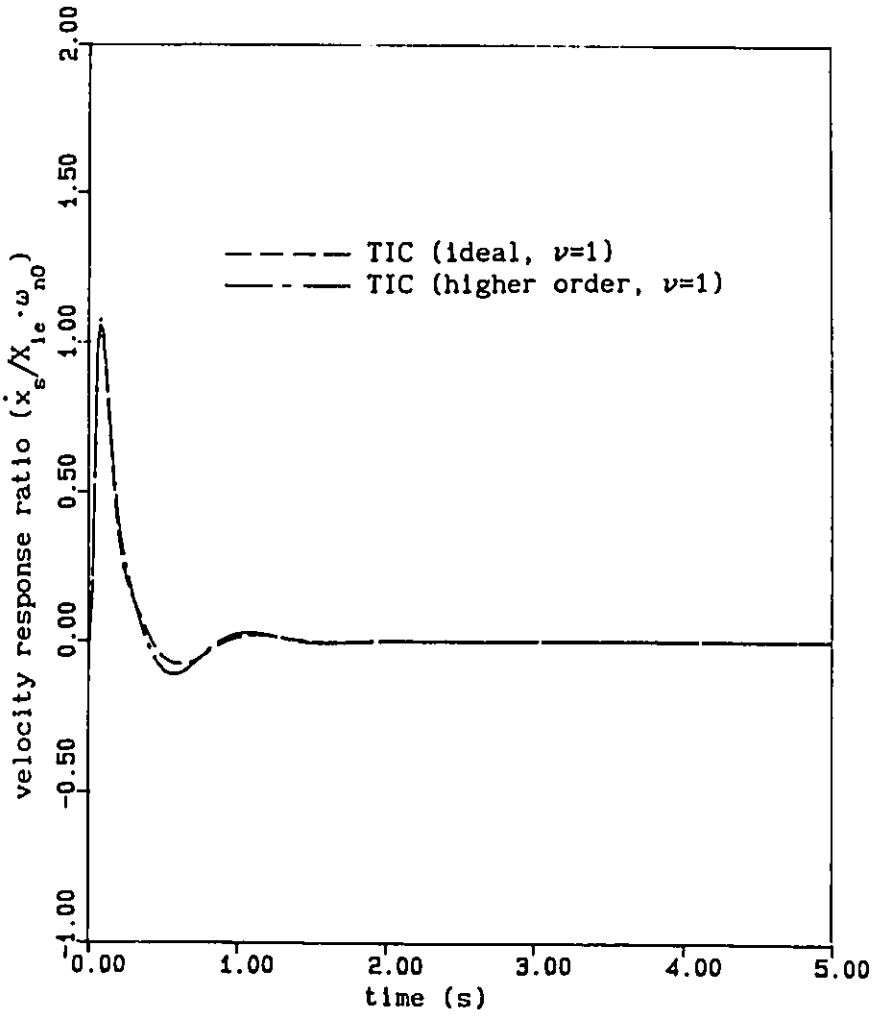

FIGURE 6.27 Transient velocity response of sprung mass of vehicle employing higher order and ideal tunable interconnected suspensions

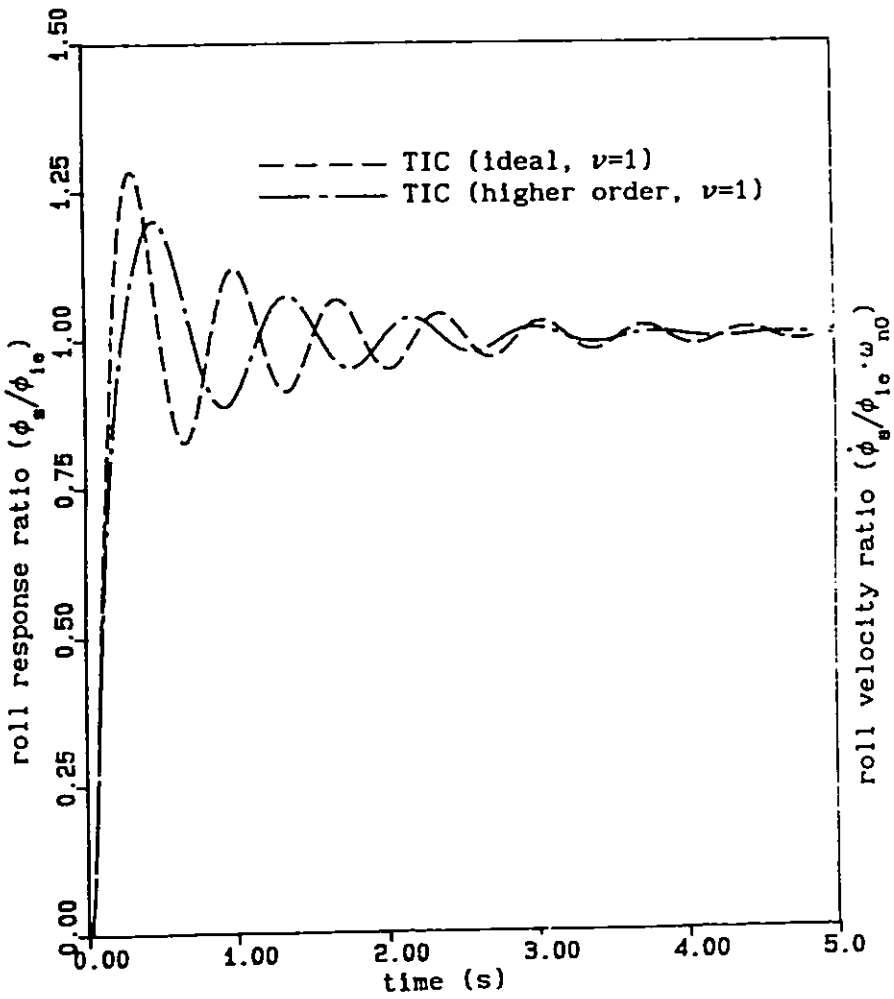

FIGURE 6.28 Transient roll angle response of sprung mass of vehicle employing higher order and ideal tunable interconnected suspensions

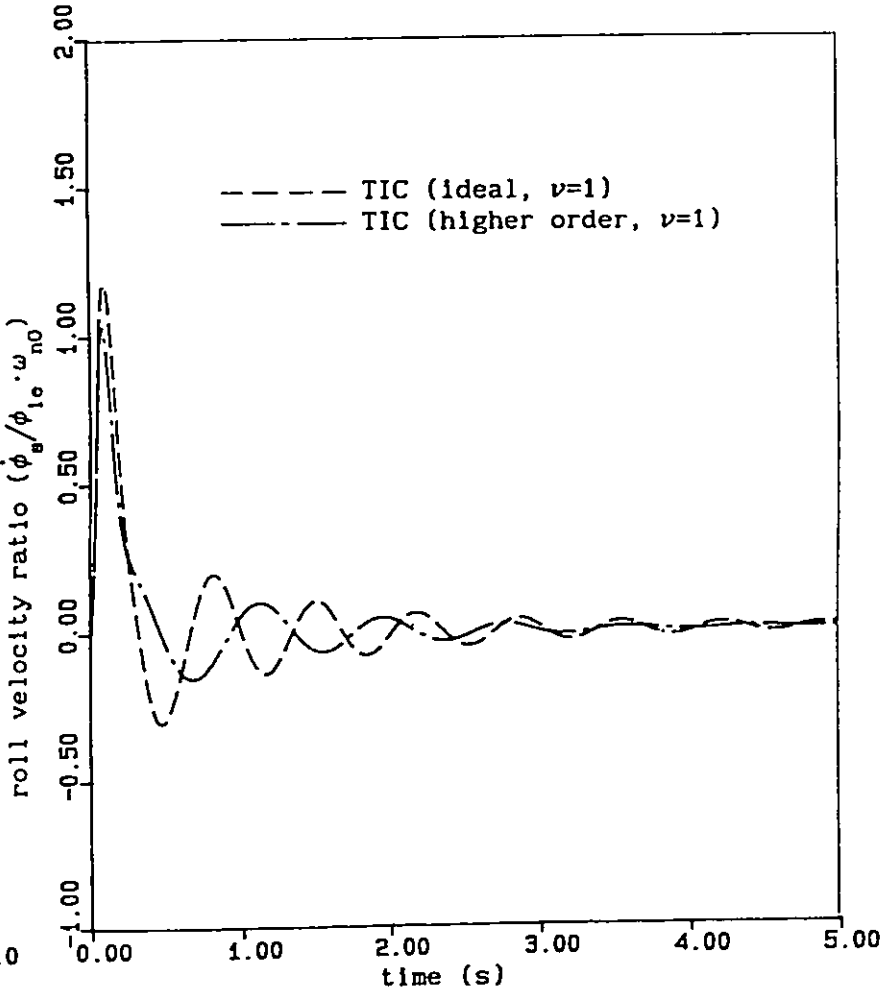

FIGURE 6.29 Transient angle velocity response of sprung mass of vehicle employing higher order and ideal tunable interconnected suspensions

isolation performance. The vibration isolation performance characteristics of the roll plane vehicle are evaluated for harmonic excitation at the contact point of the right tire and the road surface. The amplitude of harmonic displacement excitation, at the right tire, is selected as X_{ir}=0.025 m. The vibration isolation characteristics of two different suspensions are evaluated by computing the ratio of the steady state response amplitude to the equivalent excitation amplitude. Vibration isolation characteristics are expressed by the following transmissibility ratios:

vertical displacement transmissibility of sprung mass = $\left|\frac{X_s}{X_{ie}}\right|$

roll angle transmissibility of sprung mass = $\left|\frac{\phi_s}{\phi_{ie}}\right|$

vertical displacement transmissibility of unsprung mass = $\left|\frac{X_u}{X_{ie}}\right|$

roll angle transmissibility of unsprung mass = $\left|\frac{\phi_u}{\phi_{ie}}\right|$

relative displacement transmissibility of right suspension unit = $\left|\frac{Z_r}{X_{ir}}\right|$

The sprung mass displacement and roll angle, and unsprung mass displacement and roll angle transmissibility characteristics of the roll plane model of the vehicle, employing interconnected and tunable interconnected suspensions incorporating fluid compressibility and valve dynamics, are illustrated in Figures 6.30 through 6.33, respectively. The effective bulk modulus of the fluid for the two suspension systems is selected as $\beta_e = 6.9\times10^8$ (Pa). Both the interconnected suspensions in

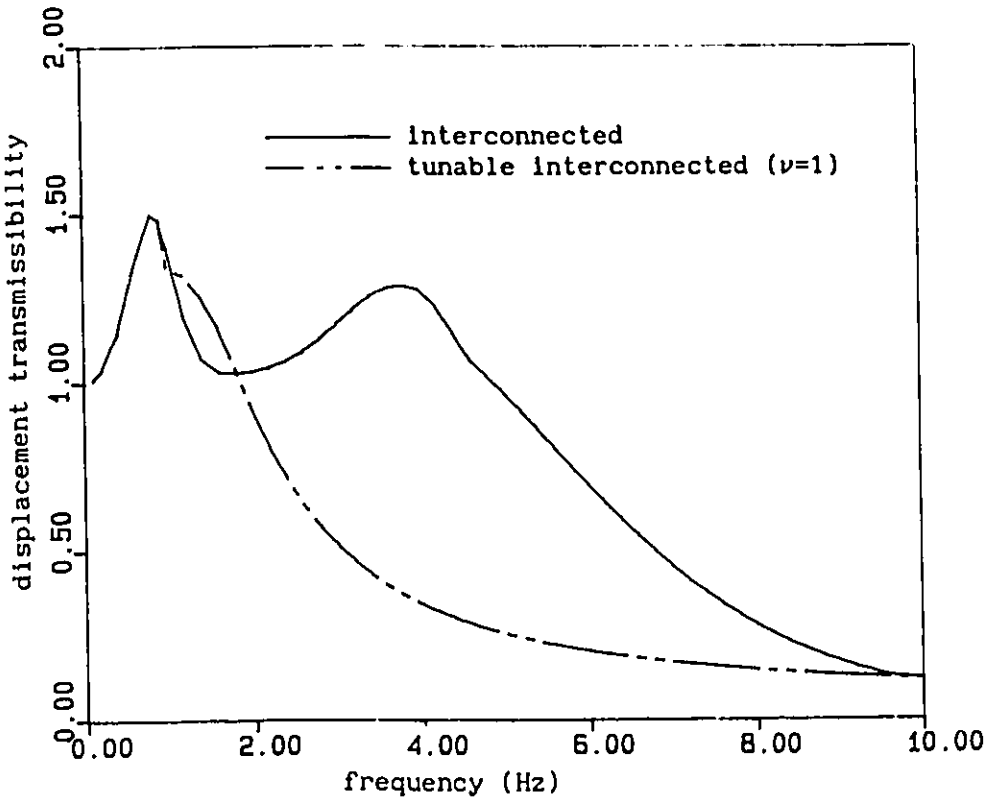

FIGURE 6.30 Displacement transmissibility of sprung mass of vehicle employing interconnected and tunable interconnected (ν=1) suspensions (β_o=6.9x10^8 (Pa))

the simulation are assumed to have identical orifice areas between chambers II and III, while a unit value of the tuning factor (ν=1) is selected for the tunable interconnected one. The displacement transmissibility of the sprung mass with the interconnected suspension yields a resonant peak response at an excitation frequency of 0.9 Hz, as shown in Figure 6.30. The response amplitude of the sprung mass reduces as the excitation frequency increases. However, the interconnected suspension yields a large second peak response of the sprung mass around excitation frequency 4 Hz corresponding to the unsprung mass resonance, due to the high damping value provided by the interconnected one at the high relative velocity. The tunable interconnected suspension yields displacement response identical to that of the interconnected suspension before and around the first resonant frequency. However, the displacement transmissibility response reveals a higher response as compared with that of the interconnected one, as the pressure relief valve starts to open and modulate the fluid flow between chambers II and III. As the excitation frequency further increases, the tunable interconnected suspension considerably reduces the displacement response amplitude through pressure limiting modulation. A comparison of the displacement transmissibility response of the two types of interconnected suspensions reveals that the tunable interconnected one yields superior vertical displacement transmissibility at excitation frequency beyond 2 Hz, as shown in Figure 6.30. The roll angle transmissibility characteristics of the sprung mass of the vehicle employing interconnected and tunable interconnected suspensions, incorporating fluid compressibility and valve dynamics, are presented in

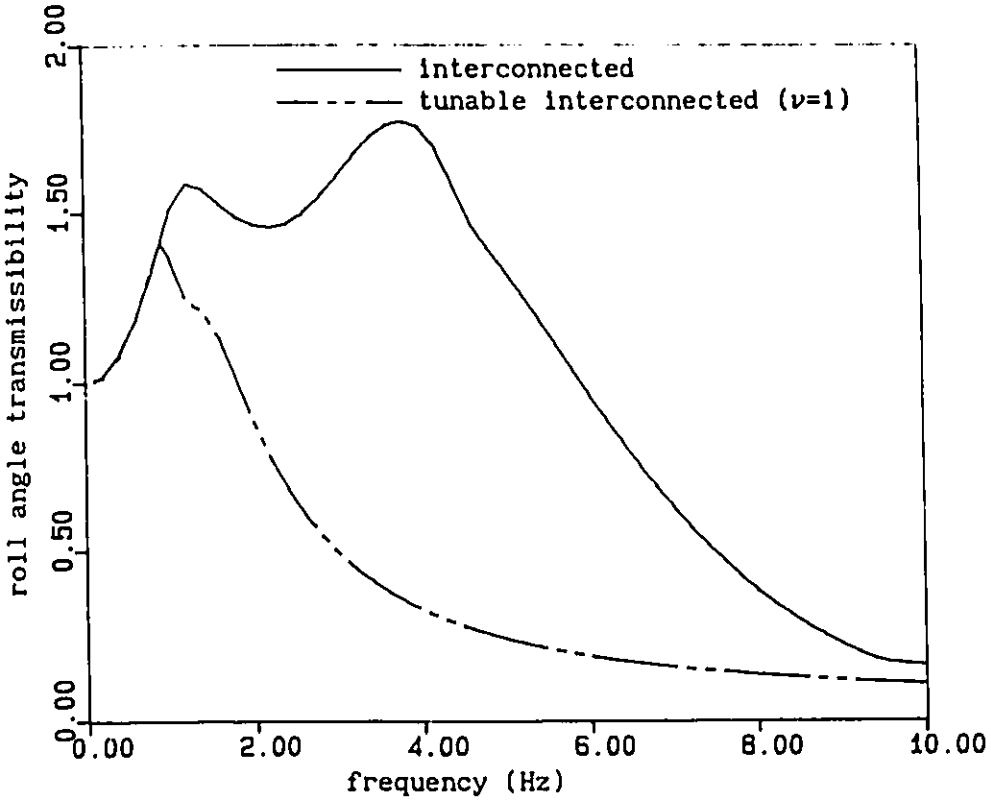

FIGURE 6.31 Roll angle transmissibility of sprung mass of vehicle employing interconnected and tunable interconnected (ν=1) suspensions (β_o=6.9x10^8 (Pa))

Figure 6.31. It is observed that the interconnected suspension yields two high peaks of roll angle response, around excitation frequencies 1.2 Hz and 3.9 Hz, respectively. The roll angle response of the sprung mass with the tunable interconnected suspension is identical to that with the interconnected one when excitation frequency is less than 0.9 Hz. The roll angle transmissibility of the sprung mass tunable interconnected suspension, however, is considerably reduced even before the first roll peak response, due to opening of the pressure relief valve around the resonant frequency of vertical displacement mode of sprung mass. It is obvious, from Figure 6.31, that the tunable interconnected suspension yields a significantly reduced roll response value, for excitation frequency beyond 1 Hz.

Figures 6.32 presents displacement transmissibility characteristics of the unsprung mass of the vehicle employing two types of interconnected suspensions. It is observed that the interconnected suspension yields a peak displacement response around 4 Hz and a reduced response amplitude corresponding higher excitation frequencies. The tunable interconnected yields an unsprung mass displacement response identical to that of the interconnected one when excitation frequency is less than 1 Hz. As the excitation frequency increases, the tunable suspension yields a reduced displacement response of the unsprung mass due to pressure limiting modulation. Due to reduced damping by the pressure limiting valves, the unsprung mass displacement response increases and approaches a resonant peak of the unsprung mass, for excitation frequency beyond 6 Hz, as shown in Figure 6.32. The roll angle response characteristics of the unsprung mass with two suspensions are presented

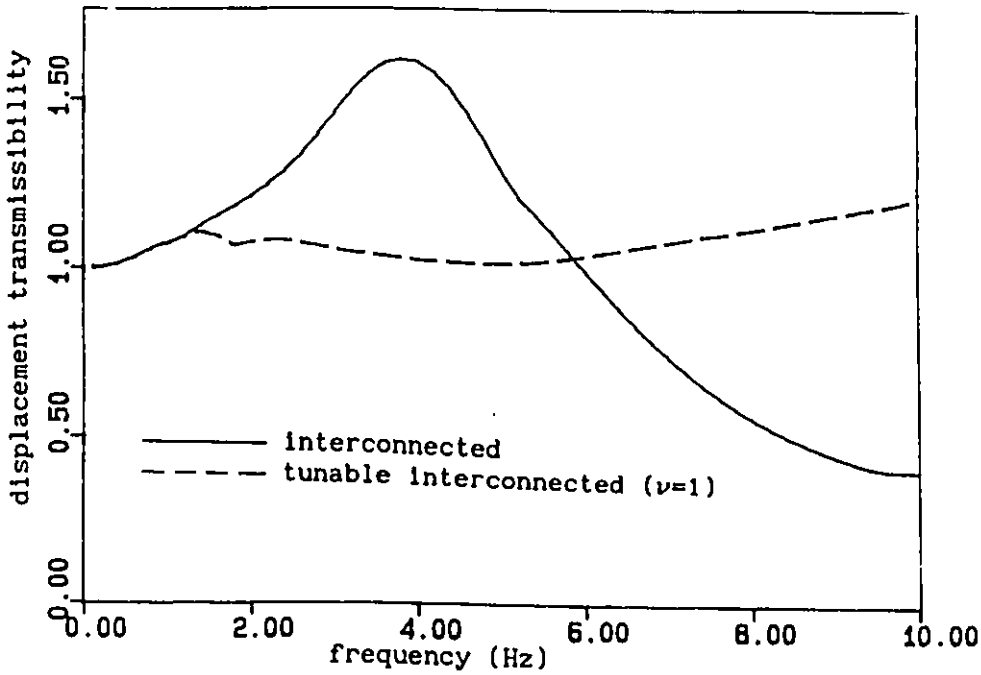

FIGURE 6.32 Displacement transmissibility of unsprung mass of vehicle employing interconnected and tunable interconnected (ν=1) suspensions (β_o=6.9x10^8 (Pa))

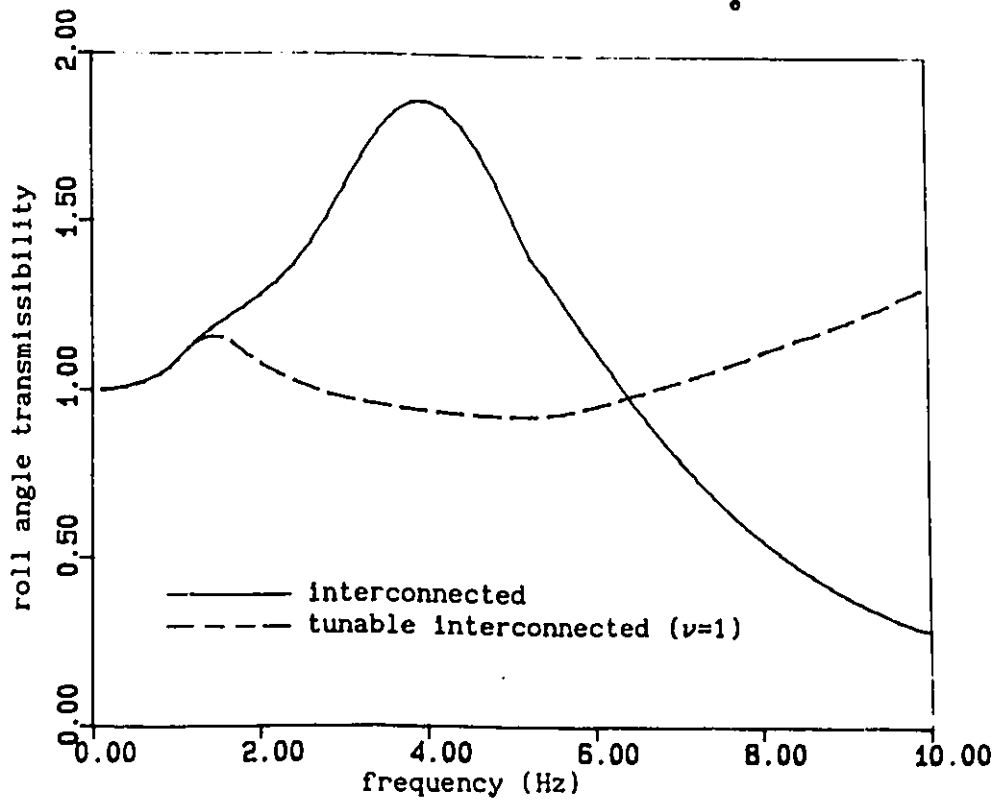

FIGURE 6.33 Roll angle transmissibility of unsprung mass of vehicle employing interconnected and tunable interconnected (ν=1) suspensions (β_o=6.9x10^8 (Pa))

in Figure 6.33. A comparison of the unsprung mass roll angle response reveals that the tunable suspension yields a reduced roll angle response for an excitation frequency less than 6 Hz. The reduced damping in the suspension due to the pressure limiting modulation results in an increased amplitude response of the unsprung mass roll angle and a higher resonant frequency corresponding to the unsprung mass mode, for excitation frequency beyond 6 Hz, as shown in Figure 6.33.

The effects of fluid compressibility and valve dynamics, upon the response characteristics of the roll plane vehicle model employing the tunable interconnected suspension, are illustrated by comparison of frequency response characteristics of ideal and higher order models, as shown in Figures 6.34 through 6.36. The effective bulk modulus of the fluid for the higher order suspension systems is selected as $\beta_e = 6.9\times10^8$ (Pa). The tuning factor for both the ideal and higher order tunable interconnected suspensions is set to be unity (ν=1). The displacement transmissibility characteristics of the sprung mass of the vehicle employing interconnected (with β_e), and ideal and higher order tunable interconnected suspensions, presented in Figure 6.34, reveal that the ideal tunable interconnected suspension yields a sprung mass displacement response identical to that of the interconnected suspension until the opening of the pressure relief valve. The displacement response of the sprung mass with ideal pressure limiting control illustrates a slightly larger response around the excitation frequency at which the pressure limiting modulation occurs. It is observed that the ideal tunable interconnected suspension yields the smallest displacement response amplitude of the sprung mass for an excitation

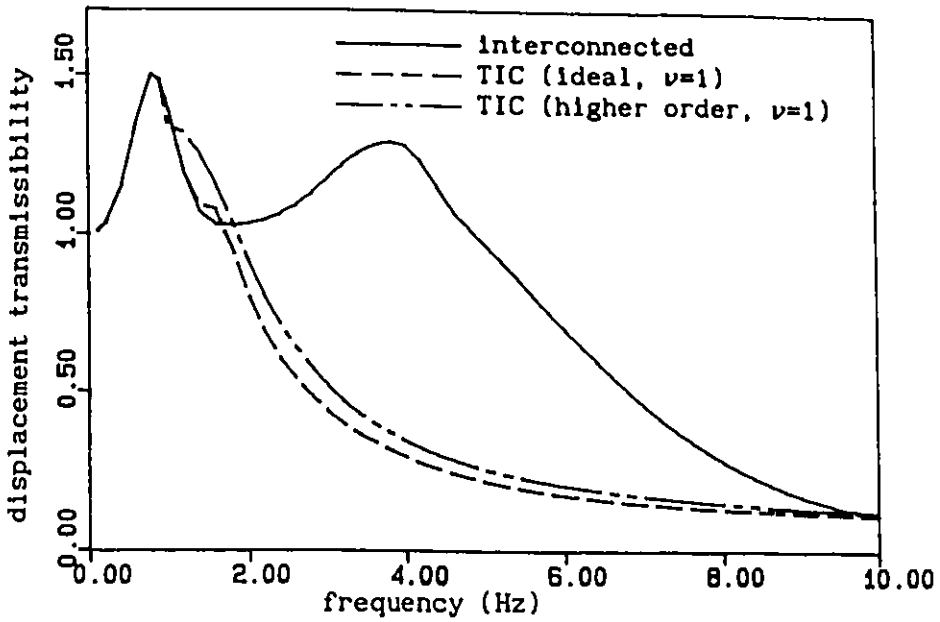

FIGURE 6.34 Displacement transmissibility of sprung mass of vehicle employing interconnected, higher order and ideal tunable interconnected (ν=1.0) suspensions

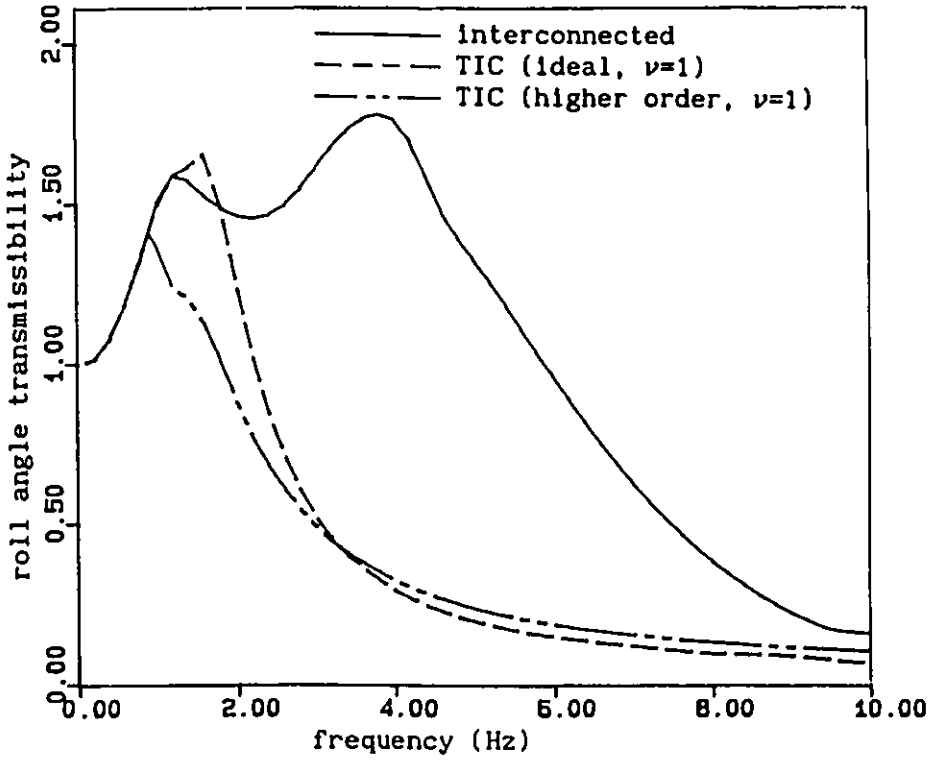

FIGURE 6.35 Roll angle transmissibility of sprung mass of vehicle employing interconnected, higher order and ideal tunable interconnected (ν=1.0) suspensions

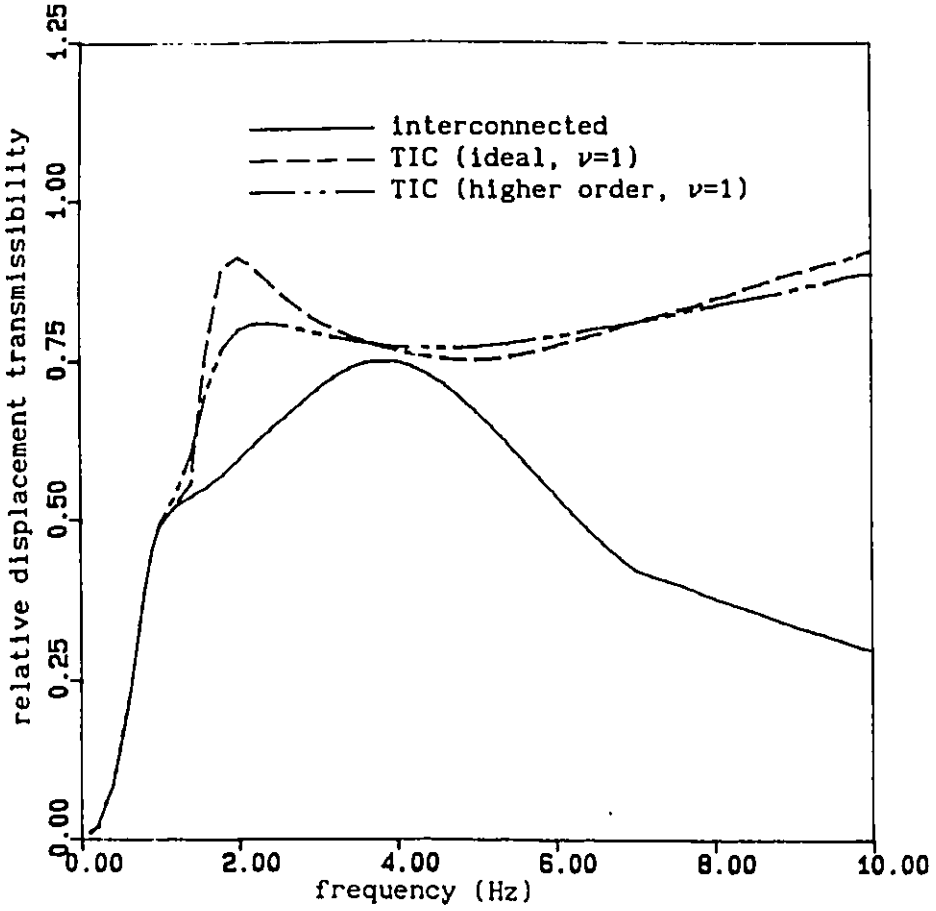

FIGURE 6.36 Relative displacement transmissibility of right suspension unit with interconnected, higher order and ideal tunable interconnected (ν=1.0) suspensions

frequency beyond 1.8 Hz. The tunable interconnected suspension deteriorates the vertical displacement response of the sprung mass slightly as compared with that of the ideal interconnected suspension, due to the dynamics of relief valve, especially around the excitation frequency at which the pressure limiting modulation starts. However, the displacement response of sprung mass with the higher order model of the tunable interconnected suspension is still superior to that with the interconnected suspension, as shown in Figure 6.34.

The roll angle transmissibility characteristics of the sprung mass of the roll plane model of the vehicle, employing interconnected, ideal and higher order tunable interconnected suspensions, are presented in Figure 6.35. It is observed that the ideal tunable suspension yields a roll angle response identical to that of the interconnected one until the excitation frequency approaches 1.1 Hz. The magnitude of the roll angle response of the sprung mass increases and reaches to a peak at the frequency 1.8 Hz at which pressure limiting modulation occurs. The roll angle response of the sprung mass with the ideal tunable suspension decreases for excitation frequencies above 1.8 Hz. The roll angle response of the sprung mass with higher order suspension is identical to that of interconnected one until 0.9 Hz. It can be seen, from equations (6.90) and (6.91), that the motion of the relief valve spool affects the fluid flow between chambers II and III even before the relief valves open. The magnitude of the roll angle response of the sprung mass with the higher order tunable interconnected suspension is thus found to be reduced for frequency less than 0.9 Hz. It is observed that the magnitude of roll angle transmissibility of sprung mass with the higher

order tunable suspension is less than that with the ideal tunable one within the frequency range 0.9 to 3.0 Hz, as shown in Figure 6.35.

The relative displacement transmissibility characteristics of the right suspension unit with interconnected, and ideal and higher order tunable interconnected suspensions are illustrated in Figure 6.36. It is observed that the magnitude of the relative displacement response of the right suspension unit with the interconnected suspension is always less than that of the tunable interconnected one, due to the higher damping value provided by interconnected suspension with fixed orifice area, especially at high frequency. The ideal tunable interconnected suspension yields a higher peak value of relative displacement response around the excitation frequency 1.8 Hz due to a sudden pressure limiting modulation of an ideal damping force control. The relative displacement response approaches to unity when the excitation frequency further increases, due to the reduced damping in the suspension by pressure limiting mechanism. The higher order tunable interconnected suspension yields a lower value of relative displacement response around frequencies of 1.8 Hz, due to the gradually opening of the relief valves, as compared with that of the ideal tunable suspension. At higher frequency, the relative displacement of right suspension unit with the higher order tunable interconnected suspension is similar to that with the ideal tunable suspension, as shown in Figure 6.36.

The vibration transmissibility characteristics of the roll plane vehicle model, employing the tunable interconnected suspension, are strongly related to the tuning factor, ν, as illustrated in Figures 6.37 through 6.39. The displacement transmissibility characteristics of the

sprung mass, employing the tunable interconnected suspension, for various values of tuning factor, are presented in Figure 6.37. It is observed that the vertical displacement response characteristics of the sprung mass with tunable interconnected suspension, around excitation frequencies at which pressure limiting modulation occurs, are significantly influenced by the tuning factor. A lower value of the tuning factor (ν=0.7) tends to limit the damping force at lower excitation frequency and thus yields a larger displacement response around the frequency at which pressure limiting modulation starts. On the other hand, a larger value of the tuning factor (ν=1.3) can be selected to limit the damping force at a higher excitation frequency and the displacement response can be reduced. However, the larger tuning factor yields a slightly higher displacement response at higher excitation frequencies, as shown in Figure 6.37. The roll angle transmissibility characteristics of the sprung mass with the tunable interconnected suspension are presented in Figure 6.38. It can be seen that a lower value of the tuning factor (ν=0.7) yields a larger peak value of roll angle response due to pressure limiting modulation at a lower excitation frequency. A larger value of tuning factor (ν=1.3) results in a smaller peak amplitude of the roll angle response, but yields a slightly higher magnitude of roll angle transmissibility at higher frequencies. Figure 6.39 shows relative displacement transmissibility of the right suspension unit with the tunable suspension, for various values of tuning factor. A comparison of the relative response characteristics reveals that a lower value of tuning factor yields a larger peak in the relative displacement response around

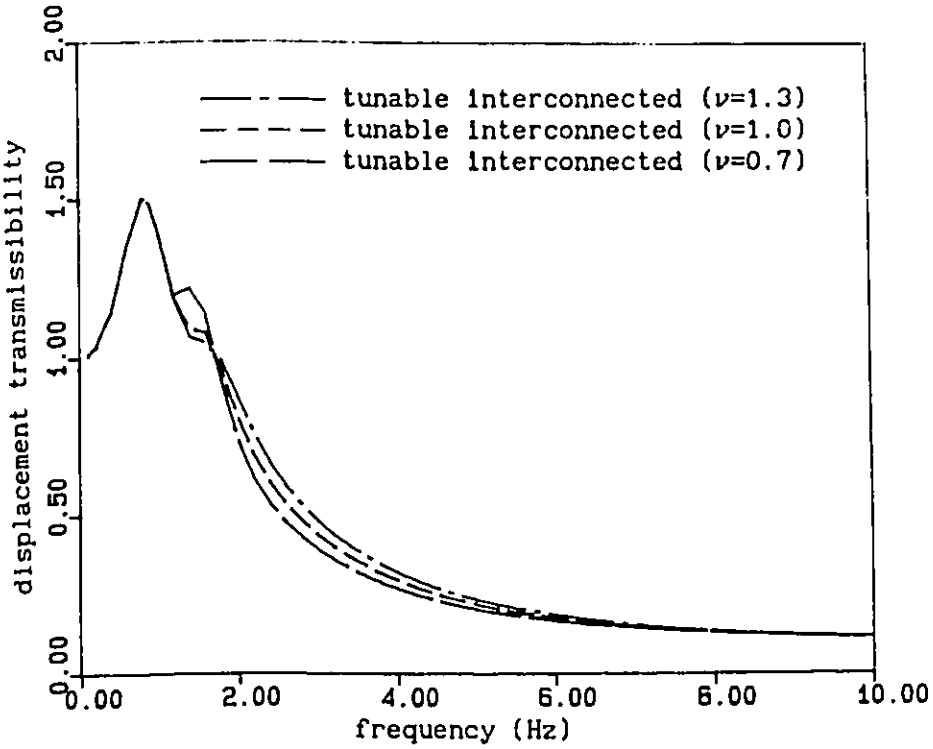

FIGURE 6.37 Displacement transmissibility of sprung mass of vehicle employing tunable interconnected suspensions (ν=0.7, 1.0 and 1.3)

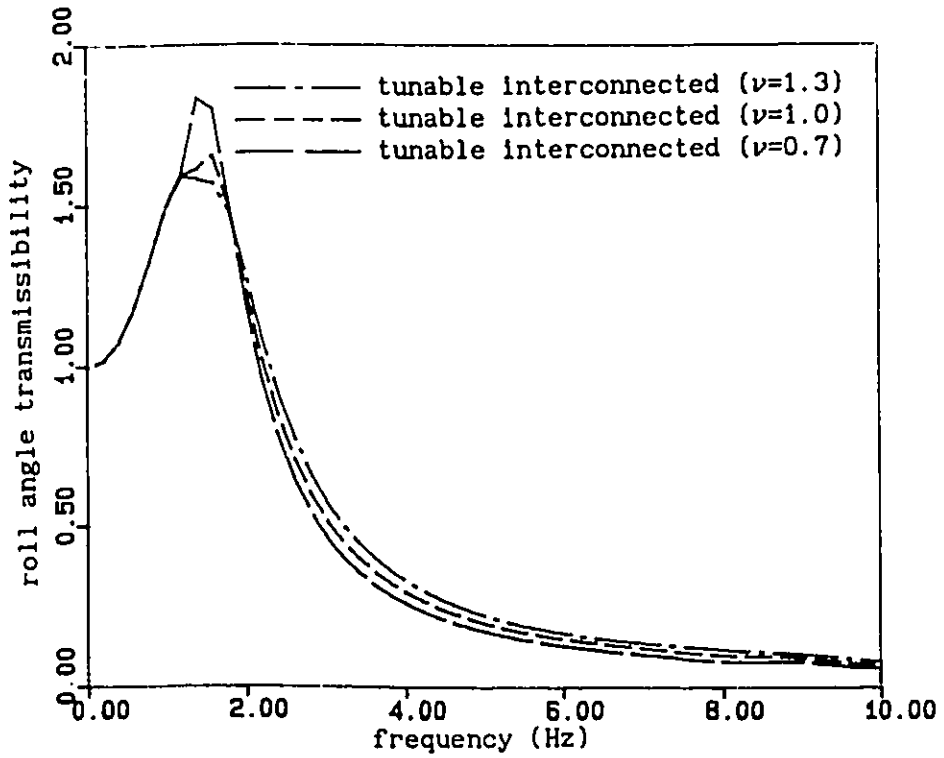

FIGURE 6.38 Roll angle transmissibility of sprung mass of vehicle employing tunable interconnected suspensions (ν=0.7, 1.0 and 1.3)

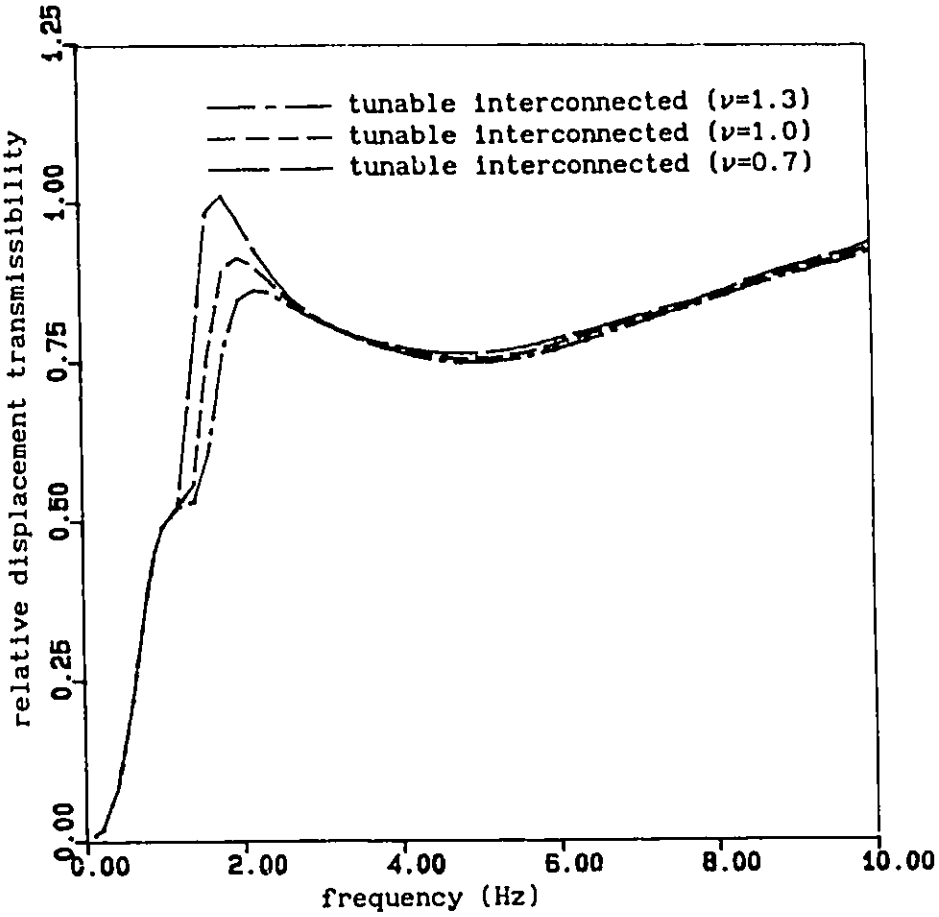

FIGURE 6.39 Relative displacement transmissibility of right suspension unit with tunable interconnected suspensions (ν=0.7, 1.0 and 1.3)

an excitation frequency of 1.8 Hz. A larger value of the tuning factor results in a lower peak amplitude around 1.8 Hz. For the excitation frequencies above 2 Hz, the lower value of the tuning factor yields a slightly larger magnitude of relative response of the right suspension unit. There is not very much difference in the relative displacement response at the high excitation frequencies, as shown in Figure 6.39. The results in Figures 6.37 through 6.39 indicate that the tunable interconnected suspension, with the tuning factor within the range 0.7 to 1.3, can yield improved vibration transmissibility characteristics of the roll plane vehicle model.

6.8 Summary

In this chapter, a tunable interconnected suspension is proposed to achieve improved overall performance of a roll plane model of a vehicle. A mathematical model of the roll plane model of the vehicle employing a tunable interconnected suspension has been developed, incorporating the effects of fluid and mechanical compliance, and tunable valve dynamics. The performance potential of a vehicle employing a tunable interconnected suspension are illustrated via turning and dynamic ride evaluation. The fluid feedback effects due to the interconnecting pipes within the hydro-pneumatic suspension are analytically demonstrated by formulating the interconnected suspension models, as well as by computer simulation. Performance evaluation of the static roll stability and dynamic ride of the roll plane model of the vehicle are presented and compared with that of a vehicle employing independent and interconnected suspensions. The static roll stability and roll performance is evaluated by simulating the roll response of the vehicle to an external moment

during a turning maneuver. The dynamic ride performance of the suspensions is illustrated in terms of the transient and frequency response characteristics. The analysis demonstrates that the fluid interconnections between the two suspension units of vehicle can provides enhanced static roll stability; while a tunable pressure limiting mechanism between the strut and the accumulator of each suspension unit can yield improved dynamic ride performance.

CHAPTER 7

CONCLUSIONS AND RECOMMENDATIONS

7.1 General

In this thesis, active and passive vibration control systems are analytically investigated in order to achieve improved shock and vibration isolation performance. Tunable passive vibration control systems are configured based upon a critical examination of passive hydraulic, as well as active and semi-active damping control mechanisms. The performance characteristics of tunable dampers and tunable interconnected suspensions are examined for improved ride and handling characteristics of road vehicles.

The vibration isolation characteristics of a hybrid active control system, comprising an electro-magnetic force generator, and passive spring and damping elements, are investigated for deterministic base excitations. The dynamics of active force generating element are appropriately incorporated in the hybrid vibration control system and the influence of the dynamics of force generator on the frequency response characteristics are presented for various control schemes.

A concept of tunable hydraulic damper is proposed to achieve sequential damping based upon the pressure differential across the piston, without requiring any external energy source, sophisticated control devices and feedback instrumentation that are essential for active and semi-active vibration isolators. Damping, as well as shock and vibration isolation, characteristics of the proposed tunable damper are investigated for deterministic excitations and compared with those of fixed orifice passive and semi-active 'on-off' dampers. A higher

order analytical model of the tunable damper, incorporating the dynamics due to the pressure modulating mechanism, as well as fluid and mechanical compliance, is developed and a tuning methodology is derived. The tunable damper model is integrated into a quarter vehicle and an in-plane vehicle models and the ride characteristics are presented to demonstrate the performance potential of the proposed damper arrangement. Discrete harmonic linearization technique is generalized for simulating nonlinear systems containing both nonlinear restoring and dissipative elements, based on the principle of energy similarity of dynamic elements. Stochastic analysis of the nonlinear in-plane vehicle model, employing tunable shock absorbers, is carried out using the generalized discrete harmonic linearization technique, and the results are presented in terms of response power spectral density.

A tunable interconnected vehicle suspension is configured by introducing tunable pressure relief valves to an interconnected hydro-pneumatic suspension. Roll-plane models of a road vehicle, incorporating independent, interconnected and tunable interconnected suspensions, are developed to investigate the ride and handling performance potential of tunable interconnected suspensions. The tunable interconnected suspension is mathematically modeled as an eighteenth order dynamic system, including fluid compressibility and valve dynamics. Shock and vibration, as well as roll response, characteristics of a road vehicle are investigated for deterministic excitations arising from road roughness, and rounded step turning moments.

7.2 Highlights of the Investigation

The major highlights of this investigation are summarized in the

following subsections.

7.2.1 Vibration Isolation Performance of Electro-magnetic Active Control Systems Including the Influence of Force Generator Dynamics

The vibration isolation characteristics of active vibration control systems are often evaluated assuming ideal control elements, while the dynamic characteristics of the control force generators are not taken into account. In this thesis, a hybrid active vibration control system, incorporating an electro-magnetic force generator along with passive spring and damping elements, is investigated to demonstrate the significance of generator dynamics as a function of the active control scheme. The electro-magnetic force generator is modeled as a first order dynamic subsystem. The vibration isolation characteristics of a SDOF system employing an electro-magnetic force generator are presented in terms of vibration transmissibility, for various control schemes. The vibration transmissibility characteristics clearly illustrate that the dynamics of the force generator influence the vibration isolation performance considerably. The stability limits of the active vibration control system are also affected by the dynamics of the generator. In most cases, the vibration isolation performance of the active system is adversely affected by the inclusion of the generator dynamics. However, for certain control schemes only, the force generator dynamics can contribute to an improved vibration isolation performance.

7.2.2 Concept of Tunable Pressure Limiting Modulation

It has been established that the damping force of a fixed orifice hydraulic damper becomes predominant at large values of the relative

velocity and thus yields poor vibration isolation performance. The semi-active or sequential dampers reduce the magnitude of the damping force at large values of the relative velocity response by actively modulating the fluid flow through the orifice using 'on-off' control schemes. An examination of the frequency response characteristics of a fixed orifice hydraulic damper clearly reveal that the pressure differential across the piston and the damping force increase rapidly with increasing relative velocity response. The vibration isolation performance of fixed orifice hydraulic damper is considerably deteriorated under a large relative velocity response. A concept of a tunable pressure limiting modulation to obtain sequential damping, by limiting the pressure differential across the damper, is proposed to achieve improved shock and vibration isolation characteristics. Pressure differential limitation and thus damping modulation is achieved via externally mounted pressure relief valves that can be tuned to achieve desirable damping characteristics. A tuning methodology is developed, based upon harmonic base excitations, to estimate the preset limiting pressure required to control the resonant response.

The shock and vibration isolation characteristics of a tunable hydraulic damper are compared with those of fixed orifice and semi-active sequential dampers. It is concluded that the performance characteristics of the tunable damper are comparable to those of a semi-active damper. The proposed tunable passive pressure limiting modulation can be realized passively and does not require sophisticated control devices and feedback instrumentation essential for a semi-active 'on-off' vibration isolator. Moreover, a semi-active 'on-off' damper exhibits discontinuities in acceleration and gives rise to large

magnitude jerk of the system mass, chatter and instability at the time of switching. The tunable damper, on the other hand, provides a sequential damping by limiting the maximum value of pressure and does not produce discontinuities in the acceleration response.

7.2.3 Significance of Fluid Compliance and Valve Dynamics

Hydraulic dampers and shock absorbers are often analytically modeled assuming incompressibility for the fluid flow. In this thesis, the tunable hydraulic damper and the interconnected hydro-pneumatic suspension are modeled incorporating the fluid and the mechanical compliance as well as the dynamics of the tunable pressure relief valves. The influence of the fluid compliance and valve dynamics on the shock and vibration isolation performance of tunable dampers is illustrated.

The fluid and mechanical compliance is characterized in terms of an effective bulk modulus, related to bulk moduli of the fluid and the chamber. Additional variables, describing the rate of change of pressure in each fluid chamber and rate of change of volume in each gas chamber, are introduced in the mathematical modeling. This general modeling methodology is applicable to other types of hydraulic dampers and shock absorbers.

The tunable pressure limiting mechanism is modeled as a second order dynamic subsystem incorporating the spring preload and various port shapes. A SDOF base excited vibration isolation system employing the tunable hydraulic damper is thus mathematically modeled as a seventh order nonlinear dynamic system. The roll-plane vehicle model (conventionally four DOF), equipped with tunable interconnected suspension, is analytically modeled as an eighteenth order nonlinear dynamic system.

The shock and vibration isolation characteristics of the tunable dampers, presented in Chapter 4, clearly illustrate the significance of fluid compressibility and valve dynamics. The simulation results reveals that the effective bulk modulus has a relatively moderate influence on vibration isolation performance. At high excitation frequency, however, the magnitude of the dynamic force changes considerably with reduced bulk modulus. Reduction in fluid bulk modulus, caused by entrapped air within the fluid, significantly affects the restoring as well as damping force characteristics, specifically at higher excitation frequencies. The variations in dynamic forces due to fluid compressibility, are of significance in active and semi-active vibration control systems and may produce serious stability problems.

7.2.4 Development of Generalized Discrete Harmonic Linearization Technique

The discrete harmonic linearization method is an extension of the frequency domain linearization [107] to stochastic analysis of nonlinear systems [105]. The discrete harmonic linearization technique, based upon energy balance, is applicable to systems with nonlinear dissipative elements. The conventional linearization technique can not provide an equivalent stiffness coefficient for a nonlinear conservative restoring element, due to the fact that the energy stored by the restoring element per cycle is zero. The discrete harmonic linearization technique is generalized in this investigation such that the nonlinear tunable dampers can be simulated in the convenient frequency domain for stochastic excitations.

The generalized discrete harmonic linearization method provides linear representations of both nonlinear conservative and dissipative

elements based on the principle of energy similarity of dynamic elements. The generalized discrete harmonic linearization technique, thus developed, is applicable to both nonlinear damping and restoring elements, while all the advantages of the original discrete harmonic linearization method are retained. The generalized technique presented is, therefore, directly applicable for deterministic and stochastic analyses of nonlinear dynamic systems.

7.2.5 Development of Tunable Interconnected Hydro-pneumatic Vehicle Suspension

Ride comfort and road holding ability of a vehicle often pose conflicting requirements on the vehicle suspension. From the study presented in this dissertation and previous studies, it has been established that an interconnected vehicle suspension can increase the effective roll stiffness and thus the roll stability. Tunable pressure limiting mechanisms can be introduced to further improve the ride performance of interconnected vehicle suspensions. A tunable interconnected vehicle suspension is thus configured to achieve improved suspension performance in view of ride and roll characteristics of the vehicles.

A roll plane model of a road vehicle employing a tunable interconnected hydro-pneumatic suspension is developed, and then investigated for excitations arising from road roughness, and roll moments imposed during turning, in order to determine overall suspension performance. The simulation results clearly illustrate that fluid couplings between the two struts of the suspension yield an improved anti-roll performance and thus enhance static roll stability; while tunable pressure limiting modulation between the strut and the accumulator of each suspension unit

offers sequential damping and thus an improved vehicle ride.

7.3 Conclusions

Based on the studies carried out in this thesis work, the following specific conclusions can be drawn:

- — Stability and vibration isolation characteristics of an active vibration control system are strongly influenced by the dynamics of the active force generator.
- — Vibration isolation characteristics of an active control system, in most cases, are adversely affected by the generator dynamics. The generator dynamics, however, can yield an improved vibration isolation response for certain control schemes, such as $\ddot{x}$.
- — Active control based on independent response variables can affect only some aspects of vibration transmissibility characteristics, while active control based upon combined variables has the potential to yield improved vibration isolation performance.
- — Active control based on absolute displacement, velocity, and relative displacement of a hybrid active system yields a superior vibration isolation performance in the presence of generator dynamics, as compared with other schemes proposed in the literature.
- — Sequential damping characteristics can be achieved via modulating the pressure differential across the damper piston.
- — The pressure limited hydraulic damper can be effectively tuned by employing a harmonic analysis for a desirable sequential damping.
- — The tunable pressure limited hydraulic damper offers an improved shock and vibration isolation performance.
- — The performance characteristics of tunable hydraulic damper are

comparable to those of a semi-active 'on-off' damper, while the tunable damper offers the following advantages:

(a) Variation in damping is realized passively.

(b) The tunable damper is simpler and does not require sensors and control devices essential for a semi-active 'on-off' damper.

(c) The jerk and chatter associated with the discontinuous behavior of a semi-active damper is essentially eliminated by the tunable passive damper.

— The shock and vibration isolation performance of a tunable damper is strongly influenced by the preset value of the limiting pressure. Too low a value of preset limiting pressure yields a high resonant peak due to insufficient damping. It is recommended that the tuning factor should be selected greater than or equal to one.

— The dynamics of the pressure limiting mechanism and fluid compliance also influence vibration isolation performance of a tunable pressure limited damper.

— Variations in fluid compliance yield a severe influence on the shock isolation performance, while the vibration isolation characteristics are only moderately influenced by variations in fluid compliance.

— Dynamic characteristics of restoring and damping forces are strongly influenced by low values of effective bulk modulus.

— Both deterministic and stochastic analyses of tunable pressure limited suspension systems indicate that the tunable damper offers considerable potential to improve vehicle ride.

— The generalized harmonic linearization technique can be implemented to achieve locally equivalent linear coefficients for both

nonlinear damping and spring elements based on the principle of energy similarity of dynamic elements. The nonlinear system can be simulated for deterministic as well as stochastic excitation, in the convenient frequency domain.

— The random ride response of a vehicle suspension system is influenced not only by the power spectral density of road roughness, but also by the preset pressure limiting values for the tunable shock absorbers at front and rear axles.

— The tunable interconnected hydro-pneumatic suspension offers considerable potential to improve vehicle ride through tunable sequential damping. The enhanced effective roll stiffness of interconnected vehicle suspension increases the rollover threshold value and thus improves static roll stability.

— The tunable pressure limiting mechanism employed in an interconnected suspension does not affect the effective roll stiffness and thus the static roll stability. Even with very small values of tuning factors, the steady state value of roll response remains unchanged.

— A low value of bulk modulus along with valve dynamics slightly increases the bounce response of the vehicle model with a tunable interconnected suspension. The vehicle roll response, however, decreases due to low fluid bulk modulus and valve dynamics.

Some of the results of this investigation have been presented at conferences and published in journals [129, 130, 131, 132].

7.4 Recommendations for Future Work

Mathematical modeling and computer simulation provide performance potential of the tunable pressure limiting control scheme, but physical

validation is necessary for realization and application of such a concept. An attempt should be made to develop and study physical models of a tunable pressure limited damper and interconnected suspension. The corresponding performance characteristics should be evaluated via laboratory experimentation and the analytical models may be appropriately tuned to achieve validated models for further analyses.

Parameter sensitivity of a tunable hydraulic damper with relief valve mechanisms should be studied, with respect to the shock and vibration isolation characteristics, and incorporating experimental validation. Parameter optimization design of a tunable hydraulic damper can be carried out to achieve shock and vibration isolation characteristics of the system close to those of an ideal tunable damper system, for specified base excitations.

Different mechanisms to realize the pressure limiting modulation should be investigated, in order to minimize the influence of valve dynamics and to achieve further effective control. Adaptive control of tunable modulation should be studied to achieve an optimal tuning of pressure modulation with respect to various excitations.

Parameter sensitivity of a tunable interconnected suspension should be studied in order to achieve an optimal compromise of roll stability and ride comfort, for various types of vehicle models.

Efforts are needed to develop and investigate more comprehensive vehicle models for evaluation of ride and handling performance characteristics. A three dimensional vehicle model with tunable interconnected suspension needs to be studied, incorporating fluid flow interconnections within both roll and pitch planes.

Stochastic analysis of the roll plane vehicle model, as well as a

three dimensional vehicle model, employing tunable interconnected suspension should be carried out to evaluate the ride performance of the suspension in terms of PSD characteristics, by using the generalized harmonic linearization technique.

Application of the generalized harmonic linearization technique to simulate the response of nonlinear dynamic systems with various types of conservative and dissipative nonlinear elements would be of interest. The stochastic response characteristics of the nonlinear systems thus obtained can be compared with those obtained via other methods in order to identify the limitations and advantages of the technique.

Nonlinearities in active vibration control systems, such as the nonlinear control force due to variation in clearance and nonlinear magnetic field, should be properly considered. The effects of these nonlinearities can be evaluated via computer simulations. Laboratory tests, however, need to be conducted to achieve an active vibration control system based upon electro-magnetic force generator.

An optimal design of a hybrid active vibration isolation system along with passive elements could be studied. The optimization can be carried out to achieve the best vibration isolation performance for a limited level of active force or external energy, and employing directly measurable response variables.

REFERENCES

1. Snowdon, J. C., *Vibration and Shock in Damped Mechanical Systems*, John Wiley and Sons, New York, N.Y., 1968.

2. Crede, C. E., *Vibration and Shock Isolation*, John Wiley and Sons, Inc., New York, N.Y., 1951.

3. Ellis, J. T. and Karbowniczek, S., "Hydraulic Shock Absorbers," *Machine Design*, May 24, 1972. pp. 22-27.

4. Simanaitis, D. J., "Shock Absorbers," *Automotive Engineering*, Vol.84, No.11, 1976, pp. 34-39.

5. Cline, R., "Shock Absorbers: An Integral Part of Recreational Vehicle Developments," *SAE* Paper No. 740678, 1974.

6. Crouse, W. H. and Anglin, L., *Automotive Chassis and Body: Suspension, Steering, Aligment, Brakes, Tires, Air Conditioning*, McGraw-Hill, New York, N.Y., 1976.

7. Young, D. W., "Aircraft Landing Gears — the Past, Present and Future," *IMechE, Proc. Instn. Mech. Engrs*, Vol.200, No.D2, 1986, pp. 75-88.

8. Harris, C. M., *Shock and Vibration Handbook*, 3rd Ed., McGraw Hill Book Company, New York, N.Y., 1988, Chapters 30-33.

9. Ruzicka, J. E. and Derby, T. F., "Vibration Isolation with Nonlinear Damping," *ASME, Journal of Engineering for Industry*, May, 1971, pp. 627-635.

10. Hundal, M. S., "Impact Absorber with Linear Spring and Quadratic Law Damper," *Journal of Sound and Vibration*, 48(2), 1976, pp.189-193.

11. Karadayi, R. and Masada, G. Y., "A Nonlinear Shock Absorber Model," Proceedings of SCGVTS, *ASME Winter Annual Meeting*, Dec., 1986, Anaheim, Cal., pp. 149-166.

12. Mercer, C. A. and Rees, R. L., "An Optimal Shock Absorber," *Journal of Sound and Vibration*, 18(4), 1971, pp. 511-520.

13. Freudenstein, F., "Dynamic Analysis of Long-Travel, High Efficient Shock Absorbers in Freight Cars," *ASME Journal of Engineering for Industry*, August, 1970, pp. 581-587.

14. Venkatesan, C., "Optimization of an Oleo-Pneumatic Shock Absorber of an Aircraft During Landing," *Journal of Aircraft*, Vol.14, No.8, 1977, pp. 812-823.

15. Alley, T. L., "Optimal Isolation of a Single-Degree-of- Freedom System with Quadratic-Velocity Damping," *ASME Journal of Applied Mechanics*, Vol.48, 1981, pp. 676-678.

16. Bank, T. A., "Some ABC's of Air Spring Suspensions for Commercial Road Vehicles," *SAE* paper No.800482, 1980

17. Moulton, A. E. and Best, A., "Hydragas Suspension," *SAE* Paper No. 790374, 1980.

18. Chu, Y. and Li, Z., "The Dynamic Response of Vehicles with Hydro-gas Suspension to Roadway Undulation," *ACTA Armamentari*, No.2, May 1984, pp. 30-42.

19. Lin, Y. and Xi, D., "Nonlinear Random Vibration of the Vehicles suspended with Oil-Pneumatic Spring," *ACTA Armamentari*, No.1, Feb., 1985, pp. 17-25.

20. Marek, L, and Winiarz, P. E., "Liquid Spring Design Methodology for Shock Isolation System Applications," *Shock and Vibration Bulletin*, 1987, pp. 17-28.

21. Burns, R. N. and Sacks, H. K., "Ride Comfort as Influenced by Asymmetric Shock Absorber Characteristics," *I.Mech.E., Proc. of the 2nd Int. Conf. on Vehicle Mechanics*, Sept., 1971, pp. 89-106.

22. van Vliet, M., *Computer Aided Analysis and Design of Off-Road Motorcycle Suspensions*, Ph.D. Thesis, Mechanical Engineering Department, Concordia University, 1983.

23. Asami, T., Sekiguchi, H. and Taniguchi, S., "Study on an Oil Damper with Variable Damping Mechanism," *Bulletin of JSME*, Vol.28, No.246, 1985, pp. 2978-2985.

24. Hundal, M. S., "Impact Absorber with Two-Stage Variable Area Orifice Hydraulic Damper," *Journal of Sound and Vibration*, 50(2), 1977, pp. 195-202.

25. Wahi, M. K., "Oil Compressibility and Polytropic Air Compression Analysis for Oleopneumatic Shock Struts," Journal of Aircraft, Vol.13, No.7, July 1976, pp. 527-530.

26. Mayne, R. W., "The Effects of Fluid and Mechanical Compliance on the Performance of Hydraulic Shock Absorbers," *ASME Journal of Engineering for Industry*, Feb., 1974, pp. 101-106.

27. Bennet, S., *A History of Control Engineering*, Petes Peregrimus LTD, New York, N.Y., 1979.

28. Chien, X. S., *Theory of Engineering Control*, Academic Press, Beijin, 1956.

29. Young. H., *Mechanical Control Engineering,* Machine Building Industry Press, Beijin, 1983.

30. Ruzicka, J. E., "Active Vibration and Shock Isolation," *SAE* Paper No. 680747, 1968.

31. Goodall, R. M. and Kortum, W., "Active Controls in Ground Transportation — A Review of the State-of-the-art and Future Potential," *Vehicle System Dynamics*, Vol.12, 1983, pp. 225-257.

32. Sharp, R. S. and Hassan, S. A., "The Relative Performance Capabilities of Passive, Active and Semi-active Car Suspension Systems," *Proc. Instn. Mech. Engrs.*, Vol.200, No.D3, 1986, pp. 219-228.

33. Cavanaugh, R. D.,"Air Suspension and Servo Controlled Isolation Systems," *Shock and Vibration Handbook*, Chapter 33, McGraw-Hill, New York, N.Y., 1961.

34. Hullender, D. A., Wormley, D. N. and Richardson, H. H., "Active Control of Vehicle Air Cushion Suspensions," *ASME Journal of Dynamic Systems, Measurement and Control*, Vol.94, 1972, pp. 41-49.

35. Cho, D. and Hedrick, J. K., "Pneumatic Actuators for Vehicle Active Suspension Applications," *ASME Journal of Dynamic Systems, Measurement and Control*, Vol.107, 1985, pp. 67-72.

36. Iwata, Y. and Nakano, M., "Optimum Vibration Control of Rigid Body Supported by Four Active Isolators," *Proceedings of JSME*, Series C, Vol.50, No.458, 1984, pp. 1955-1961.

37. Sutton, H. B., "The Potential for Active Suspension Systems," *Automotive Engineer*, April, 1979, pp. 42-45.

38. Dominy, J. and Bulman D. N., "An Active Suspension for a Formala One Ground Prix Racing Car," *ASME Journal of Dynamic Systems, Measurement and Control*, Vol.107, March 1985, pp. 73-78.

39. Calcaterra, P. C., Cavanaugh R. D. and Schubert, D. W., "Study of Active Vibration Isolation Systems for Severe Ground Transportation Environments," *NASA-Langlry Report*, CR-1454, 1969.

40. Schubert, D. and Ruzicka, J. Z., "Theoretical and Experimental Investigation of Electrohydraulic Vibration Isolation Systems," *ASME Journal of Engineering for Industry*, 1969, pp. 981-990.

41. Tanaka, N, and Kikushima, Y., "A Study of Active Vibration Isolation," *ASME Journal of Vibration, Acoustics, Stress and Reliability in Design*, Vol.107, 1985, pp. 392-397.

42. Seto, Kazuto, "Study on a Variable Stiffness-type Dynamic Damper with Eddy-Current Damping," *Bulletin of JSME*, 1978, pp. 1482-1489.

43. Ellis, R. W. and Mote, C. D. Jr., "A Feedback Vibration Controller for Circular Saws," *ASME Journal of Dynamic Systems, Measurement and Control*, Vol.101, 1979, pp. 44-48.

44. Nikolajsen, J. K., Holmes, R. and Gondhalekar, V., "Investigation of an Electromagnetic Damper for Vibration Control of a Transmission Shaft," *Proceedings of I.Mech.E.*, Vol.193, 1979, pp. 331-336.

45. Guntur, R. R. and Sankar, S., "Fail-Safe Vibration Control Using Active Force Generators," *ASME Journal of Vibration, Acoustics, Stress and Reliability in Design*, Vol.105, 1981, pp. 361-368.

46. Buzan, F. T. and Hedrick, J. K., "Lateral Active Pneumatic Suspension for Rail Vehicle Control," *Proceedings of the 1983 American Control Conference*, San Francisco, Cal., 1983.

47. Thompson, A. G., "Optimal and Suboptimal Linear Active Suspensions for Road Vehicles," *Vehicle System Dynamics*, Vol.13, 1984, pp. 61-72.

48. Klinger, D. L. and Calzado, A. J., "A Pneumatic On-Off Vehicle Suspension System," *ASME Journal of Dynamic Systems, Measurements, and Control*, 1977, pp. 130-136.

49. Karnopp, D. C., Crosby, M. J. and Harwood, R. A.,"Vibration Control Using Semi-Active Force Generators," *ASME Journal of Engineering for Industry*, Vol.92, No.2, 1974, pp. 619-626.

50. Roley, D. G., "Performance Characteristics of Cab Suspension Models," *1975 Winter Meeting of American Society of Agricultural Engineers*, Paper No.75-1517, Dec., 1975.

51. Margolis, D. L., Tylee, J. L. and Hrovat, D., "Heave Mode Dynamics of Tracked ACV with Semi-Active Airbag Secondary Suspension," *ASME Journal of Dynamic Systems, Measurement and Control*, Vol.97, No.4, Dec., 1975, pp. 399-407.

52. Krasnicki, E. J., "The Experimental Performance of an 'On-Off' Active Damper," *The Shock and Vibration Bulletin*, 51(1), May 1981, pp. 125-131.

53. Allan, R. R. and Karnopp D. C., "Semi-Active Control of Multimode Vibratory Systems Using ILSM Concept," *ASME Journal of Engineering for Industry*, Aug. 1976, pp. 914-918.

54. Margolis, D. L., "Semi-Active Suspensions for Military Ground Vehicles Under Off-Road Conditions," *the 52ed Symposium on Shock and Vibration*, New Orleans, Oct., 1981.

55. Margolis, D. L., "The Response of Active and Semi-Active Suspensions to Realistic Feedback Signals," *Vehicle System Dynamics*, 11(5-6), Dec. 1982, pp. 267-282.

56. Sharp, R. S. and Hassan, S. A., "Performance and Design Consideration for Dissipative Semi-Active Suspension Systems for Automobiles," *IMechE Proceedings of Institution of Mechanical Engineers*, Vol.201, No.D2, 1987, pp. 149-153.

57. Rakheja, S. and Sankar, S., "Vibration and Shock Isolation Performance of a Semi-Active 'On-Off' Damper," *ASME Journal of Vibration, Acoustics, Stress and Reliability in Design*, Vol.107, 1985, pp. 398-403.

58. Sireteanu, T., "The Effect of Sequential Damping on Ride Comfort Improvement," *Vehicle Noise and Vibration, IMechE Conference*, London, June, 1984, pp. 77-82.

59. Margolis, D. L. and Goshtasbpour, M., "The Chatter of Semi- Active On-Off Suspensions and Its Cure," *Vehicle System Dynamics*, Vol.13, 1984, pp. 129-144.

60. Snowdon, J. C., "Isolation from Mechanical shock with a Mounting System Having Nonlinear Dual-Phase damping," *The Shock and Vibration Bulletin*, Vol.41, No.2, Dec. 1970, pp. 21-45.

61. Venkatesan, C. and Kirshnan, R., "Harmonic Response of a Shock Mount Employing Dual-Phase Damping," *Journal of Sound and Vibration*, 40(3), 1975, pp. 409-413.

62. Guntur, R. R. and Sankar, S., "Performance of Shock Mounts Employing Different Kinds of Dual-Phase Damping," *Journal of Sound and Vibration*, 84(2), 1982, pp. 253-267.

63. Venkatesan, C. and Kirshnan, R., "Dual-Phase Damping in a Landing Gear at Touch-Down," *Journal of Aircraft*, Vol.12, No.10, Oct., 1975, pp. 847-849.

64. Burkley, T. E. and Myers, P. F., "Design and Validation of Rate Pneumatic Springs," *SAE* Paper No. 80483, 1980.

65. Felez, J. and Vera, C., "Bond Graph Assisted Models for Hydro-Pneumatic Suspensions In Crane Vehicles," *Vehicle System Dynamics*, Vol.16, 1987, pp. 313-332.

66. Moulton, A. E. and Best, A., "Rubber Springs and Interconnected Suspension Systems," *Engineering Design Show Conference*, Paper No.15a, 1970.

67. Meller, T., "Self-Energising, Hydropneumatic Levelling Systems," *SAE* Paper No. 780052, 1978.

68. Tanahashi, H., Shindo, K., Nogami, T. and Oonuma, T., "Toyota Electronic Modulated Air Suspension for the 1986 SOARER," *SAE* Paper No. 870541, 1987.

69. Horton, D. N. L. and Crolla, D. A., "Theoretical Analysis of a Semi-active Suspension Fitted to an Off-road Vehicle," *Vehicle System Dynamics*, Vol.15, 1986, pp. 351-372.

70. Crolla, D. A., Horton, D. N. L., Pitcher, R. H. and Lines, J. A.,"Active Suspension Control for an Off-Road Vehicles," *IMechE, Proc. Instn. Mech. Engrs.* Vol.201, No.D1, 1987.

71. Howard, A. B., "A Study of Control Algorithms for Active Suspension Systems," *Technical Report*, Royal Military College of Science, England, Nov., 1985.

72. Michelberger, P., Bokor, J., Karesztes, A. and Variaki, P.,"Simulation of Nonlinear Dynamics of Commercial Vehicle Structures," *Simulation and Control of Ground Vehicles and Transportantion Systems*, ASME Winter Annual Meeting, Anaheim, Cal., Dec. 7-12, 1986, pp. 287-297.

73. Caughey, T. K., "Nonlinear Theory of Random Vibrations," Advances in Applied Mechanics, Vol. 11, 1971, pp. 209-253.

74. Roberts, J. B.,"Response of Nonlinear Mechanical Systems to Random Excitation — Part 1: Markov Methods," *Shock and Vibration Digest*, Vol. 13, No.4, 1981, pp. 17-28.

75. Roberts, J. B.,"Response of Nonlinear Mechanical Systems to Random Excitation — Part 2: Equivalent Linearization and Other Methods," *Shock and Vibration Digest*, Vol. 13, No.11, 1981, pp. 15-29.

76. Crandall, S. H. and Zhu, W. Q., "Random Vibration — A Survey of Recent Developments," *ASME Journal of Applied Mechanics*, Vol. 50, 1983, pp. 953-962.

77. To, C. W. S., "Random Vibration of Nonlinear Systems," *Shock and Vibration Digest*, Vol. 19, No.3, 1987, pp 3-9.

78. Sankar, T. S. *Random Vibrations*, Class Notes for the Course ENGR 733, Concordia University, Summer, 1987.

79. Ariaratnam, S. T.,"Random Vibrations of Non-linear Suspensions," *Journal Mechanical Engineering Science*, Vol.2, No.3, 1960, pp. 195-201.

80. Caughey, T. K., "Derivation and Application of the Fokker-Planck Equation to Discrete Nonlinear Dynamic Systems Subjected to White Random Excitation," *Journal of the Acoustical Society of America*, Vol.35, No.11, 1963, pp. 1683-1692.

81. Fuller, A., "Analysis of Nonlinear Stochastic System by Means of the Fokker-Planck Equation," *International Journal of Control*, Vol.9, No.6, 1969, pp. 603-655.

82. Garrido, L. and Masoliver, J., "On a Class of Exact Solutions to the Fokker-Planck Equations," *Journal of Mathematical Physics*, Vol.23, No.6, 1982, pp. 1155-1158.

83. Khasminski, R. Z., "Principle of Averaging for Parabolic and Elliptic Differential Equations and for Markov Processes with Small Diffusion," *Theory of Probability and Its Applications*, Vol.8, 1963, pp. 1-21.

84. Roberts, J. B. and Spanos, P. D., "Stochastic Averaging: An Approximate Method of Solving Random Vibration Problems," *International Journal of Nonlinear Mechanics*, Vol.21, No.2, 1986, pp. 111-134.

85. Roberts, J. B., "First-Passage Time for Randomly Excited Nonlinear Oscillators," *Journal of Sound and Vibration*, Vol.109, No.1, 1986, pp. 33-50.

86. Langley, R. S., "A Finite Element Method for the Statistics of Nonlinear Random Vibration, " *Journal of Sound and Vibration*, Vol.101, No.1, 1985, pp. 41-45.

87. Ihrahim, R. A. and Roberts, J. W., "Parameter Vibration — Part V: Stochastic Problems," *Shock and Vibration Digest*, Vol.10, No.5, 1978, pp. 17-38.

88. Caughey, T. K., "Equivalent Linearization Techniques," *The Journal of the Acoustical Society of America*, Vol.35, No.11, 1963, pp. 1706-1711.

89. Crandall, S. H., "Non Gaussian Closure Techniques for Stationary Random Vibration," *International Journal of Nonlinear Mechanics*, Vol.20, No.1, 1985, pp. 1-8.

90. Ibrahim, R. A., Soundararajan, A. and Heo, H., "Stochastic Response of Nonlinear Dynamic Systems Based on a Non-Gaussian Closure," *ASME Journal of Applied Mechanics*, Vol.52, No.4, 1985, pp. 965-970.

91. Iyenger, R. N. and Dash, P. K., "Study of the Random Vibration of Nonlinear Systems by the Gaussian Closure Technique," *ASME Journal of Applied Mechanics*, Vol.45, No.2, 1978, pp. 393-399.

92. Roberts, J. B. and Dunne, J. F., "Nonlinear Random Vibration in Mechanical Systems," *Shock and Vibration Digest*, Vol.21, No.6, 1988, pp. 16-25.

93. Liu, Q. and Davies, H. G., "Application of Non-Gaussian Closure to the Nonstationary Response of a Duffing Oscillator," *International Journal of Non-linear Mechanics*, Vol.23, No.3, 1988, pp. 241-250.

94. Liu, X. Z., *Mechanics*, Chinese Academic Press, 1956.

95. Crandall, S. H., "Perturbation Techniques for Random Vibration of Nonlinear Systems," *The Journal of the Acoustical Society of America*, Vol.35, No.11, 1963, pp. 1700-1705.

96. Manning, J. E., "Response Spectra for Nonlinear Oscillators," *ASME Journal of Engineering for Industry*, Vol.97, 1975, pp. 1223-1226.

97. Tung, C., "The Effects of Runway Roughness on the Dynamic Response of Airplanes," *Journal of Sound and Vibration*, Vol.5, No.1, 1967, pp. 164-172.

98. Wang, Z. K., *Theory of Probability and Statistics*, Chinese Academic Press, 1972.

99. Liu, D. G., *Computer Simulation Algorithms*, Chinese Military Academic Press, 1985.

100. Hudspeth, R. T. and Borgman. L. E., "Efficient FFT Simulation of Digital Time Sequences," *ASCE Journal of Engineering Mechanics*, Vol.105 (EM2), 1979, pp. 223-236.

101. Shinozuka, M., "Simulation of Multivariate and Multidimensional Random Processes," *The Journal of the Acoustical Society of America*, Vol.49, No.1, 1971, pp. 357-368.

102. Nigam, N, C., *Introduction to Random Vibrations*, The MIT Press, Cambridge, Massachusetts, 1983, pp. 267-273.

103. Ogata, K., *Modern Control Engineering*, Prentice-Hall, Englewood Cliffs, N.J., 1970.

104. Iwan, W. and Patula, E., "The Merit of Different Error Minimization Criteria In Approximation Analysis," *ASME Journal of Applied Mechanics*, Vol.39, 1972, pp. 257-262.

105. Rakheja, S., *Computer Aided Dynamic Analysis and Optimal Design of Suspension Systems for Off-Road Tractors*, Ph.D. Thesis, Mechanical Engineering Department, Concordia University, 1983.

106. Kumar, A. S., Osman, M. O. M. and Sankar, T. S., "On Statistical Analysis of Gear Dynamic Loads," *ASME Journal of Vibration, Acoustics, Stress and Reliability in Design*, Vol.108, 1986, pp. 362-368.

107. Thompson, W. T., *Theory of Vibration with Applications*, Prentice-Hall, Englewood Cliffs, N.J., 1965.

108. Bandstra, J. P., "Comparison of Equivalent Viscous Damping and Nonlinear Damping in Discrete and Continuous Vibration Systems," *ASME Journal of Vibration, Acoustics, Stress and Reliability in Design*, Vol.105, 1983, pp. 382-392.

109. Rakheja, S., Van Vliet, M. and Sankar, S., "A Discrete Harmonic Linearization Technique for Simulation Nonlinear Mechanical Systems," *Journal of Sound and Vibration*, 100(4), 1985, pp. 511-526.

110. Chalasani, R. M.,"Ride Performance Potential of Active Suspension Systems — Part I: Simplified Analysis Based on a Quarter-car Model," *Symposium on Simulation and Control of Ground Vehicles and Transportation Systems*, Anaheim, Cal., Dec. 7-12, 1986, pp. 187-204

111. Stikeleather, L. F.,"Review of Ride Vibration Standards and Tolerance Criteria," *Trans. SAE*, Paper No. 760413, 1976, pp. 1460-1467.

112. Crandall, S. H. and Mark, W. D., *Random Vibration in Mechanical Systems*, Academic Press, New York, 1963.

113. Streeter, V., *Fluid Mechanics*, McGraw-Hill, New York, 1975.

114. Merritt, H. E.,*Hydraulic Control Systems*, John Wiley and Sons, Inc., New York, 1967.

115. Ray, A., "Dynamic Modelling and Simulation of a Relief Valve," *Simulation*, Nov., 1978, pp. 167-172.

116. Bendat, J. S. and Piersol, A. G.,*Random Data: Analysis and Measurement Procedures*, John Wiley, New York, N.Y., 1971

117. Dodds, C. J. and Robson, J. D., "The Description of Road Surface Roughness," *Journal of Sound and Vibration*, Vol.31, No.2, 1973, pp. 175-183.

118. Roa, B. K. N., Jones, B. and Ashley, C., "Laboratory Simulation of Vibratory Road Surface Inputs," *Journal of Sound and Vibration*, Vol.31, No.2, 1973, pp. 175-183.

119. Robson, J. D. and Dodds, C. J., "Stochastic Road Inputs and Vehicle Response," *Vehicle System Dynamics*, Vol.5, 1975/76, pp. 1-13.

120. Elmadany, M.,M., Dokanish, M. A. and Allan, A. B., "Road Vehicle Train Response to Random Road Surface Undulations," *ASME Paper*, 80-WA/DEC-1, PP. 1-11.

121. Segel, L., *The Mechanics of Heavy-duty Trucks and Truck Combinations*, Chapter 20, Mechanics of the Rollover Process, The Open University, Course Notes, U.K., pp. 843-909.

122. Poyser, J., "Development of a Computer Controlled Suspension System," *International Journal of Vehicle Design*, Vol.8, No.1, 1987, pp. 74-86.

123. Sharp, R. S. and Hassan, A., "On Performance Capabilities of Active Automobile Suspension Systems of Limited Bandwith," *Vehicle System Dynamics*, Vol.16, 1987, pp.213-225.

124. Hall, B. B. and Gill, K. F., "Performance Evaluation of Motor Vehicle Active Suspension Systems," *Proceedings of Instn. Mech. Engrs.*, Vol.201, No.D2, 1987, pp. 135-148.

125. Hogan, J. R. and Hubbard, M., "Active Magnetic Suspension Design Using Linear Quadratic Regulator Theory," *IEEE Trans. on Industry and General Applications*, 1980, pp.83-87.

126. Sinha, N. K., Dicenzo, C. D. and Szabados, B., "Modelling of DC Motros for Control Applications," *IEEE, Industrial Elect. and Control Inst.*, Vol. IECI-21, No.2, 1974, pp. 84-88.

127. Szabados, B., Dicenzo, C. D. and Sinha, P. K., "Dynamic Measurements of the Main Electrical Parameters of a DC Machine," *IEEE Trans. on Industry and General Applications*, 1971, pp. 109-114.

128. Weinberg, M. S., *Electromagnectic Suspensions for Ground Transportation*, Ph.D. Thesis, Massachusetts Institute of Technology, 1974.

129. Su, H., Rakheja, S. and Sankar, T. S., "Vibration and Shock Isolation Performance of a Pressure Limited Hydraulic Damper," *Mechanical Systems and Signal Processing*, Vol.3, No.1, 1989, pp. 71-86.

130. Su, H., Rakheja, S. and Sankar, T. S., "Analysis of a Modified Passive Hydraulic Damper with Variable Damping Characteristics," *Proceedings of Damping 89*, Paper No.CDB, Feb. 1989, pp.1-25.

131. Su, H., Rakheja, S. and Sankar, T. S., "Vibration Isolation Characteristics of an Active Electro-magnetic Force Generator and the influence of Generator Dynamics," *ASME Journal of Vibration and Acoustics*, Vol.112, No.1, Jan. 1990, pp.8-15

132. Su, H., Rakheja, S. and Sankar, T. S., "Response of A Nonlinear Vehicle Suspension With Tunable Shock Absorber To Random Road Excitations," *ASME Diagnostics, Vehicle Dynamics and Special Topics*, the 12th ASME Vibration and Noise Conference, Montreal, Quebec, Sept., 1989, pp. 185-193.